



<https://theses.gla.ac.uk/>

Theses Digitisation:

<https://www.gla.ac.uk/myglasgow/research/enlighten/theses/digitisation/>

This is a digitised version of the original print thesis.

Copyright and moral rights for this work are retained by the author

A copy can be downloaded for personal non-commercial research or study,
without prior permission or charge

This work cannot be reproduced or quoted extensively from without first
obtaining permission in writing from the author

The content must not be changed in any way or sold commercially in any
format or medium without the formal permission of the author

When referring to this work, full bibliographic details including the author,
title, awarding institution and date of the thesis must be given

Enlighten: Theses

<https://theses.gla.ac.uk/>
research-enlighten@glasgow.ac.uk

**DYNAMIC INELASTIC BEHAVIOUR
OF SHIP PLATES IN COLLISION**

by

Ling Zhu B.Sc. (Eng.) M.Sc.

Thesis Submitted for the Degree of Doctor of Philosophy

Department of Naval Architecture and Ocean Engineering

Faculty of Engineering

University of Glasgow

June 1990

© L. Zhu 1990

ProQuest Number: 11007404

All rights reserved

INFORMATION TO ALL USERS

The quality of this reproduction is dependent upon the quality of the copy submitted.

In the unlikely event that the author did not send a complete manuscript and there are missing pages, these will be noted. Also, if material had to be removed, a note will indicate the deletion.



ProQuest 11007404

Published by ProQuest LLC (2018). Copyright of the Dissertation is held by the Author.

All rights reserved.

This work is protected against unauthorized copying under Title 17, United States Code
Microform Edition © ProQuest LLC.

ProQuest LLC.
789 East Eisenhower Parkway
P.O. Box 1346
Ann Arbor, MI 48106 – 1346

To Glasgow University

DECLARATION

Except where reference is made to the work of others,
this thesis is believed to be original.

Acknowledgements

The work presented in this thesis has made possible by Postgraduate Scholarship and ORS Awards from the University of Glasgow.

The work has been carried out under the supervision of Professor D. Faulkner, Head of the Department of Naval Architecture and Ocean Engineering, to whom I wish to express my deepest gratitude. Without his recognition and recommendation at the very beginning, this work would not have started; Without his support and encouragement throughout this work would not have been brought to a successful completion within two years.

The experimental work was conducted in Hydrodynamics Laboratory of the Department. I am indebted to Dr. A. Incecik, Superintendent of the Laboratory, for his discussion and support in the course of the experiments. I wish to thank Mr. R.B. Christison, chief technician, and Mr. P. Miller, electrical technician for their assistance during the execution of the experiment.

During the course of this work I have received advice, assistance and encouragement from a great many people from outside. They are Professor N. Jones (University of Liverpool), Professor J.B. Caldwell (University of Newcastle), Dr. R. Dow (ARE Dunfermline), Mr. G. Woisin (West Germany) and Dr. P.A. Frieze (Advanced Mechanics & Engineering Ltd.). I wish to acknowledge a particular debt of gratitude to Professor N. Jones of University of Liverpool, whose early lecture in Wuhan inspired me to pursue research in the impact field. To them all I offer my grateful thanks.

Finally I must thank my wife, Hui Jiang and parents for their vital moral support.

CONTENTS

	page
Declaration	ii
Acknowledgements	iii
List of Figures	viii
List of Tables	xiii
Summary	1
Notation	3
CHAPTER 1 INTRODUCTION AND LITERATURE REVIEW	11
1.1 Introduction	11
1.2 Literature Review	12
1.2.1 Brief Description on Ship Collision	12
1.2.2 Global Methods	15
1.2.2.1 Minorsky's Method	15
1.2.2.2 Modified Minorsky's Method	16
1.2.3 Structural Response Analysis	18
1.2.3.1 Static and Dynamic Approach	18
1.2.3.2 Impact Force	23
1.2.3.3 Dynamic Effects	25
1.2.3.4 Dynamic Failure Mode and 'Critical Speed' of Ship	27
1.2.3.5 Dynamic Inelastic Response of Plate	29
1.3 Aim of the Thesis	30
Figures 1.1 - 1.3	32
CHAPTER 2 NUMERICAL MODELLING OF DYNAMIC RESPONSE OF PLATES UNDER IMPACT	35
2.1 Introductory Remarks	35
2.2 Minimum Principle	36
2.3 Kinematic Relationships	37
2.4 Impact Force	39
2.5 Constitutive Relationships	41
2.6 Boundary Conditions	46
2.7 Damping Effects	47

2.8	Variational Finite Difference Method	47
2.9	Description of Program: IMPACT-I	50
2.9.1	Input Data	50
2.9.2	Output of Results	51
2.10	Check of Numerical Results	52
	Figures 2.1 - 2.5	54
CHAPTER 3 EXPERIMENTAL PROGRAMME		57
3.1	Introductory Remarks	57
3.2	Experimental Rig	58
3.2.1	Runway	58
3.2.2	Striker	58
3.2.3	Plate Clamping Device	59
3.3	Plate Specimen	60
3.3.1	Dimension of Plate	60
3.3.2	Uni-axial Tensile Test	60
3.4	Instrumentation and Measurements	61
3.4.1	Recording of Data	62
3.4.2	Permanent Deflections	63
3.4.3	Impact and Rebound Velocity	63
3.4.4	Acceleration	64
3.4.5	Dynamic Strains	65
3.4.6	Calibration	65
3.4.6.1	Impact and rebound velocity	65
3.4.6.2	Accelerometer	66
3.4.6.3	Strain gauges	66
3.5	Test Results on First Impact	66
3.5.1	Permanent Deflections	68
3.5.2	Acceleration	69
3.5.3	Dynamic Strains	71
3.5.4	Failure Mode on First Impact	72
3.5.5	The Influence of Boundary Conditions	74

3.6	Test Results on Repeated Impacts	75
3.6.1	Permanent Deflections	76
3.6.2	Acceleration	77
3.6.3	Dynamic Strains	77
3.6.4	Response of Plate under More than Two Impacts	78
3.6.5	Failure Mode on Repeated Impacts	79
	Figures 3.1 - 3.31	81

CHAPTER 4 NUMERICAL RESULTS AND CORRELATION WITH EXPERIMENTAL VALUES

		109
4.1	Overall Dynamic Response	109
4.1.1	Deflection, Velocity and Acceleration History	109
4.1.2	Impact Force	110
4.1.3	Deformation Profiles	110
4.2	Dynamic Strains	111
4.3	Stress and Strain Distributions at Maximum Deflection	111
4.4	Stress and Strain Distributions in Residual State	112
4.5	Correlation with Experiments	113
4.5.1	Fully Clamped Aluminium Plates	113
4.5.2	Fully Clamped Steel Plates	113
4.5.3	Side Plates of Small Scale Ship Models	114
4.6	Discussions	117
	Figures 4.1 - 4.19	120

CHAPTER 5 PARAMETRIC STUDIES

5.1	Mass and Impact Velocity of the Striker	139
5.2	Length of the Vertical Striker	141
5.3	Plate Thickness	142
5.4	Plate Length	143
5.5	Plate Width	144
5.6	Critical Speed of Ship	145
	Figures 5.1 - 5.10	147

CHAPTER 6 RIGID PERFECTLY PLASTIC METHOD	156
6.1 Introductory Remarks	156
6.2 Formulation	156
6.2.1 Fully Clamped on Four Sides	156
6.2.2 Fully Clamped on Two Sides	160
6.3 Analytical Solution and Discussions	161
6.4 Application in Design of Plates	166
Figures 6.1 - 6.8	168
CHAPTER 7 DYNAMIC RESPONSE OF PLATE UNDER REPEATED IMPACTS	174
7.1 Introductory Remarks	174
7.2 Numerical Simulation of Elasto-Plastic Plates	175
7.3 Rigid Perfectly Plastic Analysis	177
7.3.1 Second Impact	177
7.3.2 <i>i</i> th Impact	181
7.4 Discussions	183
Figures 7.1 - 7.10	186
CHAPTER 8 CONCLUSIONS AND PROPOSALS FOR FUTURE WORK	196
8.1 Conclusions	196
8.2 Proposals for Future Work	200
REFERENCES	203
APPENDIX	213

LIST OF FIGURES

Page

CHAPTER 1

Fig. 1.1	Variation of absorbed energy with ratio of bow to side strength, according to Akita and Kitamura	32
Fig. 1.2	Minorsky's empirical correlation between resistance factor (R_T) and kinetic energy (K_T) absorbed during collision. (Labelled data is from actual ship collisions. R_T in ft^2 in and K_T in 1000 ton knot^2)	33
Fig. 1.3	Comparison of the modified Minorsky method (Jones) for various values of $W_f/2L_b$ with Minorsky's empirical relation (R_T in ft^2 in and K_T in ton knot^2)	34

CHAPTER 2

Fig. 2.1	Co-ordinate system	54
Fig. 2.2	Fictitious nodes	54
Fig. 2.3	Computational process for IMPACT-I program simulation	55
Fig. 2.4	Central deflection-time history	55
Fig. 2.5	Comparison of present numerical predictions and experimental results (Jones) for aluminium alloy plates and mild steel plates	56

CHAPTER 3

Fig. 3.1	The experimental setup	81
Fig. 3.2	The upper rails and "wheel system"	81
Fig. 3.3	The clamping device	82
Fig. 3.4	True stress-strain curves	83
Fig. 3.5	The permanent deflection measurement	84
Fig. 3.6	Impact and rebound velocity measurement	84

Fig. 3.7	The permanent deformation profile along the central line and the denting line (- <u>ST08</u> -)	85
Fig. 3.8	The permanent deformation profile along the central line and the denting line (- <u>AL06</u> -)	86
Fig. 3.9	Impact test results on the maximum permanent deflection for aluminium and steel plates	87
Fig. 3.10	The influence of strain-rate sensitivity on the maximum permanent deflection for steel plates of thickness 1.65mm when $L=250\text{mm}$.	88
Fig. 3.11	Measurement of acceleration on plate - <u>AL03</u> -	89
Fig. 3.12	Measurement of acceleration on plate - <u>AL04</u> -	89
Fig. 3.13	Measurement of acceleration on plate - <u>ST01</u> -	90
Fig. 3.14	Measurement of acceleration on plate.- <u>ST03</u> -	90
Fig. 3.15	Measurement of strain history on plate - <u>AL04</u> - at point $x=L/4,y=B/2$	91
Fig. 3.16	Measurement of strain history on plate - <u>ST01</u> - at point $x=L/4,y=B/2$	92
Fig. 3.17	Measurement of strain history on plate - <u>ST01</u> - at point $x=L/2,y=B/2$	93
Fig. 3.18	Measurement of strain history on plate - <u>ST02</u> - at point $x=0,y=B/2$	94
Fig. 3.19	Measurement of strain history on plate - <u>AL01</u> -	95
Fig. 3.20	Broken aluminium plate - <u>AL01</u> -	97
Fig. 3.21	Deformed aluminium plate - <u>AL05</u> -	98
Fig. 3.22	The permanent deformation profile along the central line and the denting line (- <u>ST17</u> -)	99
Fig. 3.23	The influence of boundary condition on failure of plate	100
Fig. 3.24	The permanent deformation profile along the central line and the denting line for two impacts (- <u>AL06</u> -)	101
Fig. 3.25	The permanent deformation profile along the central line and the denting line for two impacts (- <u>ST07</u> -)	102
Fig. 3.26	Measurement of acceleration on plate - <u>AL03</u> -	103
Fig. 3.27	Measurement of acceleration and strain history on plate - <u>ST01</u> - during the first two impacts	104

Fig. 3.28	Experimental results of repeatedly impacted plate <u>-ST03-</u> (17 impacts)	105
Fig. 3.29	Experimental results of repeatedly impacted plate <u>-ST05-</u> (15 impacts)	106
Fig. 3.30	Measurement of acceleration and strain history on plate <u>-AL04-</u> during the second impact	107
Fig. 3.31	Comparison between single impact (<u>-AL08-</u>) and repeated impacts (<u>-AL10-</u>)	108

CHAPTER 4

Fig. 4.1	Impact of fully clamped rectangular plate	120
Fig. 4.2	Overall response of impacted aluminium plate (<u>-AL04-</u>)	121
Fig. 4.3	Deformation process of plate (<u>-AL04-</u>) during collision (View from the front surface)	122
Fig. 4.4	Deformation process of plate (<u>-AL04-</u>) during collision (View from the back surface)	123
Fig. 4.5	The maximum deformation profiles of plate (<u>-AL04-</u>)	124
Fig. 4.6	The residual deformation profiles of plate (<u>-AL04-</u>)	125
Fig. 4.7	Strain time histories of plate (<u>-AL04-</u>)	126
Fig. 4.8	Stress and strain distribution at maximum deflection	127
Fig. 4.9	Stress and strain distribution in residual state	128
Fig. 4.10	Comparison between test and numerical results on maximum permanent deflection for aluminium plates	129
Fig. 4.11	Comparison between test and numerical results on rebound velocity of striker for aluminium plates	130
Fig. 4.12	Correlation between test and numerical results on the influence of impact velocity for aluminium plates <u>AL07 - AL10</u> ($L=250$ mm, $m_o=12.8$ kg)	131
Fig. 4.13	Comparison between test and numerical results on dynamic strains at point 2 of aluminium plate <u>-AL04-</u>	132
Fig. 4.14	Comparison between test and numerical results on maximum permanent deflection for steel plates	133

Fig. 4.15	Comparison between test and numerical results on dynamic strains at point 2 of steel plate - <u>ST01</u> -	134
Fig. 4.16	Comparison between test and numerical results on dynamic strains at point 1 of steel plate - <u>ST01</u> -	135
Fig. 4.17	Permanent deformation profiles of a tank in small scale ship model impact test	136
Fig. 4.18	Comparison of numerical and experimental results for dry test	137
Fig. 4.19	Comparison of theoretical and experimental results 1. Plate, elastic plastic strain hardening; *2. Plate, rigid plastic; *3. Plate strip, elastic/visco-perfectly plastic; *4. Plate strip, elastic perfectly plastic; *5. Beam elastic perfectly plastic. (*: result from the paper of Samuelides, 1984)	138

CHAPTER 5

Fig. 5.1	The influence of mass and impact velocity of striker on structural response	147
Fig. 5.2	The influence of vertical striker length on structural response	148
Fig. 5.3	The influence of plate thickness on structural response	149
Fig. 5.4	Strain time histories of plate (- <u>ESH1</u> -)	150
Fig. 5.5	Strain time histories of plate (- <u>ESH2</u> -)	151
Fig. 5.6	Strain time histories of plate (- <u>ESH3</u> -)	152
Fig. 5.7.	The influence of plate length on structural response	153
Fig. 5.8	The influence of plate width on structural response	154
Fig. 5.9	Maximum strains arising from rigid bow impacts on the side of the tanker	155
Fig. 5.10	Critical speeds for a tanker struck by a rigid bow	155

CHAPTER 6

Fig. 6.1	Deformation mode	168
Fig. 6.2	Yield curve	168
Fig. 6.3	Results from analytical method using rigid perfectly plastic material	169
Fig. 6.4	Results from numerical method using elasto-plastic work - hardening material	170
Fig. 6.5	Comparison between the rigid perfectly plastic solutions and test results on the permanent deflection of aluminium plates	171
Fig. 6.6	Maximum and permanent deflections of plates with different thickness	172
Fig. 6.7	Maximum deflection by rigid perfectly plastic analysis and permanent deflection by numerical analysis	
Fig. 6.8	Determination of thicknesses of struck steel and aluminium plates	173

CHAPTER 7

Fig. 7.1	Overall response of plate - <u>A3P2</u> - (Numerical method using elasto-plastic work-hardening material)	186
Fig. 7.2	Strain time histories on plate - <u>A3P2</u> - by numerical method	187
Fig. 7.3	Stress and strain distributions at maximum deflection	188
Fig. 7.4	Stress and strain distributions in residual state	189
Fig. 7.5	Overall response of plate - <u>A3P2</u> - (rigid perfectly plastic method)	190
Fig. 7.6	Overall response of plate - <u>A4P2</u> - (Numerical method using elasto-plastic work-hardening material)	191
Fig. 7.7	Overall response of plate - <u>A4P2</u> - (rigid perfectly plastic method)	192
Fig. 7.8	Strain time histories on plate - <u>A4P2</u> - by numerical method	193
Fig. 7.9	Rigid perfectly plastic solutions for repeatedly impacted plate - <u>ST03</u> -	194
Fig. 7.10	Comparisons between test results and rigid perfectly plastic solutions for repeatedly impacted plate - <u>ST03</u> -	195

LIST OF TABLES

Page

CHAPTER 3

Table 3.1	Dimension of plate specimens	60
Table 3.2	Mechanical properties of specimens	61
Table 3.3	Experimental records on the first impact of steel plates	67
Table 3.4	Experimental records on the first impact of aluminium plates	68
Table 3.5	Experimental records on the second impact of aluminium and steel plates	76

CHAPTER 5

Table 5.1	Parameters of struck plate	139
-----------	----------------------------	-----

CHAPTER 6

Table 6.1	Dimension of examined aluminium and steel plates	164
Table 6.2	Influence of boundary conditions on the structural response of steel plate <u>E102</u>	165
Table 6.3	Mechanical properties of materials	166

Summary

This thesis consists of eight chapters. In the first of these the literature on the structural aspects of ship collision is reviewed in terms of the specific topic in this field. Emphasis is placed on the structural response in collision in which several important aspects are addressed, such as, Minorsky's method, static and dynamic approach, impact force, dynamic effects and failure mode.

Based on the Variational Finite Difference Method, a numerical model of dynamic inelastic response of plates impacted by a rigid knife indenter is developed in the second chapter. The numerical model includes the influence of finite transverse displacement, axial restraints, bending moments, material elasticity and strain hardening. The struck plate and rigid striker are coupled in the numerical simulation, with the deformation, strain, stress and impact force as output of the calculation.

Chapter 3 presents the experimental investigation of clamped rectangular plates impacted by a knife edge indenter. A series of impact tests are conducted on aluminium and steel plates. The plate specimens are struck by a rigid knife edge indenter sliding down from a runway, and the impact loading is repeatedly applied to each plate until plate failure. Detailed experimental results are reported on impact and rebound velocities, permanent deformation, acceleration, dynamic strains and failure modes both for single impact and for repeated impacts. Different stages of plate failure are identified based on the dynamic strain recording. For the plate subjected to a number of identical impacts no pseudo-shakedown phenomenon is observed in the test. The influence of boundary conditions caused by in-plane sliding is also investigated.

In chapter 4 the numerical approach proposed in chapter 2 is used to simulate the collision process of an aluminium plate impacted by a knife edge indenter. Numerical

results provide a full picture of the response of the clamped rectangular plate under dynamic loading, giving information on the impact force, deformation, stress and strain history and distribution in the plate. Correlations are performed with the experimental results on the plate impact test described in chapter 3 as well as on the test of a small scale ship model which was conducted in the Department during 1981-1982. Very good agreement is reached.

Parametric studies are made in chapter 5 on some important parameters for ship collision, such as mass and impact velocity of the striking bow, the length of vertical bow, the struck plate length and width, and plate thickness. As an application of the numerical work, critical speed for a longitudinally framed tanker struck by a rigid vertical bow is also investigated.

Chapters 6 and 7 contain analytical solutions based on the Rigid Perfectly Plastic Method for single impact and repeated impacts respectively. An approximate theoretical procedure is developed to give the lower and upper bounds of the dynamic plastic solution to the impacted rectangular plate with finite deflections. The analytical solution obtained is compared with the experimental results and predictions of numerical program. It is found that no pseudo-shakedown occurs for the plate subjected to a number of identical impacts.

Finally, conclusions and suggestions for further work are given in chapter 8.

Notation

A, A_m	total area and sub-area of plate
$A^s_{i,j}$	coefficient in Eqns (2.40) - (2.42)
B	width of plate (see Fig. 2.1)
B_r	semi-width of plate (see Fig. 6.1)
C	coefficient in Eqns (1.7) and (1.8)
C_d	damping coefficient
C_{ij}	coefficient of matrix in Eqn. (2.31)
C_m	length of a boundary curve surrounding the sub-area A_m
C_r	coefficient in Eqns (2.40) - (2.42)
D	energy dissipation function
E	Young's Modulus
E_0	initial kinetic energy of striker $E_0 = \frac{1}{2} m_0 V_0^2$
E_i	energy absorption components
E_{ij}	the Lagrangian strain tensor
E^e_{ij}	elastic strain tensor
\dot{E}^e_{ij}	elastic strain rate tensor
E^p_{ij}	plastic strain tensor
\dot{E}^p_{ij}	plastic strain rate tensor
E_s	energy absorbed by plate $E_s = \frac{1}{2} m_0 (V_0^2 - V_s^2)$
E_{si}	energy absorbed by plate in first i impacts
dE_{si}	energy absorbed by plate in the i th impact
E_T	total energy of the striking ship
E_t	tangent Modulus
E_{xx}, E_{xy}, E_{yy}	components of the Lagrangian strain tensor

F	collision impact force
F_i	body force (per unit mass)
F_m	maximum impact force
G	scalar proportionality function
H	thickness of the plate
I	functional defined in Eqn. (2.3)
I^q	functional I at time $t=q\Delta t$
J	expressed by left hand of Eqn. (6.2)
J_2	the second invariant of the stress deviation tensor
K_T	kinetic energy lost in collision
L	length of the plate (see Fig.2.1)
L_b	semi-span of the fully clamped beam
L_d	the dent length (see Fig. 2.1)
L_r	semi-length of plate (see Fig. 6.1)
M	resultant moment along yield hinge
M_0	plastic moment of plate $M_0=1/4(\sigma_s H^2)$
M'_0	plastic moment of plate including strain rate effect $M'_0=1/4(\sigma_d H^2)$
M_A, M_B	mass of the struck and striking ship
M_{ij}	bending moment per unit length
M_x, M_y, M_{xy}	bending moment components
$(M_{xx})_{i,j}$	coefficient in Eqns (2.40) - (2.42)
$(M_{yy})_{i,j}$	coefficient in Eqns (2.40) - (2.42)
$(M_{xy})_{i,j}$	coefficient in Eqns (2.40) - (2.42)
N	membrane force along yield hinge
N_0	limit membrane force
N_{ij}	membrane force per unit length
N_x, N_y, N_{xy}	membrane force components
$(N_{xx})_{i,j}$	coefficient in Eqns (2.40) - (2.42)

$(N_{yy})_{i,j}$	coefficient in Eqns (2.40) - (2.42)
$(N_{xy})_{i,j}$	coefficient in Eqns (2.40) - (2.42)
P_c	concentrated load
Q	coefficient in Eqns (2.40) - (2.42)
Q_t	temperature
R	coefficient in Eqns (1.7) and (1.8)
R_T	resistance factor
S_0	boundary surface of the region
S_T	boundary surface with traction
dS	the initial area element
T_e	natural period of elastic vibration of plate
T_i	Lagrangian surface traction (per unit area)
U, V, W	the displacement components of a point at the mid-span along the X, Y and Z axis
U_c	common speed of two collided ships after collision
U_i	displacement vector
U_x, U_y, U_z	the physical components of the displacement vector
V	velocity of striker
V_0	initial impact velocity for first impact
\bar{V}_0	region
V_{20}	initial impact velocity for second impact
V_{2s}	rebound velocity of striker in second impact
V_B	speed of the striking ship before collision
V_s	rebound velocity of striker in first impact
W_c	central deflection of plate
W_{1c}	central deflection of plate for first impact
W_{2c}	central deflection of plate for second impact
W_f	final deflection
W_{1f}	final deflection of plate after first impact

W_{2f}	final deflection of plate after second impact
W_m	maximum deflection of plate
W_{1m}	maximum deflection of plate for first impact
W_{2m}	maximum deflection of plate for second impact
W_{im}	maximum deflection of plate for i th impact
W_r	the deflection corresponding to the maximum elastic recovery
W_{p1}	maximum permanent transverse displacement for first pressure pulse
W_{p2}	maximum permanent transverse displacement for second pressure pulse
W_s	maximum permanent transverse displacement due to static load
X_i	covariant coordinates referred to contravariant base vector g^i
X, Y, Z	the rectangular Cartesian coordinates
a	acceleration of the striker
a_0	initial acceleration of the striker
a_{10}	initial acceleration for first impact
a_{20}	initial acceleration for second impact
a_{i0}	initial acceleration for i th impact
a_m	maximum acceleration
a_{1m}	maximum acceleration for first impact
a_{2m}	maximum acceleration for second impact
a_{im}	maximum acceleration for i th impact
da	the area element after deformation
d, \bar{d}, d_2	coefficients expressed in Eqns (6.14), (6.28) and (7.9)
d_s	distance between the nearest plate structures attached to the shell and extending in the longitudinal and transverse directions
f	loading function
$f_{i,j}$	resistant pressure at plate surface (x_i, y_j)

g	gravity
g_i, g^i	covariant base vector and contravariant base vector
g_{ki}	the metric tensor
h, \bar{h}, h_2	coefficients expressed in Eqns (6.12), (6.26) and (7.7)
h_s	height of broken or heavily deformed longitudinal member
l_d	non-dimensional dent length ($l_d=L_d/L$)
l'_d	semi-length of dent line (see Fig. 6.1)
l_m	length of yield hinge
m_0	mass of striker
n_k	the covariant unit normal to da
p	transverse pressure over the surface of the plate
p_m	magnitude of pressure pulse
r	number of boundary curves
s	number of yield hinges
s^{ij}	the contravariant Kirchhoff stress tensor
s'_{ij}	the Kirchhoff stress deviation tensor
s_{xx}, s_{xy}, s_{yy}	components of the Kirchhoff stress tensor
s_t	non-dimensional area
t	real time
t_d	impact duration
t_m	time for plate to reach the maximum deflection W_m
t_{1m}	time for plate to reach the maximum deflection W_{1m}
t_{2m}	time for plate to reach the maximum deflection W_{2m}
t_{im}	time for plate to reach the maximum deflection W_{im}
t_s	thickness of broken or heavily deformed longitudinal member
u, v, w	the nondimensional displacement components in Chapter 2

$$u = \frac{U}{L}, \quad v = \frac{V}{L}, \quad w = \frac{W}{L}$$

u_b, v_b, w_b	displacement components for boundary point (see Fig.2.2)
u_{ex}, v_{ex}, w_{ex}	displacement components for fictitious point (see Fig.2.2)
u_{in}, v_{in}, w_{in}	displacement components for internal point (see Fig.2.2)
$\dot{u}_i(\bar{x}, t)$	general mode fields of velocity in Chapter 6
$\dot{u}_i^0(\bar{x})$	given initial velocity
v_0	nondimensional volume
$v_{i,j}$	velocity of the plate at point (x_i, y_j)
w	transverse displacement of plate in Chapters 6 and 7
w_I	transverse displacement of plate in region I (see Fig. 6.1)
w_{II}	transverse displacement of plate in region II (see Fig. 6.1)
$\dot{w}_*(t)$	mode velocity amplitude
\dot{w}_*^0	initial mode velocity amplitude
\ddot{w}_d	the non-dimensional acceleration of the plate at the dent line
w^P	plastic work
x, y, z	the nondimensional coordinates $x = \frac{X}{L}$, $y = \frac{Y}{L}$, $z = \frac{Z}{L}$
$\Delta x, \Delta y, \Delta z$	the chosen spacing of coordinates x, y and z
x'	$x' = x - l'_d$
\bar{x}	space variables
Δ_0	kinetic energy difference
Φ	angle in Fig. 6.1
Γ	$\Gamma = 2l'_d$
Λ	scalar function in Eqn.(2.17)
$\Theta_i(\bar{x})$	normalised vector valued shaped function of space variables \bar{x}

δ_i^k, δ_{ij}	the Kronecker symbol
$\dot{\epsilon}$	uni-axial strain rate
$\dot{\epsilon}_e$	equivalent strain rate for multi-axial stress system $\dot{\epsilon}_e = \left(\frac{2}{3}\dot{\epsilon}_{ij}\dot{\epsilon}_{ij}\right)^{\frac{1}{2}}$
ϵ_m	maximum strain
ϵ_s	uni-axial yield strain
ϵ_p	uni-axial rupture strain
$\epsilon_x, \epsilon_y, \epsilon_{xy}$	in-plane strain components
κ	the strain-hardening parameter of the material
λ, λ_1	structural impact parameter $\lambda = m_0 V_0^2 / (8M_0 H)$
λ_0	impact parameter for impulsively loaded plate $\lambda_0 = \rho L^2 V_0^2 / (4M_0)$
μ	mass per unit area of plate
ν	Poisson's ratio
ν_i	the covariant unit normal to dS
θ_c	critical overall rotation angle of beam at fracture
θ_m	rotation of adjacent rigid part of plate
ρ	mass density
ρ_0	the initial mass density
σ	uni-axial stress
$\bar{\sigma}$	equivalent stress for multi-axial stress system $\bar{\sigma} = \left(\frac{3}{2}s'_{ij}s'_{ij}\right)^{\frac{1}{2}}$
σ_d	dynamic yield stress in uni-axial state
$\bar{\sigma}_d$	equivalent dynamic stress for multi-axial stress system
σ_s	static uni-axial yield stress
τ	nondimensional time
τ_1	duration of pressure pulse
$\Delta\tau$	nondimensional time increment
$\omega, \bar{\omega}, \omega_2$	coefficients expressed in Eqns (6.13), (6.27) and (7.8)

Subscript:	i-1, i, i+1	node number in x-axis
	j-1, j, j+1	node number in y-axis
	k-1, k, k+1	node number in z-axis
Superscript:	q-1, q, q+1	time iteration number

$\frac{D^2}{Dt^2}$	the second material derivative
($\dot{\quad}$)	partial differentiation with respect to time
($\ddot{\quad}$)	second partial differentiation with respect to time
(\quad) _{;i}	covariant derivative of a variable with respect to X_i

CHAPTER ONE

INTRODUCTION AND LITERATURE REVIEW

1.1 Introduction

Between 1970 and 1980, about 25% of the total accidents involving ships were due to ship-ship collisions. These collisions often resulted in the severe damage of ships, loss of lives and property, and pollution of the sea by spillage of hazardous cargo. Because of the high frequency of collision accidents and their serious consequences, the problem of ship collision has attracted much attention since the late 50s when Minorsky published his pioneering paper on the protection of the nuclear-powered ship. Over the past 40 years a great deal of research has been carried out worldwide which covers various aspects of ship collision, experimentally, analytically and numerically.

To reduce the consequences of ship collision we should either reduce the probability of collision by adopting adequate, preventive measures (Prevention), or choose proper structural configuration against collisions (Mitigation), or by a mix of both. It seems impossible to eliminate all collisions and therefore more work on Mitigation is needed, in which minor collision should be considered at the design stage of the ship.

In the past the collision process in ships has been simulated by tests and by numerical packages. Through tests different types of failure were identified and a relationship between the amount of kinetic energy dissipated as structural energy during a collision

to values of the volume and area of the damaged materials can be established, which is simple to use for design purposes. On the other hand, modern computers make it possible to study the response of ship collision. However, it is still difficult to evaluate the numerical results, and the running cost for such a package is impractically expensive. Although some design tools were proposed and developed in collision research, they should be tested with model experiments before being applied to the ship designed. To predict the extent of damage and response of ship plate during minor collision and to optimise the structural arrangements which may minimise the damage, it is necessary to investigate fully the several important aspects of ship collision and to develop some simple analytical methods or efficient numerical programs for the preliminary design of ship plate against collision.

1.2 Literature Review

The collision of ship and offshore platforms was studied extensively and continue to occupy the attention of naval architects and the general public. Jones [1979, 1983], Ellinas and Valsgard [1985] have presented a broad review on collision problems related to ship and offshore structures. The field of collision protection is not only relevant to the design of nuclear-powered ships examined in the earlier work, but now includes oil tankers, LNG carriers, chemical carriers with hazardous cargoes and various types of offshore platforms.

The literature review focuses on the structural response of ships during collisions.

1.2.1 Brief Description on Ship Collision

Let us first discuss the collision phenomena. In the following discussion it is assumed that A is the struck ship which is stationary before collision and B the striking ship.

When the two ships, A and B, are involved in a collision, the collision impact force, F , is a function of the stiffness of the structure of the two ships in the contacted area. The structure of both A and B will be deformed, crushed or penetrated in terms of relative stiffness of the two structures, viz. there is a complicated interaction between the two striking ships. The collision response is highly transient and non-linear, involving continuous changes in geometry and boundary of the structure and the properties of the materials.

The collision problem can be divided into two categories: one dealing with external mechanics and the other with internal mechanics. External mechanics is defined as the motion of two ships. Internal mechanics is defined as the deformation and destruction of local ship structures.

The behaviour of two ships and their structural members following a collision involves the global dynamics of the ship structures in way of the collision. Both sets of dynamics are functions of the interaction forces between the ships, including the inertia forces of the ships and the hydrodynamic forces of the surrounding water [Incecik and Samuelides, 1981].

From the view point of energy distribution, the total energy of the striking ship will be absorbed by the striking and struck ships during the collision as follows:

- (1) Energy absorption due to the rigid body motion of the struck ships.
- (2) Energy absorption due to the overall elastic deformation of the struck and striking ships.
- (3) Energy absorption due to the elasto-plastic deformation of the structural members around the impact region of the struck ship and striking ship.
- (4) Energy absorption due to the crack or rupture of the structural elements of the struck ship and striking ship.

- (5) Energy absorption due to the motion of the fluid which surrounds the struck and striking ship.

The energy conservation equation may be written as

$$E_T = \sum_{i=1}^5 E_i \quad (1.1)$$

where E_T is total energy of the striking ship and E_i is the energy absorption components as summarised above.

It is clear that external collision parameters are E_1 and E_5 while E_2 , E_3 and E_4 belong to internal ones. The ship collision is often classified as 'major collision' and 'minor collision', depending on the existence and absence of E_4 . The energy absorption, E_5 , exists because of hydrodynamic effects in the entrained water around the ships. This phenomenon can be accounted for by the added mass effects. Following Minorsky [1959], most researchers took the added mass of a struck ship as $0.4M_A$. The added mass of the striking ship is ignored by Minorsky, but is assumed to be $0.1M_B$ by several other authors.

In respect of the structural part, the relative strength of the bow of a striking ship and the side of the struck ship is an important factor which determines the partition of energy absorption between the two ships. This is shown in Fig.1.1 from the experimental results of Akita and Kitamura [1972].

As mentioned above, the interaction between the two colliding ships is very complicated. Therefore, most papers studied the two extreme cases, namely, a rigid bow against a soft side shell and a soft bow against a rigid side structure. The former

was widely used for the study of the side structure of the ship and the latter for the study of the bow structure.

1.2.2 Global Methods

Existing solutions for internal mechanics consists of the solution developed by Minorsky [1959] based on the collected data on damaged ships and the modified Minorsky's formulae based on experimental data and theoretical analysis. Minorsky's method and the modified ones are called Global Method [ISSC 1982], because they establish a simple relationship between the amount of kinetic energy dissipated as structural energy during a collision to values of the volume and area of the damaged materials.

1.2.2.1 Minorsky's Method: In the original paper of Minorsky [1959], the general case of two vessels with an arbitrary angle of encounter was studied. For simplicity of demonstration, the collision scenario is assumed as striking ship (B) travelling with a speed V_B and impacting a stationary ship (A) at right angles.

According to the conservation of momentum and energy principle, we have

$$M_B V_B = (M_A + 0.4M_A + M_B) U_c \quad (1.2)$$

$$K_T = \frac{1}{2} M_B V_B^2 - \frac{1}{2} (M_A + 0.4M_A + M_B) U_c^2 \quad (1.3)$$

where U_c is the common speed of both ships after collision and $0.4M_A$ is the added mass of the struck ship. The kinetic energy lost in the collision, K_T , is the difference between the initial kinetic energy and the final kinetic energy remaining in the system after impact.

Minorsky collected information on 26 damaged ships and identified the loss of kinetic energy (K_T) and the resistance factor (R_T) as two parameters which largely describe the structural damage associated with major ship collision. Through calculation, a straight line relationship was found between the value of K_T and R_T (Fig.1.2).

The resistance of ship's structure to collision is extremely difficult to estimate. The calculation of R_T is given in detail in the paper. It should be noted in Fig. 1.2 K_T and R_T do not follow a straight line relationship near the origin. This means that the Minorsky approach is only applicable to major collision which does not allow direct calculation of energy absorption prior to the rupture of the ship plate.

1.2.2.2 Modified Minorsky's Method: The Minorsky method is used extensively by designers all over the world despite its limitations. Because of its simplicity, several modified Minorsky's formulae were proposed separately by Woisin [1979 and 1986], Jones [1979], NCRE¹ [ISSC,1967] and Vaughan [1978]. In the Jones' formula, Minorsky's method was extended to the study of minor collision.

Based on the experimental results of GKSS, Hamburg, and his long time working experience in this field, Woisin [1979] proposed a modified formula as follows:

$$K_T = 47 R_T + 0.5 \sum h_s t_s^2 \quad (1.4)$$

where K_T [MJ] is the loss of kinetic energy, R_T [m³] represents the volume of the steel plates involved, h_s [m] is the height of broken or heavily deformed longitudinal member, and t_s [cm] is the thickness of member.

Recently Woisin [1986] made a little change in his original proposal of equation (1.4)

¹Naval Construction Research Establishment, and now Admiralty Research Establishment (ARE).

$$K_T = 47 R_T + 0.19 \sum d_s h_s t_s \quad (1.5)$$

where d_s [m] is the distance between the nearest plate structures attached to the shell and extending in the longitudinal and transverse directions, such as decks, inner decks and ship's bottom. In this formula three spatial dimensions were used but without the dimensions in the longitudinal direction, such as the distance between webframe or transverse bulkhead.

During a minor collision, the membrane energy absorbed in stiffened hull plating and in stiffened decks is the dominant energy absorption in a struck ship. Jones [1979] developed a simple formula to extend Minorsky's method to minor collision problems. Considering a rigid perfectly plastic beam with fully clamped supports across a span $2L_b$ subjected to a concentrated load P_c at the mid-span, Jones presented the formula as

$$K_T = 0.030288 \sigma_s R_T \left(\frac{W_f}{L_b} \right)^2 \quad (1.6)$$

where R_T is the volume of side-shell assumed to be involved in membrane mechanism, σ_s is the yield stress and W_f is the final deflection. This approach was used to estimate the energy which could be absorbed by a struck ship before the rupture of the side shell. This formula (Eqn (1.6) with $\sigma_s = 30,000 \text{ lb/in}^2$) for various values of $W_f/2L_b$ was compared with Minorsky's empirical relation (see Fig.1.3), which gives a family of lines radiating from the origin of Fig.1.3 in which minor or low energy collision was contained.

Formulae for the calculation of the energy required to tear the deck and/or the bottom of the ship structures has been proposed by researchers at NCRE [ISSC,1967] and Vaughan [1978].

The formulae by Woisin and Jones are two typical works of modified Minorsky's method, but extended in different ways. Woisin followed Minorsky's method, placing emphasis on the analysis of the results from real collision cases and the large scale collision experiments, making the Minorsky's formula close to the statistical data. However, Jones analysed the problem theoretically, whose analytical model is of clear mechanic sense, and implemented a structural damage parameter W_f .

The Minorsky and modified methods are simple to use for design purposes, and can predict the total volume of material damaged in collision for a given required energy absorption K_T . After a ship collision accident happens, the collision resistance can be calculated by observation of the damaged area thereby adding more information to the statistical data bank of ship collision. However, for the striking and struck ships given, the method can not predict the ships' damages due to the absence of consideration on the stiffness of the structures. Ship collision is an extremely complicated phenomena which involves dynamic effects, structural failure mode, interaction between the two colliding ships and hydrodynamic forces, etc. For better understanding of the phenomena each aspect of collision must be thoroughly studied.

1.2.3 Structural Response Analysis

A great number of papers have been published on the structural response of ship structures and elements to collision [Jones, 1983, Ellinas and Valsgard, 1985]. In this section the literature is reviewed under several important and specific subjects which are limited to a side structure of ship under rigid bow impact.

1.2.3.1 Static and Dynamic Approach:

(a) Static Approach

McDermott et al [1974] developed an approximate plastic analysis procedure to study

the behaviour of a longitudinally framed oil tank structure during a minor collision. The structural elements in the analysis procedure follow the various phases during the collision - bending and stiffener buckling of the stiffened hull plating followed by membrane stretching, web frame failure, etc. up to hull rupture. In the analysis, the striking location is chosen to be midway between flanking web frames and bulkheads and the collision force is evenly distributed along the length of contact area. The impact of the assumptions and suitability of the overall procedure developed in M. Rosenblatt & Son, Inc. were evaluated by Jones [Van Mater et al, 1979].

The ship structure is considered as an assemblage of many basic elements. The total local deformation relationship is found by adding the contribution to the energy dissipation from all the elements. Various folding mechanisms of energy dissipation in ship collision are identified and described by Amdahl [1983]. Using the kinematic method of plasticity, analytical solutions are obtained and are also compared with experiments on single elements. Wierzbicki [1983] studied the crushing behaviour of plate intersections. The theory of folding mechanics was developed in a systematic way starting from elementary concepts of bending, extension of flat sheets and plastic inversion of tubes. Yang and Caldwell [1988] used the kinematic method of plasticity to study the crushing strength of ship's bow structures during a collision. The crushing strength of a ship's bow structure is obtained by summing the energy dissipated in all individual elements.

To simulate the ship-ship collision process, a lot of work has been done in which the structure is subjected to impact from knife edge indentors. Akita et al [1972] reported two distinctly different failure types in transversely framed side structure when penetrated statically with rigid bow. One is deformation type and the other is crack type. The former occurred when the strain underneath a bow was less than about 0.3. The latter was observed for large strain. Various series of tests and simple theoretical

analysis were carried out. In the paper of Ando and Arita [1976], experiments were reported on double-hull models penetrated statically by a rigid bow model to estimate the amount of energy absorbed in the hull plating during a minor collision. This is neglected in the design procedure due to Minorsky. Ito et al [1984 and 1985] performed static tests to destruction on large scale models of side and bilge structures similar to those on ships with a double-hull construction. The striking bow was taken as rigid and the type of collision was classified into five groups from a geometric point of view between a colliding bow and hull. A simple theoretical procedure was developed using a displacement method formulated in matrix form and quite good agreement was obtained with corresponding experimental results.

Pettersen [1981] used the simplified non-linear Finite Element program to make a static analysis of the damaged region of a struck vessel involved in collision. The use of 'simplified element' reduced the computing cost but the results generated by this particular procedure have not been verified. Valsgard and Pettersen [1982] developed this procedure further to allow for interaction between the bow and side structures and for rupture of the side-shell.

Ronalds and Dowling [1986] investigated the plastic behaviour of a T-shaped beam under central point loading and derived simple formulae for modelling the denting process of the beam with finite deflections. The formulae were extended to the longitudinally stiffened plates and shells. Small scale model tests on stiffened plates and shells were conducted and comparisons with the theoretical results were made. Parallel to the experimental investigation of Ronalds, Onoufriou et al [1987] developed a numerical approach, using the Finite Element Method, in which the damage process was treated as a static problem by denting the ring-stiffened member through a knife edge indenter and the residual deformation and stress were predicted. On the other hand, much more attention has been placed on the effect of damage on structures to

evaluate the influence of residual deformation and residual stress on the residual strength of structures. Frieze and Sachinis [1983] studied the compressive strength of ring-stiffened cylinders including local damage, but there was no information on the residual stresses in their work.

In summary, the static approach can be applied providing dynamic effects, e.g. inertia force of the impacting bodies and strain-rate sensitivity of the material, are insignificant. Therefore the energy absorbed by the ship can be determined by integrating the static force-deformation curve maintaining force equilibrium. In adopting the static approach for predicting the damage of the colliding ships, the problem remaining to be solved is how to construct the force-deformation relationship for the striking and struck ships.

(b) Dynamic Approach

Strictly speaking, all impacts and collisions will involve some dynamic effects. Kinetic energy will by some mechanism be transferred to elastic or plastic energy during structural deformation, and the global motion of all involved bodies should be described dynamically.

In the early 60s, a series of impact experiments were conducted in Japan [Harima et al 1962], from the beam of various shaped cross-section to stiffened plates as well as double-hull side structure models. For the fully clamped plates and stiffened plate, a ball-end striker was used to hit the plate centre dynamically. However, in the theoretical analysis, the static solution for a circular plate model was adopted.

Ueda et al [1989] studied the dynamic elastic response of tubular beam under collision through point contact, using an equivalent mass-spring model incorporated with the Finite Element Method in which the local and bending deformation of the beam was considered. Based on the analysis, the phenomena were classified into three groups depending on the ratio of the stiffness and mass.

Liu and Jones made experimental [1987] and theoretical [1988] studies on the dynamic response of clamped beams made of aluminum alloy and steel struck transversely by a mass. The transverse shear and bending response and influence of finite deflection were examined by rigid, perfectly plastic models. The ABAQUS Finite Element program was used to examine the experiment by Liu and Jones for a clamped aluminum alloy beam [Yu and Jones, 1989]. Significant differences were found between the behaviour of flat-end beams and beams with enlarged ends. The strain time history and strain distribution along the beam were given.

Samuelides [1984] made studies on the structural dynamics and rigid body response coupling in ship collision both numerically and experimentally. The proposed procedure solved the governing equation using a time-marching technique which included the hydrodynamic force acting on the struck ship. The structural analysis incorporated predicted the behaviour of a beam and a plate-strip. The numerical model significantly over-estimated the deflection with the theoretical predictions being 1.5 to 2.0 times the experimental results.

It is generally accepted that using the Finite Element Method is the best way to analyse the structural response of ship structure in collision. In 1976, the Finite Element package ANSYS was used in Hydronautics Inc.[Van Mater et al 1979] to study the structural response of energy resisting collision barriers developed by GKSS. In the calculations, the dynamic loading time history used was taken from very rough GKSS measurements, which makes firm correlation difficult with the GKSS data. One good run of the program requiring three or four trials could cost as much as 15,000 dollars.

Chang et al [1980] proposed a methodology for the prediction of the structural response, which used the Finite Element techniques collaborated with plastic collapse theorem. The method gave a lower-bound for the prediction of the resistance capacity

of the structure and is valid only when the collapse theorem is properly applied.

The Finite Element Approach is potentially a more powerful and flexible tool. However, it is not practical for use as a routine design tool because of high cost, uncertainties in the input loading and appropriate modelling of boundary conditions, etc. Nevertheless, it could be used to check final designs and for particularly critical cases.

From the review above, it can be seen that impact force is important both for a static and a dynamic approach. In fact, the impact force is much concerned with the stiffness of the side structures of the struck ship and the characteristics of colliding vessels, particularly the mass, size and impact velocity of the striking ship when the bow is assumed rigid.

1.2.3.2 Impact Force: One of the most difficult problems in collisions is the determination of impact force because of the interaction between striker and struck structure. The impact force problem has been investigated experimentally and theoretically by many researchers. In the literature, many experimental works using knife edge indentors were reported in ship collision research to investigate the characteristics of impact force.

McDermott et al [1974] reported ten test results conducted by the U.S. Steel Research Laboratory, each consisting of the application of a concentrated static lateral load on a 1:5 scale model. Two types of structural components were studied, namely, stiffened plate and flat plate, and the load-indentation curves were shown in Figs. 16 and 17 of the paper [McDermott et al 1974]. Ronalds and Dowling [1986] reported similar experimental work on stiffened plates and shells.

Soreide and Amdahl [1982] studied the behaviour of bracing structure loaded dynamically by a knife edge indenter through a hydraulic machine. The dynamic and static load-indentation curves were compared and an increase in the load was observed as a result of the dynamic effects.

In the experimental work of Samuelides [1984] and Cho [1987], a V-shaped striker was used to hit the structure and to measure the deceleration of the striker during impact using an accelerometer attached to a dummy in order to establish the history of the interactive force between the striker and the model. However, from the recorded results, it was difficult to separate the rigid body acceleration of the striker from the vibrations of the member on which the instrument was mounted.

To overcome the difficulties encountered in the experiments, some researchers propose theoretical methods to calculate the impact force. Mass-spring model is a simple method which was used by Davies [1980] and Ueda et al [1989]. However, the stiffness at the impact point is difficult to estimate, therefore this method must be incorporated with some other method, e.g. Finite Element Method.

The Finite Element approach is a more practical and flexible tool and some computer packages, such as DYNA-3D and AUTODYN, can be used in collision research. However, several months are required to develop the necessary familiarity to run such codes with some feeling of confidence [Zukas,1982]. Moreover, as running time for 3-D codes is still measured in terms of hours and tens of hours, it is not practical for use as a routine tool due to the high cost.

Using Finite Element techniques and a plastic collapse theorem, Chang et al [1980] predicted the impact force of the model test conducted by GKSS in Germany. The correlation between the calculation and experiment is encouraging, but in view of the doubtful character of test data, conclusive validation of Chang's work cannot be expected [Van Mater et al, 1979].

1.2.3.3 Dynamic Effects: When studying dynamic effects two important aspects should be considered: inertia force and strain-rate sensitivity.

(a) Inertia force

As mentioned in 1.2.3.1, all impacts and collisions will involve some dynamic effects which are reflected by the term 'inertia force'. When the collision duration is much longer than the natural period of elastic vibration of the hull plating, the static approach is often used [McDermott et al, 1974]. However, if the duration of impact is less than the natural period of plating, considerable errors can arise, as shown by Jones [1973] for the slamming damage of ships.

(b) Strain-rate sensitivity

Hot-rolled mild steel is sensitive to the strain-rate, which has been shown by much experimental work on dynamic, uni-axial, constant strain-rate tests [Manjoine, 1944, Marsh and Campbell, 1963]. The effect of strain-rate, $\dot{\epsilon}$, on the mild steel dynamic yield stress, σ_d , has been expressed empirically by Cowper and Symonds to be

$$\frac{\sigma_d}{\sigma_s} = 1 + \left(\frac{\dot{\epsilon}}{C} \right)^{\frac{1}{R}} \quad (1.7)$$

with $C=40.4 \text{ S}^{-1}$ and $R=5$ [Symonds, 1965].

The generalised counterpart of Eqn. (1.7) was proposed by Jones [1972] for multi-dimensional stress states as:

$$\frac{\bar{\sigma}_d}{\sigma_s} = 1 + \left(\frac{\dot{\epsilon}_e}{C} \right)^{\frac{1}{R}} \quad (1.8)$$

$$\text{where } \bar{\sigma}_d = \left(\frac{3}{2} s'_{ij} s'_{ij} \right)^{\frac{1}{2}} \text{ and } \dot{\epsilon}_e = \left(\frac{2}{3} \dot{\epsilon}_{ij} \dot{\epsilon}_{ij} \right)^{\frac{1}{2}}$$

but no experimental confirmation was reported for 2-D and 3-D dynamic testing of materials.

Perrone [1965 and 1967] has shown for some simple structures loaded impulsively and made from a strain-rate material that the influence of strain-rate sensitivity on the structural response can be adequately catered for with a time independent yield stress which is evaluated from Eqn. (1.8) for initial strain-rates. This observation was used for impulsively loaded annular plates and shells [Jones, 1968 and 1974]. For arbitrary pulse loading, the elastic/visco-perfectly plastic model was used in which the dynamic yield stress was calculated in terms of Eqn. (1.8) [Samuelides, 1984].

As is known, the strain-rate of real ships in collision is very complicated which is both space- and time- dependent, so it is difficult to estimate the strain-rate magnitudes in structural components. Since the strain-rate effects are significant within a short period of time at some local area in ship collision, they are generally ignored. However, for the problem of ship models, the strain-rate becomes significant because of scale effects. Even for quasi-static processes the strain-rate effect can also be important.

Soreide and Amdahl [1982] and Amdahl [1983] performed a series of static and dynamic tests on tubular members. It was observed for a certain range of impact velocity that the load-indentation curve is raised by about 10% due to dynamic effects, while very little influence is obtained on the opposite side of the cross section. This phenomenon indicates that the dynamic loading primarily affects the local deformation at point of impact, and that the increase in load carrying capacity is caused by a rise in the material stress-strain curve due to strain-rate sensitivity. Since the strain-rate effects

increase the yield stress, the dynamic yield stress is multiplied by a factor to allow for the strain-rate sensitivity of yield stress in struck beams [Parkes, 1958] and in the side shell of a struck tanker [Jones, 1979].

1.2.3.4 Dynamic Failure Mode and 'Critical Speed' of Ship: Menkes and Opat [1973] investigated the failure mode of a fully clamped beam subjected to uniformly distributed impulsive velocity. Three failure modes of metal beam were identified, i.e. large permanent ductile deformation (Mode 1), tensile tearing (Mode 2) and transverse shear failure (Mode 3). Jones made theoretical studies [1971 and 1976] on these failure modes using a rigid-plastic method. The theoretical prediction gave good agreement with the experimental results. Recently Liu and Jones [1987] reported their experimental work on aluminum and steel beams under impact loading. These modes defined by Menkes and Opat for the impulsive-velocity loading of beams remain valid for impact loading. Articles published on the dynamic inelastic failure of beams are summarised by Jones [1988].

The difficulties in the study of structural failure come in two aspects. Firstly, material properties under dynamic loading are generally not available and, secondly, it is extremely difficult to accurately calculate the stress and strain distribution in the structure. Therefore, in most papers dealing with plate the failure criteria are based on the simple philosophy that the rupture will occur when elongation of the side plate exceeds the ultimate strain limit (approximately 30% for mild steel).

Because of the great influence the rupture of the shell will have on the load-deformation pattern and the energy absorption of the hull, it is important to determine this failure condition with some degree of confidence. In the reference [Yu and Jones, 1989] the ABAQUS finite element numerical code was used to calculate the behaviour of a beam which had just cracked in an experimental test [Liu and Jones, 1987] when motion ceased. It was concluded [Yu and Jones, 1989] that a maximum tensile strain criterion

of failure may be suitable for the tensile tearing of an aluminum alloy beam under impact loading. Jones [1989-b], basing on a series of test, proposed a geometric criterion of tearing failure for the locally impacted aluminium beam: $\theta_c = 0.341$ rads, which was only demonstrated for 7.62 mm thick aluminium alloy beams. The crack criterion is dependent on the failure surface which is not clear yet for the material in multi-dimensional stress state. Therefore Embury and LeRoy [1977] concluded that no one failure criterion is expected to remain valid for a wide range of materials and loading states and that it is difficult to select the relevant one for a given problem.

For ship structure the failure modes are concerned with the definition of 'Critical Speed' of the striking vessel. In practice, the critical speed was defined according to the extent of the deformation of side plating or the intrusion of the striking ship's bow. Applying the Minorsky method to the several separate cases of ships, an encounter of 90 degrees has given rise to a relationship between loaded displacement and critical impact speed causing a spill of hazardous cargoes. Various estimates were made for the normal impact speed of a striking vessel to reach the inner hull of large LNG carriers [NMAB, 1980]. Critical state assumed by Kinkead [1983] involves a very large intrusion of rigid striking bow which is sufficient to take the cargo tank up to the point of rupture.

Samuelidies [1984] used a relationship between the deflection and the span as the rupture criterion proposed by Van Mater et al [1980], in which rupture occurs when their ratio is 0.226 corresponding to a strain of 0.1 for a mid-span strike. As an example, the critical speed of a longitudinally framed tanker struck by a rigid vessel of different mass was calculated. The tanker examined is one of those which had been considered for the full scale tests planned by the US Coast Guard [Van Mater et al, 1980]. However, the rupture strain of 0.1 in the critical state can not generally be accepted even for the beam. As discussed above, the stress state for the plate is more complicated than for the beam, so further detailed work should be done on this important topic.

1.2.3.5 Dynamic Inelastic Response of Plate: Rectangular plate is a widely used structural type in ships and other marine vessels, which often suffers from dynamic load, such as slamming, collision and grounding. If the dynamic loads are large enough to cause severe deformation of the plates, then the response of a structure can often be studied with the aid of plasticity theory [Jones, 1972]. Lee and Symonds [1952] were the first to use the rigid, perfectly plastic method to predict the inelastic response of a beam under dynamic loads. In using the rigid plastic method, it is often assumed that elastic effects may be neglected when the dynamic energy is at least three times larger than the maximum elastic strain energy capacity, and that the pulse duration is smaller than the fundamental period of the structure. For rectangular plate, because of the difficulties arising from the complication of the generalised stresses (M_x , M_y , M_{xy}) for infinitesimal deflection and (M_x , M_y , M_{xy} , N_x , N_y , N_{xy}) for finite deflection, the only exact rigid-plastic solution of a flat plate loaded dynamically is the special case of a simply supported square plate subjected to a uniformly distributed dynamic load which produces infinitesimal deflections [Cox and Morland, 1959].

The convenient use of bound theorem attracts many researchers. Martin [1964] derived a theorem for the upper bound to the permanent displacements of a rigid, perfectly plastic continuum which was subjected to an initial impulsive velocity field. A corresponding lower bound displacement theorem has been derived by Morales and Nevill [1970]. As the influence of finite deflections was not accounted for, these theorems over-estimated the actual permanent deflections of axially restrained plates in the case of large deflection.

Since it is almost impossible to obtain the exact solution for the dynamic response of a rectangular plate at finite deflections, several approximate methods have been proposed. The mode approximation technique proposed by Martin and Symonds [1966] was first applied to the beam with infinitesimal deflections, and then to that of finite deflections. In the mode approximation technique the general mode fields of velocity are expressed

as the product of a normalised, vector valued 'shape function', and the scalar velocity amplitude of a point of main interest. The initial velocity field is obtained by minimising the difference between the given initial velocity and the mode solution in a mean square sense. However, this initial velocity field can not account for the distribution of initial velocity over the structure and the continuity of velocities is satisfied only in an average fashion when more than one mode shape is present.

The energy method is another possible approximation approach to the dynamically loaded plates, which is based on the idea that the energy input to a structure is equal to the plastic work done. In determining the initial kinetic energy, the minimising technique in the mode approximation method is used to get the initial velocity of the plate. The plastic work can be determined by integrating the static load deflection curve. The energy method was used by Martin and Ponter [1972] for an impulsive loading case, and by de Oliveira [1981] for impact load due to dropped objects. This method tends to over-estimate the magnitude of the permanent displacement, as discussed by Symonds and Wierzbicki [1979].

An approximate rigid-plastic method, which retains the influence of finite deflections, was developed by Jones [1971] for the dynamic behaviour of arbitrarily shaped plates. This analysis has proved to be quite powerful, and reduces to that presented by Sawczuk [1964] for the influence of finite displacements on the behaviour of rigid perfectly plastic plates loaded statically. The correlation was made with the experimental results [Jones et al 1970] on the impulsively loaded aluminum alloy and steel plates and showed reasonable agreement.

1.3 Aim of the Thesis

Ship collision is a very complex phenomenon and a large number of parameters are

associated with it. The functions of these parameters and some dynamic characteristics of collision have not been clearly understood. In this thesis the side structure of a struck ship is simplified as a fully clamped rectangular plate and the striking vessel as a rigid knife edge indenter. The experimental, numerical and analytical methods are used to study the dynamic inelastic response of the impacted plate in the course of collision. The main purpose in all this work is the use of theoretical modelling, computational techniques and analytical method, backed by experimental verification, to provide an insight into the material and structural behaviour which dominate in the collision. It is hoped that the methods proposed may prove to be a useful tool in gaining a better understanding of ship collision and in providing ship designers with information about the behaviour of impacted ship plates.

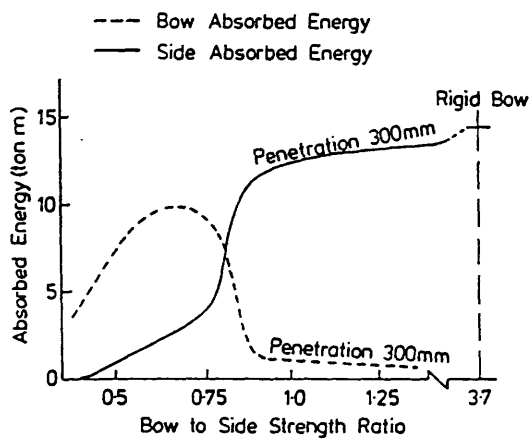


Fig. 1.1 Variation of absorbed energy with ratio of bow to side strength, according to Akita and Kitamura

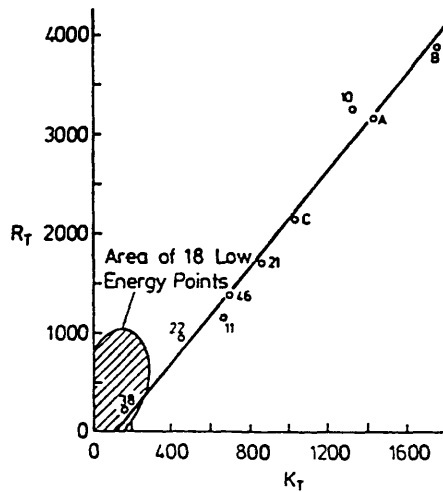


Fig. 1.2 Minorsky's empirical correlation between resistance factor (R_T) and kinetic energy (K_T) absorbed during collision. (Labelled data is from actual ship collisions.
 R_T in ft^2 in and K_T in 1000 ton knot^2)

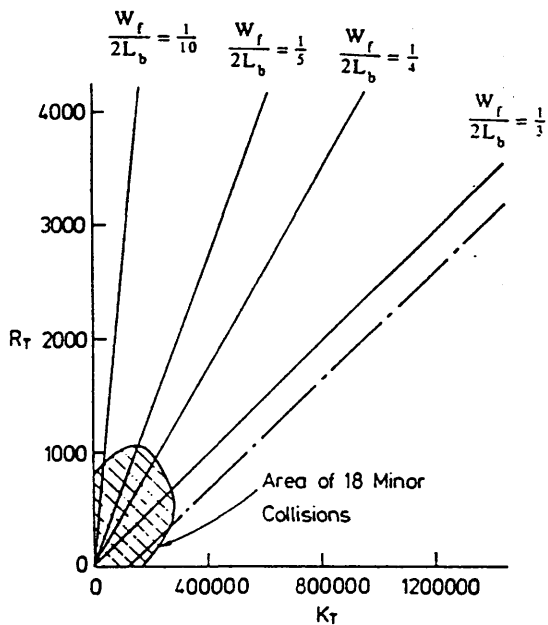


Fig. 1.3 Comparison of the modified Minorsky method (Jones) for various values of $\frac{W_f}{2L_b}$ with Minorsky's empirical relation (R_T in $ft^2 in$ and K_T in $ton\ knot^2$)

CHAPTER TWO

NUMERICAL MODELLING OF DYNAMIC RESPONSE OF PLATES UNDER IMPACT

2.1 Introductory Remarks

The prediction of large dynamic and permanent deformations of structures is important in engineering problems. There are mainly two kinds of analytical methods, i.e. rigid-plastic and energy. The former can be used for simple structural elements to get analytical solutions and is applicable only to problems for which the initial kinetic energy is much larger than the maximum elastic strain energy. Moreover, it can not provide any information about the stress and strain distributions, particularly in the residual state. The latter is based on the idea that the energy input to a structure is equal to the plastic work done. The success of this method depends upon a reasonable estimate of the primary mode of deformation which may occur during the large deformation process. For the large deformation of a complex structure under arbitrary transient loading, it is difficult to use either of these two methods. Their limitation and deficiencies have been overcome by various numerical methods [Jones, 1989-a]. There are a number of Finite Element packages, e.g. ADINA and ABAQUS. There are also some Finite Difference codes. The Variational Finite Difference Method (VFDM) was developed by Ni and Lee [1974] based on a minimum principle in dynamic finite plasticity [Lee and Ni, 1973]. VFDM refers to the procedures in which the finite difference expression, written in terms of grid or nodal values, is directly inserted into the governing variational principle. In this method no continuity requirements are generally enforced on the integration sub-domain boundary, therefore lower-order polynomials can be used in the numerical integrations to reduce the computational

effort. The best VFDM has been observed to converge significantly faster than "conforming" finite element idealisation with a similar number of unknowns or degrees of freedom [Ni, 1982].

In reference [Ni and Lee, 1974] the dynamic behaviour of inelastic cylindrical shells under impulsive loading was investigated. In this chapter the Variational Finite Difference Method is developed to simulate the denting process of a fully clamped rectangular plate subjected to a knife edge impact.

2.2 Minimum Principle

For the problem of large deformations the reference configuration [Fung, 1965] must first be chosen. In this chapter, the initial configuration was used as reference configuration and the formulation is termed Total Formulation.

In the convected curvilinear co-ordinate system $X_i(X^i)$ the Lagrangian strain tensor is defined as:

$$E_{ij} = \frac{1}{2}(U_{j;i} + U_{i;j} + U_{k;i}U^k_{;j}) \quad (2.1)$$

Herein, $()_{;i}$ denotes a covariant derivative of a variable with respect to X_i , and the repetition of an index in a term indicates summation.

For finite deformations, the equation of equilibrium on surface S_T (boundary condition) takes the form

$$T_k = (g_{ki} + U_{k;i})v_j s^{ij} \quad \text{on } S_T \quad (2.2)$$

where g_{ki} is the metric tensor.

It has been shown [Lee and Ni, 1973] that the true acceleration field, $\ddot{U}_k = \frac{D^2 U_k}{Dt^2}$, of the body, which has known or predetermined displacement and velocity fields at time t , is distinguished from all kinematically admissible ones by having the minimum value of the following functional:

$$I = \int_{V_0} s^{ij} \ddot{E}_{ij} d\bar{V}_0 + \frac{1}{2} \int_{V_0} \rho_0 \ddot{U}^k \ddot{U}_k d\bar{V}_0 - \int_{S_T} T^k \ddot{U}_k dS - \int_{V_0} \rho_0 F^k \ddot{U}_k d\bar{V}_0 \quad (2.3)$$

in which ρ_0 is the initial mass density. The minimum principle is valid for continuous as well as sectionally discontinuous acceleration fields.

2.3 Kinematic Relationships

Consider the rectangular Cartesian co-ordinate (X, Y, Z) shown in Fig. 2.1 which lies in the mid-plane of an initially flat plate of length L , width B and thickness H . Let (U_X, U_Y, U_Z) be the corresponding physical components of the displacement vector of a point in the plate, respectively. In order to express the displacement of a particle at any position through the thickness of the plate in terms of the corresponding displacements and their derivatives at the mid-plane, the Kirchhoff assumption is used.

Thus:

$$\begin{aligned} U_X &= U - ZW_{,X} \\ U_Y &= V - ZW_{,Y} \\ U_Z &= W \end{aligned} \quad (2.4)$$

where U, V and W are the displacement components of a point at the mid-span along the X, Y and Z axis, respectively.

The following non-dimensional quantities are introduced to simplify the subsequent computations:

$$\begin{aligned} x &= \frac{X}{L} & y &= \frac{Y}{L} & z &= \frac{Z}{L} \\ u &= \frac{U}{L} & v &= \frac{V}{L} & w &= \frac{W}{L} \\ \tau &= \sqrt{\frac{E}{\rho_0 L^2}} t \end{aligned} \quad (2.5)$$

Taking the covariant derivatives in Eqn. (2.1), we obtain:

$$\begin{aligned} E_{xx} &= \frac{\partial U_x}{\partial X} + \frac{1}{2} \left[\left(\frac{\partial U_x}{\partial X} \right)^2 + \left(\frac{\partial U_y}{\partial X} \right)^2 + \left(\frac{\partial U_z}{\partial X} \right)^2 \right] \\ E_{yy} &= \frac{\partial U_y}{\partial Y} + \frac{1}{2} \left[\left(\frac{\partial U_x}{\partial Y} \right)^2 + \left(\frac{\partial U_y}{\partial Y} \right)^2 + \left(\frac{\partial U_z}{\partial Y} \right)^2 \right] \\ E_{xy} &= \frac{1}{2} \left[\left(\frac{\partial U_x}{\partial Y} \right) + \left(\frac{\partial U_y}{\partial X} \right) + \left(\frac{\partial U_x}{\partial X} \right) \left(\frac{\partial U_x}{\partial Y} \right) + \left(\frac{\partial U_y}{\partial X} \right) \left(\frac{\partial U_y}{\partial Y} \right) + \left(\frac{\partial U_z}{\partial X} \right) \left(\frac{\partial U_z}{\partial Y} \right) \right] \end{aligned} \quad (2.6)$$

Substituting equations (2.4) and (2.5) into (2.6) and taking derivatives of the Lagrangian strain, with respect to the non-dimensional time τ , the dimensionless strain-accelerations are cast in the following form:

$$\begin{aligned} \ddot{E}_{xx} &= \frac{\partial \ddot{u}}{\partial x} - z \frac{\partial^2 \ddot{w}}{\partial x^2} + \left(\frac{\partial \dot{u}}{\partial x} \right)^2 + \frac{\partial u}{\partial x} \frac{\partial \ddot{u}}{\partial x} + \left(\frac{\partial \dot{v}}{\partial x} \right)^2 + \frac{\partial v}{\partial x} \frac{\partial \ddot{v}}{\partial x} + \left(\frac{\partial \dot{w}}{\partial x} \right)^2 + \frac{\partial w}{\partial x} \frac{\partial \ddot{w}}{\partial x} \\ \ddot{E}_{yy} &= \frac{\partial \ddot{v}}{\partial y} - z \frac{\partial^2 \ddot{w}}{\partial y^2} + \left(\frac{\partial \dot{u}}{\partial y} \right)^2 + \frac{\partial u}{\partial y} \frac{\partial \ddot{u}}{\partial y} + \left(\frac{\partial \dot{v}}{\partial y} \right)^2 + \frac{\partial v}{\partial y} \frac{\partial \ddot{v}}{\partial y} + \left(\frac{\partial \dot{w}}{\partial y} \right)^2 + \frac{\partial w}{\partial y} \frac{\partial \ddot{w}}{\partial y} \\ \ddot{E}_{xy} &= \frac{1}{2} \frac{\partial \ddot{u}}{\partial y} + \frac{1}{2} \frac{\partial \ddot{v}}{\partial x} - z \frac{\partial^2 \ddot{w}}{\partial x \partial y} + \frac{1}{2} \frac{\partial \ddot{u}}{\partial x} \frac{\partial u}{\partial y} + \frac{\partial \dot{u}}{\partial x} \frac{\partial \dot{u}}{\partial y} + \frac{1}{2} \frac{\partial u}{\partial x} \frac{\partial \ddot{u}}{\partial y} \\ &+ \frac{1}{2} \frac{\partial \dot{v}}{\partial x} \frac{\partial v}{\partial y} + \frac{\partial \dot{v}}{\partial x} \frac{\partial \dot{v}}{\partial y} + \frac{1}{2} \frac{\partial v}{\partial x} \frac{\partial \ddot{v}}{\partial y} + \frac{1}{2} \frac{\partial \dot{w}}{\partial x} \frac{\partial w}{\partial y} + \frac{\partial \dot{w}}{\partial x} \frac{\partial \dot{w}}{\partial y} + \frac{1}{2} \frac{\partial w}{\partial x} \frac{\partial \ddot{w}}{\partial y} \end{aligned} \quad (2.7)$$

where $(\dot{})$ denotes partial differentiation with respect to non-dimensional time τ .

2.4 Impact Force

Before modelling the impact force, let us first discuss the arbitrarily distributed pressure.

The general relationship between the Lagrangian surface traction T_i at the initial configuration and the pressure p at the deformed configuration can be expressed as

$$T_i dS = p \delta_i^k n_k da \quad (2.8)$$

where dS is the initial area element, da the corresponding area element after deformation, δ_i^k the Kronecker symbol and n_k the covariant unit normal to da . When the deformation is relatively small, the surface traction T_i can be simplified as

$$T_i = p \left(v_i + v_i U_{;k}^k + v_k U_{;i}^k \right) \quad (2.9)$$

where v_i is the covariant unit normal to dS .

For the plate in the rectangular Cartesian coordinate, we have

$$\begin{aligned} T_X &= p \frac{\partial W}{\partial X} \\ T_Y &= p \frac{\partial W}{\partial Y} \\ T_Z &= p \left(1 + \frac{\partial U_X}{\partial X} + \frac{\partial U_Y}{\partial Y} \right) \end{aligned} \quad (2.10)$$

Using the strain-accelerations by Eqn. (2.7) and the traction term in Eqn. (2.10), the functional I in Eqn. (2.3), for the rectangular plate under uniformly distributed

pressure p but no body force, may be specified in the form:

$$\begin{aligned}
 I = & \frac{E^2 L}{\rho_0} \left\{ \int_{v_0} \frac{1}{E} (s_{xx} \ddot{E}_{xx} + 2s_{xy} \ddot{E}_{xy} + s_{yy} \ddot{E}_{yy}) dv_0 \right. \\
 & + \frac{1}{2} \int_{v_0} \left[\left(\ddot{u} - z \frac{\partial \ddot{w}}{\partial x} \right)^2 + \left(\ddot{v} - z \frac{\partial \ddot{w}}{\partial y} \right)^2 + \ddot{w}^2 \right] dv_0 \\
 & - \int_{s_t} \frac{p}{E} \left[\frac{\partial w}{\partial x} \left(\ddot{u} - z \frac{\partial \ddot{w}}{\partial x} \right) + \frac{\partial w}{\partial y} \left(\ddot{v} - z \frac{\partial \ddot{w}}{\partial y} \right) \right. \\
 & \left. + \left(1 + \frac{\partial u}{\partial x} + \frac{\partial v}{\partial y} - z \frac{\partial^2 w}{\partial x^2} - z \frac{\partial^2 w}{\partial y^2} \right) \ddot{w} \right] ds \left. \right\}
 \end{aligned} \tag{2.11}$$

where v_0 and s_t are the non-dimensional volume and area, respectively; s_{xx} , s_{xy} and s_{yy} are the components of the Kirchhoff stress tensor which may be expressed in terms of the displacements and their rates by the constitutive relationships.

The difficulties in modelling the impact force arise from the impact load history being unknown. There is interaction between the striker and struck plate and hence the plate can not be analysed in isolation. To simplify the problem, the following assumptions are adopted

- 1 The striker hits the centre of the plate and with the knife-edge perpendicular to the X-axis (see Fig 2.1).
- 2 The striker keeps contact with the plate at a line during the collision and moves along with the plate until the interactive force decreases to zero.

Applying Newton's laws of motion to the striker

$$F = - m_0 a \tag{2.12}$$

where F is the interactive force ($F=pL_d$), m_0 and a the mass and acceleration of the

striker. At the dent line, we have:

$$\frac{\partial w}{\partial x} = 0 \quad \text{and} \quad \frac{\partial w}{\partial y} = 0 \quad (2.13)$$

Using the contact condition of the striker and the plate, Eqn. (2.11) has the form

$$\begin{aligned} I = & \frac{E^2 L}{\rho_0} \left\{ \int_{v_0} \frac{1}{E} (s_{xx} \ddot{E}_{xx} + 2s_{xy} \ddot{E}_{xy} + s_{yy} \ddot{E}_{yy}) dv_0 \right. \\ & + \frac{1}{2} \int_{v_0} \left[\left(\ddot{u} - z \frac{\partial \ddot{w}}{\partial x} \right)^2 + \left(\ddot{v} - z \frac{\partial \ddot{w}}{\partial y} \right)^2 + \ddot{w}^2 \right] dv_0 \\ & \left. + \int_{l_d} \frac{m_0}{\rho_0 L_d L_d^2} \left(1 + \frac{\partial u}{\partial x} + \frac{\partial v}{\partial y} - z \frac{\partial^2 w}{\partial x^2} - z \frac{\partial^2 w}{\partial y^2} \right) \ddot{w}_d^2 dl \right\} \end{aligned} \quad (2.14)$$

where L_d is the dent length, l_d the non-dimensional dent length and \ddot{w}_d the non-dimensional acceleration of the plate at the dent line.

2.5 Constitutive Relationships

In dealing with the problems of both propagation of stress waves and dynamic response of structures, the vital problem encountered is to find constitutive relations which are not only correct to describe the dynamic behaviour of materials but also convenient for calculation or computation of the dynamic response. The study in this field is carried out at two levels, namely macroscopic experiment and microstructure mechanism analysis. The former gives quite good results for one-dimensional problems but for multi-dimensional problems the experimental investigations become difficult. Microstructure analysis is concerned with irreversible thermodynamics and the dislocation theory of crystals.

A general typical rate-type internal state variable constitutive model may be represented in the form [Perzyna, 1980]:

$$\dot{E}_{ij}^P = F(\sigma_{ij}, Q_t, q) \quad (2.15)$$

This assumes that the macroscopic inelastic strain rate tensor \dot{E}_{ij}^P is a function of the current value of the stress tensor σ_{ij} , the temperature Q_t and the structural parameter q , which is either scalar or tensor representing some kind of average measures of the current material structure, e.g. dislocation density and arrangement. In the problem discussed below, we assume that the deformation process is isothermal and the constitutive equation is independent of strain-rate. The loading (yield) function vanishes:

$$f(s_{ij}, E_{ij}^P, \kappa) = 0 \quad (2.16)$$

where κ is the strain-hardening parameter.

According to Drucker's postulate, the normality of the plastic strain rate vector at a smooth point of the loading surface requires that:

$$\dot{E}_{ij}^P = \Lambda \frac{\partial f}{\partial s_{ij}} \quad (2.17)$$

where Λ is a function which may depend on stress, stress rate, strain and strain history. Assume κ to be a function of E_{ij}^P , then during loading we must have:

$$\dot{f} = \frac{\partial f}{\partial s_{ij}} \dot{s}_{ij} + \frac{\partial f}{\partial E_{ij}^p} \dot{E}_{ij}^p + \frac{\partial f}{\partial \kappa} \frac{\partial \kappa}{\partial E_{ij}^p} \dot{E}_{ij}^p = 0 \quad (2.18)$$

Substituting Eqn. (2.17) into (2.18), we have:

$$\Lambda = \frac{-\frac{\partial f}{\partial s_{ij}} \dot{s}_{ij}}{\left(\frac{\partial f}{\partial E_{ij}^p} + \frac{\partial f}{\partial \kappa} \frac{\partial \kappa}{\partial E_{ij}^p} \right) \frac{\partial f}{\partial s_{ij}}} \quad (2.19)$$

Combining Eqn. (2.17) with (2.19), we obtain

$$\dot{E}_{ij}^p = G \frac{\partial f}{\partial s_{ij}} \frac{\partial f}{\partial s_{kl}} \dot{s}_{kl} \quad (2.20)$$

where:

$$G = \begin{cases} -\frac{1}{\left(\frac{\partial f}{\partial E_{mn}^p} + \frac{\partial f}{\partial \kappa} \frac{\partial \kappa}{\partial E_{mn}^p} \right) \frac{\partial f}{\partial s_{mn}}} & \text{for } f = 0 \text{ and } \frac{\partial f}{\partial s_{ij}} \dot{s}_{ij} > 0 \\ 0 & \text{for } f < 0 \text{ or } \frac{\partial f}{\partial s_{ij}} \dot{s}_{ij} \leq 0 \end{cases} \quad (2.21)$$

For an isotropic hardening material we adopt von Mises yield function which is a reasonable description of the behaviour of certain metal materials. The loading functions are cast in the form:

$$f = J_2 - \kappa = \frac{1}{2} s'_{ij} s'_{ij} - \kappa = 0 \quad (2.22)$$

where J_2 is the second invariant of the stress deviation tensor and s'_{ij} is the Kirchoff stress deviation tensor. From Eqn. (2.22), we have:

$$\left. \begin{aligned} \frac{\partial f}{\partial E^P_{ij}} &= 0 \\ \frac{\partial f}{\partial \kappa} &= -1 \\ \frac{\partial f}{\partial s_{ij}} &= s'_{ij} \end{aligned} \right\} \quad (2.23)$$

$$\frac{\partial \kappa}{\partial E^P_{ij}} = \frac{\partial \kappa}{\partial \bar{\sigma}} \frac{\partial \bar{\sigma}}{\partial w^P} \frac{\partial w^P}{\partial E^P_{ij}} = \frac{\partial \kappa}{\partial \bar{\sigma}} \frac{\partial \bar{\sigma}}{\partial w^P} s_{ij} \quad (2.24)$$

where w^P is plastic work, $dw^P = s_{ij}dE^P_{ij}$, and $\bar{\sigma} = \left(\frac{3}{2}s'_{ij}s'_{ij}\right)^{\frac{1}{2}}$.

For the uniaxial tension, we have:

$$\kappa = \frac{1}{3}\sigma^2 \quad (2.25)$$

Thus:

$$\left. \begin{aligned} \frac{\partial \kappa}{\partial \bar{\sigma}} &= \frac{\partial \kappa}{\partial \sigma} = \frac{2}{3}\sigma \\ \frac{\partial \bar{\sigma}}{\partial w^P} &= \frac{\partial \sigma}{\partial w^P} = \frac{d\sigma}{\sigma dE^P} = \frac{1}{\sigma} \left(\frac{1}{E_t} - \frac{1}{E} \right) \end{aligned} \right\} \quad (2.26)$$

Substituting Eqn. (2.26) into (2.24), we obtain:

$$\frac{\partial \kappa}{\partial E^P_{ij}} = \frac{2}{3}s_{ij} \frac{1}{\left(\frac{1}{E_t} - \frac{1}{E}\right)} \quad (2.27)$$

in which E_t is the tangent modulus which may be obtained from the uniaxial Kirchoff

stress vs Lagrangian strain curves of the material. Substituting Eqns. (2.23) and (2.27) into Eqn. (2.21), G can be determined as follows:

$$G = \begin{cases} \frac{3}{4J_2} \left(\frac{1}{E_t} - \frac{1}{E} \right) & \text{for } f = 0 \text{ and } \frac{\partial f}{\partial s_{ij}} \dot{s}_{ij} > 0 \\ 0 & \text{for } f < 0 \text{ or } \frac{\partial f}{\partial s_{ij}} \dot{s}_{ij} \leq 0 \end{cases} \quad (2.28)$$

The elastic stress-strain relationship obey Hooke's law

$$\dot{E}_{ij}^e = \frac{1}{E} [(1 + \nu) \dot{s}_{ij} - \nu \delta_{ij} \dot{s}_{kk}] \quad (2.29)$$

in which ν is Poisson's ratio and δ_{ij} is the Kronecker symbol. The Lagrangian strain may be expressed as the sum of two parts

$$\dot{E}_{ij} = \dot{E}_{ij}^e + \dot{E}_{ij}^p \quad (2.30)$$

Combining Eqns. (2.20), (2.29) and (2.30), we have:

$$\begin{Bmatrix} \dot{E}_{xx} \\ \dot{E}_{yy} \\ 2\dot{E}_{xy} \end{Bmatrix} = \begin{bmatrix} C_{11} & C_{12} & C_{13} \\ C_{12} & C_{22} & C_{23} \\ C_{13} & C_{23} & C_{33} \end{bmatrix} \begin{Bmatrix} \dot{s}_{xx} \\ \dot{s}_{yy} \\ \dot{s}_{xy} \end{Bmatrix} \quad (2.31)$$

The stress-strain relationship may be explicitly written as

$$\begin{Bmatrix} \dot{s}_{xx} \\ \dot{s}_{yy} \\ \dot{s}_{xy} \end{Bmatrix} = \begin{bmatrix} f_{11} & f_{12} & f_{13} \\ f_{12} & f_{22} & f_{23} \\ f_{13} & f_{23} & f_{33} \end{bmatrix} \begin{Bmatrix} \dot{E}_{xx} \\ \dot{E}_{yy} \\ 2\dot{E}_{xy} \end{Bmatrix} \quad (2.32)$$

where the symmetric matrix of coefficients f_{ij} may be expressed in terms of the inverse of the symmetric matrix C_{ij} as

$$f_{ij} = C_{ij}^{-1} \quad i,j=1,2,3 \quad (2.33)$$

and where

$$\left. \begin{aligned} C_{11} &= \frac{1}{E} + \frac{G}{9}(2s_{xx} - s_{yy})^2 \\ C_{12} &= -\frac{\nu}{E} + \frac{G}{9}(2s_{xx} - s_{yy})^2(2s_{yy} - s_{xx}) \\ C_{13} &= \frac{G}{3}(2s_{xx} - s_{yy})2s_{xy} \\ C_{22} &= \frac{1}{E} + \frac{G}{9}(2s_{yy} - s_{xx})^2 \\ C_{23} &= \frac{G}{3}(2s_{yy} - s_{xx})2s_{xy} \\ C_{33} &= \frac{2(1+\nu)}{E} + 4Gs_{xy} \end{aligned} \right\} \quad (2.34)$$

2.6 Boundary Conditions

For the fully clamped rectangular plate it is required that

$$\left. \begin{aligned} u &= 0 \\ v &= 0, \quad \frac{\partial v}{\partial x} = 0 \\ w &= 0, \quad \frac{\partial w}{\partial x} = 0 \end{aligned} \right\} \quad \text{for } x=0, x=1 \quad (2.35)$$

and

$$\left. \begin{aligned} u &= 0, \quad \frac{\partial u}{\partial y} = 0 \\ v &= 0 \\ w &= 0, \quad \frac{\partial w}{\partial y} = 0 \end{aligned} \right\} \quad \text{for } y=0, y=B/L \quad (2.36)$$

The second-order differential equation requires two boundary conditions for each displacement variable, so we introduce fictitious nodes (Fig. 2.2). When the end ($x=0$) is axially restrained then $u_b=0$. The relationship between the in-plane displacements of the fictitious and internal node $u_{ex} = -u_{in}$ can be added to Eqn. (2.35). Similarly, equation $v_{ex} = -v_{in}$ may be added to Eqn. (2.36).

2.7 Damping Effects

In almost all the results of non-linear dynamic analysis programs, the central deflection oscillates about a certain value with the same magnitude after the elastic recovery, which makes it difficult to select the residual state. In fact, there is a back-and-forth motion of the plate after the separation. However, with the lapse of time, the magnitude of the vibration becomes smaller and smaller due to damping effects. Finally the deflection of the plate tends to be constant, and at this moment the residual state is achieved. In the numerical analysis the damping effects are simulated by adopting resistant pressure over the whole surface of the plate:

$$f_{i,j} = -C_d v_{i,j} \quad (2.37)$$

where $f_{i,j}$ is resistant pressure at plate surface (x_i, y_j) , $v_{i,j}$ the velocity of the plate at (x_i, y_j) and C_d the damping coefficient.

2.8 Variational Finite Difference Method

In the Variational Finite Difference Method (VFDM) the finite difference expression, written in terms of grid or nodal values, is directly inserted into the governing variational principle.

As the first step in the computation, the plate can be discretised as follows:

$$\begin{aligned}
 x_i &= i \Delta x, \quad i=1,2,\dots,m \\
 y_j &= j \Delta y, \quad j=1,2,\dots,n \\
 z_k &= k \Delta z, \quad k=0, \pm 1, \dots, \pm l
 \end{aligned} \tag{2.38}$$

where Δx , Δy and Δz are chosen spacing of co-ordinates x , y and z , respectively. Then every term in functional I (Eqn. (2.14)) is replaced by discrete values through a central finite differences scheme. The functional I may be replaced by a finite summation through using the 'trapezoidal rule' for integration. With the calculus of variations, the expressions for accelerations at every nodal point at any time step, $t^q = q \Delta t$, may be obtained by minimising the functional, I , with respect to the discrete accelerations as

$$\frac{\partial I^q}{\partial \ddot{u}_{i,j}^q} = 0 ; \quad \frac{\partial I^q}{\partial \ddot{v}_{i,j}^q} = 0 ; \quad \frac{\partial I^q}{\partial \ddot{w}_{i,j}^q} = 0 \tag{2.39}$$

We have

$$\begin{aligned}
 \ddot{u}_{i,j} &= C_1 \left[\left(1 + A_{i+1,j}^1\right) (N_{xx})_{i+1,j} - \left(1 + A_{i-1,j}^1\right) (N_{xx})_{i-1,j} \right. \\
 &\quad \left. + A_{i+1,j}^4 (N_{xy})_{i+1,j} - A_{i-1,j}^4 (N_{xy})_{i-1,j} \right] \\
 &\quad + C_2 \left[A_{i,j+1}^4 (N_{yy})_{i,j+1} - A_{i,j-1}^4 (N_{yy})_{i,j-1} \right. \\
 &\quad \left. + \left(1 + A_{i,j+1}^1\right) (N_{xy})_{i,j+1} - \left(1 + A_{i,j-1}^1\right) (N_{xy})_{i,j-1} \right] \\
 &\quad + QA_{i,j}^3
 \end{aligned} \tag{2.40}$$

$$\begin{aligned}
\ddot{v}_{i,j} = & C_1 \left[A_{i+1,j}^2 (N_{xx})_{i+1,j} - A_{i-1,j}^2 (N_{xx})_{i-1,j} \right. \\
& + \left. \left(1 + A_{i+1,j}^5 \right) (N_{xy})_{i+1,j} - \left(1 + A_{i-1,j}^5 \right) (N_{xy})_{i-1,j} \right] \\
& + C_2 \left[\left(1 + A_{i,j+1}^5 \right) (N_{yy})_{i,j+1} - \left(1 + A_{i,j-1}^5 \right) (N_{yy})_{i,j-1} \right. \\
& + \left. A_{i,j+1}^2 (N_{xy})_{i,j+1} - A_{i,j-1}^5 (N_{xy})_{i,j-1} \right] \\
& + QA_{i,j}^6
\end{aligned} \tag{2.41}$$

$$\begin{aligned}
\ddot{w}_{i,j} = & \left\{ C_1 \left[A_{i+1,j}^3 (N_{xx})_{i+1,j} - A_{i-1,j}^3 (N_{xx})_{i-1,j} \right. \right. \\
& + \left. \left. A_{i+1,j}^6 (N_{xy})_{i+1,j} - A_{i-1,j}^6 (N_{xy})_{i-1,j} \right] \right. \\
& + C_3 \left[(M_{xx})_{i-1,j} - 2(M_{xx})_{i,j} + (M_{xx})_{i+1,j} \right] \\
& + C_4 \left[(M_{yy})_{i,j-1} - 2(M_{yy})_{i,j} + (M_{yy})_{i,j+1} \right] \\
& + C_5 \left[(M_{xy})_{i-1,j-1} - (M_{xy})_{i+1,j-1} - (M_{xy})_{i-1,j+1} + (M_{xy})_{i+1,j+1} \right] \\
& + Q \left[1 + C_6 (A_{i-1,j}^3 - A_{i+1,j}^3) + C_7 (A_{i-1,j}^6 - A_{i+1,j}^6) + A_{i,j}^1 + A_{i,j}^5 \right. \\
& + \left. \frac{H}{2L} A_{i,j}^7 + \frac{H}{2L} A_{i,j}^8 \right] \left\{ \left[1 + \frac{m_0}{\rho_0 H L L_d \Delta x} \left(1 + A_{i,j}^1 + A_{i,j}^5 + \frac{H}{2L} A_{i,j}^7 + \frac{H}{2L} A_{i,j}^8 \right) \right]^{-1} \right.
\end{aligned} \tag{2.42}$$

where $i=2, \dots, m-1$; $j=2, \dots, n-1$; C_r ($r=1, 2, \dots, 7$), $A_{i,j}^s$ ($s=1, 2, \dots, 9$), Q ,

$(N_{xx})_{i,j}$, $(N_{yy})_{i,j}$, $(N_{xy})_{i,j}$, $(M_{xx})_{i,j}$, $(M_{yy})_{i,j}$, $(M_{xy})_{i,j}$ are given in

Appendix.

The proposed procedure solves simultaneously the equation governing the structural response of the struck rectangular plate and that of the rigid body response of the striker using a time-marching technique. The solution procedure consists of the following steps:

-
- Step 1 Update strains from known displacements
 - Step 2 Calculate strain increments
 - Step 3 Determine the value of G
 - Step 4 Calculate stress increments
 - Step 5 Update stresses
 - Step 6 Calculate N_{xx} , N_{yy} , N_{xy} , M_{xx} , M_{yy} and M_{xy}
 - Step 7 Calculate accelerations
 - Step 8 Apply displacement boundary conditions
 - Step 9 Update displacements
 - Step 10 Go to Step 1 and repeat.

2.9 Description of Program: IMPACT-I

For the numerical solution of dynamic response of the plate under rigid bow impact, a computer program named IMPACT-I (Fig. 2.3) was written in FORTRAN and mounted on the main frame computer IBM-3090 at Glasgow University.

2.9.1 Input Data

The data needed for execution of the program are listed as follows:

1. Geometric size and material properties of the struck plate
 $L, B, H, \rho, E, E_p, \sigma_s$
2. Mass and initial velocity of the striking bow and length of denting line
 m_0, V_0, L_d
3. Controlling parameters of the program
 $\Delta x, \Delta y, \Delta z, \Delta t$

4. Initial deformation distributions
5. Initial stress distributions

2.9.2 Output of Results

The output generated by the program IMPACT-I is stated below

1. Deformations of the struck plate
 - * The deformation history of the plate centre
 - * The maximum deformation profile
 - * The permanent deformation profile
2. Velocity and acceleration history of the striking bow
3. Interactive impact force history and force-indentation curve
4. Strain of the struck plate
 - * The strain-time history of given points
 - * The maximum strain distribution
 - * The residual strain distribution
5. Stress of the struck plate
 - * The maximum stress distribution
 - * The residual stress distribution
6. Strain-rate history of given point

In output 1,4,5 and 6, the position of point of interest and the amount of output is left to the user to decide.

Using graphic package GHOST-80 the plotting programs were developed which automatically transform the output numerical data into graphic form.

2.10 Check of Numerical Results

To validate this newly developed program which embodies the foregoing theoretical formulations, the iterative time-simulation technique has been checked against two examples. The first example is the dynamic elastic-plastic response of a rectangular plate made of aluminum alloy 6061-T6, loaded impulsively with an initial velocity [Jones et al, 1970]. The target areas of all specimens measured $3 \times 5 \frac{1}{16}$ in². The density of Aluminum alloy is 0.0988 lb/in³. The yield stresses are 41166 psi, 40750 psi and 41450 psi corresponding to the plate thicknesses 0.122 in, 0.188 in and 0.244 in.

Figure 2.4 illustrates the typical predicted central deflection of the plate versus time. For all the 19 cases of aluminum plates listed in Table 2 of Ref.[Jones et al, 1970], Numerical calculations are performed (see Fig. 2.5(a)) and surprisingly good agreement has been found for aluminum material.

As a second example a comparison of numerical prediction and experimental results is shown in Fig. 2.5(b) for 22 hot-rolled mild steel specimens listed in the table 1 of the same paper. As the dynamic yield stress was adopted as static yield stress, the numerical values of W_f/H are a little larger than the experimental ones.

It should be noted that for real elastic-plastic dynamic response of a plate the three different kind of deflections should be distinguished:

W_m - the maximum deflection of plate,

W_r - the deflection corresponding to the maximum elastic recovery, and

W_f - the permanent deflection of plate at which the plate come to rest.

It transpires, from the numerical results, that there are obvious differences for these three deflections defined according to the loading conditions, geometric and physical parameters of the plate. Unfortunately, neither the bound theorem nor rigid perfectly-plastic model can explain the differences among these three deflections. Moreover, for dynamic inelastic response of plate with large deflection, no bound theorem is available and the error in the prediction of rigid perfectly-plastic method becomes large when the elastic effects can not be neglected.

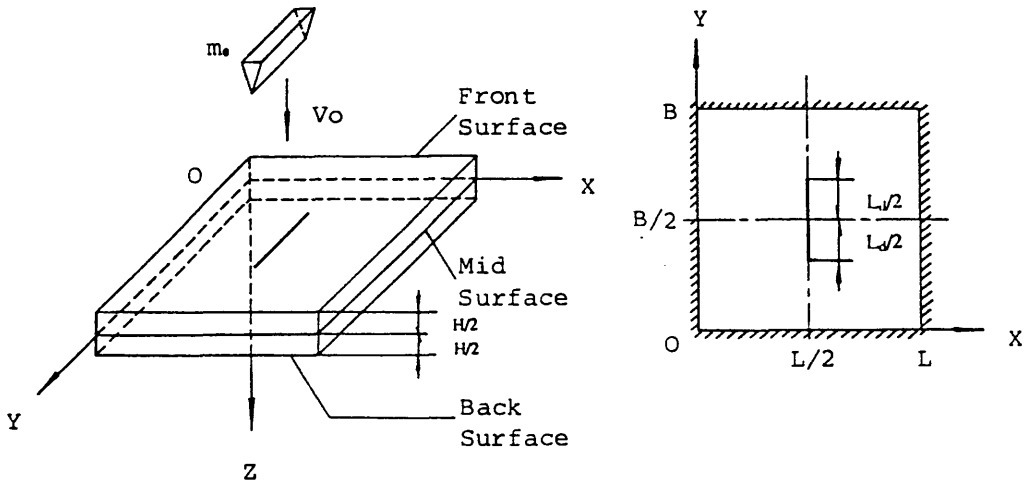


Fig.2.1 Co-ordinate System

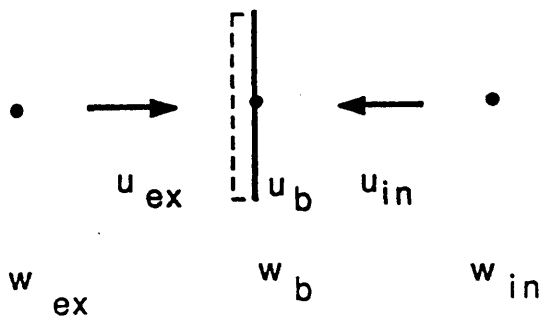


Fig. 2.2 Fictitious nodes

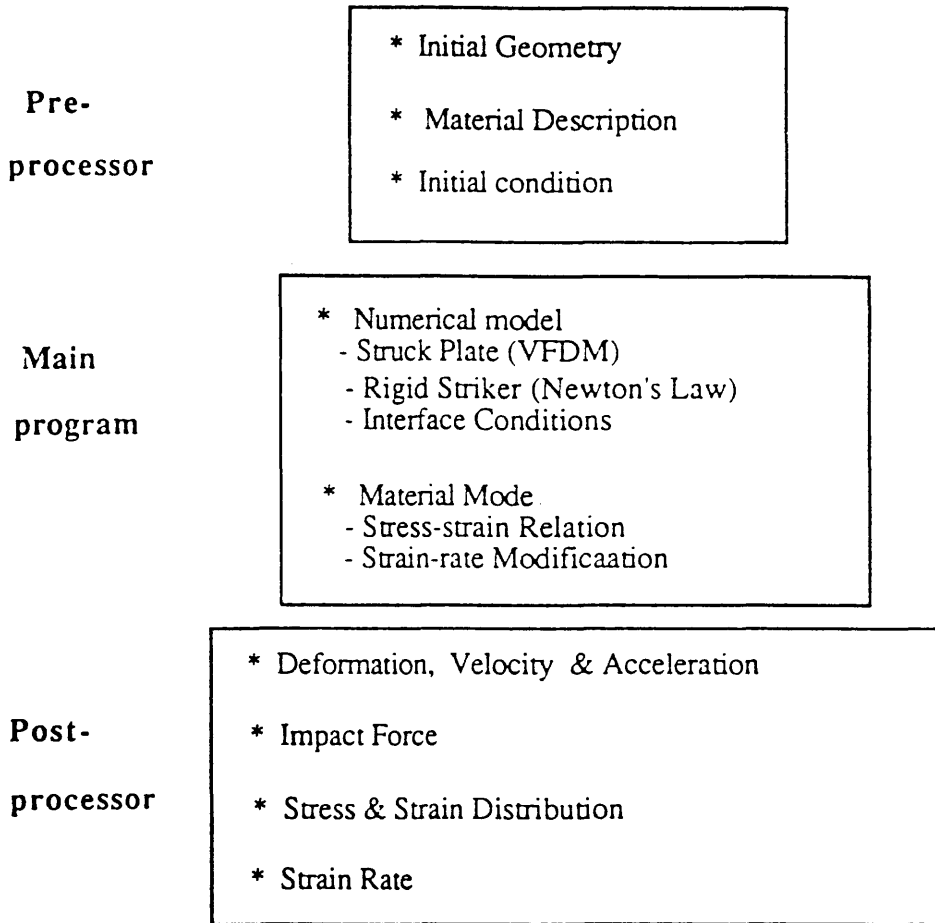


Fig. 2.3 Computational process for IMPACT-I program simulation

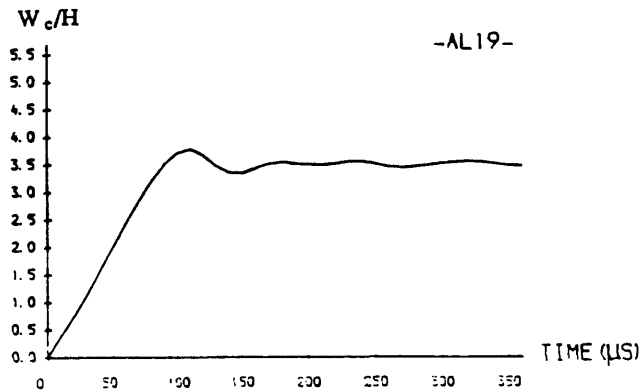
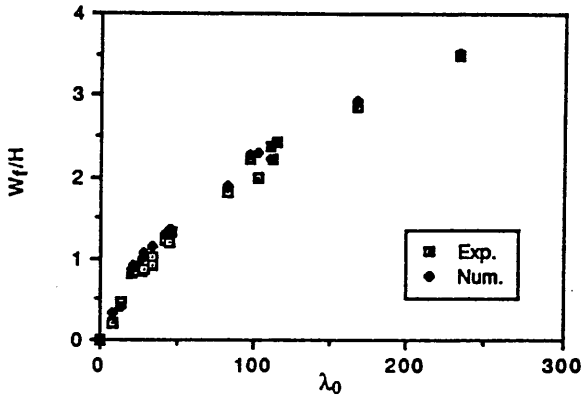
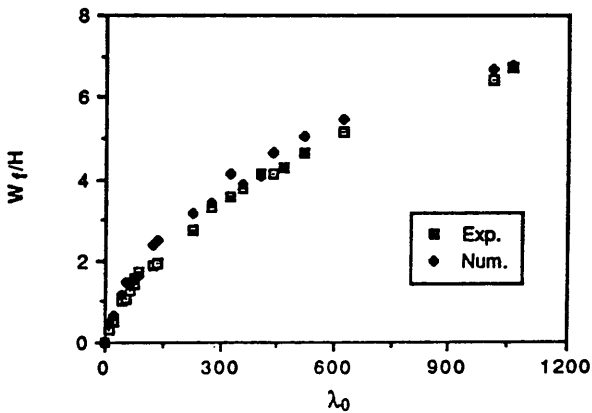


Fig.2.4 Central Deflection-Time History



(a) Aluminium Alloy



(b) Mild Steel

Fig. 2.5 Comparison of numerical predictions and experimental results for aluminium alloy plates and mild steel plates

- Experimental results [Jones, et al 1970]
- Present numerical analysis.

CHAPTER THREE

EXPERIMENTAL PROGRAMME

3.1 Introductory Remarks

The dynamic inelastic behaviour of clamped plates, with finite deflections, impacted transversely by a knife edge indenter at the plate centre, has been examined theoretically by Zhu and Faulkner [1989 and 1990]. It transpires that the membrane force plays an important role in the dynamic response of a plate when the transverse deformations are sufficiently large. High levels of stress and strain develop at the dent line, particularly at the end of the dent line where there are extreme stress and strain concentrations.

It is the objective of the experimental programme to examine the accuracy of the numerical elasto-plastic analysis [Zhu and Faulkner, 1990] and analytical rigid-plastic solution [Zhu, 1989 and 1990], establish their limitations, and explore and identify the various failure modes of impacted plates.

During 1981-1982 an experimental programme on the collision of small scale ship models was conducted in the Department of Naval Architecture and Ocean Engineering, University of Glasgow [Samuelides, 1984]. The experiment consisted of bringing a rigid striker into violent contact with a deformable model. To gain kinetic energy the striker was released from a pre-determined height to run freely along a runway. In the experiment reported in this thesis, the runway was adopted and modified and will be

described in the next section. The struck structural model is a fully clamped rectangular plate which was struck at its centre by a knife edge indenter. The plate was made either from mild steel (0.95 mm and 1.65 mm thick), which is strong strain rate sensitive material, or from a strain-rate insensitive aluminium (1.65 mm thick).

In the test, the width of the plate was 200 mm and the length of the striker was 100 mm. The length of the plate was 150 mm and 250 mm respectively. The impact loading was repeatedly applied to each plate specimen until plate failure. For each impact the initial impact velocity, rebound velocity, and permanent deflections were measured. The acceleration and dynamic strains at four different points (two at front surface and two at back) of the plate were measured for some specimens.

3.2 Experimental Rig

3.2.1 Runway

The runway consisted of a pair of angled rails mounted on a frame (Fig. 3.1). The rails were formed into two straight sections with a curved linking one. One straight section was inclined at 30 degrees and the other was horizontal leading to the struck plate. The upper rails were mounted over the transition section on the frame (see Fig. 3.2), which included a curved and a straight section. The upper rails were built to prevent the severe pitch motion of the striker sliding down along the runway.

3.2.2 Striker

The striker used in this test was similar to the one used by Samuelides [1984]. The

striker was reconstructed under the following two considerations:

- to reduce the severe fluctuation in the measured acceleration curve, and
- to demolish the pitch motion of the striker.

The striker consisted of a box mounted on a plate base with four wheels. A V-shaped 8 mm thick vertical steel wedge was attached to the front of the box. A triangle-sectioned steel prism was welded inside the wedge in which the accelerometer was mounted. The tip of the wedge was sharp and of vertical length 100 mm. The striker was considered to be rigid and after the tests no deformations were found. The mass range of the striker can be varied from 15 kg to 60 kg by changing the mass fixed in the box. By releasing the striker from a different height on the inclined section of the runway the speed of the striker could be varied up to 5.0 ms^{-1} . At the rear of the plate base the "wheel system" was mounted which, together with the upper rails on the runway, prevented the pitch motion of the striker (Fig. 3.2). The transverse movement of the striker was controlled by the "roller system" which was placed at the four corners of the plate base [Samuelides, 1984].

3.2.3 Plate Clamping Device

A fully clamped rectangular plate was chosen for the impact test. The boundary condition allowed no rotation, axial or lateral movement. This configuration was achieved with a clamping device bolted to the front face of two rigid frames which in turn were bolted to the laboratory floor (Fig. 3.1). The clamping device was designed shown in Fig. 3.3, with fixed plate width and aspect ratio of plate L/B ranging from 0.5 to 1.5.

3.3 Plate Specimen

3.3.1 Dimension of Plate

Six types of plate specimen were used in the test, as listed in Table 3.1.

Table 3.1 Dimension of plate specimens

<u>Type No.</u>	<u>Material</u>	<u>Thickness</u> [mm]	<u>Length</u> [mm]	<u>Width</u> [mm]
1	Steel	0.95	150	200
2	Steel	0.95	250	200
3	Steel	1.65	150	200
4	Steel	1.65	250	200
5	Aluminum	1.65	150	200
6	Aluminum	1.65	250	200

3.3.2 Uni-axial Tensile Test

The tensile tests on the mechanical properties of the plate material were performed in the Mechanical Engineering Department laboratory. Four tensile tests were conducted for each thickness of the material, steel and aluminum respectively. The tensile specimens of the same material and thickness as the plate specimens were fabricated in accordance with British Standards. To evaluate the influence of the strain rate on the stress-strain relationship tensile tests were performed both quasi-statically and dynamically.

The specimens were cut from aluminum plate (S.I.C. Half hard, BS.1470) and steel plate (C.R.4, Cold reduced). The densities of the aluminium and steel were 2700 kg/m³ and 7800 kg/m³ respectively. Two standard static tensile tests were conducted for each piece of material at an average strain rate of $9.25 \times 10^{-6} \text{ S}^{-1}$ approximately, and

two dynamic tensile tests were conducted at a strain rate of $1.86 \times 10^{-2} \text{ S}^{-1}$ for each piece of material. Typical uni-axial stress-strain curves for the aluminium and steel are shown in Fig. 3.4. The average yield flow stress was used for steel, while the offset method with 0.2 % strain was used to give the flow stress for the aluminium. The mean values of the material property parameters are listed in Table 3.2.

Table 3.2 Mechanical properties of specimens

<u>Material</u>	<u>Thickness</u> [mm]	<u>Density</u> [kg/m ³]	<u>E</u> [N/mm ²]	<u>Yield stress</u> [N/mm ²]	<u>UTS</u> [N/mm ²]	<u>Rupture strain</u> %
Steel	0.95	7800	207000	143.5	322.5	47.0
Steel	1.65	7800	207000	312.0	580.8	21.0
Aluminium	1.65	2700	51500	103.3	125.4	6.0

Because of the limit on the loading speed of the machine the dynamic tensile test was only conducted at strain rate $1.86 \times 10^{-2} \text{ S}^{-1}$. At this specific strain rate, the experimental yield stress was smaller than the value predicted by Cowper-Symonds formula ($C=40.4$ and $R=5$) by 13.4% for 1.65 mm thick plate and 2.8% for 0.95 mm thick plate.

3.4 Instrumentation and Measurements

During the period of impact the acceleration of the striker and dynamic strains of specimen plates were measured. The signals from the impact tests were processed by high speed instrumentation and recorded on a tape recorder at high speed. The test results were then played back at a slower speed and recorded into the computers and on the chart recorders as required. After analysing the series of preliminary tests it was decided to use Wideband mode with Tchebychev filtering for the impact test.

3.4.1 Recording of Data

The tape recorder used was a Racal Store-7DS. The outputs from the accelerometer and strain gauges were recorded on the tape recorder recording at the highest possible tape speed of 60 inches per second. Replay from the tape recorder was played at a tape speed of 15/16 inches per second. It must be noted that if the system bandwidth is inadequately small the amplitude of spike will be reduced, and its apparent duration increased. The combination selected had a quoted bandwidth of 16 kHz. One consequence of the large bandwidth is the large amount of noise that is superimposed on the required signal. The objective of the experiment is to measure short duration, large amplitude events so some noise is inevitable and must be accepted.

After the data has been recorded it is replayed and recorded into the computer which is to be used to process the information. In this case it is the Laboratory's VAX 11/730 with an AD11-K/AM11-K analogue input system. A limitation of this system is the limited sampling rate of 250 samples per second per channel. Five channels of data are recorded: the accelerometer output and the four strain gauges. Playback was effectively sampled at 16000 samples per second.

To improve the "readability" of test data the analog filters were incorporated to reduce "noise" introduced by the vibrations of the system components and to eliminate high-frequency noise from the computer and other external sources. The filter used has a cut-off frequency of 36Hz at the computer inputs which corresponds to a cut-off frequency of 2300 Hz at the tape recorder's input. A first-order low pass filter was used which rolls off at 3 db per octave above the cut-off frequency. In this test the filters which were positioned between the tape recorder and the computer were used after the original, unfiltered data were saved. In this way the filtered data can be compared with the original data, allowing the effect of the filtering to be easily seen.

For the acceleration curves, filtering significantly reduces the amplitude of the oscillation at an early stage of the impact. However, little influence was observed on the maximum value of the acceleration and whole response time. The measured strain curves were quite smooth and little difference was observed between the original curves and the filtered ones.

3.4.2 Permanent Deflections

The permanent deflection of the plate after impact is measured by using a Linear Vertical Displacement Transducer (LVDT) mounted in a jig. An LVDT and associated instrumentation produces a voltage output proportional to the displacement of the armature of the LVDT. The jig holding the LVDT allows it to be moved anywhere over the surface of the deformed plate, which allows the deflection of the plate to be measured at any point. The position of the measured point can be read from the ruler mounted on the top of the frame. As the LVDT moves along the plate surface the out-of-plane deflections are measured (Fig. 3.5). The LVDT in use has a spring loaded armature to force the measuring tip of the probe into contact with the object to be measured. The measuring tip of the LVDT has a machined hemispherical tip so that contact with the surface to be measured is made at a single point. The output of the LVDT and associated instrumentation is recorded on a conventional pen recorder, the deflection of the trace being proportional to the deflection of the test specimen. The calibration of the system may be readily checked by placing a piece of thin metal shim of known thickness between the measuring tip of the LVDT and the test specimen.

3.4.3 Impact and Rebound Velocity

The impact and rebound velocity of the moving striker is measured by the use of an optical gate system (Fig. 3.6). On one side of the striker there is a light source and on the other side there are two light detectors spaced about 30 mm apart. A projector lamp

with an internal reflector is used as the light source, so that it is virtually a point source of light to minimise errors due to the light sensors having differing switching thresholds. The light detectors and source are arranged so that the moving striker will shadow the two light detectors in turn just before it hits the test specimen. The outputs from the light detectors are processed by some electronic logic and then provided to two independent time units. The first timer unit measures the time delay between the first and second sensor sensing no light. The distance that the striker moves through to cut off the light from the first and second sensors is easily measured and so from the reading on the timer the velocity of the moving striker is readily calculated. A similar process happens when the striker is rebounding from the test specimen, using the second timer unit. It is important to measure the speed of the striker as near to the test specimen as possible to minimise errors due to the significant amount of friction from the track. For impact velocity the light source and detectors were so arranged that the speed of the striker was measured just before the striker touched the plate surface. For rebound velocity measurement the light source and detectors were planted at the same position so that the rebound velocity of the striker was measured a little after it separated from the surface of the plate. This resulted in that the measured rebound velocity was smaller than the real value.

3.4.4 Acceleration

Inside the back of the V-shaped wedge mounted on the box is an accelerometer (see Fig. 3.6) which is used to measure the deceleration of the striker during the impact. The accelerometer used is a piezo-electric type which is characterised by the ability to measure very high accelerations (0.1 g to 8000 g) and the unit has a wide bandwidth suitable for use with impact tests. The measured acceleration has a substantial amount of noise superimposed on it due to mechanical "ringing" caused by the structural components involved. The striker is made as rigid as possible to minimise this effect.

3.4.5 Dynamic Strains

Both sides of the plate were gauged with strain gauges to record the strain history during impact. The position of the gauges was changed between tests. The yield linear gauges were 2 mm and 5 mm in length and were supplied by Showa Measuring Instrument Co. Ltd. The 2 mm gauges were used near the dent line and the boundary of the plate and the 5 mm ones for the quarter-span positions. On the back surface of the plate the strain gauge can be placed at any position, but for front surface the gauge must be kept some distance from the dent line to avoid being cut by the sharp end of the striker. It should be noted that the output from a strain gauge is the mean value of the strain along its active length.

Four single strain gauges were used on each test specimen. Each strain gauge was wired up part of a quarter bridge, using a three wire system to compensate for thermal effects. The bridge completion resistors were placed as close to the gauges as possible to minimise the effects of the longer leads to the instrument electronics. The strain gauge amplifier had a bandwidth (50 kHz) for the tests, made by Fylde Electronics Ltd. and the adhesive used was made by Micro-Measurements Inc. Great care had to be taken during the instrumentation of the gauges to ensure that the adhesive used to attach the strain gauges did not fail during the experiment.

3.4.6 Calibration

3.4.6.1 Impact and rebound velocity: The calibration of the impact and rebound velocity is reasonably simple. The striker was moved slowly through the optical gate by hand and the position where the first timer starts to count was marked. The striker was moved on and the position where the first timer stops counting was marked. This test was repeated a number of times to ensure repeatability of the result and to enable a mean value to be taken. The second timer used the same sensors as the first timer. The timers

used had a resolution to at least $1\mu\text{s}$. The electronic logic and sensors used are intended for high speed counting applications and so the system is more than fast enough for this application.

3.4.6.2 Accelerometer: The accelerometer was the hardest part of the equipment to calibrate. The accelerometer and associated electronics were made by Environmental Equipment Ltd. The equipment was difficult to use because of very little information available and the manufacturer has ceased trading. The unit was calibrated using a shaker table for one acceleration namely, 1 "g" and the results obtained were consistent with the manufacturer's nominal calibration value. However, the acceleration in the test was of the order of around 100 "g" for which there were no calibration facilities.

3.4.6.3 Strain gauges: The gauges used throughout the series of experiments were provided with calibration data about their sensitivity (Gauge Factor). To calibrate the system a bend test specimen was made and a strain gauge bonded to it. This was used to set the amplifiers up so that the system gain on each channel was identical. Therefore, as strain gauges were changed with test specimens, the system sensitivity can be obtained by changing the gauge factor of the gauge in use. It should be noted that the calibration was performed statically for very small deflection, but the real strain measured and set-up range of instrument were much larger than the calibration. It was found in calibration that the scale factor increased with the value of strain. This means that the calibrated strain tends to underestimate the real strain.

3.5 Test Results on First Impact

The experimental records on the first impact of 0.95 mm and 1.65 mm thick steel plates are given in Table 3.3, while the data for the aluminium specimens are presented in Table 3.4. In Table 3.3 and 3.4 L is the plate length perpendicular to the denting line, m_0 is the mass of the striker. V_0 and V_s are the impact velocity and rebound velocity of the striker. W_f is the permanent transverse deformation of a plate centre.

Table 3.3 Experimental records on the first impact of steel plates

<u>No.</u>	<u>L</u> [mm]	<u>H</u> [mm]	<u>m₀</u> [kg]	<u>V₀</u> [m/s]	<u>V_s/V₀</u>	<u>W_{1f}/H</u>	<u>No.of</u> <u>Impacts</u>	<u>Comments</u>
ST01	150	1.65	21.75	1.516	0.511	1.588	2	
ST02	150	1.65	21.80	3.476	X	X	1	
ST03	150	1.65	23.30	2.744	0.367	3.155	17	
ST04	150	0.95	23.30	2.357	0.209	7.152	2	
ST05	250	1.65	23.30	2.788	0.386	3.477	15	
ST06	250	1.65	23.30	3.161	0.371	3.776	4	
ST07	250	0.95	23.30	3.562	0.188	12.138	2	
ST08	250	0.95	23.30	4.266	0.142	14.562	1	necking \$
ST09	250	1.65	33.50	4.154	0.109	5.986	2	
ST10	250	0.95	33.50	4.751	0.000	rupture	1	
ST11	250	0.95	33.50	3.687	0.144	15.830	1	crack \$
ST12	250	0.95	33.50	3.727	0.000	rupture	1	
ST13	250	0.95	33.50	3.227	0.170	13.990	1	
ST14	250	1.65	33.50	3.513	0.231	5.563	2	
ST15	250	0.95	33.50	3.128	0.177	13.920 @	1	
ST16	250	0.95	33.50	4.296	0.113	16.750 @	1	rupture \$
ST17	250	0.95	33.50	3.539	0.154	15.080 @	1	
ST18	250	0.95	33.50	4.874	0.132	16.350 @	1	rupture \$

X - The striker hit the top end first

\$ - At the two ends of the dent line

@ - Free in-plane sliding is allowed at the top and bottom boundaries (see 3.5.5).

Table 3.4 Experimental records on the first impact of aluminium plates

<u>No.</u>	<u>L</u> [mm]	<u>H</u> [mm]	<u>m₀</u> [kg]	<u>V₀</u> [m/s]	<u>V_s/V₀</u>	<u>W_{1f}/H</u>	<u>No.of</u> <u>Impacts</u>	<u>Comments</u>
AL01	150	1.65	23.05	3.268	0.050	rupture	1	
AL02	150	1.65	23.05	2.276	0.238	4.088	2	
AL03	150	1.65	23.30	2.021	0.301	4.741	3	
AL04	150	1.65	23.30	2.313	0.234	5.060	2	
AL05	250	1.65	23.30	2.619	0.240	6.581	1	crack \$
AL06	250	1.65	23.30	2.057	0.274	4.933	2	
AL07	250	1.65	12.80	2.413	0.384	4.819	2	
AL08	250	1.65	12.80	3.234	0.276	6.440	1	crack \$
AL09	250	1.65	12.80	3.000	0.313	5.950	1	
AL10	250	1.65	12.80	1.826	0.464	3.361	5	

\$ - At the two ends of the dent line.

3.5.1 Permanent Deflections

The permanent transverse deflections at the plate centre were summarised in Tables 3.3 and 3.4. Figures 3.7 and 3.8 show the permanent transverse deformation distribution along the symmetry lines of the steel and aluminium plates. It can be seen from Figs. 3.7 and 3.8 that the deformation profile is only a straight line at the denting line. This means that the local bending effects are still significant for the impacted rectangular plates. It is obvious from Figs. 3.7 and 3.8 that along the x-direction the severe local deformation occurs near the denting line, while along the y-direction the local plastic deformation is more severe at the end of the denting line.

The fact that the plate has almost a constant transverse deformation along the dent line justifies the assumption in the numerical approach that the striker keeps contact with the

plate at a line during the collision and moves along with the plate until the interactive force decreases to zero. It should be noted that the drop rig can simulate the ship collision only when the amplitude of the acceleration of the plate is much larger than gravity g . Moreover, in the drop rig the plate actually sustains repeated impact [Liu and Jones, 1988]. Even though the rebound does not affect the maximum deformation of the impacted plate, it influences the permanent deformation of the plate, especially for large mass of the striker.

Figure 3.9 gives all the first impact test results in which the variation of dimensionless maximum permanent deflection W_f/H with either dimensional absorbed energy E_s or dimensionless external dynamic energy λ is presented. It can be seen that if the dynamic energy parameter chosen is dimensional (E_s), the $W_f/H - E_s$ curves for different material and thickness are different (Fig. 3.9(a)), but for dimensionless parameter λ , the $W_f/H - \lambda$ relationship yields an approximately identical curve, as shown in Fig. 3.9(b).

To evaluate the effect of strain-rate sensitivity, the permanent deflection of 1.5 mm thick aluminium and steel plates are plotted against the dimensionless parameter λ in Fig. 3.10(a) in which the plate is 250 mm long but with different impact mass. It is obvious from Fig. 3.10(a) that the points for aluminium plates lie a little above those for steel due to the strain-rate sensitivity. However, if the dynamic yield stress is introduced above two sets of data will coincide (Fig. 3.10(b)).

3.5.2 Acceleration

It is well-known that it is difficult to perform data evaluation for dynamic tests. Two extraneous physical phenomena which influence the data are inertial loads and harmonic oscillations [Cheresh, 1987]. These dynamic effects are particular to the test setup and

may obscure the actual response. To obtain reliable response data free of these effects it is necessary to have a thorough understanding of the physical process involved in the impact testing.

The inertial load is known as the load required to accelerate the specimen plate from zero velocity up to the velocity of the striker. Inertial loads are most often characterised by a sharp peak followed by a decaying oscillation at the beginning of the response curve. The harmonic oscillations are caused by vibration arising from the system components (striker, specimen and clamping device) which react to the impact by oscillating at their natural frequencies. The oscillations are reflected in the instrumentation.

Even though these two effects arising from different sources, both amplitudes are proportional to the impact velocity and they act simultaneously.

Figures 3.11 - 3.14 give the measured acceleration curves. The aluminium material specimens AL03 and AL04 have approximately the same impact velocity so that the maximum value and response time are nearly the same, which shows the good repeatability of the test (see Figs. 3.11 and 3.12).

In Figs 3.13 and 3.14 the steel plates ST01 and ST03 have the same experimental condition except that the velocity of case ST03 is larger than that of ST01. It was found that larger fluctuation exists at the beginning of the acceleration curve of ST03 caused by the higher inertial load.

It can be concluded from the acceleration records that during the impact the impact force on the plate increases steadily from zero value to the maximum and then declines a little more quickly to zero. According to numerical analysis [Zhu and Faulkner, 1989] and correlation between acceleration and dynamic strains, the time for the plate to reach its

maximum deflection is approximately the time when acceleration has its maximum value. The time for maximum deformation can therefore be obtained from the acceleration measurement. After the plate reaches the maximum deflection it will bounce back and when the impact force decreases to zero the striker will separate from the plate. The separation time is the period of the impact process.

3.5.3 Dynamic Strains

During the test the x-strain time histories at different points of the plate were recorded on steel and aluminium plate specimens. Because of the limitation on the length of the strain gauges it is difficult to measure the strains near the denting line where extreme strain concentrations exist.

The strains of the aluminium plate AL04 at the quarter span of the central line are shown in Fig.3.15. It was found that the strains were tensile on both the front and back surfaces of the plate throughout the entire response, and the value of strains on the front surface were larger than those on the back surface. A small strain pulse was observed at the beginning of the impact on the strain curves for both surfaces of the plate, being positive for the front surface and negative for the back. The response time obtained from the strain curves is the same as that for the corresponding acceleration record (see Fig. 3.12).

Similar strain curves were obtained (Fig. 3.16) on the same position of the steel plate specimen ST01, but the residual strain on the back surface was compressive because the maximum permanent deformation was not large enough ($W_f/H=1.588$).

The strains at the centre of the steel plate ST01 are given in Fig. 3.17. It appears that there were some differences on the shape of the strain curves for the front and back

surface. In fact, the strains on the back surface show a small delay to response. Nevertheless, the values of the strains on the back surface were larger than those on the front, in contrast to the quarter-span point (see Figs 3.15 and 3.16).

The strains at the support, as shown in Fig. 3.18, show that the gauge on the back surface was compressed, while that on the front surface was tensile and the amplitude of the tensile strain was four times as large as that of the compressed one. It is worth pointing out that the strain at the support of the flat end is smaller than that of the enlarged end [Yu and Jones, 1989] on the front surface of the plate. However, in this test all the plate specimens were flat-ended because the span/thickness ratio is very large and therefore the difference between support of flat end and of enlarged end is not significant.

3.5.4 Failure Mode on First Impact

Menkes and Opat [1973] investigated the failure mode of a fully clamped beam subjected to uniformly distributed impulsive velocity. Three failure modes of the metal beam were identified, i.e. large permanent ductile deformation (Mode 1), tensile tearing (Mode 2) and transverse shear failure (Mode 3). These concepts on failure are also important for the study of plate failure.

Figure 3.19 presents the strains at four points of the aluminium plate (AL01) during the impact process. In the test, strain gauge No.1 was cut by the sharp end of the striker and gauges No.3 and 4 peeled off from the plate due to the failure of the adhesive at large dynamic strains. The broken plate is shown in Fig. 3.20.

Observations on the broken plate in Fig. 3.20 and study on the strain history of gauge No.2 in Fig. 3.19-1 makes it possible to analyse the failure process of plate AL01

struck by the striker at an initial velocity of 3.27 m/s. When the plate was hit by the striker, both transverse shear and bending effects were present at the end of dent line. When the deflection at the end of the dent line was about 7 times the plate thickness ($t=4.76$ ms), the denting went through the plate thickness at this point because of the large transverse shear force, which was reflected as a reduction in the strain curve of point No. 2 (Fig. 3.19-1). The plate then developed tearing from this point along the line perpendicular to the dent line and meanwhile the plate deformed further. At the time of 11.78 ms the plate ruptured along the dent line due to tensile tearing and the striker penetrated the plate. The striker's velocity decreased to zero at the time of 16.8 ms after which it bounced back. Finally the striker separated from the plate and the whole process is approximately 27.73 ms.

In the test a general failure mode was large ductile deformation, e.g. the plate specimens AL02, AL03, AL04 and AL06. When the impact velocity was increased the plate was dented through the thickness at two ends of the dent line.

For aluminium plate AL05 of length 250 mm, under impact velocity 2.619 m/s, cracks just occurred at the two ends of the dent line due to large tensile strain. This denting did not go through the whole plate thickness. In the uni-axial tension test, contraction of the specimen happens when it is stretched near breaking point. This phenomenon is referred to as "necking". It was interesting to find that the phenomenon of "necking" happened along the dent line and the plate was about to rupture (Fig. 3.21).

For steel plate ST10 of length 250 mm, under the impact mass 33.7 kg and velocity 4.751 m/s, it was observed that the failure mode was exactly the same as described above for the aluminium plate AL01. When the impact velocity was reduced to 3.687 m/s (ST11), no denting through the thickness occurred. Instead, there were small cracks at the two ends of the dent line due to tensile strain. In other words, the steel plate specimen ST11 had the same failure mode as that of specimen AL05.

In short, the failure process of the plate can be classified as four stages:

1st stage: The behaviour of the plate consisted of bending, membrane stretching and transverse shearing at the end of the dent line.

2nd stage: This stage began either when the denting went through the plate thickness at the end of the dent line or when the plate cracked due to the large tensile strain at the end of the dent line. Large ductile deformation developed along the dent line and meanwhile the tearing occurred from the end of the dent line in the direction perpendicular to the dent line.

3rd stage: This stage started when the plate ruptured along the dent line. The tearing process continued and severe bending deformation existed near the dent area until the striker ceased to move forward.

4th stage: The plate bounced back along with the striker until the striker separated from the plate.

It should be noted that at the end of the dent line there are two possibilities of failure at the beginning of the 2nd stage. One is denting through caused by transverse shearing and another is cracking caused by large in-plane tension. This is determined by the intensity of the impact (impact mass and velocity) and the relative strength of shear and tension of the plate. If the plate keeps intact during the impact only the 1st and 4th stages are involved. The plate reaches its maximum deflection and bounces back at the beginning of the 4th stage. In this case the dynamic inelastic response of the impacted plate can well be studied by the numerical program developed in chapter 2.

3.5.5 The Influence of Boundary Conditions

Tests with four specimen plates were conducted to investigate the influence of boundary

conditions in which the free in-plane sliding along the top and bottom bounds of the plate was allowed.

It was seen that there was a slight in-plane sliding along the top and bottom bounds of the plate and the maximum deflection was a little larger than that of a fully clamped plate (see Fig. 3.9). The permanent deformation profiles of plate ST17 along the symmetry lines are shown in Fig. 3.22. It was noted that near the end of the dent line the slope of the deformation curve in y-direction (Fig. 3.22(b)) was smaller than that for the fully clamped plate ST08 (see Fig. 3.7(b)), while in the x-direction little difference was seen between Fig. 3.22(a) and Fig. 3.7(a).

It must be pointed out that the above changes in the boundary conditions had significant effect on the failure mode of the plate. Under the same experimental condition the fully clamped plate (ST12) was dented through at the end of the dent line and ruptured along the whole dent line at the impact velocity of 3.73 m/s; but at the impact velocity 4.87 m/s cracks occurred only at the end of the dent line due to large bi-axial tension for the plate (ST18) which allowed free in-plane sliding at two boundaries (Fig. 3.23).

For all four plates a wrinkling phenomenon was observed at the edge area right over and under the dent line (see Fig. 3.23).

3.6 TEST RESULTS ON REPEATED IMPACTS

The experimental data recorded on the flat steel and aluminium plates are presented in Table 3.5, and will be presented in detail in 3.6.1-3. The test results for more than two impacts are reported in 3.6.4.

Table 3.5 Experimental records on the second impact of aluminium and steel plates

No.	L [mm]	H [mm]	m ₀ [kg]	V ₂₀ [m/s]	V _{2s} /V ₂₀	W _{2f} /H	(W _{2f} -W _{1f})/W _{1f} [%]	Comments
AL02	150	1.65	23.05	1.165	0.293	rupture		
AL03	150	1.65	23.30	1.959 *	0.245	4.814	1.54	off centre
AL04	150	1.65	23.30	2.313 *	0.128	rupture		
AL06	250	1.65	23.30	2.045 *	0.000	7.263	47.23	rupture \$
AL07	250	1.65	12.80	2.528 *	0.370	6.488	34.63	
AL10	250	1.65	12.80	1.802 *	0.470	44.850	44.30	
ST01	150	1.65	21.75	2.164	F	2.586	22.23	
ST03	150	1.65	23.30	2.661 *	0.412	3.672	16.39	
ST04	150	0.95	23.30	1.667	0.319	7.904	10.51	off centre
ST05	250	1.65	23.30	2.785 *	0.442	4.559	31.12	
ST06	250	1.65	23.30	3.232 *	0.417	4.509	31.09	
ST07	250	0.95	23.30	3.320	0.200	16.250	33.88	
ST09	250	1.65	33.50	3.630	0.268	7.655	27.88	off centre
ST14	250	1.65	33.50	3.656	0.230	7.225	29.88	

F - Failure on instrument.

\$ - At the two ends of the dent line.

* - The 1st and 2nd impacts have approximately the same impact velocity

$$\left| \frac{V_{10} - V_{20}}{V_{10}} \right| \leq 0.05$$

3.6.1 Permanent Deflections

Comparison of permanent deflections for the first and second impact is shown in Fig. 3.24 for aluminium plate (AL06), and Fig. 3.25 for steel plate (ST07). The aluminium plate AL06 just cracked at two ends of the denting line in the second impact.

Figure 3.24 shows that significant increase on the permanent deformation occurs on the aluminium plate near the impacted area for the second impact, but the area near the support remains as it was. On the other hand, for the steel plate with large deflection

after the first impact ($W_f/H=12.14$), the second impact causes further deformation throughout the whole plate and again the increase of the deformation near the impacted area is most significant (Fig. 3.25).

Under two identical impacts, the values of $(W_{2f}-W_{1f})/W_{1f}$ for aluminium and steel plate are 47.23% and 33.88% for the two cases listed above. From Table 3.5 it can be seen that for the second impact, when the striker hits the plate at a different position nearby the first dent line, the value of $(W_{2f}-W_{1f})/W_{1f}$ is only 1.54% for AL03. Therefore, it is safer to impact the plate at a different position.

3.6.2 Acceleration

Figure 3.26 shows the typical acceleration curves for steel plate specimen AL03 under two identical impacts. It is obvious that the amplitude of acceleration on the second impact is larger than the first, but the overall response time is shorter than the first one. Moreover, the acceleration on the second impact increases more quickly than that on the first impact to reach the maximum value as expected [Zhu, 1990].

3.6.3 Dynamic Strains

To get details of the structural response under repeated impacts, the strain histories of plate ST01 were measured for the first two impacts. The overall accelerations and strains are plotted in Fig. 3.27.

It is shown in Fig. 3.27(b) that near the centre of the plate the maximum tensile strain and residual strain on the back surface increase in the second impact, but decrease on the front surface. Strictly speaking, the strain at the centre of the plate on the front surface is compressive for both impacts [Zhu and Faulkner, 1989]. However, to avoid

being hit by the sharp end of the striker, the strain gauges attached to the front surface of the plate were a little off the plate centre. Thus, it is hardly possible to obtain the strain at the very centre of the plate in the test especially as the strain gradient is high. It can also be seen from Fig. 3.27(b) that, during the whole process of the two impacts, the strain on the back surface was larger than that on the front surface except for the beginning of each impact.

Figure 3.27(c) shows the strain histories at the quarter span of the central line. For both impacts the strain on the front surface was larger than on the back surface. The maximum tensile strain on both surfaces increases in the second impact. The residual strain on the front surface is tensile but compressive on the back surface. The strain difference on the two surfaces implies that the bending effect is still significant and, in the circumstances, the response of the plate is not dominated by membrane behaviour.

3.6.4 Response of Plate under More than Two Impacts

The rigid perfectly plastic analysis [Zhu, 1990] indicates that the plastic deformations are accumulated in repeated identical impacts and no pseudo-shakedown occurs. To confirm this conclusion, experimental work was carried out on the steel plate (ST03) of length 150 mm, width 200 mm and thickness 1.65 mm. The dent line was 100 mm and impact velocity was 2.66 m/s. In the case ST03, the same striker of mass 23.3 kg hit the plate repeatedly up to 17 times when the plate had just cracked at the end of the dent line in the test. During each impact the acceleration, impact velocity and rebound velocity of the striker were measured and after each impact the maximum permanent deflection of the plate was measured. The experimental results for case ST03 are shown in Fig. 3.28. As predicted by the rigid perfectly plastic analysis [Zhu, 1990], no pseudo-shakedown phenomenon was observed in the test (Fig. 3.28(a)). The response time becomes smaller as the number of impacts increases (Fig. 3.28(c)). Due to difficulties in the instrumentation of the dynamic test there are fluctuations in the

curves of rebound velocity (Fig. 3.28(b)) and maximum acceleration (Fig. 3.28(d)). The energy absorbed by the plate in each impact and the variation of maximum permanent deflection with the absorbed energy are shown in Figs. 3.28 (e) and (f) respectively.

A similar test on steel plate ST05 was conducted, which is of length 250 mm, width 200 mm and thickness 1.65 mm. The denting line is 100 mm. The plate was repeatedly impacted up to 15 times by the striker of mass 23.3 kg at 2.79 m/s velocity and experimental results are shown in Fig. 3.29.

As the strength of the aluminium plate specimens is not large enough to sustain more than two impacts, most aluminium plates fail at the second or third impact.

3.6.5 Failure Mode on Repeated Impacts

The failure mode of a plate under repeated impact was also investigated in the test. Figure 3.30 shows the measurement of acceleration and strains on the aluminium plate AL04 under second impact, in which the plate was broken. It can be seen from the broken plate and Fig. 3.30(b) that the four stages of the failure process described in 3.5.4 can be applied to this plate specimen under second impact. The time needed for each stage is as follows:

1st stage: 0.00 - 2.25 ms (7.79% t_d),

2nd stage: 2.25 - 7.32 ms (17.56% t_d),

3rd stage: 7.32 - 19.61 ms (42.57% t_d),

4th stage: 19.61 - 28.87 ms (32.07% t_d).

where t_d is the total time of impact (28.87 ms).

At the beginning of the 2nd stage, the plate was dented through the thickness at the end of the dent line. The period of time spent in the 1st stage is about half that of the plate AL01 in the first impact (see Fig. 3.19-1), even though the impact velocity for plate AL01 is larger than for AL04. The reason is that during the first impact plate AL04 had denting in the direction of thickness which reduced the effective thickness of the plate at the ends of the dent line.

Analogue to the discussion in 3.5.4, the denting through plate thickness does not always occur. The crack caused by large tensile strain might occur rather than denting through, particularly for the case in which the impact velocity is not very large but the number of repeated impacts is large, e.g. for plate ST03.

Figure 3.31 presents a comparison between single impact (AL08) and 5 repeated impacts (AL10) on the deflection-energy relationship. The aluminium specimen (AL08) impacted by the striker at 3.234 m/s with the absorbed energy being 61.83 J, and just cracked at two ends of the dent line. The central permanent deflection is 6.44 H. For aluminium plate (AL10), the striker hit the plate 5 times at an average velocity of 1.825 m/s and significant cracks were observed at two ends of the dent line. After the 4th impact, no crack occurred for the total absorbed energy of 65.98 J. This means that more energy is needed for repeated impact to reach the failure point of the plate. However, the repeatedly impacted plate cracked at the end of the dent line with nearly the same deflection 6.44 H as that under single impact.

It is worth mentioning that it is more reliable and accurate to monitor the failure process by means of strain gauge than by accelerometer.

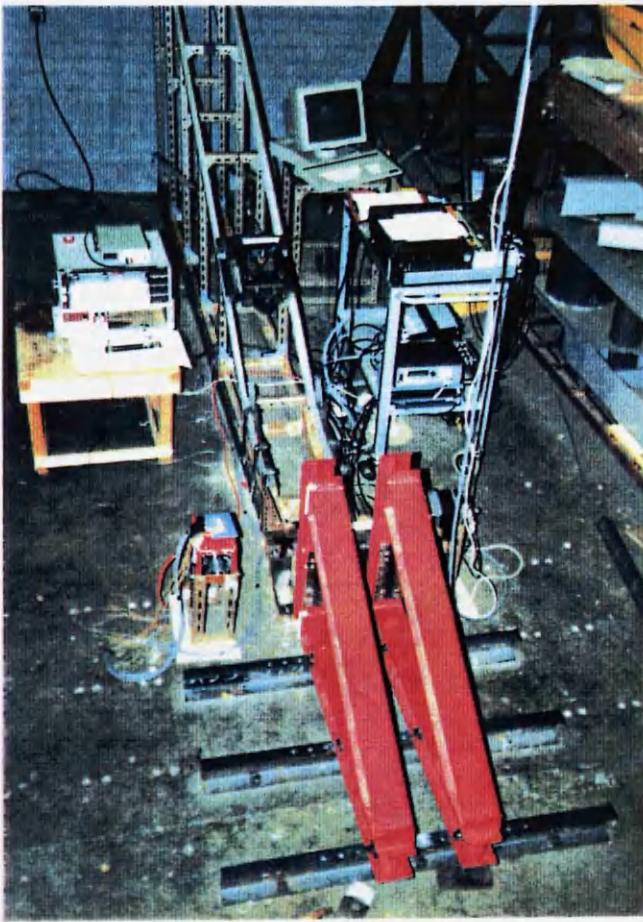


Fig. 3.1 The experimental setup

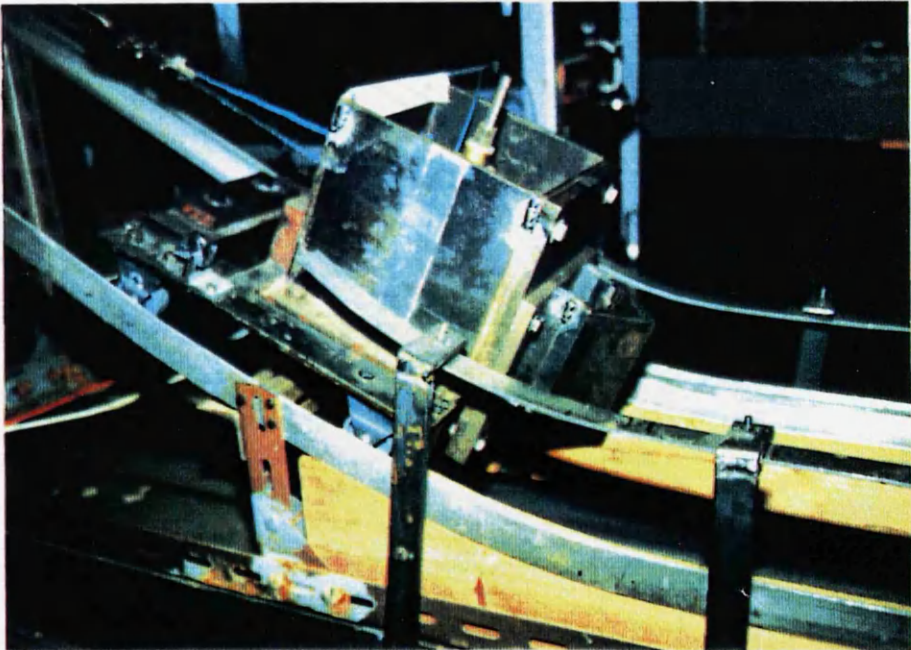


Fig. 3.2 The upper rails and "wheel system"

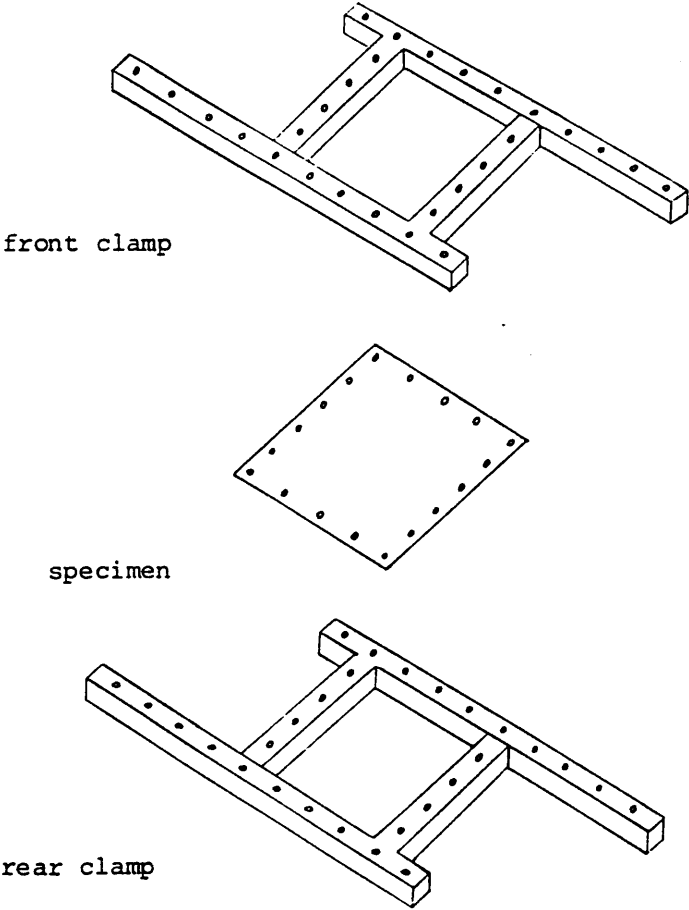
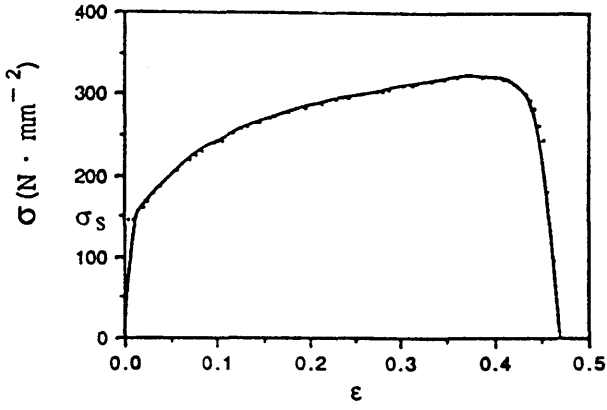
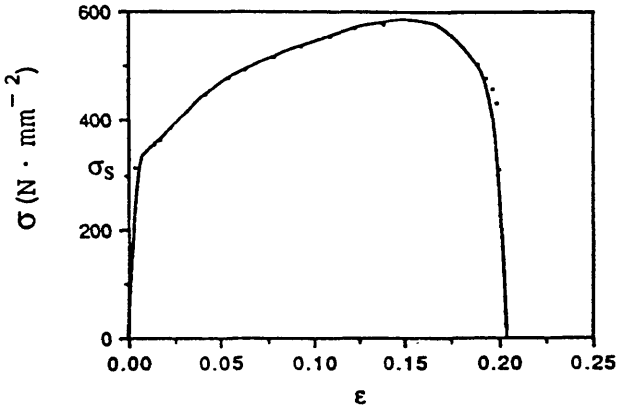


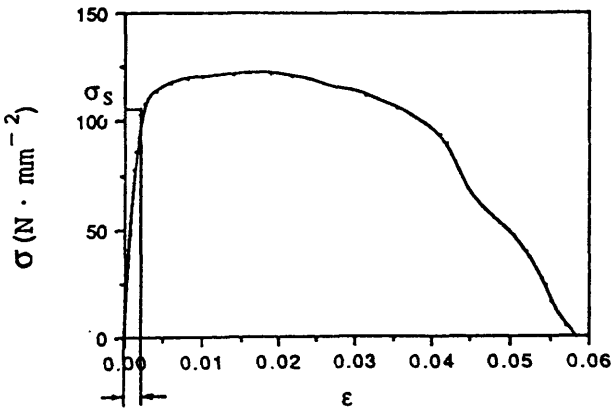
Fig. 3.3 The clamping device



(a) Steel (0.95 mm thick)



(b) Steel (1.65 mm thick)



(c) Aluminium (1.65 mm thick)

Fig. 3.4 True stress-strain curves

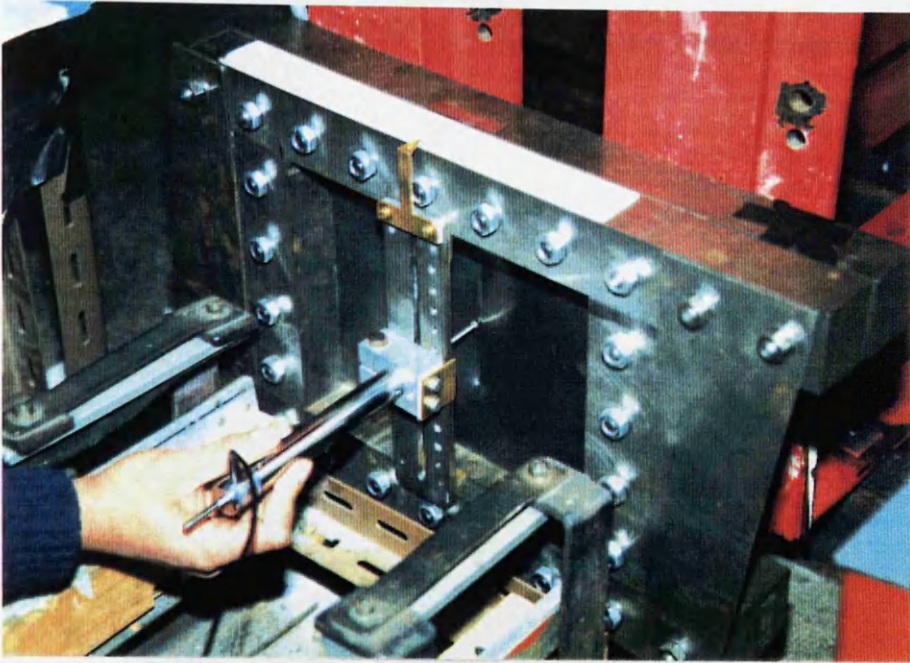


Fig. 3.5 The permanent deflection measurement

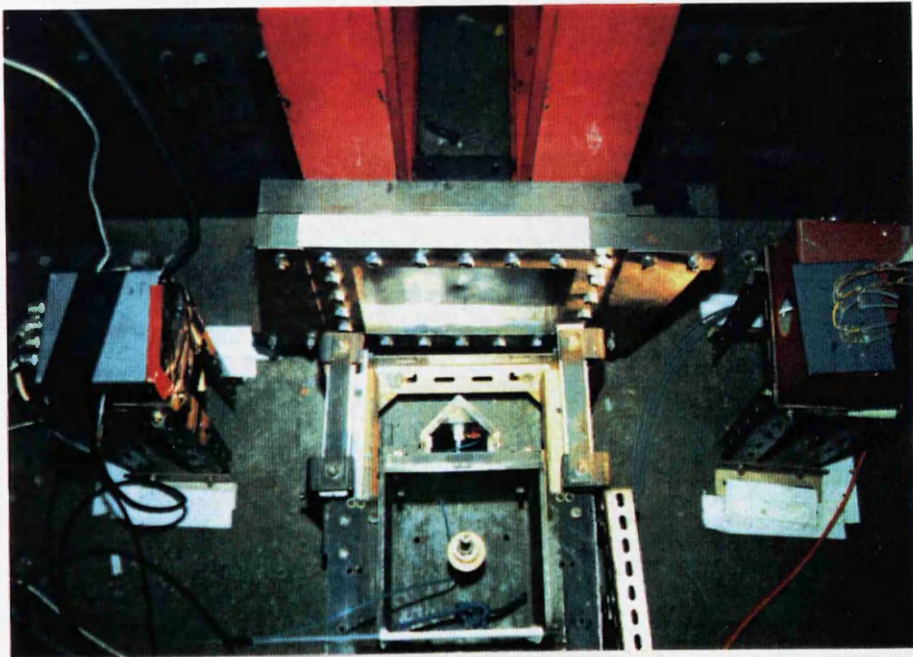


Fig. 3.6 Impact and rebound velocity measurement

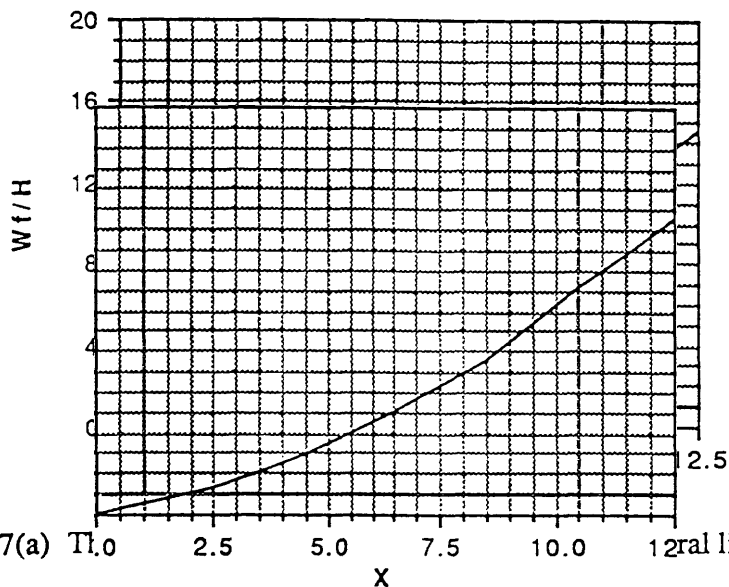


Fig. 3.7(a) Dental line(-ST08-)

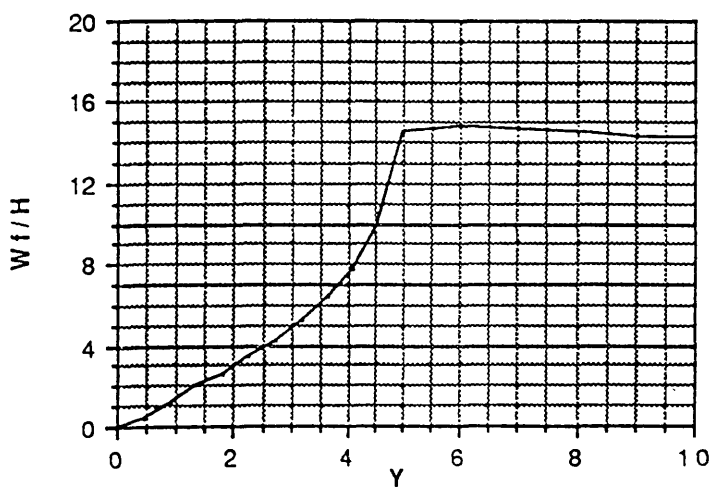


Fig. 3.7(b) The permanent deformation profile along the denting line(-ST08-)

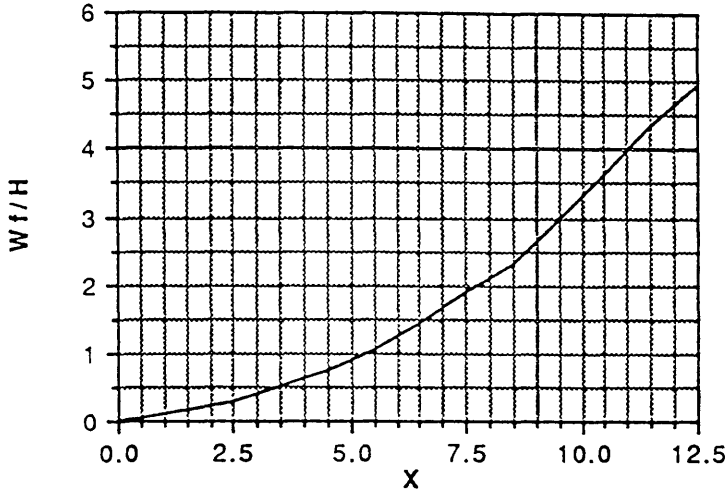


Fig. 3.8(a) The permanent deformation profile along the central line (-AL06-)

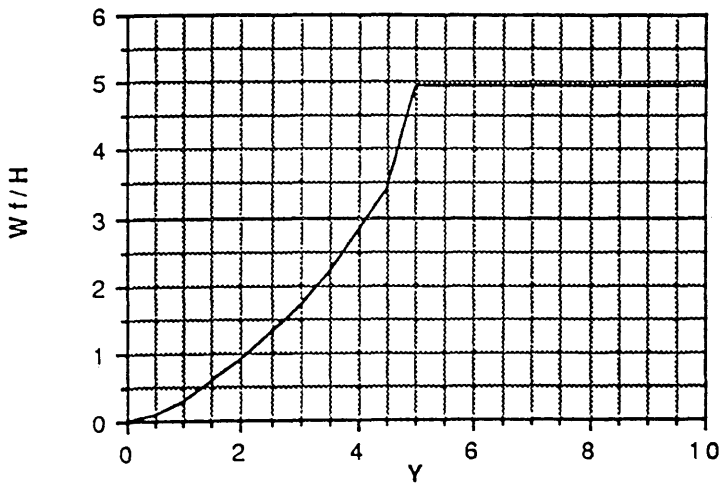
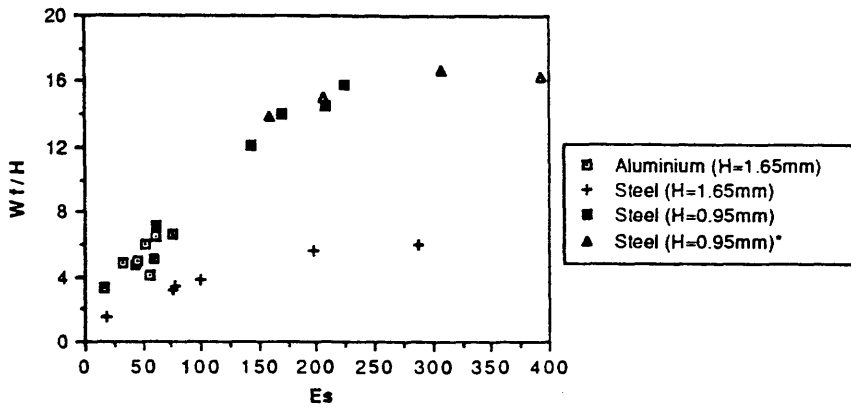
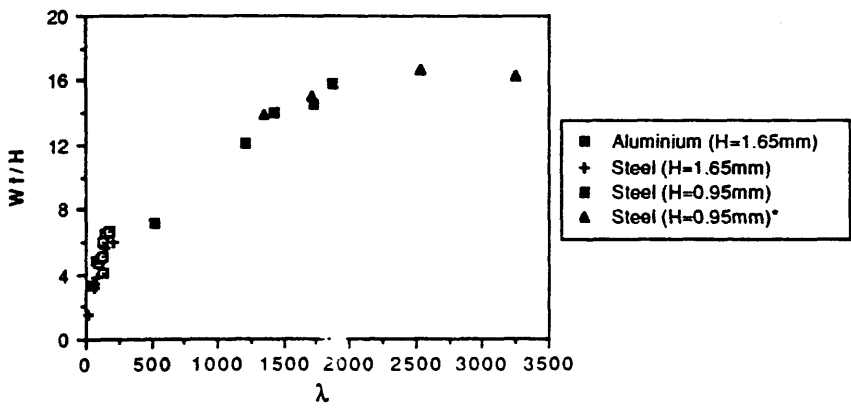


Fig. 3.8(b) The permanent deformation profile along the denting line (-AL06-)



(a) Wf/H - E_s relationship

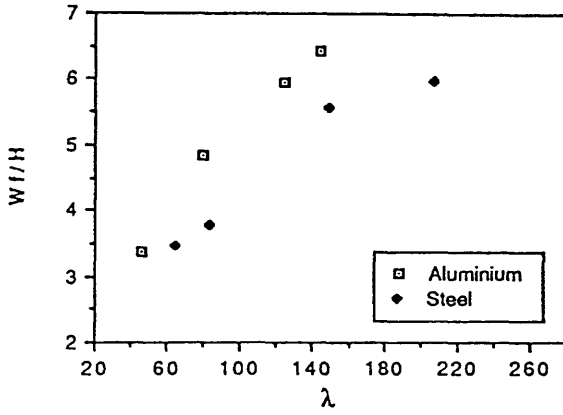


(b) Wf/H - λ relationship

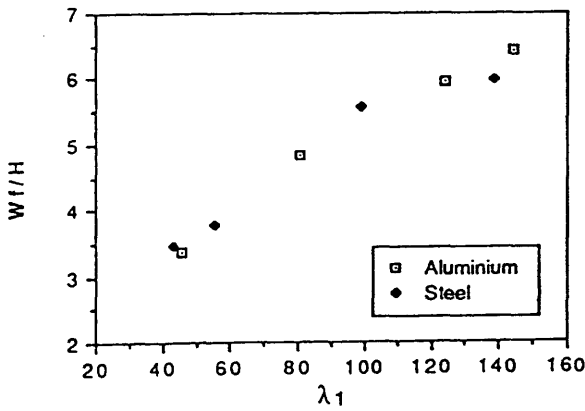
Fig. 3.9 Impact test results on the maximum permanent deflection for Aluminium and Steel plates

(a) $E_s = \frac{1}{2} m_0 (V_0^2 - V_s^2)$ and (b) $\lambda = \frac{m_0 V_0^2}{8M_0 H}$

* Free in-plane slide is allowed at the top and bottom boundaries.



(a) $Wf/H - \lambda$ relationship ($\lambda = \frac{m_0 V_0^2}{8M_0 H}$)



(b) $Wf/H - \lambda_1$ relationship ($\lambda_1 = \frac{m_0 V_0^2}{8M_0 H}$)

Fig.3.10 The influence of strain-rate sensitivity on the maximum permanent deflection for steel plates of thickness 1.65 mm when $L=250$ mm. (a) $\sigma_d = \sigma_s$ and (b) $\sigma_d = 1.5\sigma_s$.

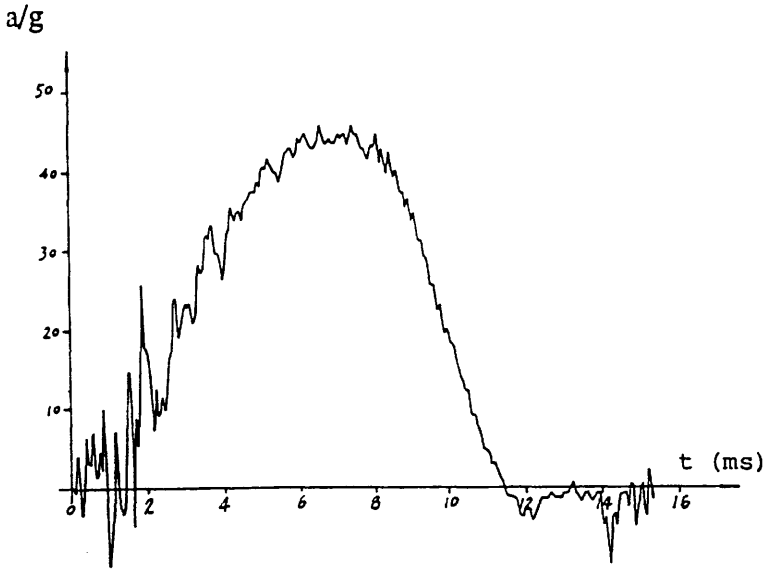


Fig. 3.11 Measurement of acceleration on plate -AL03-

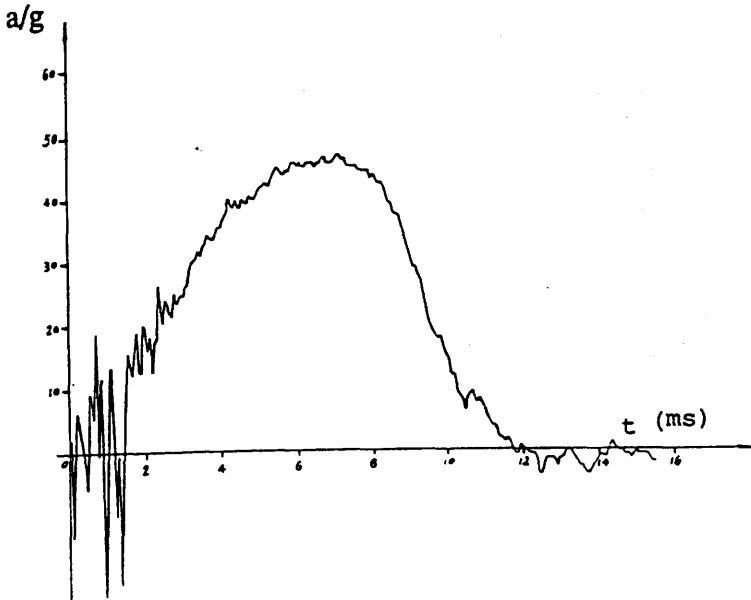


Fig. 3.12 Measurement of acceleration on plate -AL04-

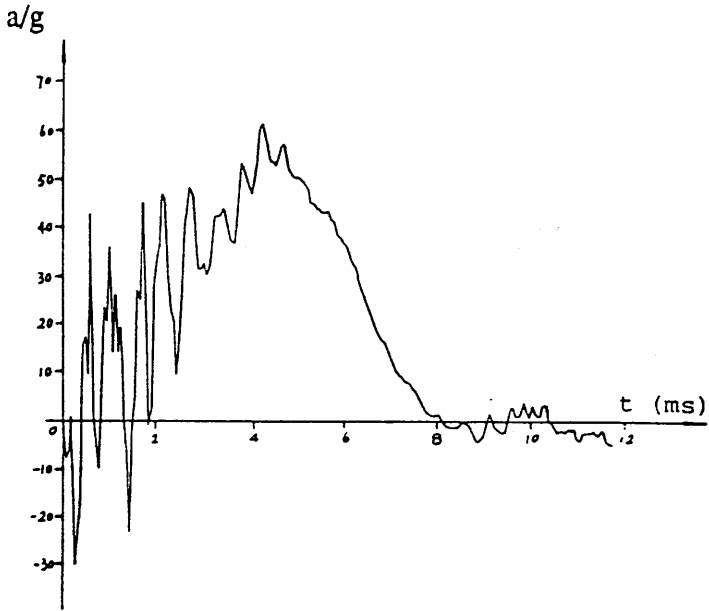


Fig. 3.13 Measurement of acceleration on plate -ST01-

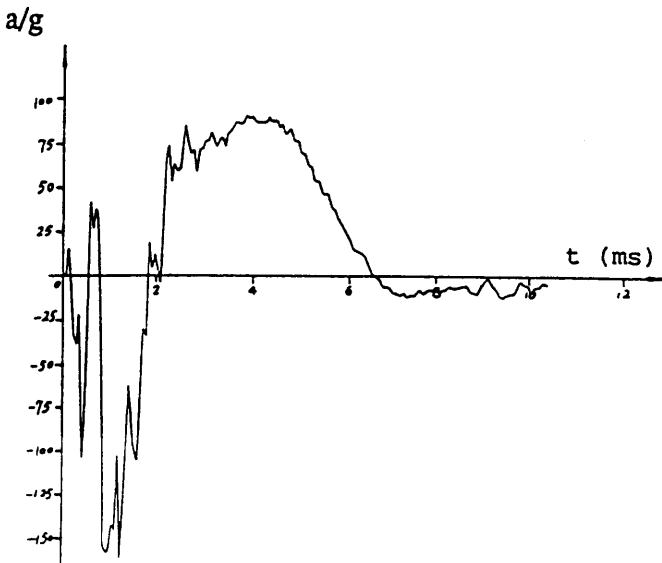
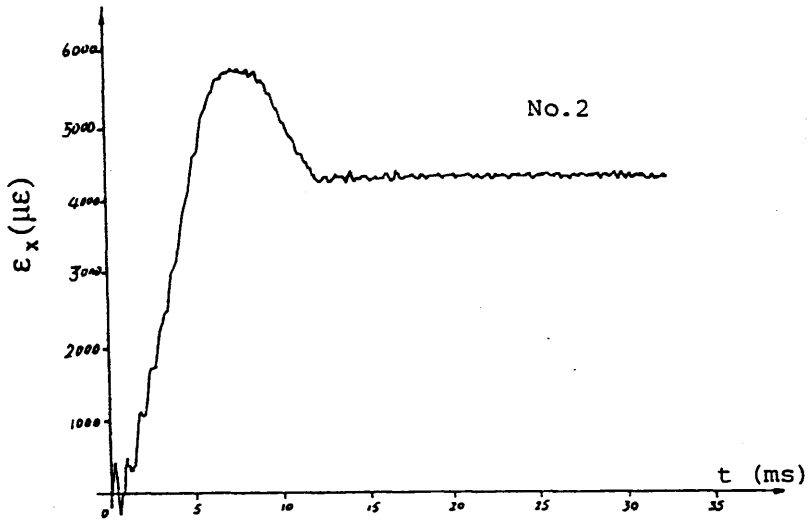
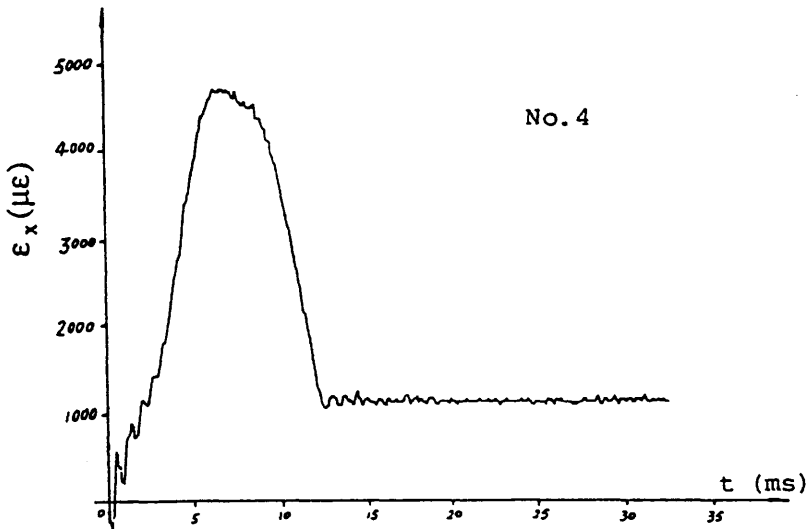


Fig. 3.14 Measurement of acceleration on plate -ST03-

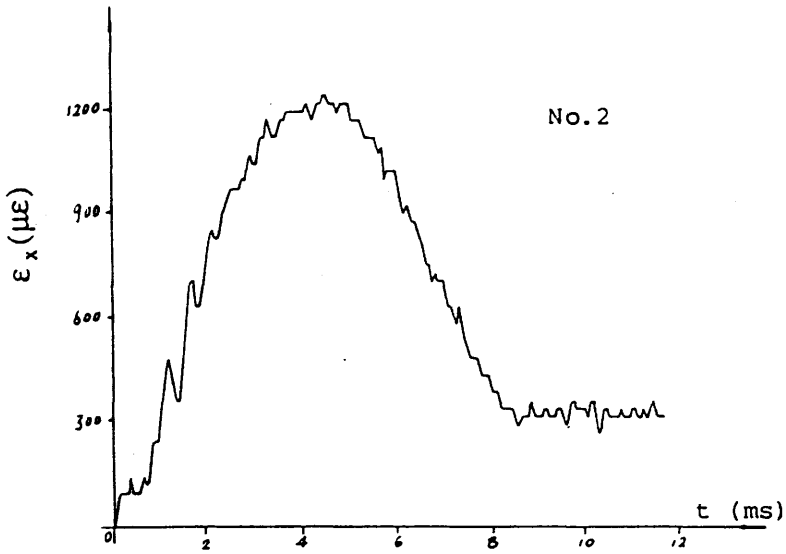


(a) front surface

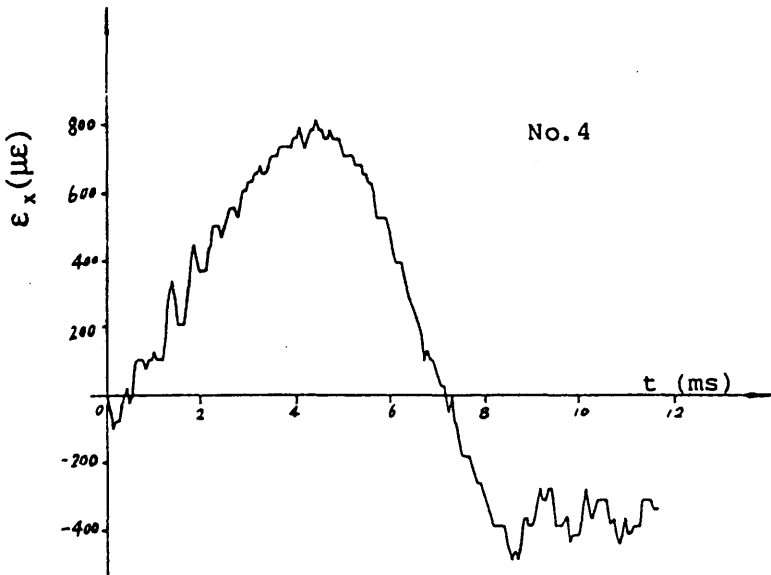


(b) back surface

Fig. 3.15 Measurement of strain history on plate -AL04- at point $x=L/4$, $y=B/2$.

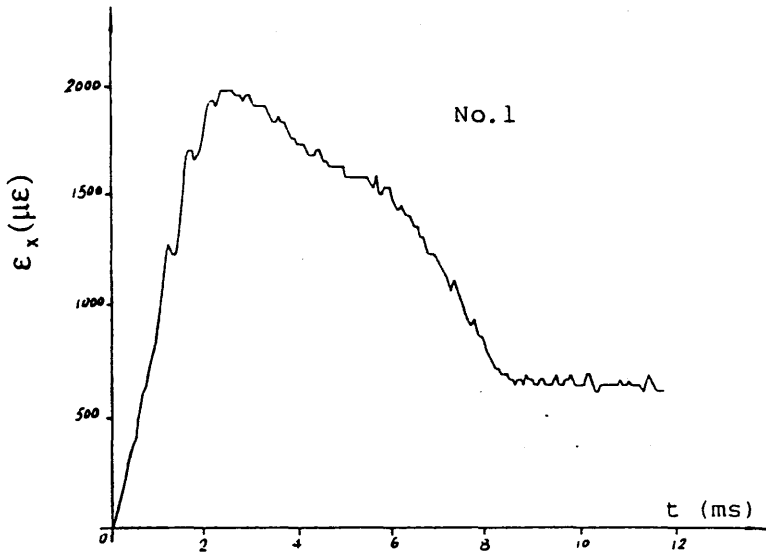


(a) front surface at point $(L/4, B/2)$

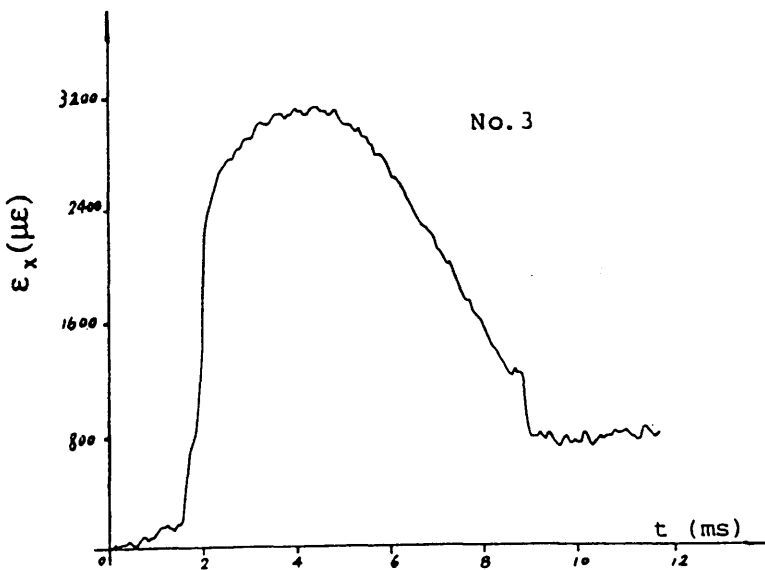


(b) back surface at point $(L/4, B/2)$

Fig. 3.16 Measurement of strain history on plate -ST01- at point $x=L/4, y=B/2$.

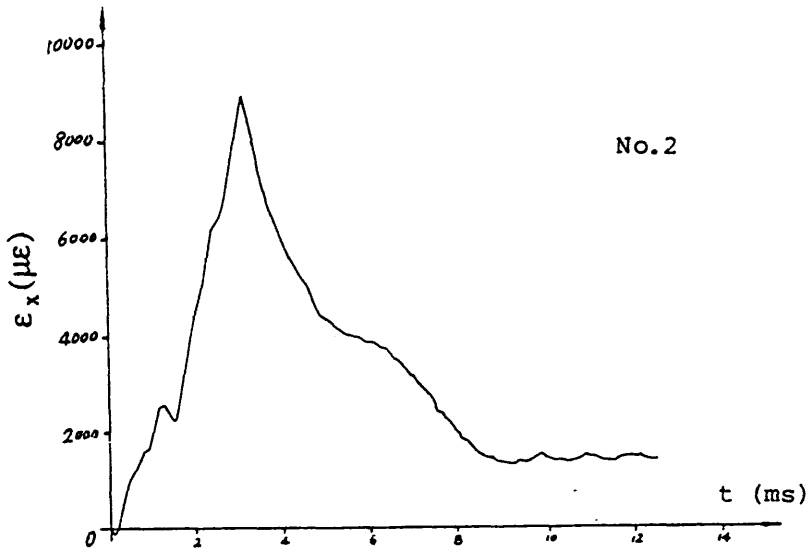


(a) front surface at point $(L/2, B/2)$

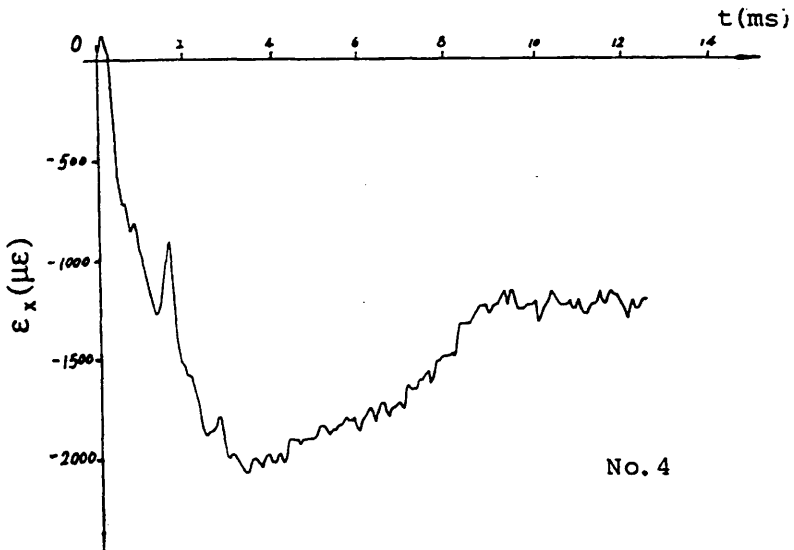


(b) back surface at point $(L/2, B/2)$

Fig. 3.17 Measurement of strain history on plate -ST01- at point $x=L/2, y=B/2$.

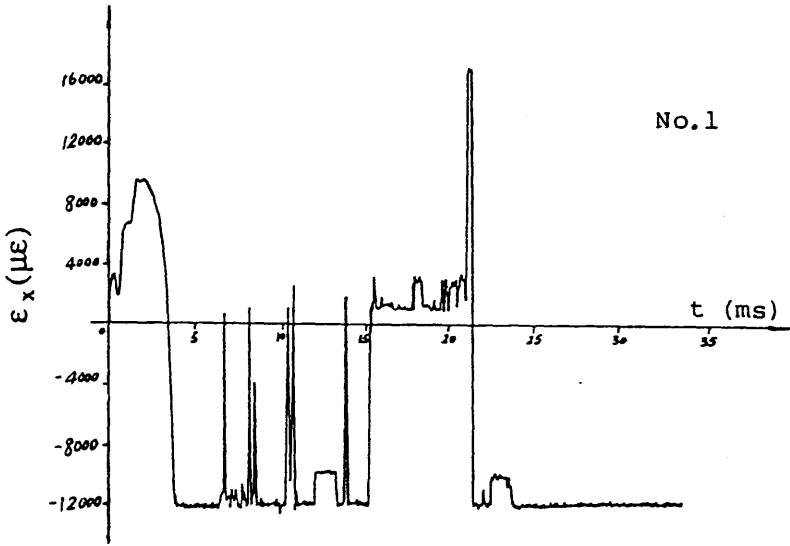


(a) front surface

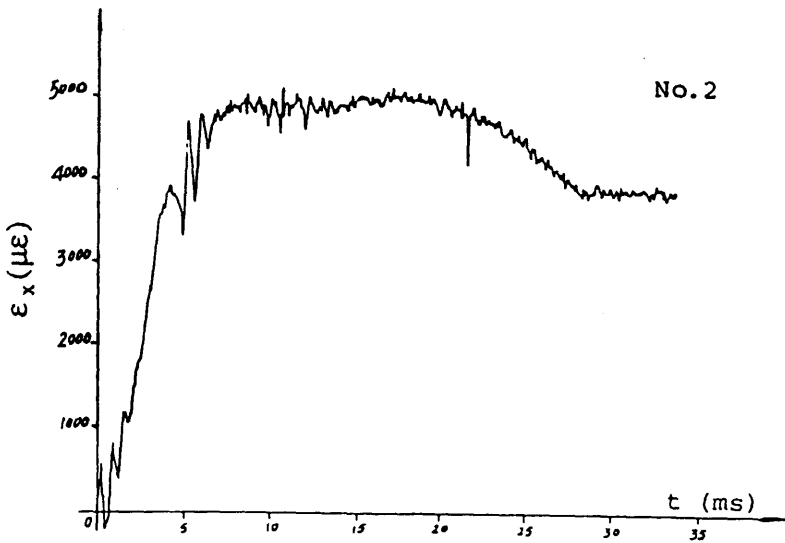


(b) back surface

Fig. 3.18 Measurement of strain history on plate -ST02- at point $x=0, y=B/2$.

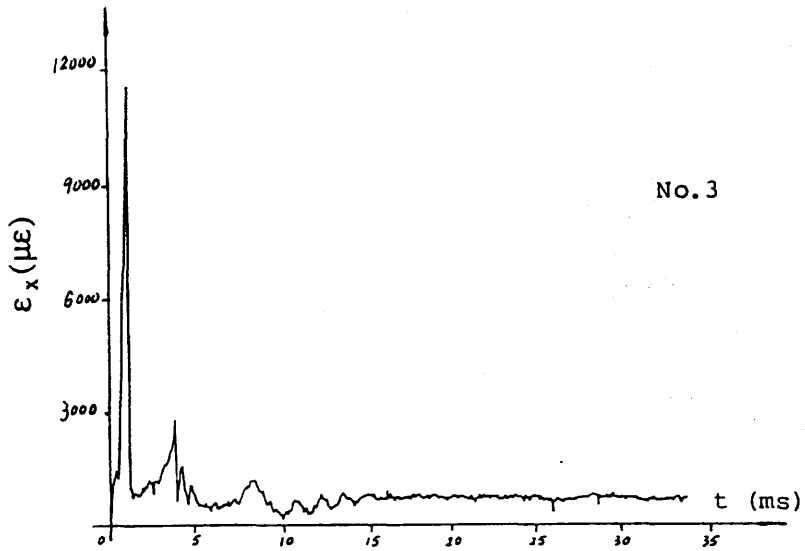


(a) front surface at point (L/2, B/2)

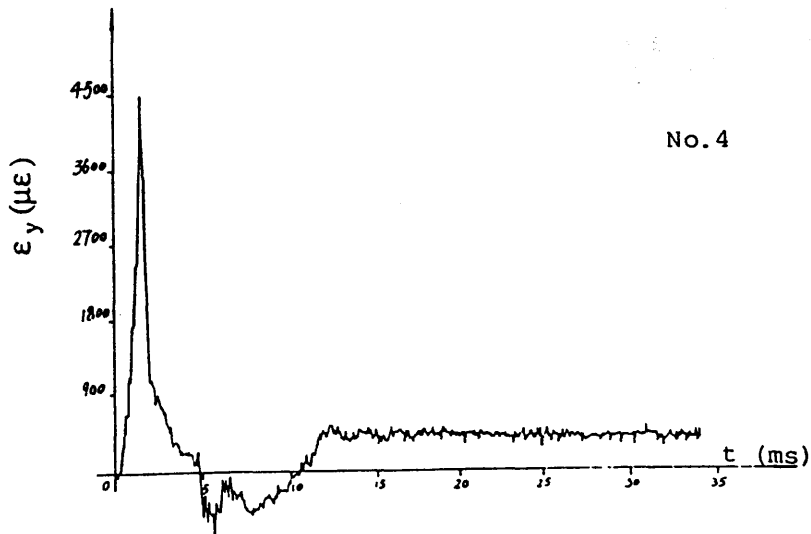


(b) front surface at point (L/4, B/2)

Fig. 3.19-1 Measurement of strain history on plate -AL01-

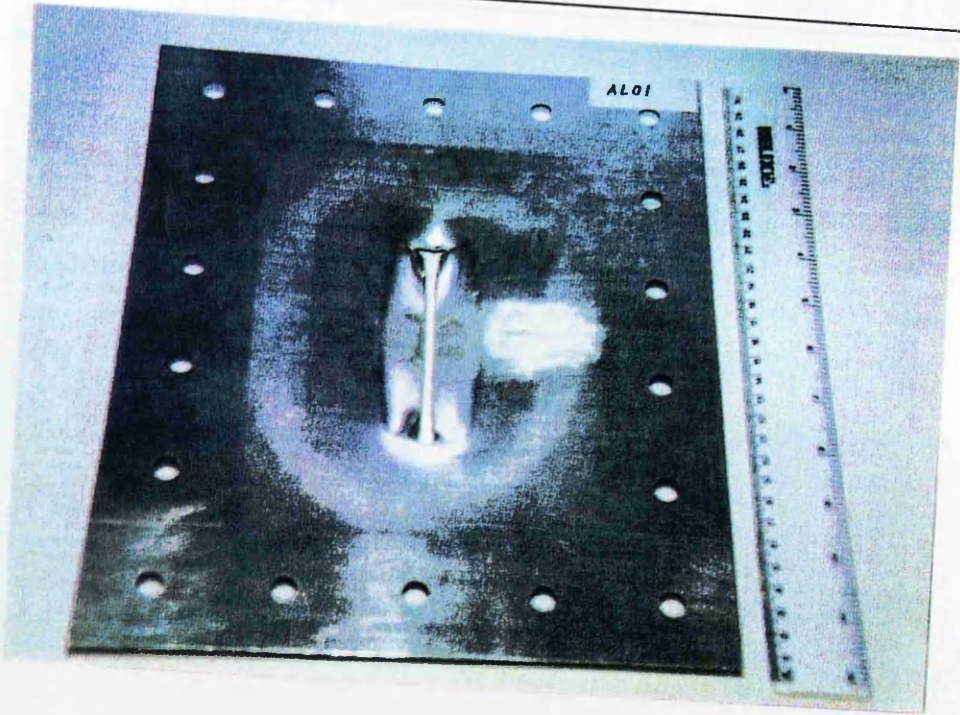


(c) back surface at end of dent line

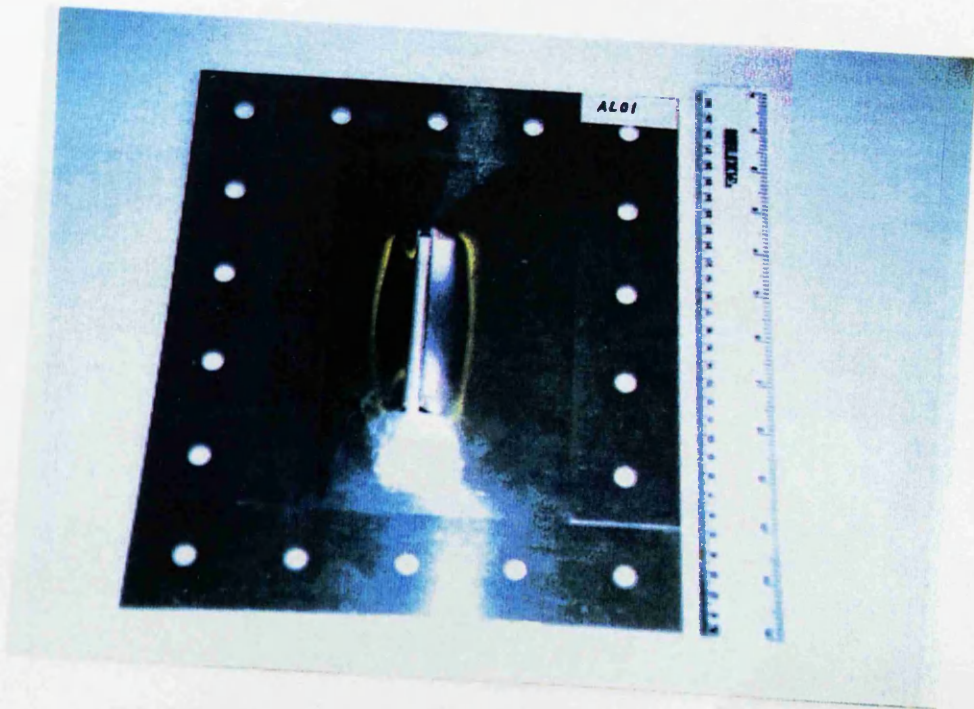


(d) back surface at end of dent line

Fig. 3.19-2 Measurement of strain history on plate -AL01-

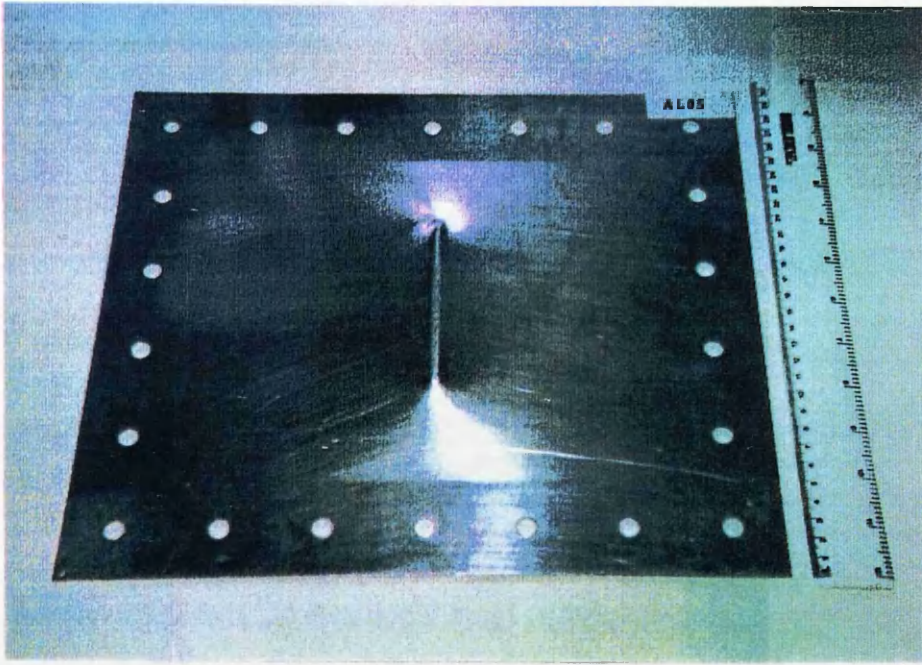


(a) front side

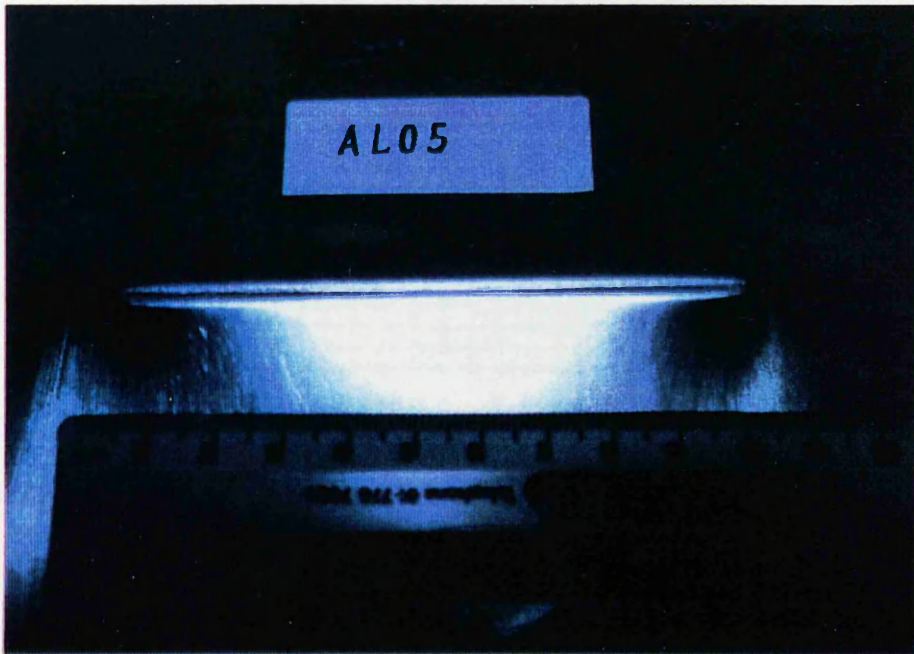


(b) back side

Fig. 3.20 Broken aluminium plate -AL01-



(a) back side



(b) "Necking" along the dent line on back side

Fig. 3.21 Deformed aluminium plate -AL05-

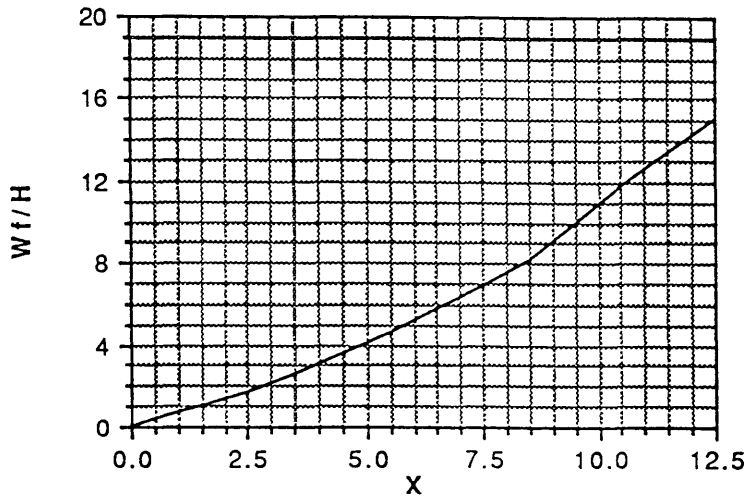


Fig. 3.22(a) The permanent deformation profile along the central line (-ST17-)

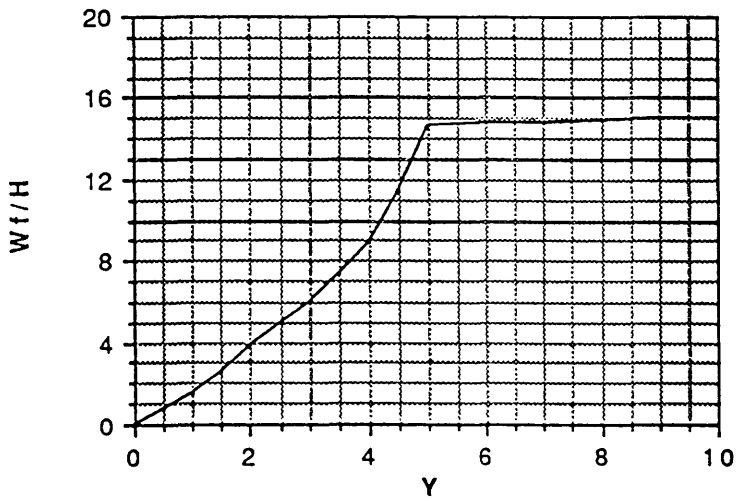


Fig. 3.22(b) The permanent deformation profile along the denting line (-ST17-)

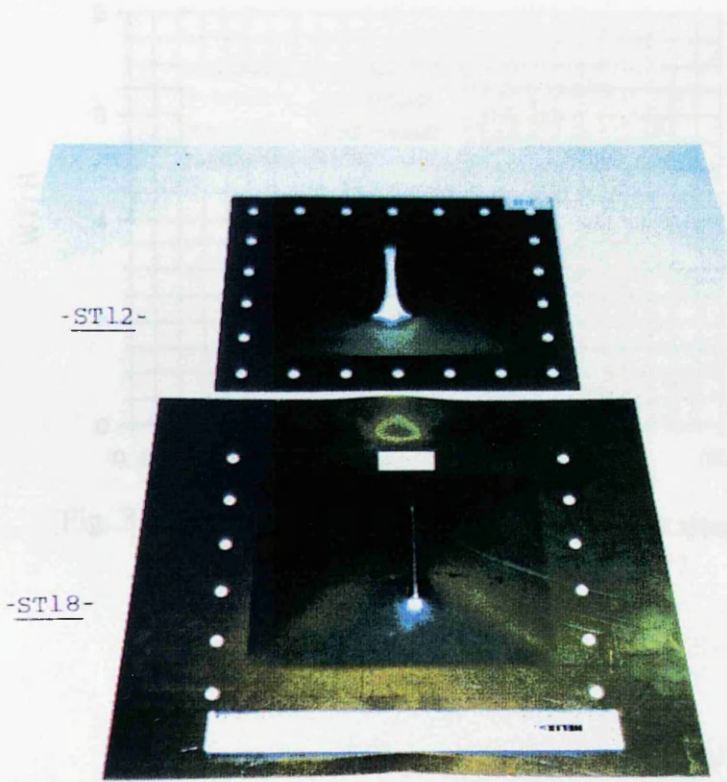


Fig. 3.23 The influence of boundary condition on failure of plate

Fig. 3.24(a) The possible deformation of a plate
under a central point load

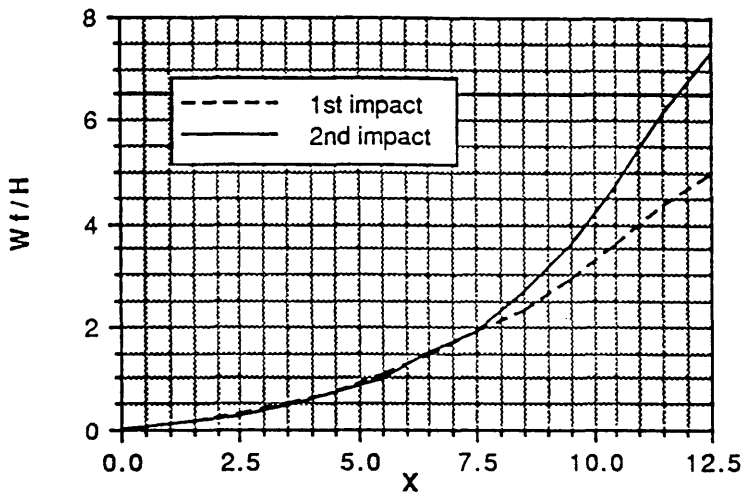


Fig. 3.24(a) The permanent deformation profile along the central line for two impacts (-AL06-)

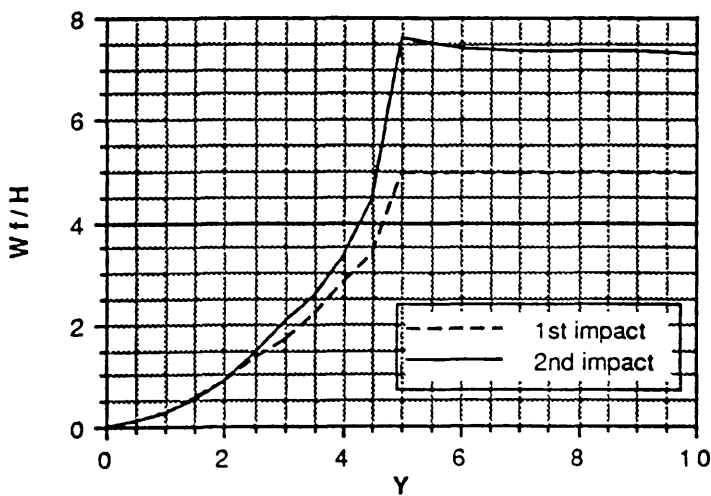


Fig. 3.24(b) The permanent deformation profile along the denting line for two impacts (-AL06-)

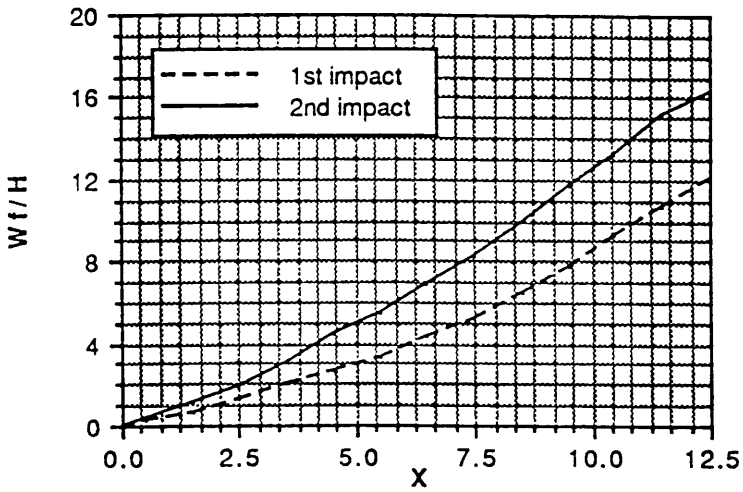


Fig. 3.25(a) The permanent deformation profile along the central line for two impacts(-ST07-)

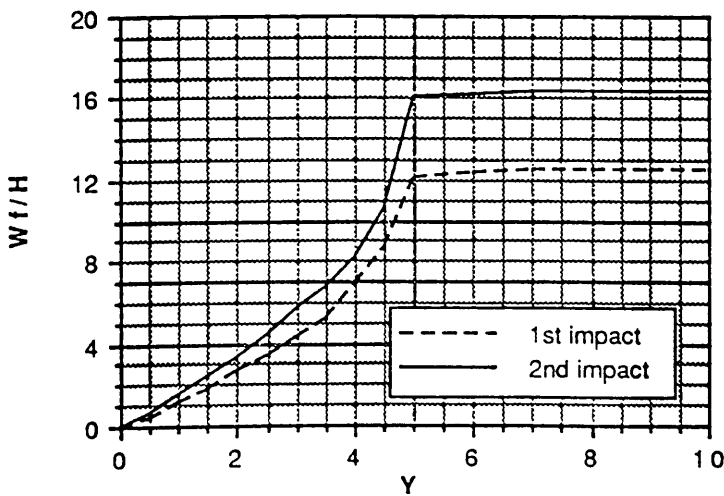


Fig. 3.25(b) The permanent deformation profile along the denting line for two impacts(-ST07-)

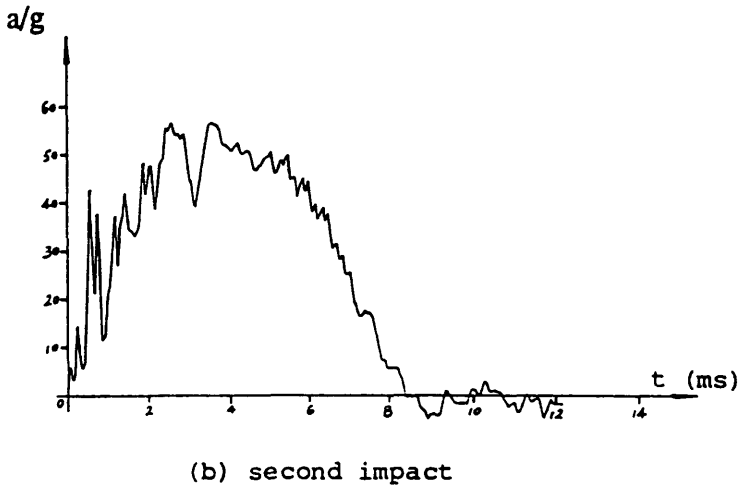
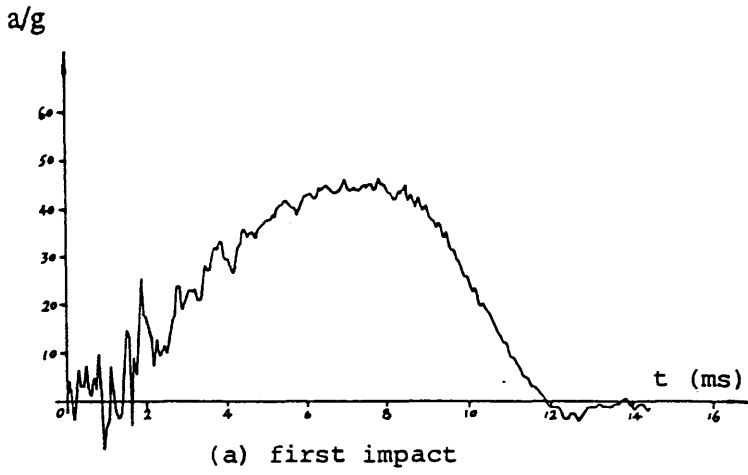
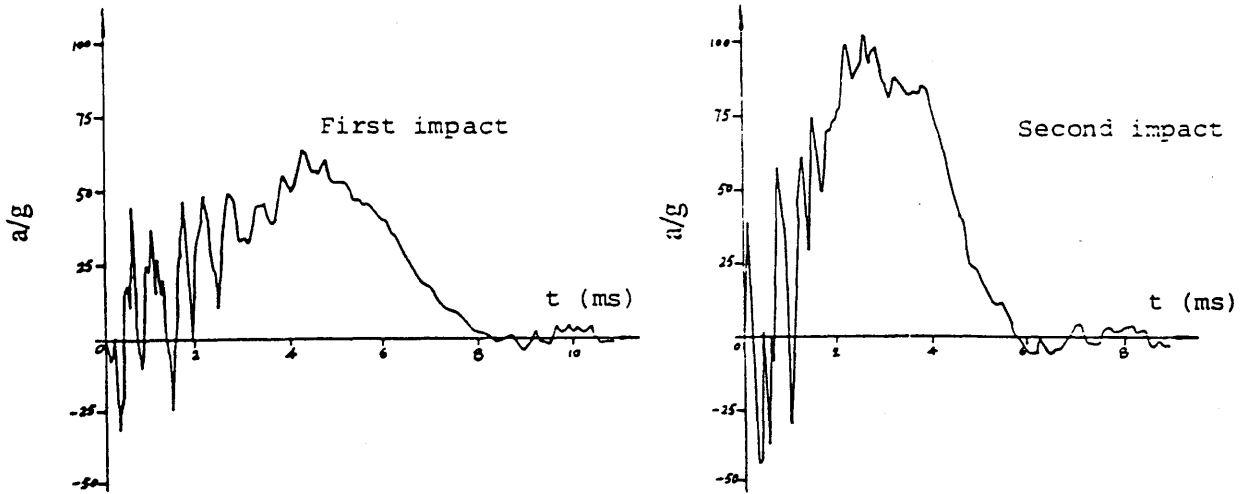
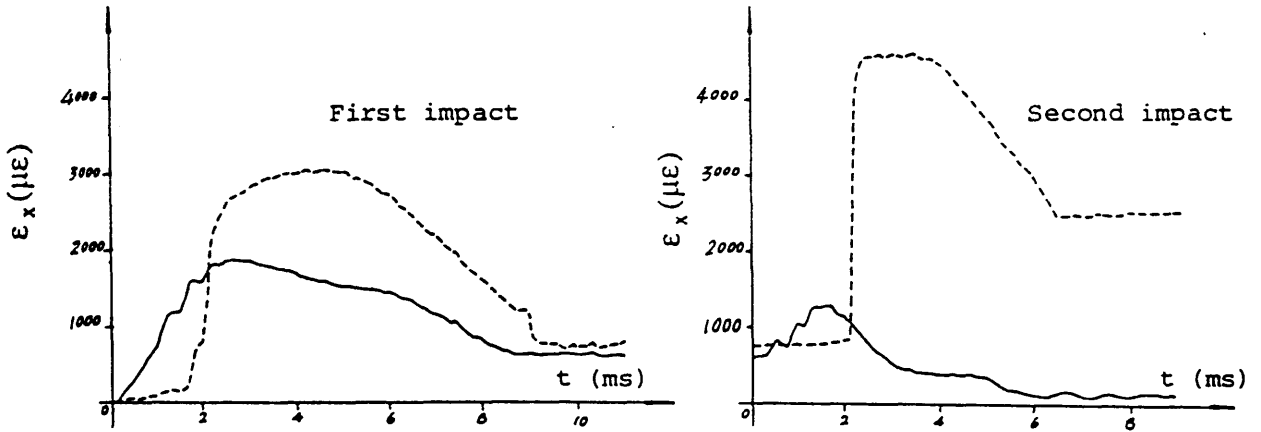


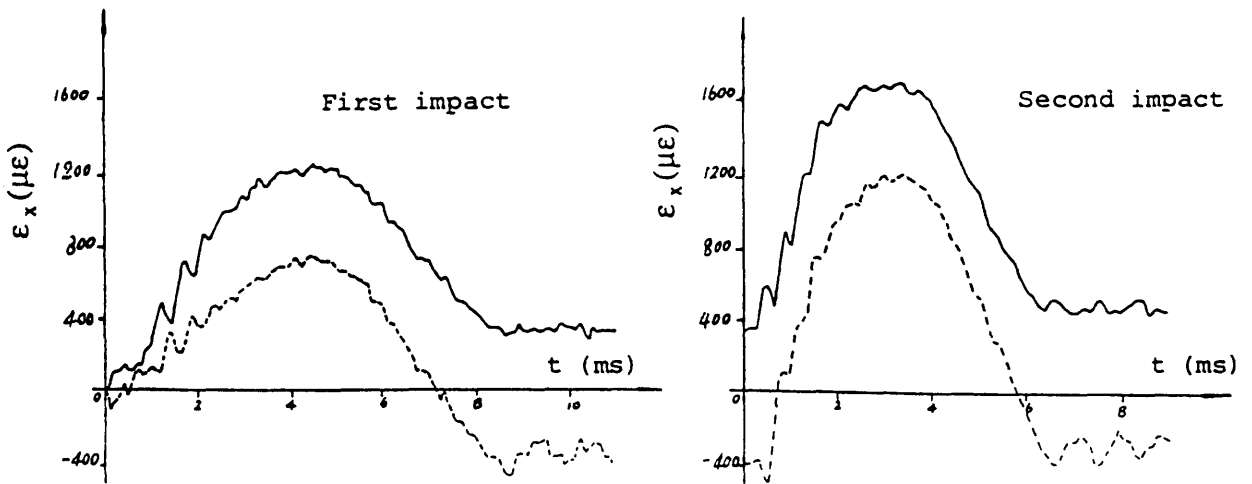
Fig. 3.26 Measurement of acceleration on plate -AL03-



(a) Acceleration curves



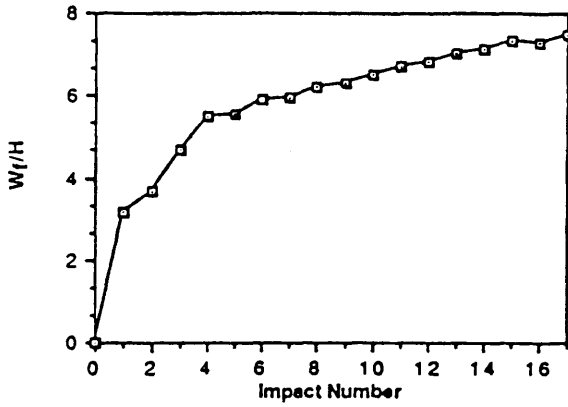
(b) Strains at point (L/2, B/2)



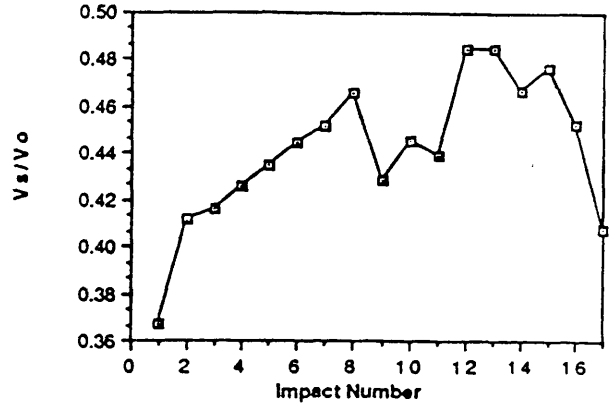
(c) Strains at point (L/4, B/2)

Fig. 3.27 Measurement of acceleration and strain history on plate -ST01- during the first two impacts

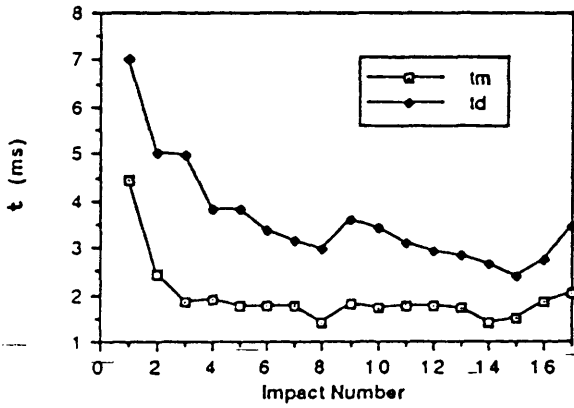
———— front surface
 - - - - - back surface



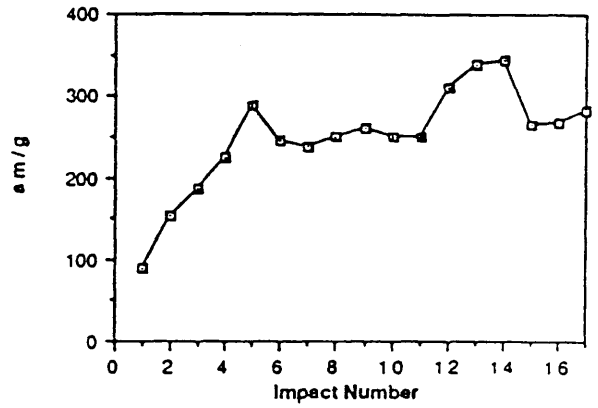
(a) Maximum permanent deflection



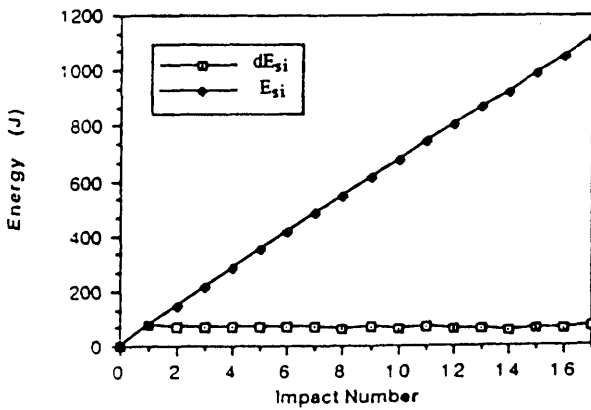
(b) Rebound velocity



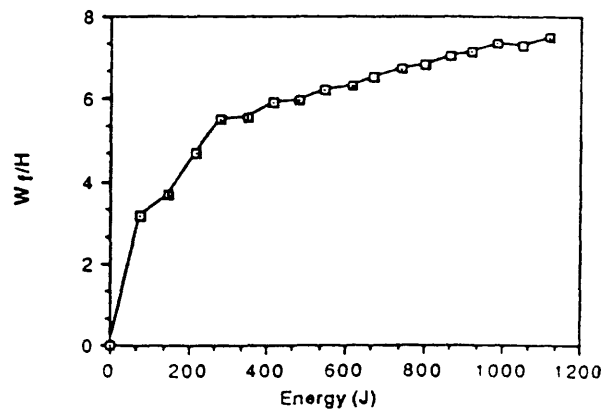
(c) Response time



(d) Acceleration

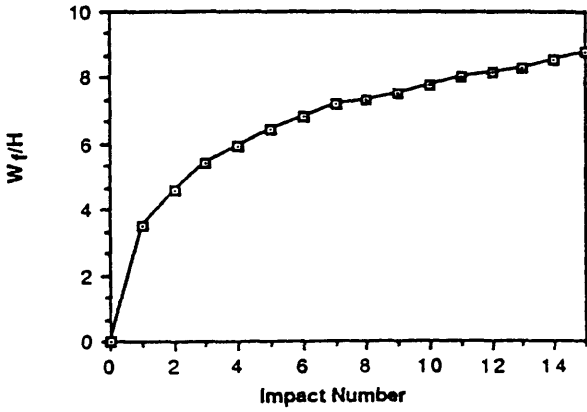


(e) Energy absorbed by the plate

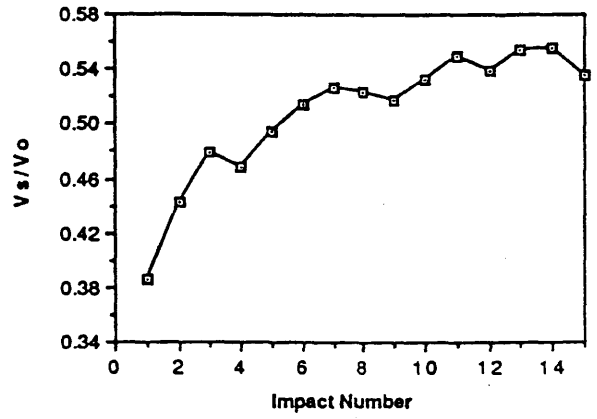


(f) Maximum permanent deflection - energy relation

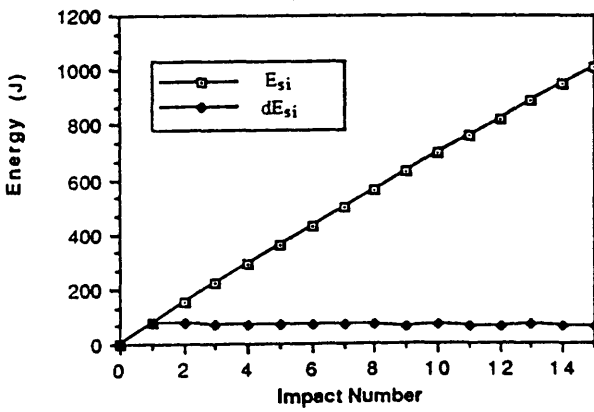
Fig. 3.28 Experimental results of repeatedly impacted plate-ST03-(17 impacts)



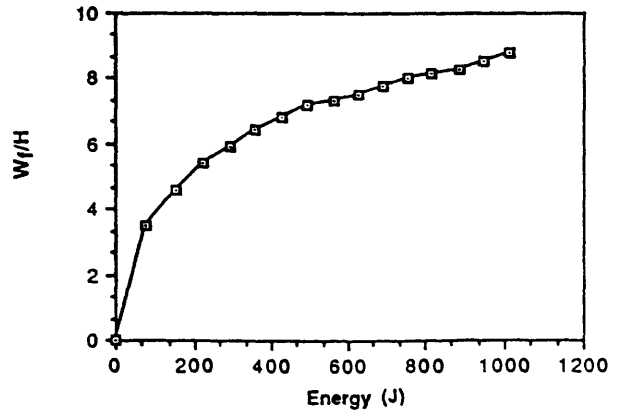
(a) Maximum permanent deflection



(b) Rebound velocity



(c) Energy absorbed by the plate



(d) Maximum permanent deflection - energy relation

Fig. 3.29 Experimental results of repeatedly impacted plate -ST05- (15 impacts)

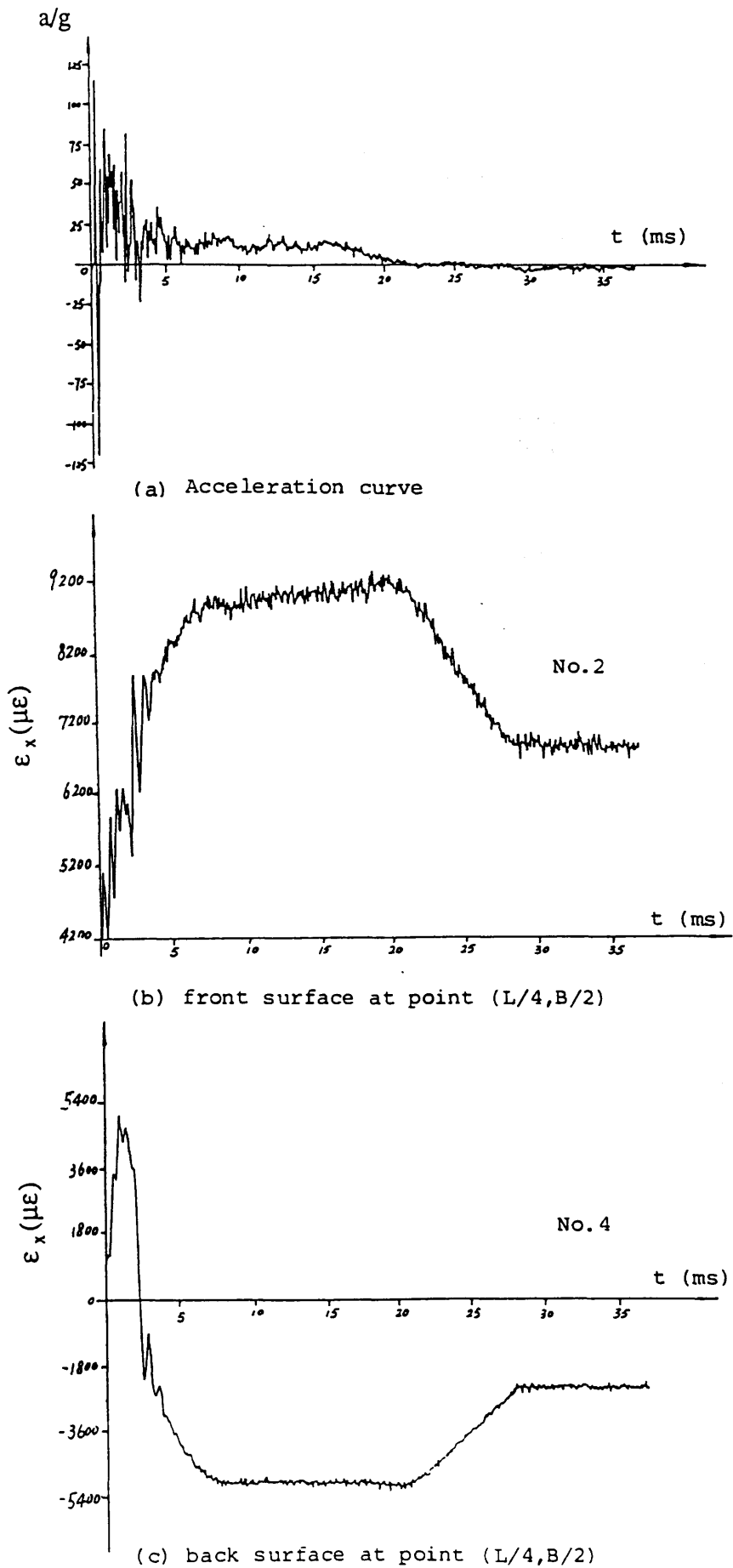


Fig. 3.30 Measurement of acceleration and strain history on plate -AL04- during the second impact

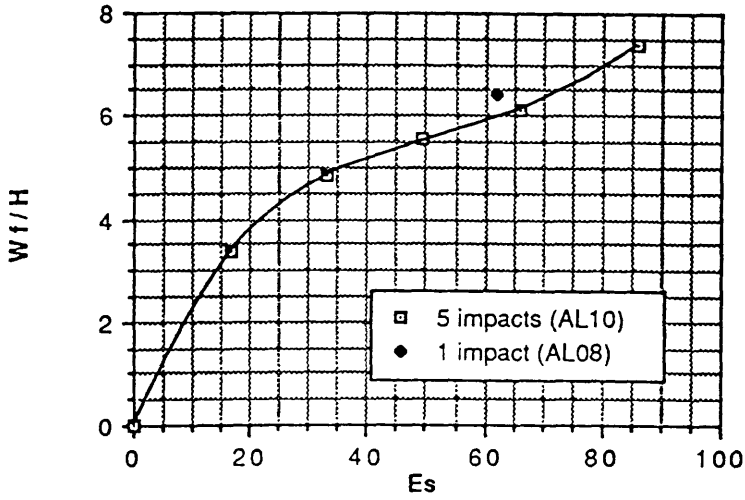


Fig. 3.31 Comparison between single impact (AL08) and repeated impacts (AL10)

CHAPTER FOUR

NUMERICAL RESULTS AND CORRELATION WITH EXPERIMENTAL VALUES

In this chapter the numerical approach developed in chapter 2 is used to simulate the collision process of an aluminium plate impacted by a knife edge indenter. Correlations are performed with the experimental results on the plate impact test described in chapter 3 as well as on the test of a small scale ship model which was conducted in the Department of Naval Architecture and Ocean Engineering during 1981-1982. Impact of the plate tested is depicted in Fig. 4.1 with strain gauge distributions.

4.1 Overall Dynamic Response

4.1.1 Deflection, Velocity and Acceleration History

Deflection history at the plate centre is shown in Fig. 4.2(a). The velocity and acceleration history of the striker are shown in Figs 4.2(b) and (c) respectively. From the correlation of these curves it can be seen that point A in Fig. 4.2(b) indicates impact which is the beginning of collision, point B represents the maximum deflection, and point C represents the separation between the striker and the struck plate. The central deflection oscillates about a certain value in the absence of damping. In the real case such kind of oscillation declines quickly [Harima et al, 1962] and the permanent deflection is at the position close to lowest point of elastic recovery at the deflection history curve. This phenomenon was modelled by incorporating the damping factor in

the numerical approach.

From the energy point of view it is known that the energy dissipated during impact is normally stored or transferred in combinations of two main modes: elastic and plastic strain energy. The former is completely recoverable which is reflected in the rebound velocity of the striker. The latter is dissipated by the development of plastic deformation of the plate.

4.1.2 Impact Force

The impact force versus central deflection is presented in Fig. 4.2(d). It can be seen that at the beginning of impact the force increases slowly, which corresponds to the bending of the plate. The fact that there is a relatively flat portion of the curve during this phase was also observed in the static test on clamped plate strip (see Fig. 17 of the paper by Mc Dermott et al [1974]). The bending phase terminates at a low load level. When the deflection increases and the plate becomes stiffer, the impact force rises steady and is nearly proportional to the central deflection of the plate during which the membrane behaviour is important. When reaching its maximum value the impact force decreases linearly with the central deflection.

4.1.3 Deformation Profiles

The deformed shapes of the plate during the process of collision are shown in Fig. 4.3 for the front surface and Fig. 4.4 for the back. Figures 4.3 and 4.4 illustrate the principal events sketched in Fig. 4.1.

The maximum deflection profiles are plotted in Fig. 4.5 and Fig. 4.6 shows the deformation profiles when the plate comes to rest, which is defined as residual state.

4.2 Dynamic Strains

The strain-time histories at four points of the plate (see Fig. 4.1(b)) are shown in Fig. 4.7. For points 1, 2 and 3 only x-strains are given (Fig. 4.7(a)-(c)) and three components of strain are presented at point 4 (Fig. 4.7(d)-(f)).

Among these four points, point 4 has the largest maximum x-strain and point 1 is next. Maximum x-strain at point 2 is smallest which reflects the membrane force. At this point the strains at front, mid and back surface nearly coincide and maximum x-strain is 4 times as large as the uni-axial static yield strain.

The y-strain at point 4 is also significantly large (Fig. 4.7(e)), but the in-plane shear strain is extremely small (Fig. 4.7(f)). Therefore the strains in x and y directions are principal strains, and the point at the end of the dent line is in the state of bi-axial tension.

4.3 Stress and Strain Distributions at Maximum Deflection

Figure 4.8 gives the x-stress and x-strain distributions along the plate's lines of symmetry at the moment the plate centre reaches its maximum deflection. To demonstrate the stress and strain concentration in the area near the dent line, stresses and strains on the front, mid and back surface are plotted separately.

Along the x-direction, the stress and strain are smooth at quarter-span area, with peaky bending changes at the boundary and at the dent area (Figs. 4.8(a) and (b)). For the front surface, the stress and strain at the boundary are a little larger than those at quarter-span because of the inward deformation, and they decrease sharply to compressive values near the dent area due to contact with the striker, while for the back surface they are a little smaller at the boundary, with peaky increases near the dent area.

From Figs.4.8(c) and (d) it can be seen that, along the y-direction, there are even more remarkable changes of the x-stress and x-strain on the back surface of plate at the end of the dent line. It is anticipated that for a sufficiently large impact energy the plate cracks at the dent line, or at the boundary, due to maximum tensile strain. The cracking is initiated at the tip of the dent line on the back surface because of bi-axial tension. This was observed in the plate impact tests and small scale ship model impact tests [Samuelides, 1984]. When the thickness of the plate increases, the point of boundary on the front surface experiences large strain and may also be the starting point for a crack. This was observed in the experiment of Liu and Jones [1987] on a clamped beam. However, for a real ship it may be impossible for this type of failure to occur due to the large ratio of the length between the bulkheads and the plate thickness.

It is noted that at the mid-surface of the plate the tensile membrane stress and strain can be observed over all the plate as a result of the large membrane tension caused by the dent.

4.4 Stress and Strain Distributions in Residual State

Figure 4.9 shows the x-stress and x-strain distributions when the plate comes to rest. There is a large reduction in all the stresses and the distributions are totally different from those at the maximum deflection. However, the strain distributions are the same as those at maximum deformation with a little reduction in the values. It should be noted that, in the residual state, the value of the stresses at mid-surface are not between those of front and back surface, which results from the fact that the elastic recovery causes the plate to deform in the opposite direction.

4.5 Correlation with Experiment

4.5.1 Fully Clamped Aluminium Plates

For all the aluminium plates tested (except a ruptured one) the comparisons between test and numerical results are shown in Fig. 4.10 on the maximum permanent deflection, in which both W_f/H - E_s curves and W_f/H - λ curves are given. Because the data include different combinations of structural size and impact condition, there are fluctuations in these curves. Correlations on the rebound velocity of the striker are presented in Fig.4.11. The agreement shown in Figs. 4.10 and 4.11 is satisfactory.

For the same structural geometry and impact mass the variations of W_f/H and V_s/V_o with impact velocity (V_o) are plotted in Fig. 4.12. The test and numerical results shown in Fig. 4.12 reveal that the W_f/H increases with impact velocity, but V_s/V_o decreases with it. This will be studied in the parametric study in 5.1.

Figures 4.13(a) and (b) gives a comparison of measured and calculated strains, in which it can be seen that the shapes of the strain curves from these two different methods are the same. The numerical approach predicts the impact duration very well. However, the calculated maximum strain is still 1.5 times larger than the measured value. This is mainly due to the problem in the calibration of the strain gauge measuring system, as discussed in 3.4.6.

4.5.2 Fully Clamped Steel Plates

The correlation of numerical results with experimental values on the maximum permanent deflections are plotted in Fig. 4.14, which consists of all the tested steel plates (0.95 mm and 1.65 mm thick) except the ruptured. In 3.5.1 the influence of the

strain-rate sensitivity on the 1.65 mm thick steel plate was evaluated by comparing with the strain-rate insensitive aluminium plate of the same thickness. The ratio of dynamic and static yield stress was found to be 1.5. As shown in Fig. 4.14, for the 1.65 mm thick plates the agreement between test data and numerical predictions is excellent, but the experimental results are apparently smaller than the numerical predictions for the steel plates of the thickness 0.95 mm, which implies that actual dynamic yield stress is larger than 1.5 times the static yield stress.

The dynamic strains at point 2 and plate centre (point 1) are plotted in Figs. 4.15 and 4.16. As seen from Figs 4.8(b) and 4.9(b), there is a plateau halfway between the boundary and dent line ($0.025 < x/L < 0.475$), and the measurement of strain in this area, e.g. point 2, is easier as compared with the plate centre where the gradient of strain is so high that it is extremely difficult to measure by using strain gauges. This is reflected in Fig. 4.16, in which the difference on shape of the strain curves between the numerical results and tested ones is noticed. In fact, the measured strain curves shown in Fig. 4.16(a) represent the strain histories of the point located in $x/L=0.48$ (see Figs 4.8(b) and 4.9(b)) where there is steep change in strain. In contrast the agreement for point 2 is good. However, the calculated maximum strain at point 2 is 1.4 times as large as the measured value.

4.5.3 Side Plates of Small Scale Ship Models

The proposed numerical model has been used to analyse the denting of small scale ship models impacted by a rigid striker. The experimental work was part of a collision project conducted in the Department during 1981-1982 which consisted of bringing a rigid striker into violent contact with a deformable model. The struck model represented approximately the parallel section of a tanker, but no local stiffeners were included in the model. Impact occurred with the struck models either rigidly supported or free-floating. The former tests are named 'dry tests' and the latter 'wet tests'. Four

models were tested. The first was used purely to examine the test procedures. The second was tested 'dry' and the last two 'wet'. More than one impact was performed on each model, generally at different locations. The scale of the struck models was roughly 1:60. The sides and the bottom were formed from one piece of 1/32" (0.79 mm) steel sheet bent to shape and to which a deck of the same thickness was riveted. The plating which formed the model ends was 1/16" (1.58 mm) thick and was soldered to the hull. The inside of the model was divided by two longitudinal and four transverse bulkheads of the same plate thickness as the ends. The testing procedure and results were reported by Samuelides [1984].

It is concluded from the tests that:

- 1 No shortening of the distance between the transverse bulkheads was observed after any of the tests.
- 2 The transverse permanent deflections keep constant along the line of impact (see Fig. 4.17).

These conclusions support the assumptions made in the numerical approach that the striker keeps contact with the plate at the dent line and the plating at transverse bulkheads is fully clamped.

In calculation the side structure of ship model is simplified as a fully clamped rectangular plate of length 243 mm, width 255 mm and thickness 0.8 mm. The dent line is 145 mm. For four dry tests, comparisons between the experimental and numerical results of the permanent central deflection of the plate and of the rebound velocity of striker are shown in Fig. 4.18. The numerical approach underestimates the permanent central deflection (Fig. 4.18(a)) and overestimates the rebound velocity (Fig.4.18(b)). In the numerical approach the boundaries at $y=0$ and $y=B$ are assumed

to be fully clamped which means that the interactions between the plate and adjoining structure (deck and bottom) are not accounted for. The allowance of in-plane sliding and rotation along the boundaries will increase the deflection of the plate. On the other hand, there is some energy dissipated during the impact process due to the friction between the roller of the striker and the runway, which contributes to the reduction of the measured rebound velocity. The rebound velocity of the striker was defined as the velocity when the striker separated from the surface of the plate but, in the test, the rebound velocity was measured after the separation. Delay in triggering of the measuring instrument may lead to significant reduction of the measured rebound velocity because, during the period of delay, the velocity of the striker reduces quickly.

Results for all the test cases are plotted in Fig. 4.19 in which the test data are compared with existing theoretical methods. In this diagram the maximum available energy to cause structural damage is plotted against final deflection. The available energy was determined as the difference between the kinetic energies of the striker before and after impact. The measured sway and yaw velocities for wet test were used and the effects of hydrodynamic forces were accounted for by added mass.

It is seen that the test data lie between the curves obtained using the present approach, a plate-strip approach [Samuelides, 1984] and an analytical method in which rigid-plastic behaviour was assumed. The results obtained using the present approach involving the complete plate are seen to lie closest to the test data and quite a good correlation is achieved. It should be pointed out that there are different kinds of energy dissipation in the test, thus the measured permanent deflection is less than the 'real' value, especially for wet tests. The energy dissipation due to the rolling motion of the model in wet tests is obvious, which was observed by using a high-speed camera. This accounts for the fact that the test data lie to the lower side of the predicted curve in Fig. 4.19.

4.6 Discussions

Strictly speaking, all impacts and collisions will involve some dynamic effects. Kinetic energy will by some mechanism be transferred to elastic or plastic strain energy during structural deformation, and the motion of all involved bodies should be described dynamically. When calculating load effects, inertia forces due to structural deformation were often neglected, which means the collision is treated as a quasi-static problem. This point of view is adequate only when the duration of impact is much longer than the corresponding natural period of elastic vibration of the struck structure. However, considerable errors can arise if the duration of impact is less than the natural period. It should be noted that, even when the impact duration is much longer than the natural period of the plate, the dynamic analysis is still necessary to obtain the maximum impact force caused by the striker of mass m_0 and initial velocity V_0 because the impact force from the dynamic interactive process is unknown.

The material elasticity plays an important role in the collision problem. The rebound velocity of the striker reflects the elastic effects. Moreover, the residual stress and strain of the plate are significantly influenced by its elastic property.

Collision and impact forces can be extremely important for structural reliability and hence for design. However, the difficulties in determining the impact force exist both in experimental measurements and in theoretical prediction. The numerical model proposed gives the impact force history and the impact force-indentation relationship, providing a convenient and economical basis for parametric studies.

Another important factor affecting dynamic response is strain-rate sensitivity. For 1.65 mm thick steel plates the numerical approach gives very good correlation with the experimental measurements when the dynamic yield stress which was determined by comparing the test results of steel and aluminium plates was used. In analysing the

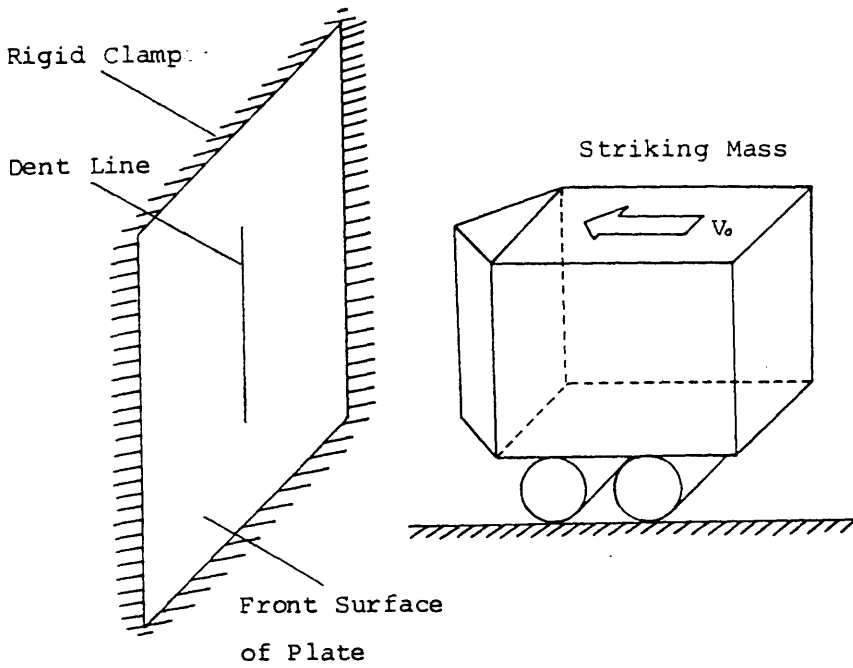
strain-rate sensitivity of the side plate of ship model the program gave the strain-rate histories at different points of the plate. Adopting the average strain-rate at point 2 during the impact, the dynamic flow stress can be determined according to the Cowper-Symonds formula. The numerical study carried out in this research using the characteristics of the dry tests [Samuelides, 1984] reveals that, when the average strain-rate increases from 1.266 s^{-1} ($\sigma_d/\sigma_s=1.5$) to 6.807 s^{-1} ($\sigma_d/\sigma_s=1.7$), the maximum permanent deflection decreases by only 5 percent approximately.

At maximum deflections the same shape distributions were found between stress and strain. The membrane tension caused by denting spread all over the plate. High levels of stress and strain develop at the dent line, particularly at the end of the dent line where there are extreme stress and strain concentrations and where cracking initiates. There are only small reductions in value between the maximum strains and the residual ones. The residual stress distributions are complex which make it hard to assess their influence on the residual strength of the plate. This topic is worthy for further study.

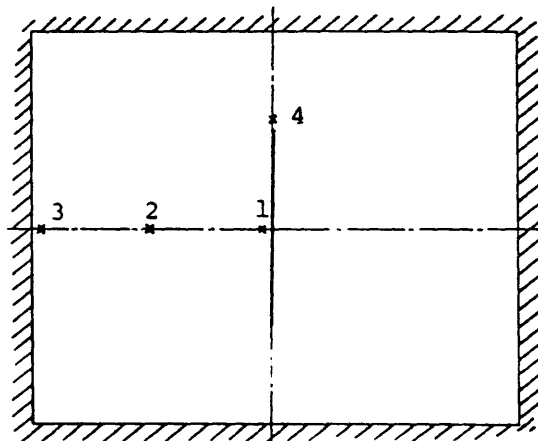
In the numerical simulation the side structure of the ship was simplified as a fully clamped rectangular plate. However, ship collision is a very complicated phenomenon which includes external mechanics dealing with motion of the collided ships and internal mechanics dealing with the deformation and, in some cases, destruction of ship structures. It is hard to establish the physical model which can be used in practical numerical simulation even just for the response of side structures of the struck ship. As collision causes extremely local damage, it is normally accepted that the response of the side structure of the ship can be studied by taking the side structure between two adjacent bulkheads, provided collision occurs halfway between these two bulkheads. For the side structures between the two bulkheads it is still difficult to determine the boundary conditions at the top and bottom sides because of the interaction between the side structures and deck structures, as well as interaction between side and bottom

structures. The effect of longitudinal and transverse stiffeners is another difficulty encountered. To study this sophisticated phenomenon step by step it was decided to adopt the fully clamped rectangular plate model in this thesis. The influence of in-plane sliding along the boundaries was investigated in the experiment reported in chapter 3, and in chapter 6 the influence of rotation about the boundary will be discussed. For future study this numerical approach can be developed by implementing the various boundary conditions and stiffeners.

In conclusion, the numerical model of the dynamic inelastic response of plates impacted by a rigid knife edge indenter is developed and correlates well with experimental results. The theory includes the influence of finite transverse displacements, axial restraints, bending moments, material elasticity and strain hardening. Numerical results are given of the plate impact test and small scale ship model collision test, which provides a full picture of the response of the clamped rectangular plate under dynamic load. It provides information on the impact force, deformation, stress and strain everywhere in the plate. Such data could not be obtained experimentally or by simple plastic formulations. The numerically predicted residual deformation, stress and strain can be used as an initial condition for subsequent load analysis in order to evaluate the influence of denting on the residual strength of the structure.

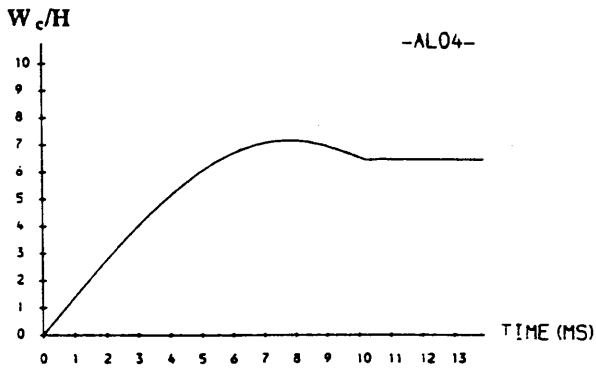


(a) Set-up

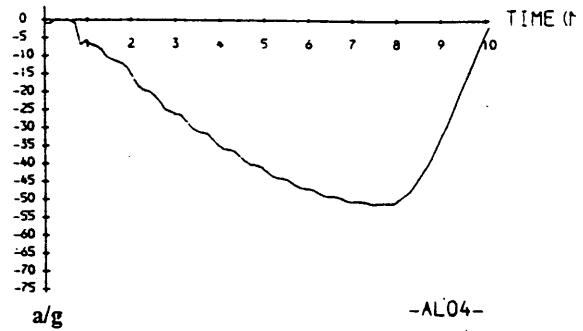


(b) Strain Gauges Distribution

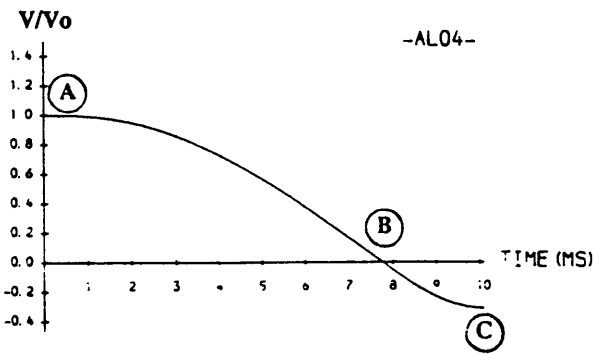
Fig. 4.1 Impact of Fully Clamped Rectangular Plate



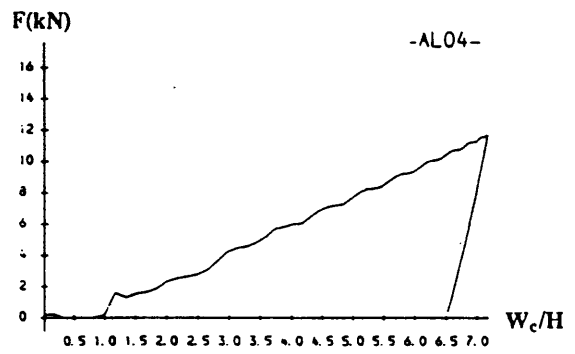
(A) CENTRAL DEFLECTION-TIME HISTORY



(C) ACCELERATION-TIME HISTORY OF STRIKER



(B) VELOCITY-TIME HISTORY OF STRIKER



(D) IMPACT FORCE-INDENTATION CURVE

Fig. 4.2 Overall response of impacted aluminium plate (-AL04-)

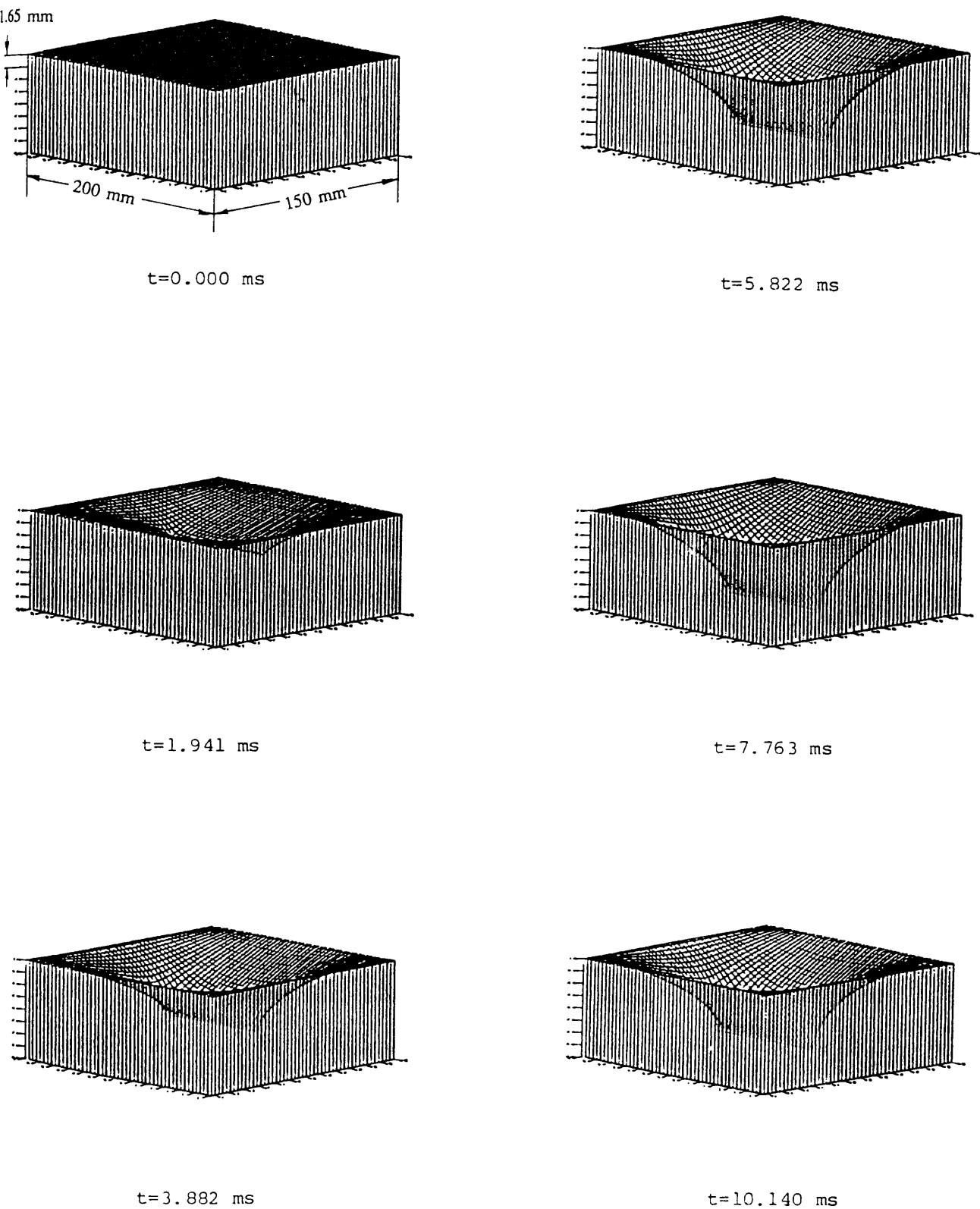


Fig. 4.3 Deformation Process of Plate (AL04) during Collision
(View from the Front Surface)

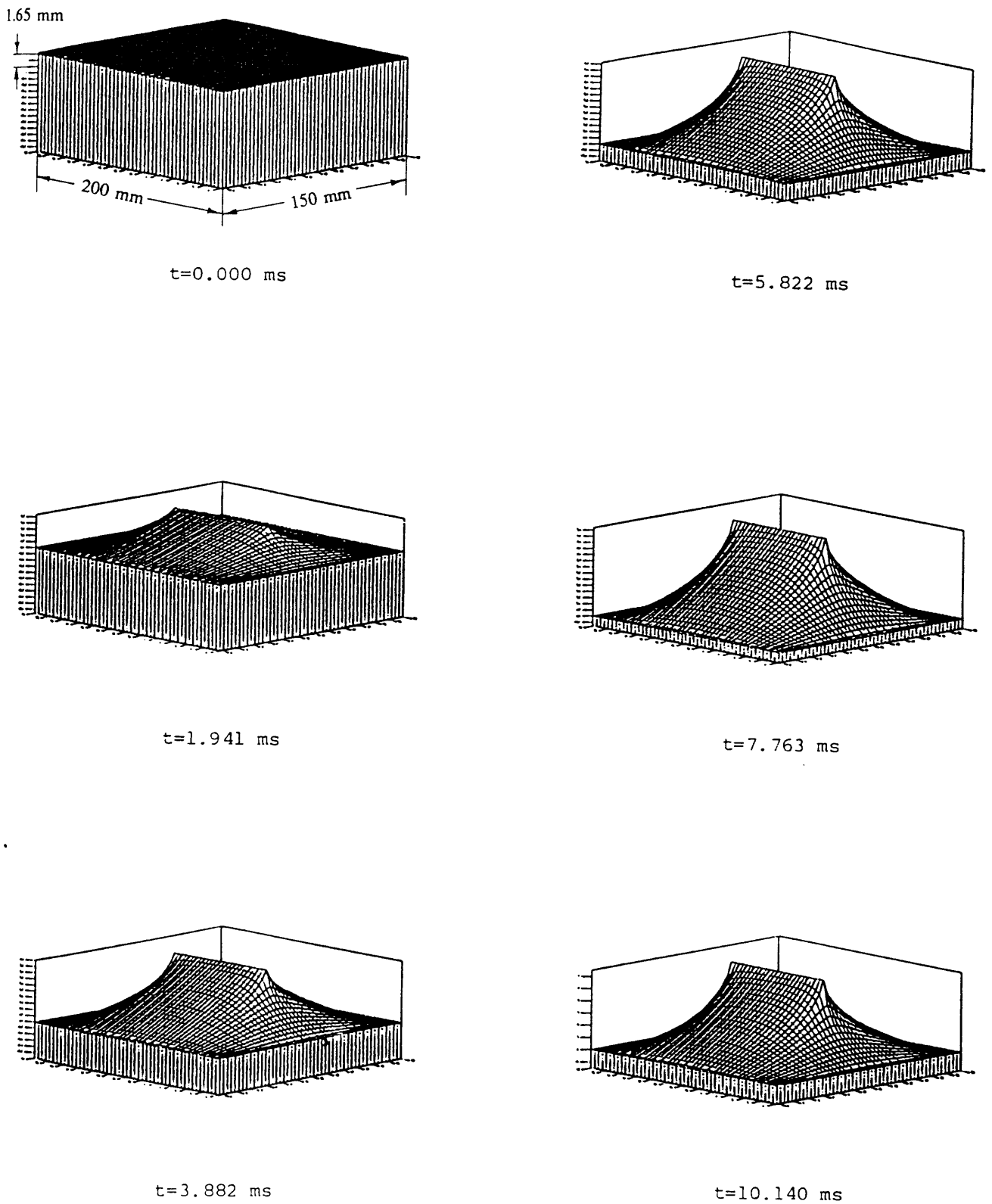
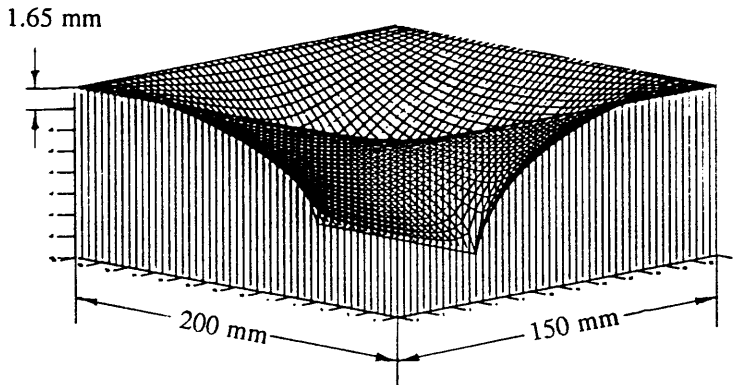
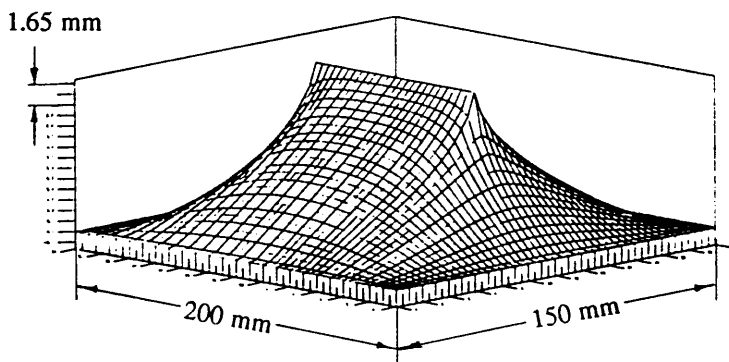


Fig. 4.4 Deformation Process of Plate (AL04) during Collision
(View from the Back Surface)



(A) THE MAXIMUM DEFORMATION PROFILE [FRONT SURFACE]

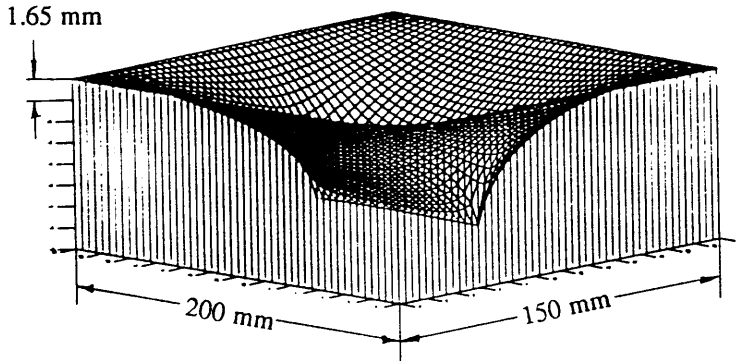
-AL04-



(B) THE MAXIMUM DEFORMATION PROFILE [BACK SURFACE]

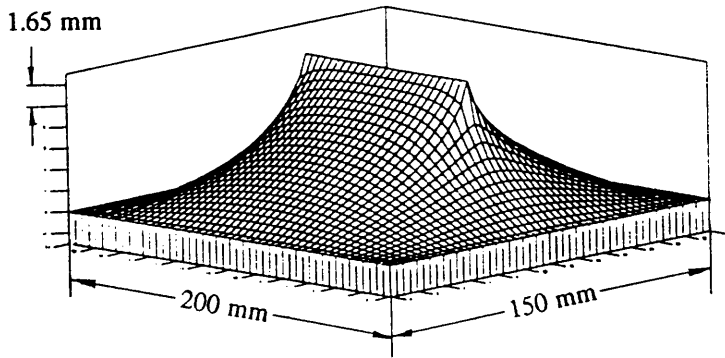
-AL04-

Fig. 4.5 The maximum deformation profiles of plate (-AL04-)



(A) THE RESIDUAL DEFORMATION PROFILE [FRONT SURFACE]

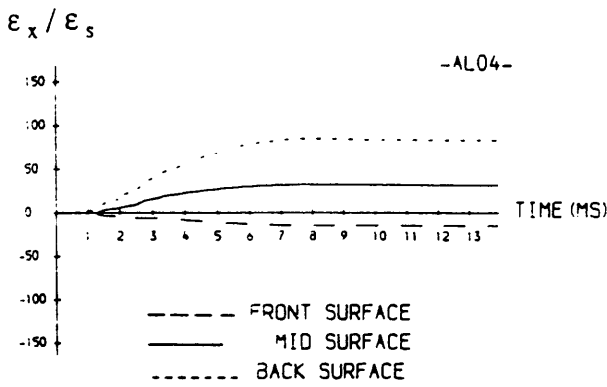
-AL04-



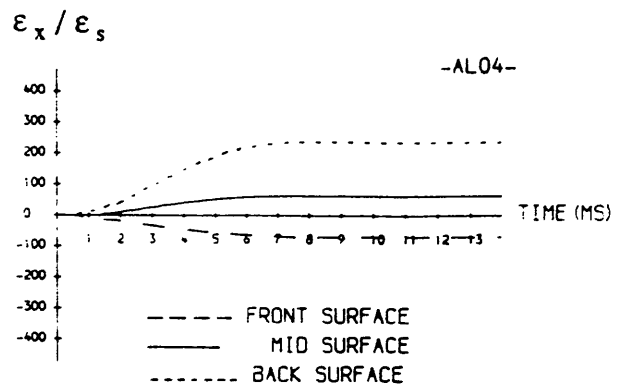
(B) THE RESIDUAL DEFORMATION PROFILE [BACK SURFACE]

-AL04-

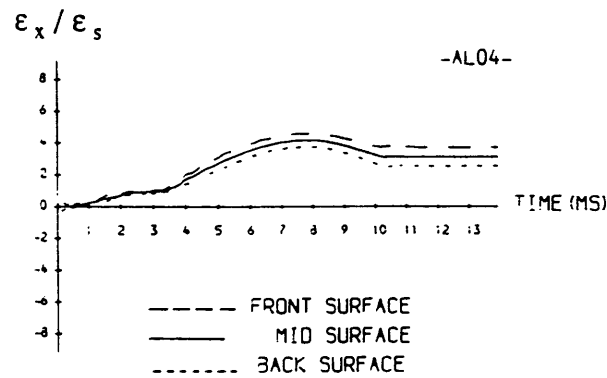
Fig. 4.6 The residual deformation profiles of plate (-AL04-)



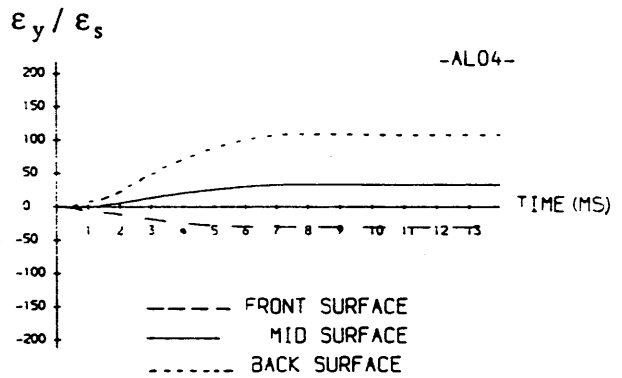
(A) STRAIN-TIME HISTORY (1)



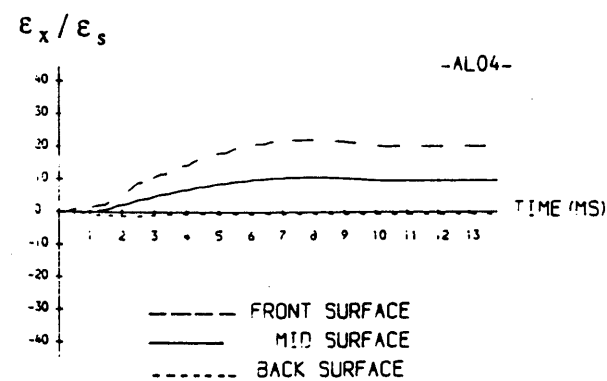
(D) STRAIN-TIME HISTORY (4)



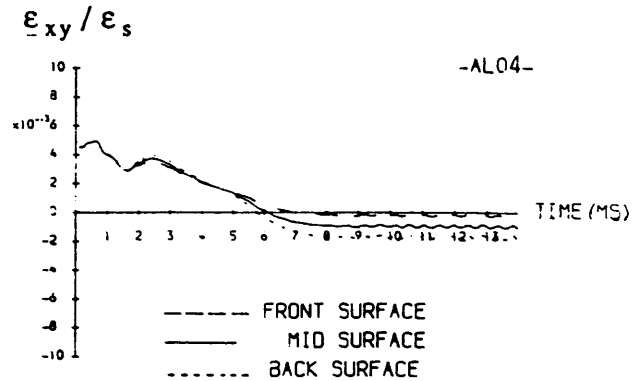
(B) STRAIN-TIME HISTORY (2)



(E) STRAIN-TIME HISTORY (4)



(C) STRAIN-TIME HISTORY (3)



(F) STRAIN-TIME HISTORY (4)

Fig. 4.7 Strain time histories of plate (-AL04-)
(ϵ_s - Static uniaxial yield strain)

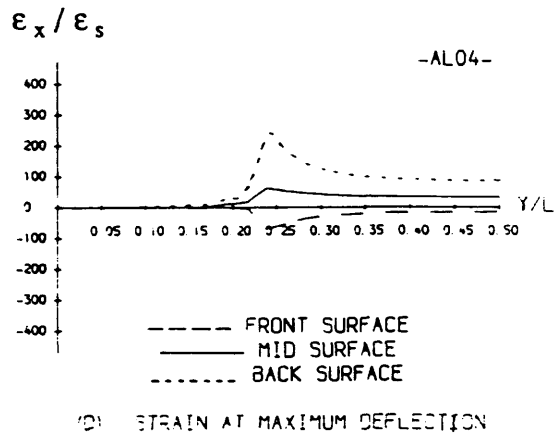
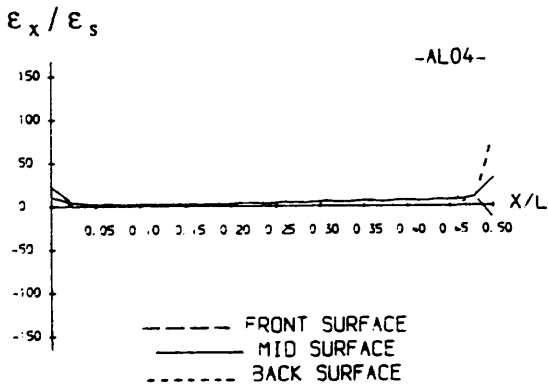
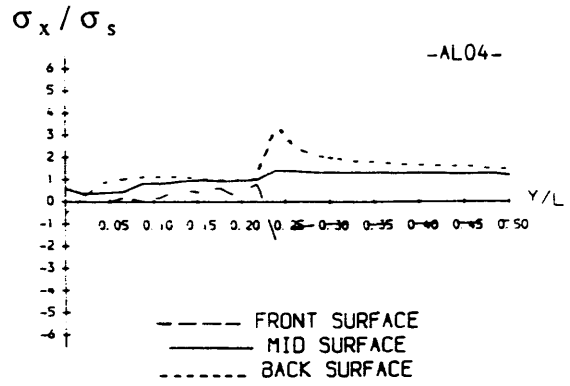
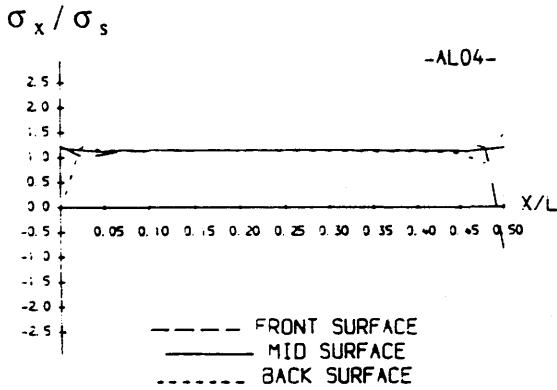


Fig. 4.8 Stress and strain distribution at maximum deflection
 σ_s - Static uniaxial yield strain, and
 ϵ_s - Static uniaxial yield stress.

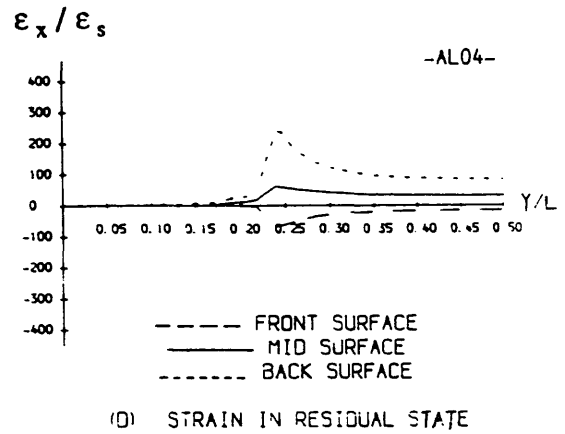
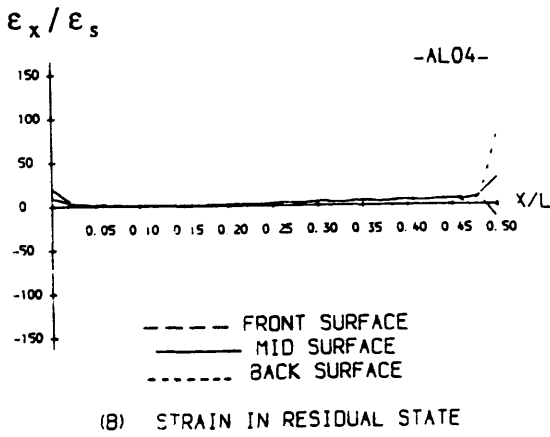
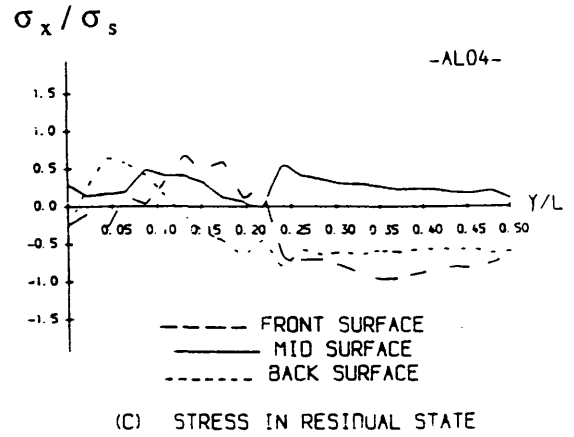
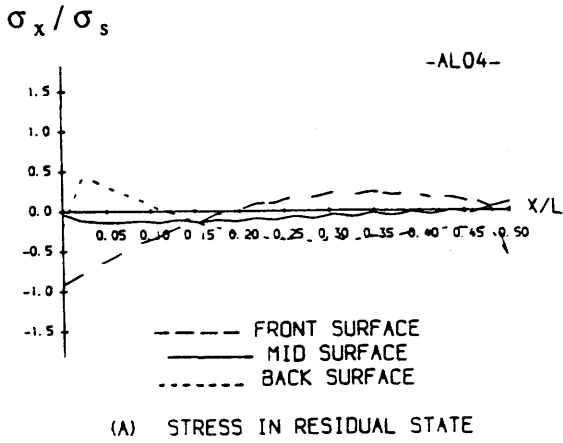
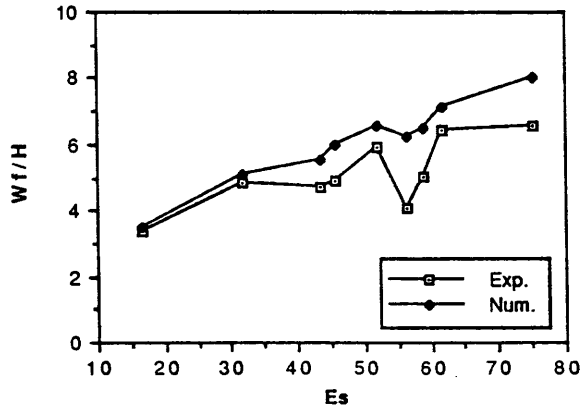


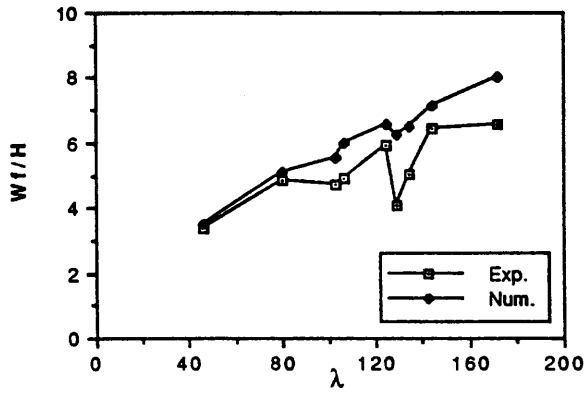
Fig. 4.9 Stress and strain distribution in residual state

σ_s - Static uniaxial yield stress, and

ϵ_s - Static uniaxial yield strain.

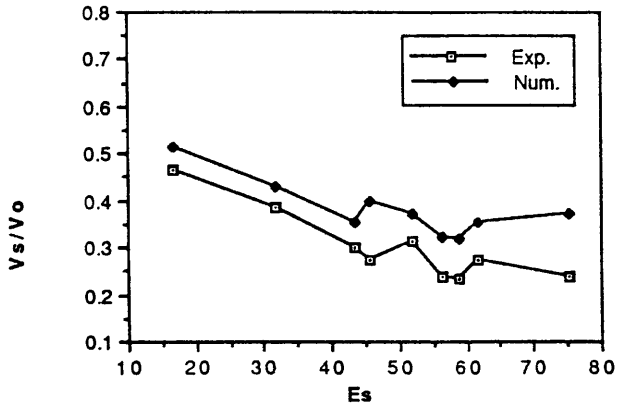


(a) Wf/H - Es curves

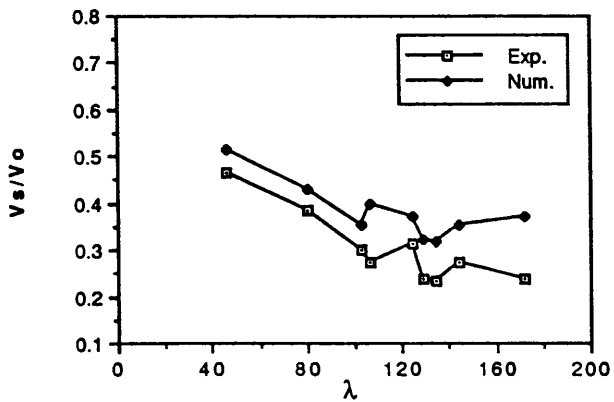


(b) Wf/H - lambda curves

Fig. 4.10 Comparison between test and numerical results on maximum permanent deflection for aluminium plates



(a) Vs/Vo - Es curves



(b) Vs/Vo - lambda curves

Fig. 4.11 Comparison between test and numerical results on rebound velocity of striker for aluminium plates

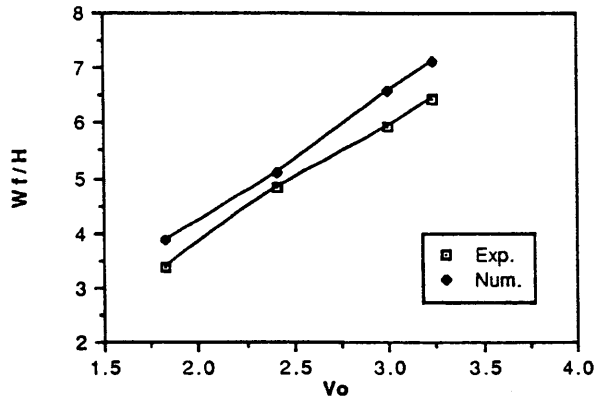
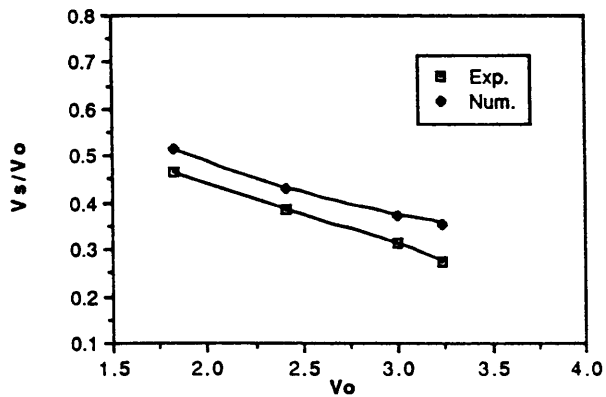
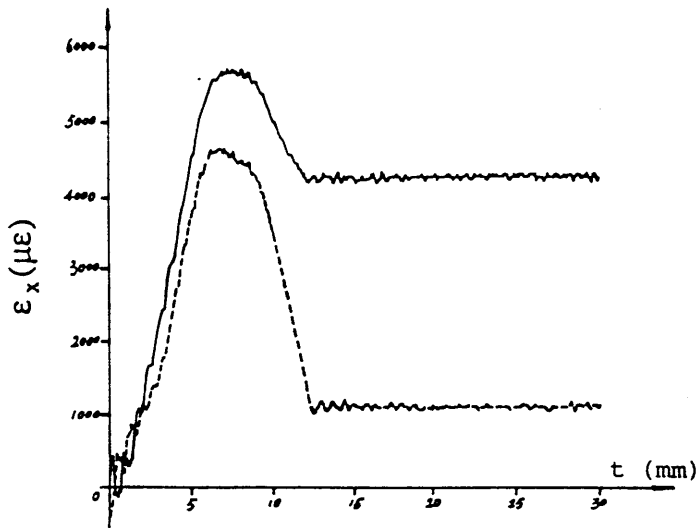
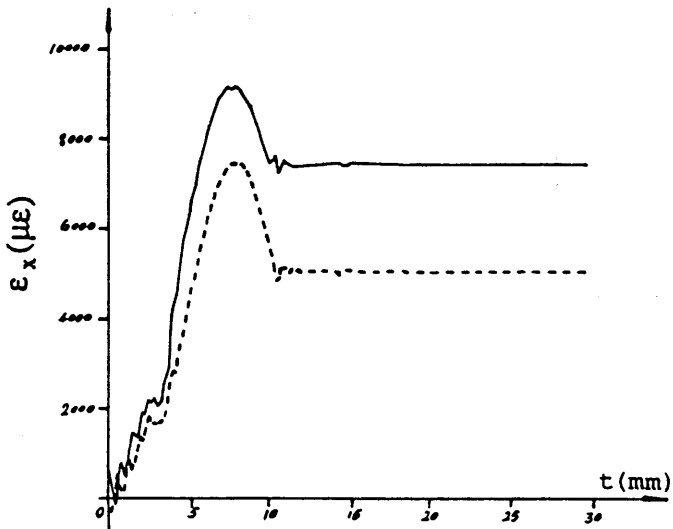
(a) Variation of Wf/H with impact velocity (V_o)(b) Variation of V_s/V_o with impact velocity (V_o)

Fig. 4.12 Correlation between test and numerical results on the influence of impact velocity for aluminium plates AL07 - AL10 ($L=250$ mm, $m_o=12.8$ kg).



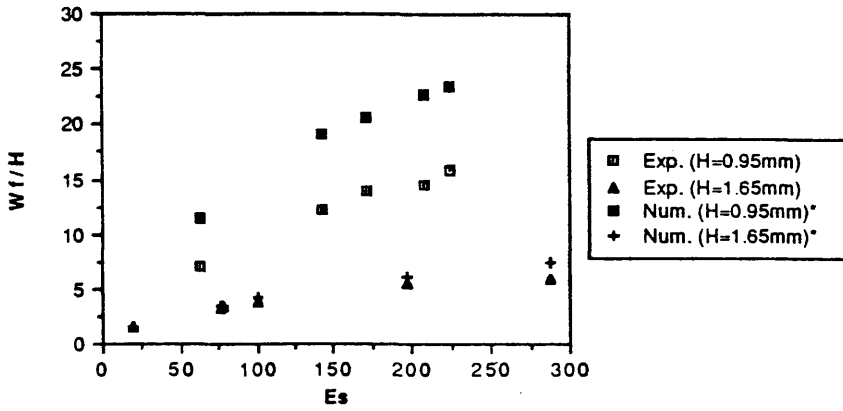
(a) Measured strain curves



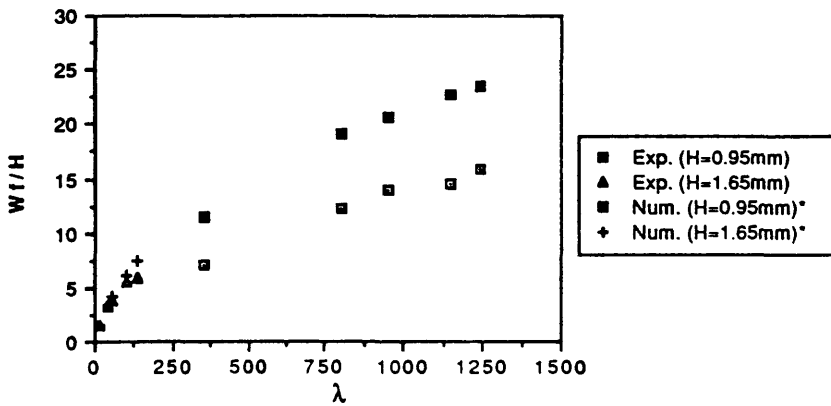
(b) Numerical predictions

Fig. 4.13 Comparison between test and numerical results on dynamic strains at point 2 of aluminium plate -AL04-

———— front surface
 - - - - - back surface

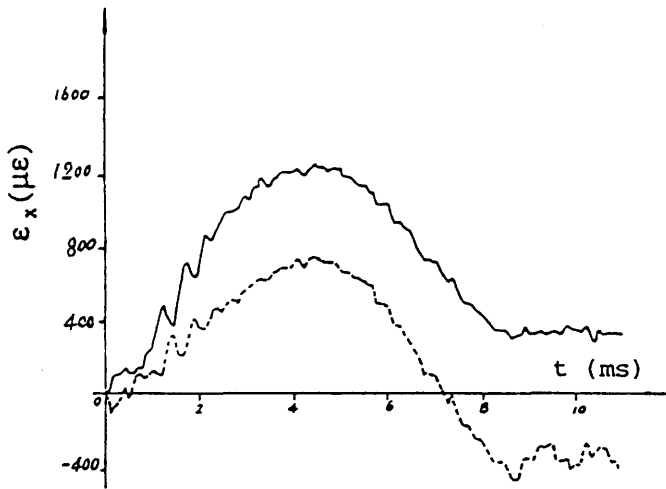


(a) $W_f/H - E_s$ relationship

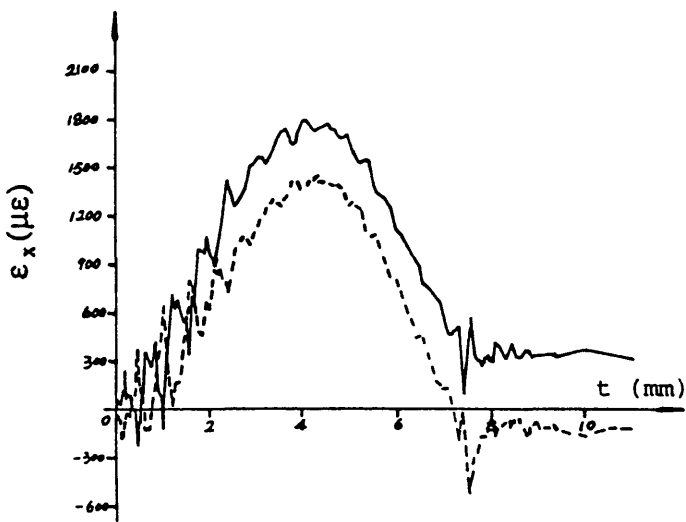


(b) $W_f/H - \lambda$ relationship

Fig. 4.14 Comparison between test and numerical results on maximum permanent deflection for steel plates
 * Dynamic yield stress/static yield stress=1.5



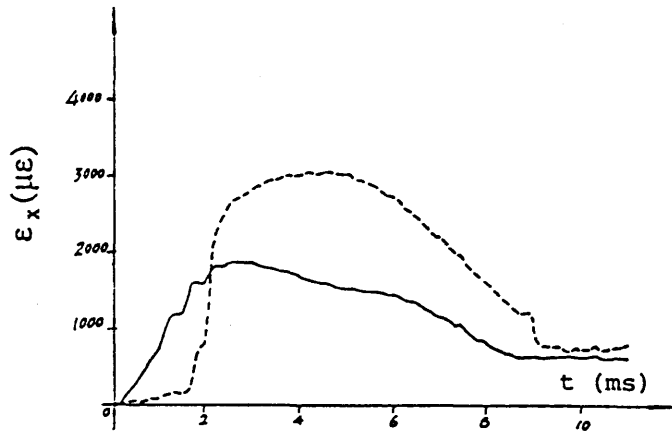
(a) Measured strain curves



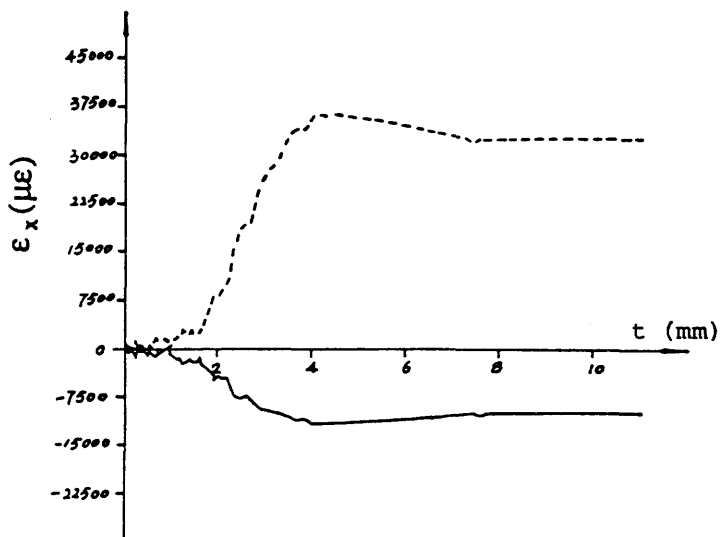
(b) Numerical predictions

Fig. 4.15 Comparison between test and numerical results on dynamic strains at point 2 of steel plate -ST01-

———— front surface
 - - - - - back surface



(a) Measured strain curves



(b) Numerical predictions

Fig. 4.16 Comparison between test and numerical results on dynamic strains at point 1 of steel plate -ST01-

———— front surface
----- back surface

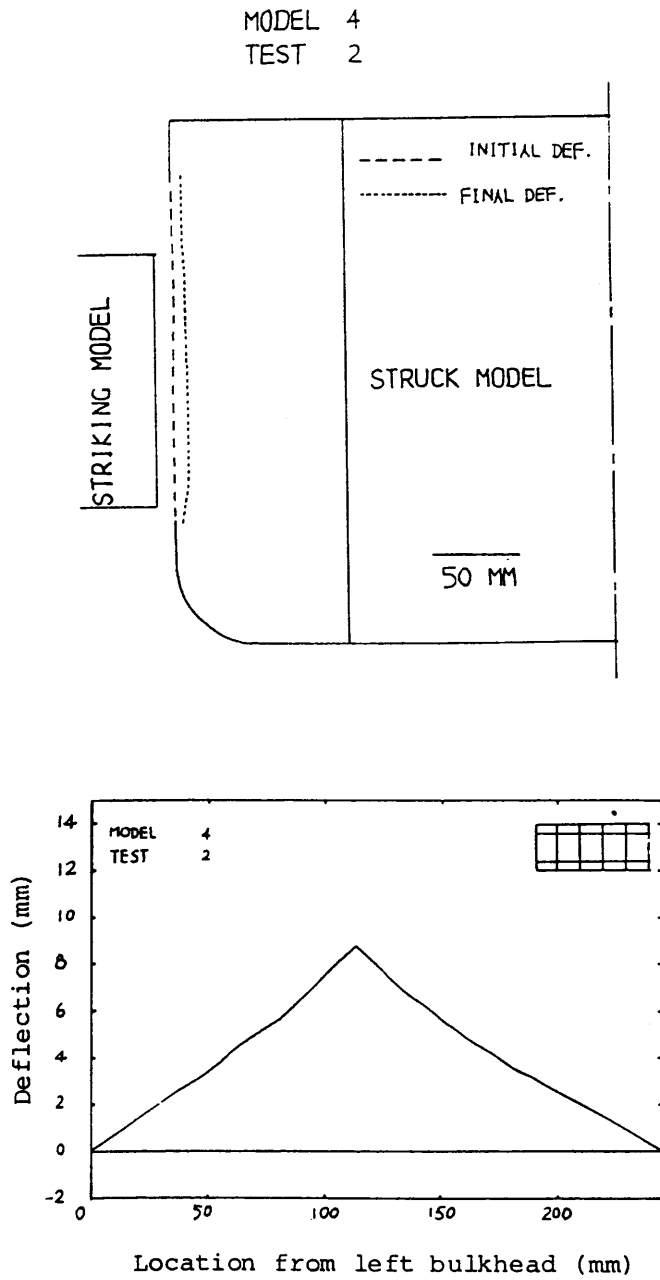
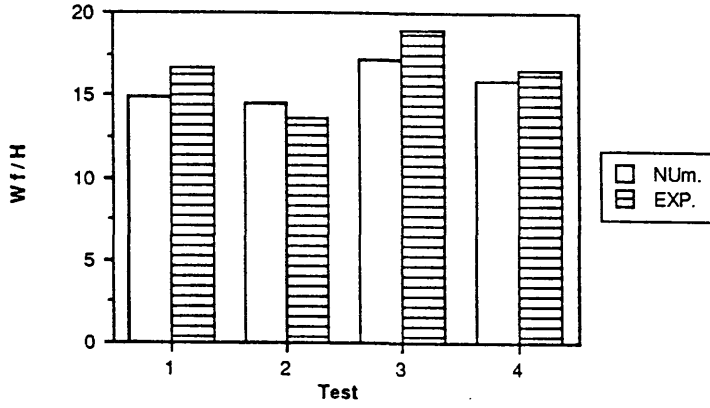
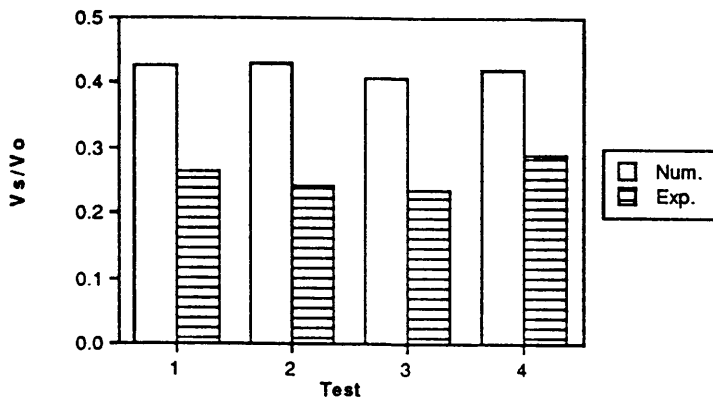


Fig. 4.17 Permanent deformation profiles of a tank in small scale ship model impact test



(a) Maximum permanent deflection



(b) Rebound velocity of striker

Fig. 4.18 Comparison of numerical and experimental results for dry test

Test	mo (kg)	Vo (m/s)
1	28.6	3.4
2	28.6	3.3
3	39.9	3.4
4	39.9	3.1

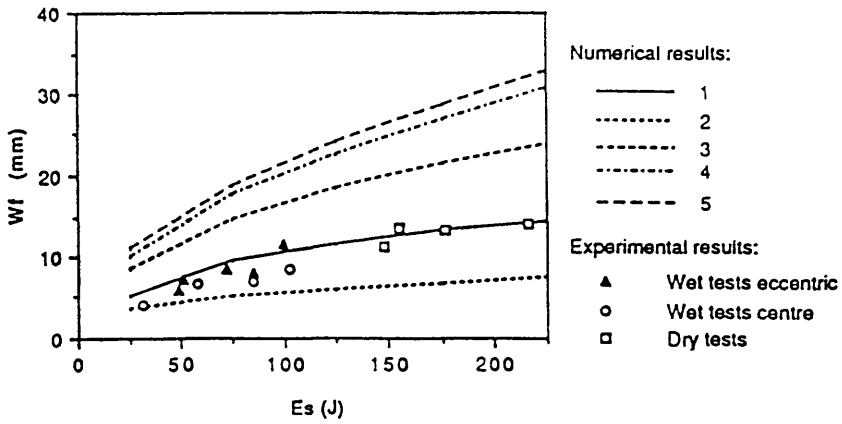


Fig.4.19 Comparison of theoretical and experimental results

- 1. Plate, elastic plastic strain hardening;
 - *2. Plate, rigid plastic;
 - *3. Plate strip, elastic/visco-perfectly plastic;
 - *4. Plate strip, elastic perfectly plastic;
 - *5. Beam elastic perfectly plastic.
- (*: results from the paper of Samuelides, 1984)

CHAPTER FIVE

PARAMETRIC STUDIES

Using the numerical program developed in chapter 2 parametric studies are carried out in this chapter to investigate the effects of several important parameters, such as mass and impact velocity of the striking vessel, length of vertical bow, thickness of the struck side plate, plate length and width. The critical speed of the ship is also investigated.

5.1 Mass and Impact Velocity of the Striker

To investigate the effects of mass and impact velocity of the striker on the structural response of the struck plate, different combinations of mass and impact velocity are chosen to evaluate the impact loading on the struck plate of the same properties. The structural parameters used are listed in Table 5.1. The masses assumed are 20.0, 28.6, 39.9 kg respectively and three impact velocities are 2.0, 2.5 and 3.4 m/s.

Table 5.1 Parameters of struck plate

Plate Dimensions	mm ³	243*255*0.8
Mass Density	kg/m ³	7800
Young's Modulus	GPa	207
Tangent Modulus	MPa	207
Poisson's Ratio		0.33
Yield Stress	MPa	217
Length of impact line	mm	117

For the three different mass and impact velocity assumed and structural parameters listed in Table 5.1, the non-dimensional maximum deflection of the plate, the rebound velocity, the collision duration and the maximum impact force are shown in Fig. 5.1.

The maximum deflection of the plate increases almost linearly with the increase of impact velocity of the striker (Fig. 5.1(a)). The larger the mass of the striker, the larger is the maximum deflection.

The non-dimensional rebound velocity of the striker decreases as the impact velocity increases. For the same impact velocity, the non-dimensional rebound velocity decreases as the mass of the striker increases (Fig. 5.1(b)). For a given structure, the maximum elastic strain energy is constant. When the external impact energy is much larger than the maximum elastic strain energy, more input energy is dissipated in plastic deformation of the plate.

It can be seen from Fig. 5.1(c) that the collision duration decreases as the impact velocity increases and as the mass of the striker decreases. For a large striking mass and small impact velocity, the collision duration is much larger than the structural elastic period, which often occurs in most of the real ship collision and is treated as a quasi-static problem. In contrast, for a small striker mass and large impact velocity, the collision duration is much smaller than the structural elastic period, e.g., a bullet hitting a plate.

From Fig. 5.1(d) it is clear that the maximum impact force becomes large when the impact velocity increases. The larger the mass of the striker, the larger the maximum impact force. It should be noted that the increase in F_m/M_o caused by increase in mass of the striker at high impact velocity is much larger than that at low impact velocity with the same increase in mass of the striker.

5.2 Length of the Vertical Striker

How does the length of the vertical striker affect the dynamic behaviour of the plate? This will be discussed in this section, in which five cases of different length of the striker are checked. The variations of structural response parameters with the length of the striker are as shown in Fig. 5.2, including maximum deflection, rebound velocity of the striker, maximum impact force, collision duration, maximum strain and total energy absorbed by the plate.

From Figs. 5.2(a), 5.2(c) and 5.2(d), it can be seen that the maximum deflection and collision duration decrease with the increase of the length of the striker, while the maximum impact force increases as the length of the striker increases. When the length of the striker is about half of the plate width, the rebound velocity reaches its maximum value (Fig. 5.2(b)). Figure 5.2(f) shows the initial impact energy distribution between the plate and the striker. When the length of the striker is about half of the plate width, the total energy absorbed by the plate has minimum value - approximately 76% of the initial impact energy. The energy absorbed by the plate is consumed by plastic deformation during collision as well as elastic vibration after collision.

It should be pointed out that it is not the maximum deformation but deformation distribution that reflects the amount of energy absorbed by the plate. In Fig. 5.2(a), when L_d/B equals 0.8, even though the maximum deflection is small, the energy absorbed is large due to the long length of the denting line (Fig. 5.2(f)).

From the point of view of failure, the results in Fig. 5.2(e) are quite interesting. With the increase of length of the striker, x-strain at the central point (point 1) decreases. However, the x-strain and y-strain at the end of the dent line (point 4) have their minimum values when L_d/B is 0.5. For the given aspect ratio of the plate, the x-strain is larger than the y-strain at the end of the dent line. The fact that the small value L_d/B

leads to the high level of strains at the end of the dent line does not necessarily mean that the plate suffers more severe damage on the whole, but that the damage is more local. From a practical background, the rupture of the ship plate results in the spillage of liquified gas cargo or chemical substance. If we define the critical speed of the ship according to the failure of the ship plate, we must take into account the effect of the length of contact between two colliding ships.

5.3 Plate Thickness

Plate thickness is an important factor which affects the strength of the plate in collision. Three different thickness (0.8, 1.6 and 2.4 mm) are used to demonstrate the influence of thickness on the structural response under the same impact conditions.

Figure 5.3 shows the non-dimensional maximum deflection of the plate, the rebound velocity of the striker, the collision duration and the maximum impact force respectively. It is evident from Fig. 5.3(a) that the maximum deflection of the plate decreases as the plate thickness H increases. As pointed out in 4.1.1, the rebound velocity to some extent reflects the amount of elastic strain energy of the plate. When the plate thickness increases the maximum elastic strain energy increases accordingly. This phenomena can be explained by Fig. 5.3(b), that is, the rebound velocity of the striker increases with increase in the plate thickness.

From Figs. 5.3(c) and (d), it can be seen that with increase of the plate thickness the non-dimensional collision duration increases but the non-dimensional maximum impact force decreases. However, it should be noted that the actual collision duration decreases and the actual maximum impact force increases, with increase of the plate thickness. This is because the elastic vibration period T_e and the limit plastic bending moment M_o are proportional to $1/H$ and H^2 respectively.

In Figs. 5.4, 5.5 and 5.6, the strain-time histories for three different plate thickness cases are plotted. For all the cases the strains located at the central point (point 1) and at the boundary (point 3) are larger than those at the quarter span (point 2). At the central point the strain-time curves for different thickness have the same character so that the strain at the back and mid-surfaces of the plate are tensile, while those at the front surface are compressive (Figs. 5.4(a), 5.5(a) and 5.6(a)). It can also be observed that the thicker the plate the earlier the strains start to response.

At the boundary (point 3) the strains at the front and at the mid-surfaces of the plate are tensile, while at the back surface they are compressive (Figs. 5.4(c), 5.5(c) and 5.6(c)). The absolute values of compressive strains at the back surface increase with the plate thickness, and the strains are more or less tensile for the very small plate thickness (Fig.5.4(c)).

The strains at the quarter span (point 2) are shown in Figs.5.4(b), 5.5(b) and 5.6(b). The strains at the back surface are a little smaller than those at the mid-surface and these at the front surface are a little larger than those at the mid-surface. For the small plate thickness the strains at any surface of the thickness are tensile during impact, with almost the same value. For the large plate thickness the residual strain at the back surface may be compressive (Fig. 5.6(b)). This phenomena was observed in the impact test for the plate (see Fig. 3.16(b)).

5.4 Plate Length

In the study of the plate problem, aspect ratio is an important parameter for the behaviour of the plate. In this section, with fixed value of B (255 mm) and L_d/B (0.5), different values of L/B 0.5, 0.75, 1.00, 1.25 and 1.75 are adopted for the parametric studies.

The maximum deflection and rebound velocity of the striker increase with the increase of the plate length (see Figs.5.7(a) and 5.7(b)). The maximum impact force decreases with increase of the length of the plate (Fig. 5.7(c)). From Fig. 5.7(d) we can see that the non-dimensional time for maximum deflection and collision duration decrease with the increased plate length. It can be seen from Fig. 5.7(e) that the change of plate length has significant influence on the x-strain at the plate centre and at the end of the dent line. For the given value of the length of the striker and the plate width, the change of y-strain at the end of the dent line is not obvious when the plate length decreases. As the plate length increases, the energy absorbed by the plate becomes less, due to increase of the rebound velocity of the striker (Fig. 5.7(f)).

5.5 Plate Width

In the last section the influence of aspect ratio with fixed width (B) and value of Ld/B was studied. Here another case is discussed in which the plate length and the striker length are constant, but the width of the plate will change over a certain range, with ratio of B/L being 0.5, 0.75, 1.00, 1.25 and 1.50 respectively and ratio of Ld/B being 0.667, 0.444, 0.333, 0.267 and 0.222 correspondingly.

It is shown in Fig. 5.8 that as the width of the plate increases the maximum deflection and rebound velocity of the striker increase (see Figs 5.8(a) and (b)), but the maximum impact force and ratio of collision duration and elastic period decrease (see Figs.5.8(c) and (d)). With regard to maximum strain (Fig. 5.8(e)), when B/L changes from 0.50 to 1.0, the value of non-dimensional strain in the y-direction at the end of the dent line decreases from 150 to 55. For the x-strain at the same point there is a slight decrease in value. However, the x-strain at the plate centre increases a little with the increase of the plate width. It is evident from Fig. 5.8(f) that the energy absorbed by the plate becomes less as the width increases, especially when the change of B/L ranges from 0.50 to 1.00.

5.6 Critical Speed of Ship

The maximum strains which occur when a longitudinally framed tanker is struck by a rigid bow are presented in this section. The critical speed of the bow is then calculated on the basis that the maximum strain of the side shell reaches a certain value. The tanker examined is one of those which had been considered for the full scale tests planned by the US Coast Guard [Van Mater et al, 1980]. This tanker was checked by Samuelides [1984] for critical speed using a beam structural model.

To make comparisons with the prediction of Samuelides [1984], the same structural and impact data are used. A mean thickness for the tank plating was adopted to account for the effect of the longitudinals. The adoption of mean thickness is based on the area of the equivalent plate being equal to that of the stiffened plate. This assumption is only applicable to the collision in which the membrane response is dominant.

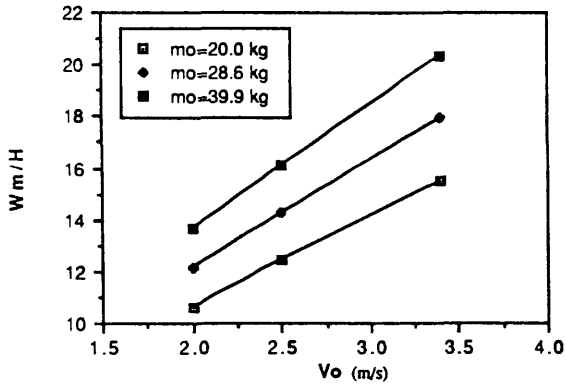
As indicated in chapter 4, severe stress and strain concentration occurs at the end of the dent line. Using the numerical program the strain component time histories in the vicinity of the failure point, viz. the end of the dent line, are obtained. It can be seen from the numerical results that the in-plane shear strain at the end of the dent line is extremely small and can be neglected. Therefore, the strains in x and y directions are principal strains, and the failure point is in the state of bi-axial tension.

It is assumed that rupture of the plate occurs when the larger one of the maximum x-strain and y-strain reaches the static uni-axial rupture strain of the material. Relation between the maximum strain and impact velocity is shown in Fig. 5.9, in which different values of vessel mass are examined. Taking a rupture strain of 30%, a critical speed corresponding to different displacements of the striking vessel can be obtained.

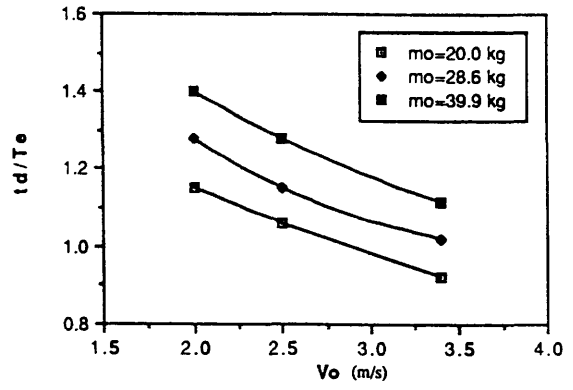
From Fig. 5.9, the curves of critical speed versus displacement of the striking vessel are also obtained and are plotted in Fig. 5.10. The predictions of Jones and Samuelides are plotted in Fig. 5.10 for comparison.

It should be stressed that the three curves in Fig. 5.10 for critical speed rely on different methods. In Jones' method, a rigid perfectly plastic beam with fully clamped supports across a span $2L_b$ subjected to a concentrated load P_c at the mid-span was considered. The effective stress was taken as the mean value of the yield and ultimate stresses. Basically, this method is an extension of Minorsky's method. Samuelides used a model for coupling the structural dynamic and rigid body response of the colliding ships. The structural type of the struck ship is beam or plate strip. The rupture strain adopted was 0.1. However, the strain analysis of the impacted plate indicated that even though the rupture strain was assumed to be 30%, the critical speed is still smaller than those calculated by the above two methods. As a more severe situation was considered in some detail, the critical speed obtained here tends to be conservative, compared with those of the other two.

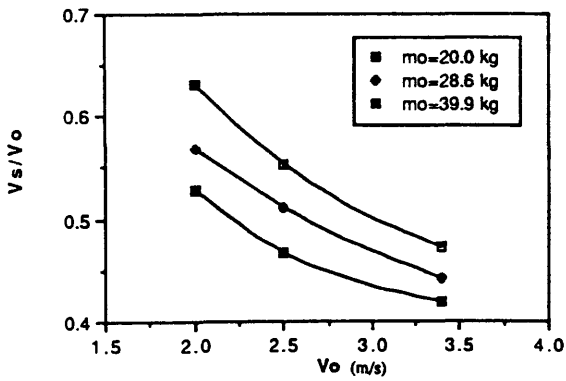
The failure criterion assumed in the above case is that the larger one of the maximum x-strain and y-strain reaches the static uniaxial rupture strain. As indicated in the literature review, the mechanism of crack failure is not fully understood so far, therefore it is extremely difficult to select a failure criterion for the given problem. When further research is carried out on this specific topic, the criterion assumed above should be replaced by a more appropriate one.



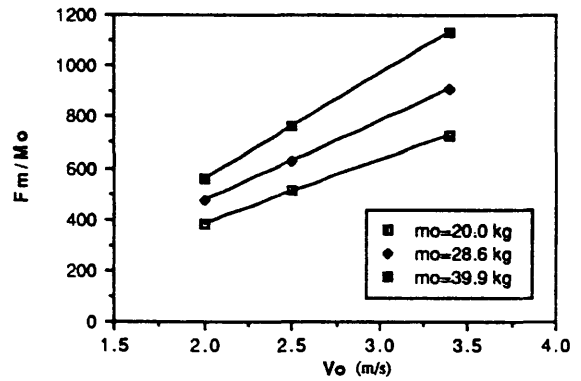
(a) Maximum Deflection



(c) Collision Duration

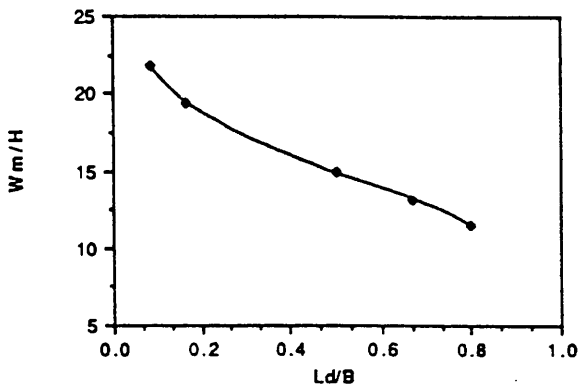


(b) Rebound Velocity of Striker

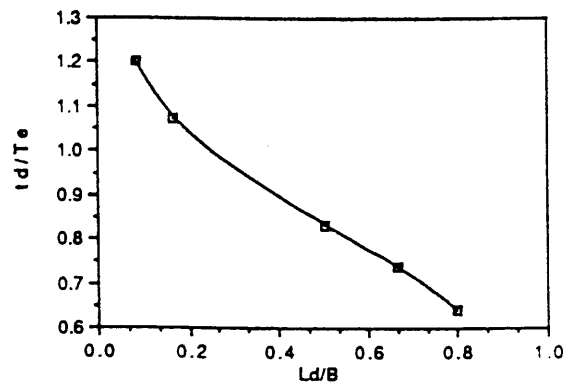


(d) Maximum Impact Force

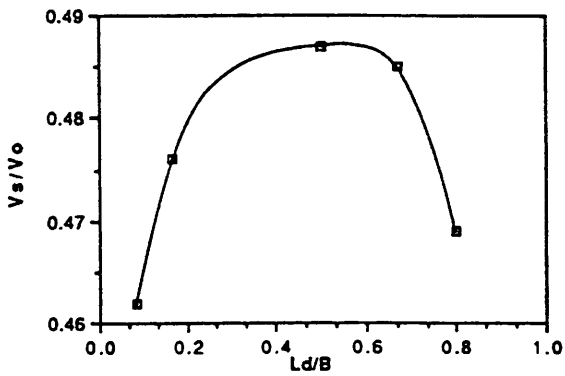
Fig. 5.1 The influence of mass and impact velocity of striker on structural response



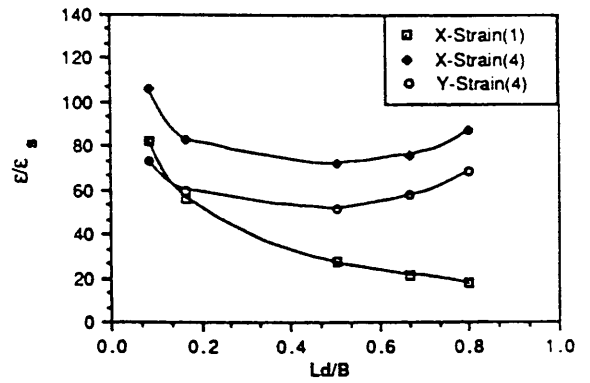
(a) Maximum deflection



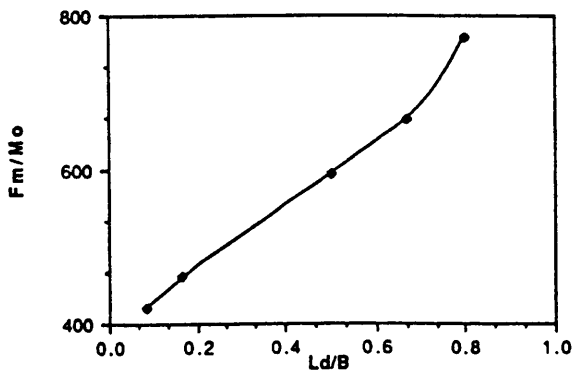
(d) Collision duration



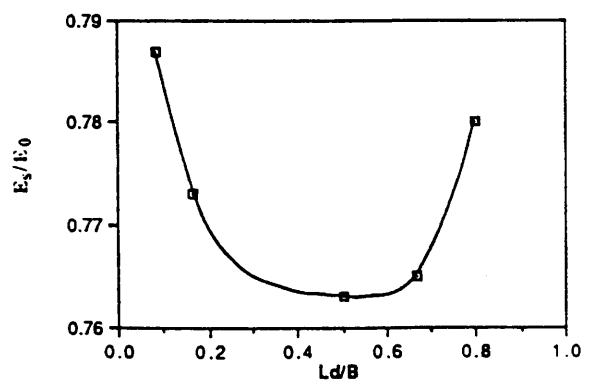
(b) Rebound velocity of striker



(e) Maximum strains

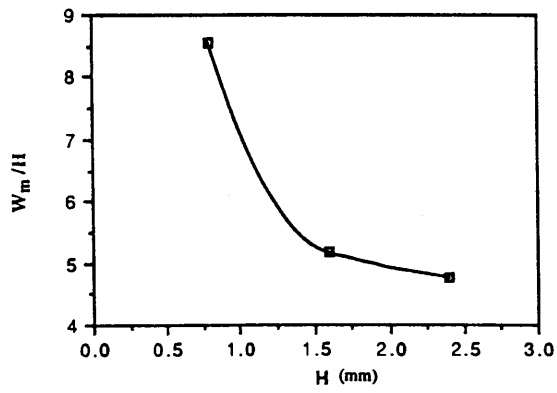


(c) Maximum impact force

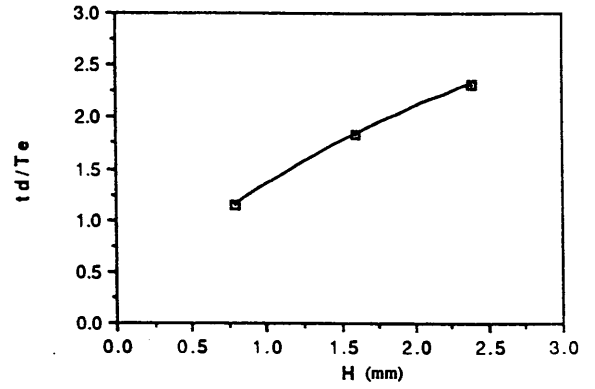


(f) Energy absorbed by plate

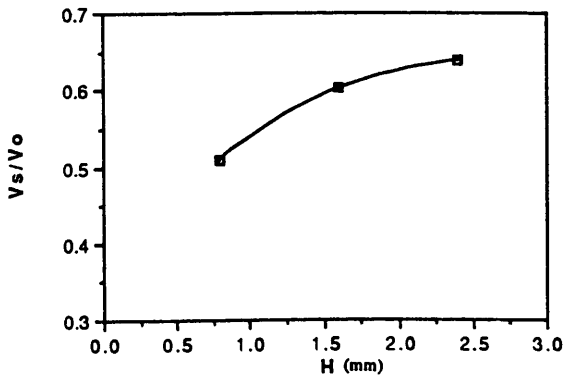
Fig. 5.2 The influence of vertical striker length on structural response



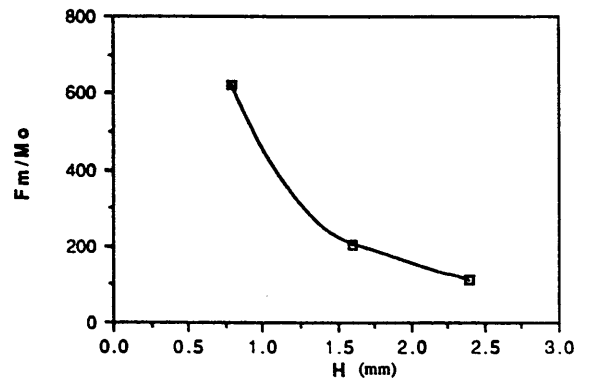
(a) Maximum Deflection



(c) Collision Duration

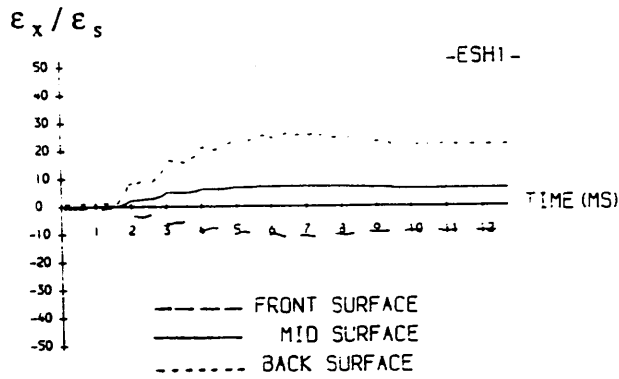


(b) Rebound Velocity of Striker

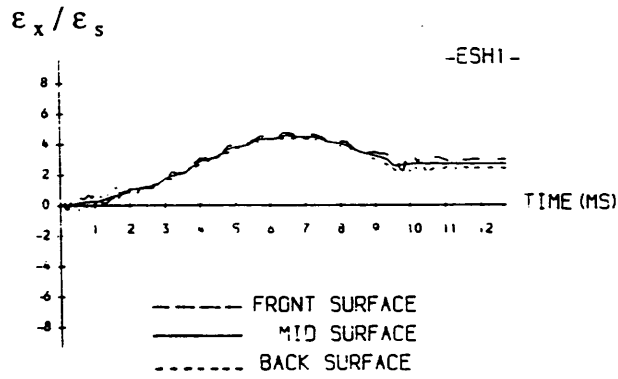


(d) Maximum Impact Force

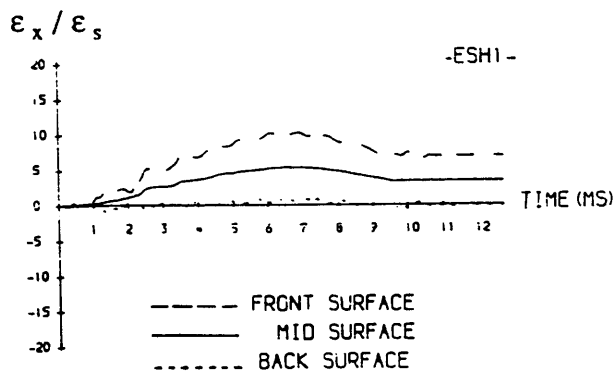
Fig. 5.3 The influence of plate thickness on structural response



(A) STRAIN-TIME HISTORY (1)

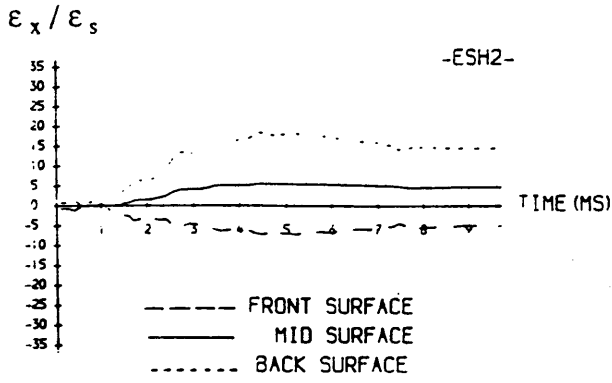


(B) STRAIN-TIME HISTORY (2)

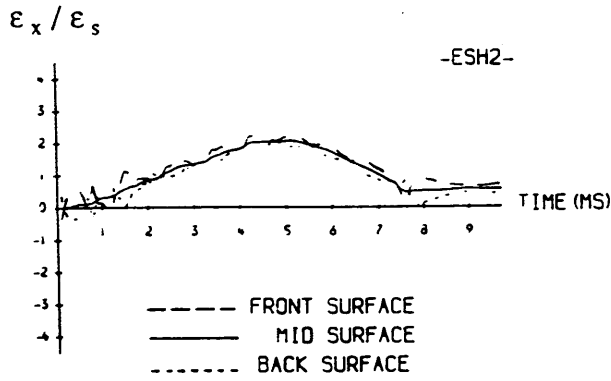


(C) STRAIN-TIME HISTORY (3)

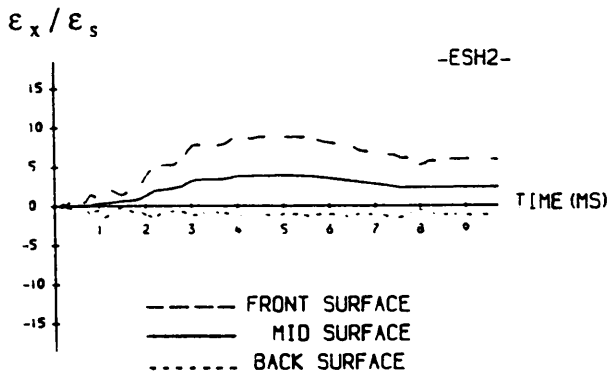
Fig. 5.4 Strain time histories of plate (-ESH1-)
 (ϵ_s - Static uniaxial yield strain)



(A) STRAIN-TIME HISTORY (1)

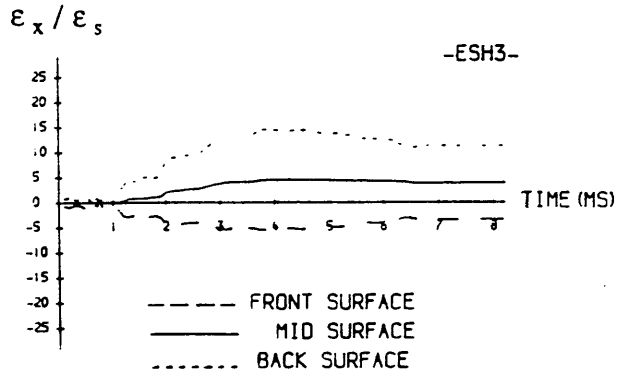


(B) STRAIN-TIME HISTORY (2)

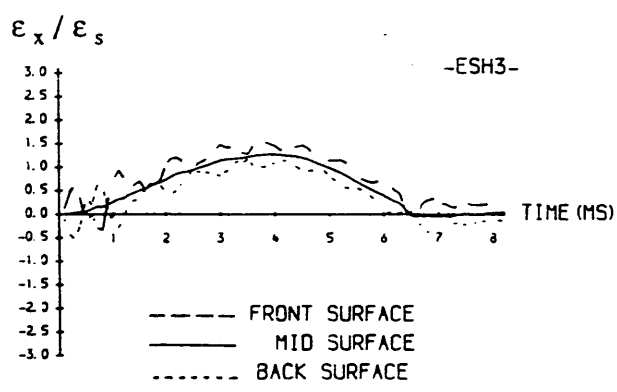


(C) STRAIN-TIME HISTORY (3)

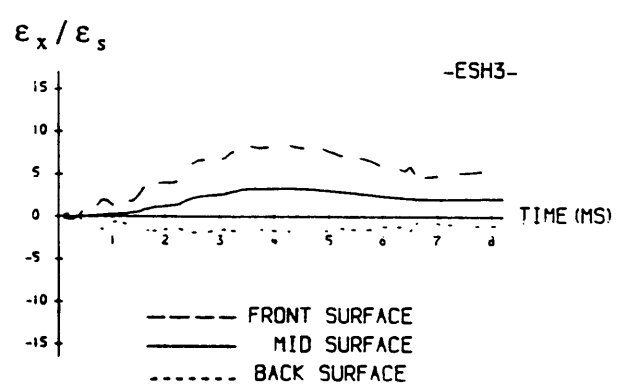
Fig. 5.5 Strain time histories of plate (-ESH2-)
 (ϵ_s - Static uniaxial yield strain)



(A) STRAIN-TIME HISTORY (1)

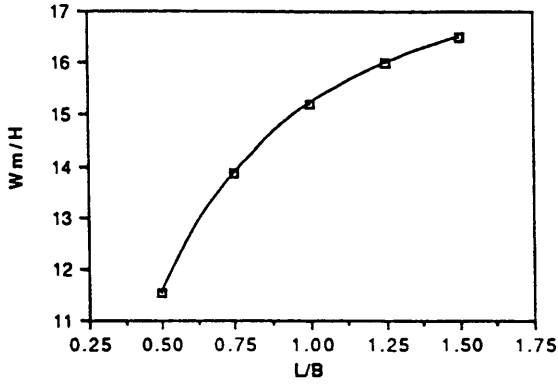


(B) STRAIN-TIME HISTORY (2)

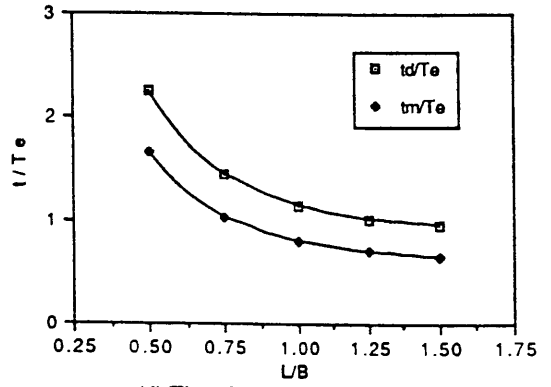


(C) STRAIN-TIME HISTORY (3)

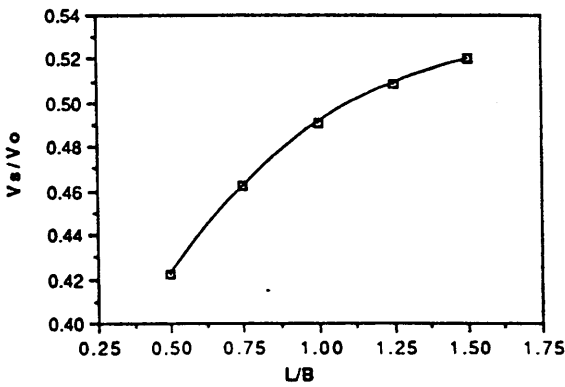
Fig. 5.6 Strain time histories of plate (-ESH3-)
 (ϵ_s - Static uniaxial yield strain)



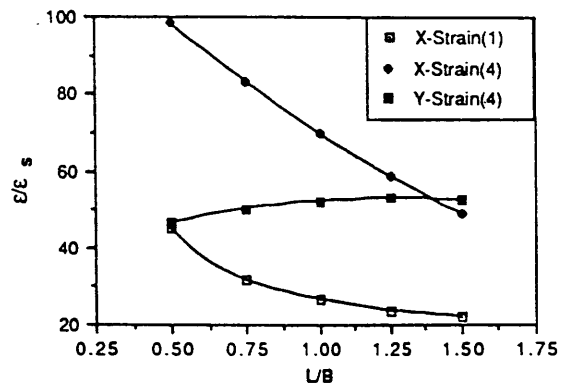
(a) Maximum deflection



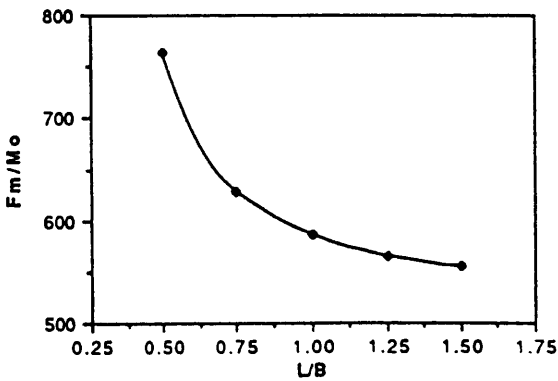
(d) Time for maximum deflection and collision duration



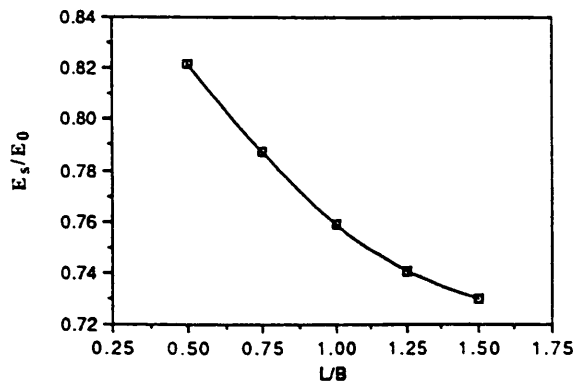
(b) Rebound velocity of striker



(e) Maximum strains

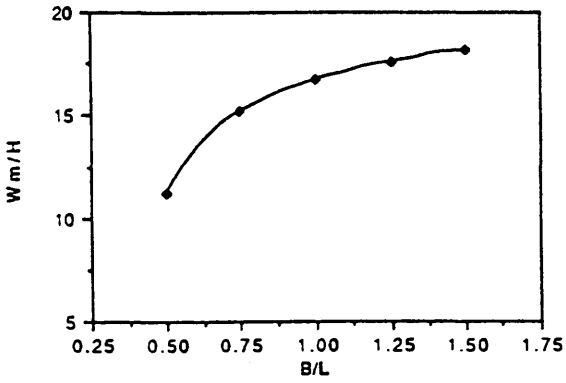


(c) Maximum impact force

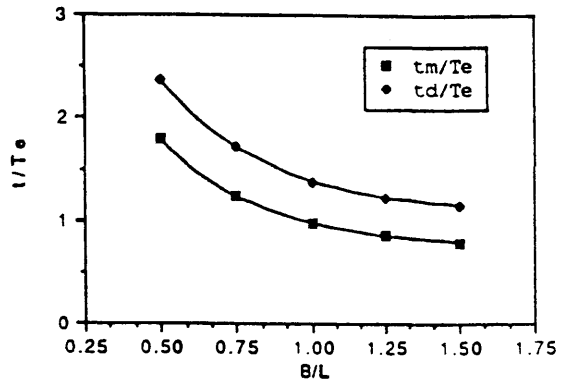


(f) Energy absorbed by plate

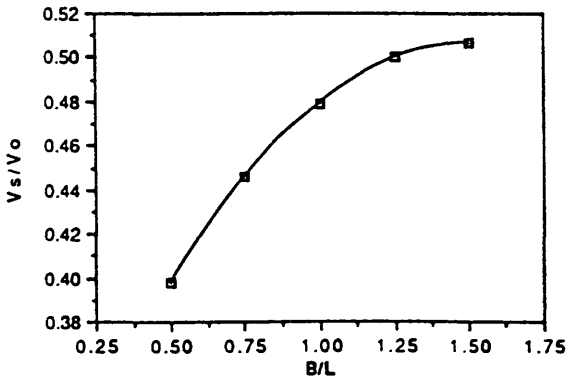
Fig. 5.7 The influence of plate length on structural response



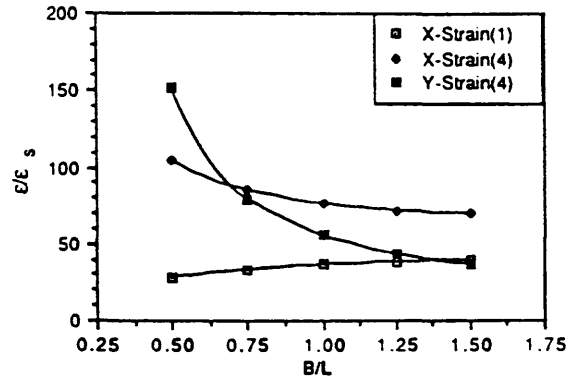
(a) Maximum deflection



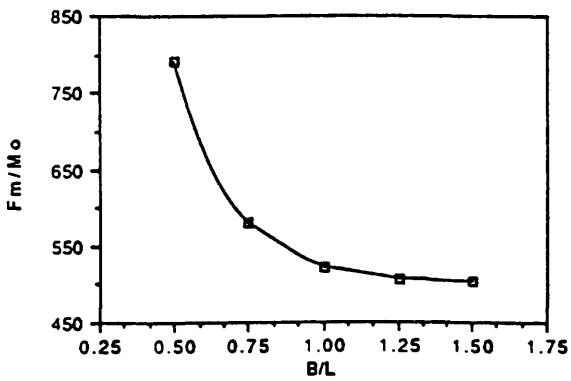
(d) Time for maximum deflection and collision duration



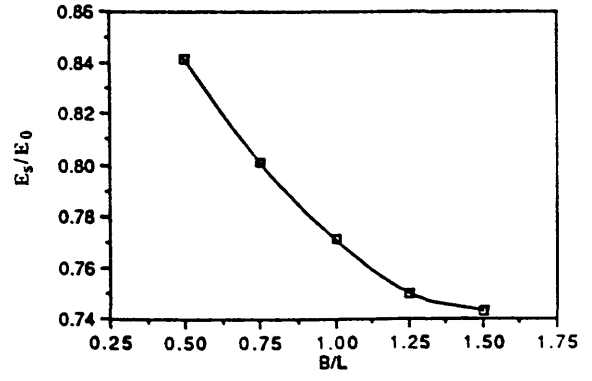
(b) Rebound velocity of striker



(e) Maximum strains



(c) Maximum impact force



(f) Energy absorbed by plate

Fig. 5.8 The influence of plate width on structural response

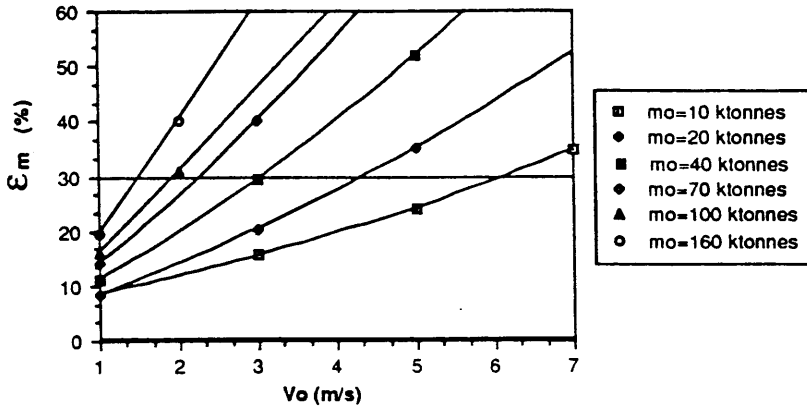


Fig. 5.9 Maximum strains arising from rigid bow impacts on the side of the tanker

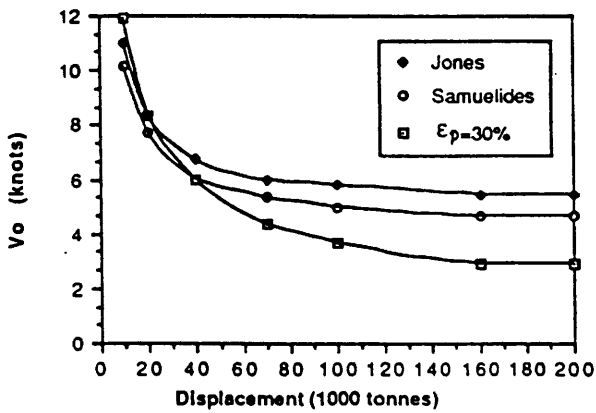


Fig. 5.10 Critical speeds for a tanker struck by a rigid bow

CHAPTER SIX

RIGID PERFECTLY PLASTIC METHOD

6.1 Introductory Remarks

To predict the extent of damage and response of a plate subjected to impact and to optimise the structural arrangements which may limit the damage, it is necessary to develop some simple analytical method for the preliminary design of the plate against impact. In this chapter the Rigid Perfectly Plastic Method has been developed to give the lower and upper bounds of the dynamic plastic solution to the impacted rectangular plate with finite deflections. The analytical solution obtained is compared with the experimental results and predictions of the numerical program in which elasto-plastic work-hardening material was assumed. The analytical solution provides formulae which can be used for the design of fully clamped plates against impact.

6.2 Formulation

6.2.1 Fully Clamped on Four Sides

The general form of the dynamic equation for a rectangular plate subjected to transverse pressure p is [Jones, 1971]:

$$\int_A (p - \mu \ddot{w}) \dot{w} dA = \sum_{m=1}^r \int_{C_m} (N_{ij} w - M_{ji}) \dot{w}_{,i} n_j dC_m + \int_A (M_{ji} - N_{ij} w) \dot{w}_{,ji} dA \quad (6.1)$$

where μ is mass per unit area of plate, M_{ji} and N_{ij} are the bending moment and membrane force per unit length respectively, C_m is the length of a boundary curve surrounding the sub-area. A_m and A is the total area of plate.

The first term on the right hand side of Eqn. (6.1) gives the internal energy dissipated at any travelling plastic "hinge", while the remaining term in Eqn. (6.1) is the energy dissipated in continuous deformation fields. Sawczuk's method [1964] for static behaviour of the plate rests on the assumption that the deformed plate can be subdivided into a number of rigid regions separated by s straight line hinges each of length l_m . Adopting this assumption, Eqn. (6.1) simplifies to:

$$\int_A (p - \mu \ddot{w}) \dot{w} dA = \sum_{m=1}^s \int_{l_m} (Nw - M) \dot{\theta}_m dl_m \quad (6.2)$$

where w is the transverse deflection, M and N denote the resultant moment and membrane force along the yield hinge, and θ_m is the rotation of adjacent rigid parts of the plate.

In the previous study [Jones, 1971] for the rectangular plates subjected to uniformly distributed impulsive loading, the deformation mode assumed for the plate is the one suggested by the well known collapse profile initially adopted by Wood [1961]. For a rectangular plate impacted by a knife edge indenter, the contact area between the plate and the indenter is a line. In this circumstance Wood's mode is reasonable. The plate can be divided into two regions I and II, shown in Fig. 6.1. The displacements are given:

$$w_I = \frac{W_{1c}(B_r \tan \Phi - x')}{B_r \tan \Phi} \quad \text{for region I} \quad (6.3a)$$

$$w_{II} = \frac{W_{1c}(B_r - y)}{B_r} \quad \text{for region II} \quad (6.3b)$$

where W_{1c} is the displacement at the centre of the plate.

The left hand side of Eqn. (6.2) is represented by J:

$$J = \int_{\Gamma} p \dot{w} dl + \int_A (-\mu \ddot{w}) \dot{w} dA \quad (6.4)$$

where Γ is dent line ($\Gamma = 2l_d$).

For the uniformly distributed impact loading along the dent line, the impact force is:

$$F = -m_0 \ddot{W}_{1c} \quad (6.5)$$

$$p = \frac{F}{2l'_d} \quad (6.6)$$

where m_0 is mass of the striker. J can be expressed as:

$$J = -\left[m_0 + \frac{2}{3} \mu B_r (2L_r - B_r \tan \Phi) \right] \dot{W}_{1c} \ddot{W}_{1c} \quad (6.7)$$

It is defined

$$D = (Nw - M) \dot{\theta}_m \quad (6.8)$$

where D is the dissipation function which reflects the internal energy dissipation per unit length of a hinge.

If the square yield criterion is chosen, then:

$$D = M_0 \left(1 + \frac{4w}{H} \right) \dot{\theta}_m \quad (6.9)$$

The total energy dissipation at the right hand of Eqn. (6.2) can be written as:

$$D_T = 8M_0 \left(\frac{L_r}{B_r} + \cot \Phi \right) \dot{W}_{1c} + 8M_0 \left(2\frac{L_r}{B_r} - \tan \Phi + \cot \Phi \right) \frac{W_{1c}}{H} \dot{W}_{1c} \quad (6.10)$$

Substituting (6.7) and (6.10) into (6.2) gives:

$$\ddot{W}_{1c} + hW_{1c} = d \quad (6.11)$$

where:

$$h = \frac{8M_0(2L_r - B_r \tan \Phi + B_r \cot \Phi)}{HB_r \left[m_0 + \frac{2}{3}\mu B_r(2L_r - B_r \tan \Phi) \right]} \quad (6.12)$$

$$\omega = \sqrt{h} \quad (6.13)$$

$$d = -\frac{8M_0(L_r + B_r \cot \Phi)}{B_r \left[m_0 + \frac{2}{3}\mu B_r(2L_r - B_r \tan \Phi) \right]} \quad (6.14)$$

$$\tan \Phi = \frac{L_r - l'_d}{B_r} \quad (6.15)$$

The solution to Eqn. (6.11) may be obtained which satisfies the following initial conditions:

$$W_{1c}(0) = 0 \quad (6.16)$$

$$\dot{W}_{1c}(0) = V_0 \quad (6.17)$$

The solution to Eqn. (6.11) is written as:

$$W_{1c}(t) = \frac{V_0}{\omega} \sin \omega t + \frac{d}{h}(1 - \cos \omega t) \quad (6.18)$$

The velocity and acceleration are:

$$\dot{W}_{1c}(t) = V_0 \cos \omega t + \frac{d}{\omega} \sin \omega t \quad (6.19)$$

$$\ddot{W}_{1c}(t) = -V_0 \omega \sin \omega t + d \cos \omega t \quad (6.20)$$

It may be shown that the duration of response of the plate is:

$$t_m = \frac{1}{\omega} \left[\tan^{-1} \left(-\frac{V_0 \omega}{d} \right) \right] \quad (6.21)$$

and that the maximum permanent deflection is:

$$W_{1m} = \frac{\sqrt{d^2 + (V_0 \omega)^2} + d}{h} \quad (6.22)$$

The initial acceleration is:

$$a_0 = d \quad (6.23)$$

and the maximum acceleration is:

$$a_m = -\sqrt{d^2 + (V_0 \omega)^2} \quad (6.24)$$

which occurs at the same time as the maximum deflection.

6.2.2 Fully Clamped on Two Sides

In the above rigid perfectly plastic modelling and numerical approach, the boundary

condition for the plate was assumed to be fully clamped. This is an extreme case but, in reality, both rotation and in-plane sliding can often be found. It is therefore necessary to investigate the influence of boundary conditions.

If the boundary conditions at $X=L_r$ and $X=-L_r$ become simply supported which allows free rotation about the edge but no in-plane sliding, the form of the dynamic equation is:

$$\ddot{W}_{1c} + \bar{h}W_{1c} = \bar{d} \quad (6.25)$$

where:

$$\bar{h} = \frac{8M_0(2L_r - B_r \tan \Phi + B_r \cot \Phi)}{HB_r \left[m_0 + \frac{2}{3}\mu B_r(2L_r - B_r \tan \Phi) \right]} \quad (6.26)$$

$$\bar{\omega} = \sqrt{\bar{h}} \quad (6.27)$$

$$\bar{d} = - \frac{4M_0(2L_r + B_r \cot \Phi)}{B_r \left[m_0 + \frac{2}{3}\mu B_r(2L_r - B_r \tan \Phi) \right]} \quad (6.28)$$

$$\tan \Phi = \frac{L_r - l'_d}{B_r} \quad (6.29)$$

As compared with the formulae for the fully clamped plate (Eqns (6.11) - (6.15)), the only coefficient changed is d in Eqn. (6.28). Therefore, the solution to Eqn. (6.11) becomes the solution to Eqn. (6.25) by taking the coefficient in Eqn. (6.28).

6.3 Analytical Solution and Discussions

The analytic procedure outlined above has been used to study the dynamic response of impacted fully clamped rectangular plates, providing information on the permanent transverse deflection, velocity and acceleration of the striker as well as interactive impact force.

In Fig. 6.2 two square yield curves are indicated. One circumscribes the corresponding maximum normal stress curve while another with dimensions 0.618 times as large would inscribe it. The rigid perfectly plastic solutions for these two square yield curves are shown in Fig. 6.3. Thus, for maximum permanent deflection and impact duration the 'lower bound' was predicted by a theoretical solution using a square yield curve which circumscribes the maximum normal stress yield curve, while the 'upper bound' corresponds to an inscribing yield curve.

For the same input data of case E102, the results generated from the numerical method described in chapter 2 are plotted in Fig. 6.4, in which elasto-plastic work-hardening materials are adopted. It may be seen that the permanent deflection predicted by the numerical method lies well between the upper and lower bound of the rigid perfectly plastic solution. However, the rigid perfectly plastic model underestimates the impact duration due to neglect of the elastic effects. The time for the maximum deflection predicted by the numerical method is equal to the average value of upper bound and lower bound of impact duration approximately. It should be noted from this example case that even though the permanent deflection is 10 times larger than the corresponding plate thickness, the elastic effects are still significant. This is quite different from the plate subjected to uniformly distributed impulsive loading because the deformation for the impacted plate is very local near the area of dent line.

As indicated in the introduction, in the mode approximation technique the initial velocity field was obtained by minimising the kinetic energy difference between the given initial velocity and that of the mode solution.

If we assume:

$$\dot{u}_i(\bar{x}, t) = \dot{w}_*(t)\Theta_i(\bar{x}) \quad (i=1,2,3) \quad (6.30)$$

where $\dot{u}_i(\bar{x}, t)$ is general mode fields, $\dot{w}_*(t)$ represents the velocity amplitude and

$\Theta_i(\bar{x})$ is a normalised vector valued shape function of space variables \bar{x} .

The kinetic energy difference Δ_0

$$\Delta_0 = \frac{1}{2} \int_V \rho (\dot{u}_i^0(\bar{x}) - \dot{w}_*^0 \Theta_i(\bar{x})) (\dot{u}_i^0(\bar{x}) - \dot{w}_*^0 \Theta_i(\bar{x})) dV \quad (6.31)$$

where $\dot{u}_i^0(\bar{x})$ is the given initial velocity. \dot{w}_*^0 is the initial mode velocity amplitude defined by:

$$\dot{w}_*(\bar{x}) = \dot{w}_*^0 \Theta_i(\bar{x}) \quad (6.32)$$

Minimising Δ_0 with respect to \dot{w}_*^0 , we have:

$$\dot{w}_*^0 = \frac{\int_V \rho \Theta_i(\bar{x}) \dot{u}_i^0(\bar{x}) dV}{\int_V \rho \Theta_i(\bar{x}) \Theta_i(\bar{x}) dV} \quad (6.33)$$

In the case of the plate being considered here, \dot{w}_*^0 can be obtained from Eqn. (6.33)

$$\dot{w}_*^0 = \frac{V_0}{\frac{2\rho H B_r (L_r + l'_d)}{3m_0} + 1} \quad (6.34)$$

For the ship collision problem, the mass of the striking vessel m_0 is much larger than the mass of the side structure involved in collision. This means that the mode initial velocity is almost the same as the given initial velocity.

In the study of the impacted plate problem there is an important parameter, λ . To study

the variation of structural response of plate with the parameter, λ ($\lambda = \frac{m_0 V_0^2}{8M_0 H}$), the

structural groups considered are listed in Table 6.1.

Table 6.1 Dimensions of examined aluminium and steel plates

<u>Group No.</u>	<u>Material</u>	<u>$2L_r*2B_r*H$ [mm³]</u>	<u>$2ld'$ [mm]</u>
1	Aluminium	200*150*1.65	100
2	Aluminium	200*250*1.65	100
3	Steel	255*243*0.8	145
4	Steel	255*243*1.6	145

Let us first check groups 1 and 2 taken from the impact test reported in chapter 3. The rigid perfectly plastic solutions on the maximum permanent deflections are shown in Fig. 6.5 in which the experimental values are also plotted. The range of λ examined is from 40 to 180. All but one of the test data scatter within the range of upper bounds and lower bounds and the correlation between the test results and the rigid perfectly plastic solutions is as good as that between the test results and the numerical predictions as discussed in chapter 4. The fluctuation in the curves is caused by different structural dimensions and different combinations of mass and impact velocity.

For the structural groups 3 and 4 listed above the deflection- λ curves are shown in Fig.6.6, with value of λ ranging from 100 to 2100. It can be seen that, for different plate thickness, the values of Wm/H predicted by the Rigid Perfectly Plastic Method are the same. This means that the rigid perfectly plastic solutions are independent of plate thickness and two parameters Wm/H and λ are sufficient to determine response behaviour. In elasto-plastic numerical results the thicker plate has smaller permanent

deflection than the thinner plate (Fig. 6.7) for the same value of λ ($\lambda > 600$) and the difference becomes larger with increase of the value λ . However, for $\lambda < 600$ these results are reversed and the conditions for the use of Rigid Perfectly Plastic Method are not satisfied. In summary, the fluctuations may occur in the W_f/H vs. λ curve due to the different plate thickness. When the plate sustains severe plastic deformation in which the Rigid Perfectly Plastic Method is generally adopted, the maximum and permanent deformations of the thicker plate are smaller than those of the thinner one. Similar phenomena were observed for the impulsively loaded plate problem both in the experimental results and in the corresponding elasto-plastic numerical predictions [Zhu and Jones, 1989].

The corresponding solutions to Eqn. (6.25) for case -E102- are listed in Table 6.2 for which free rotation along two boundaries is allowed. For comparison purposes solutions for the fully clamped plate are also given. It can be seen that, allowing rotation leads to increase of maximum permanent deflection and impact duration, but decrease of maximum impact force. For the specific case examined, changes in the solutions caused by the above variation in boundary condition are very small.

Table 6.2 Influence of boundary conditions on the structural response of steel plate E102

	<u>Fully clamped at 4 sides</u>		<u>2 sides fully clamped, 2 simply supported</u>	
	Ins*	Cir*	Ins*	Cir*
W_m/H	11.00	14.21	11.27	14.48
tm[ms]	5.67	7.29	5.76	7.38
am/g	-67.64	-53.13	-67.55	-53.08
ao/g	-4.83	-2.98	-3.19	-1.97
F_m[kN]	18.96	14.89	18.93	14.88

Ins*, Cir* for inscribing and circumscribing square yield curve.

For a rectangular plate under local impact the suitable range of λ for the Rigid Perfectly Plastic Method varies with material properties and the dimensions of the plate. Fluctuations in the $W_f/H-\lambda$ curve exist due to different plate thicknesses and a different combination of mass and impact velocity of the striker. The allowance of rotation at boundaries results in a little increase of maximum permanent deflection of the plate. The analytical solutions provide formula which can be used for the design of rigidly clamped steel plates against impact, and provide information on maximum deflection, impact duration and maximum impact force.

6.4 Application in Design of Plates

Given a clamped rectangular plate ($2L_r * 2B_r = 2400 * 600 \text{ mm}^2$) it is to withstand being struck by a rigid indenter of mass $2 * 10^6 \text{ kg}$ at impact velocity of 1.0 m/s . The dent line is 1200 mm long and in the central line of the plate parallel to the longer side of the plate. If the material properties are known (Table 6.3) and the maximum permanent deflection is not larger than 5 times the plate thickness, determine the thicknesses for steel and aluminium plate.

Table 6.3 Mechanical properties of materials

<u>Material</u>	<u>σ_s [N/mm²]</u>	<u>E [N/mm²]</u>	<u>ρ [kg/m³]</u>
Steel	350	207000	7800
Aluminium	150	51500	2700

For each thickness assumed, the lower and upper bounds of the maximum permanent deflection can be calculated by the Rigid Perfectly Plastic Method (Eqn. (6.22)). Taking the average value of the lower and upper bounds the $W_f/H - H$ curves are plotted in Fig. 6.8 and the design thicknesses for steel and aluminium plates are 24 mm

and 35 mm respectively. In the calculation for the steel plate the dynamic yield stress is assumed to be 1.3 times as large as static yield stress to account for the strain-rate sensitivity which is based on the average strain-rate at point 2 during the impact.

It is noticed from Fig. 6.8 that, when the thickness of the steel plate increases from 16 mm to 20 mm, the value of W_f decreases from 155.2 mm to 130.4 mm; while the change of thickness from 28 mm to 32 mm causes the change of W_f from 106.4 mm to 96.0 mm. This means that very little improvement in the capability to withstand impact can be gained by increasing the plate thickness when the thickness is larger than a certain value.

The impact loading on the frames has not been considered in this study. It would be relatively straightforward to evaluate the normal impact force transferred to the adjacent frames from the plating and apply a simple beam analysis for their design.

For interest the effect of the same impact on a large unsupported steel plate ($2L_r \times 2B_r = 3600 \times 4200 \text{ mm}^2$) is shown in Fig. 6.8 identified by steel-B. From this it will be seen that to limit the indent to five thicknesses only requires a 31 mm thickness. This illustrates that even without side framing the plate thickness required to meet local impact does not increase dramatically. The increment of 7 mm in thickness can be thought of as the mean thickness including the frames over the whole area. Frames are needed in practice of course to withstand other loads.

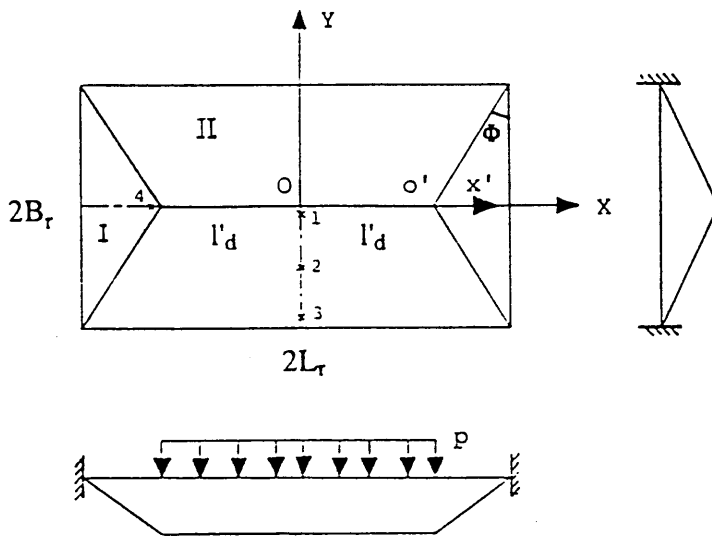


Fig. 6.1 Deformation mode

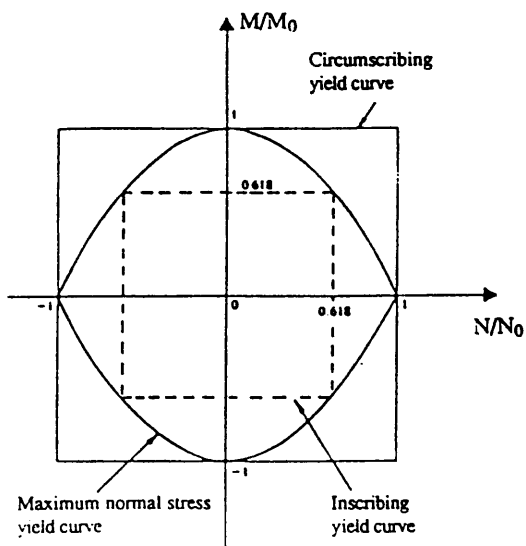
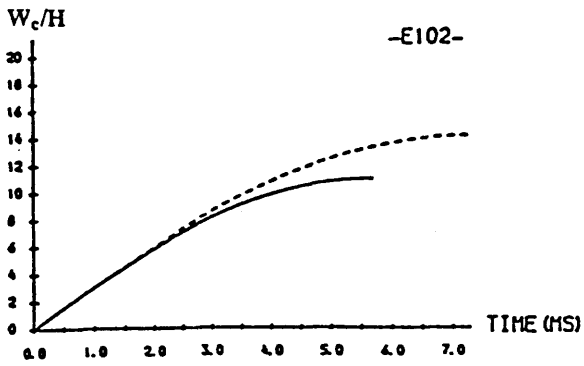
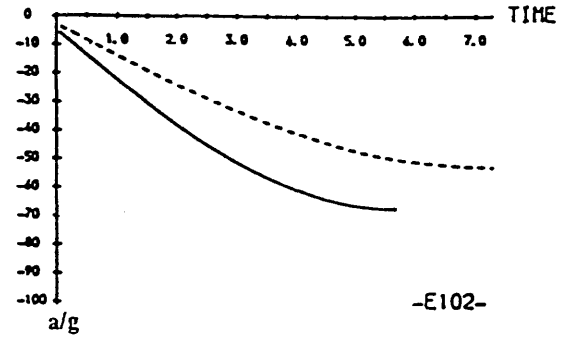


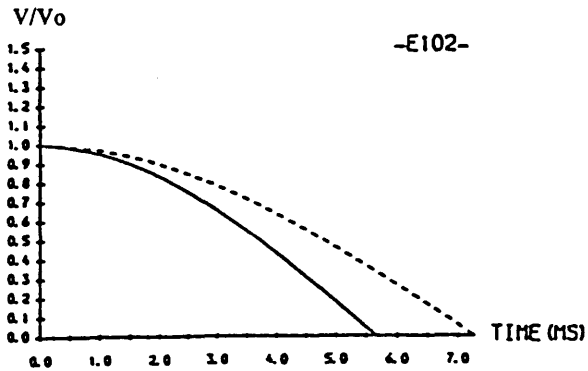
Fig. 6.2 Yield curve



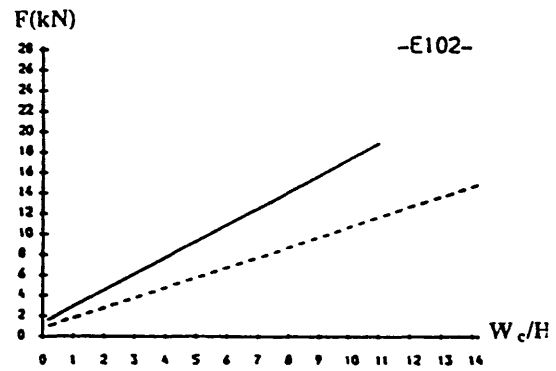
(a) CENTRAL DEFLECTION-TIME HISTORY



(c) ACCELERATION-TIME HISTORY OF STRIKER

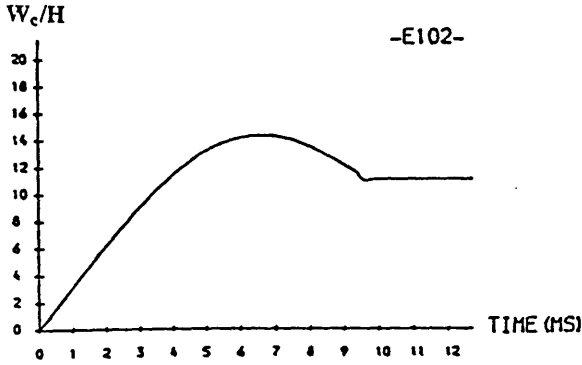


(b) VELOCITY-TIME HISTORY OF STRIKER

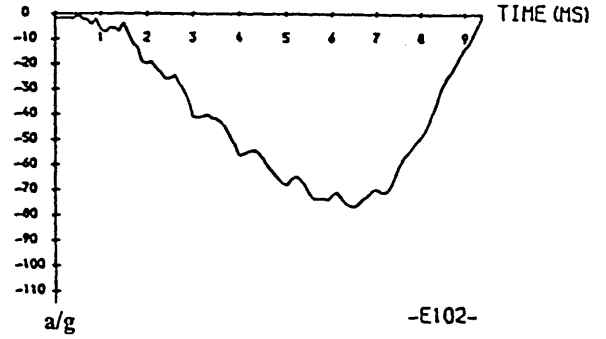


(d) IMPACT FORCE-INDENTATION CURVE

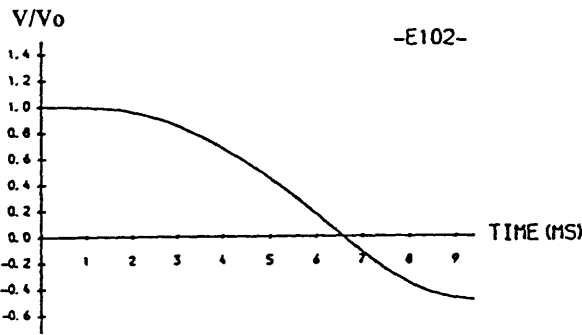
Fig. 6.3 Results from analytical method using rigid perfectly plastic material
 ----- for inscribing square yield curve
 ————— for circumscribing square yield curve



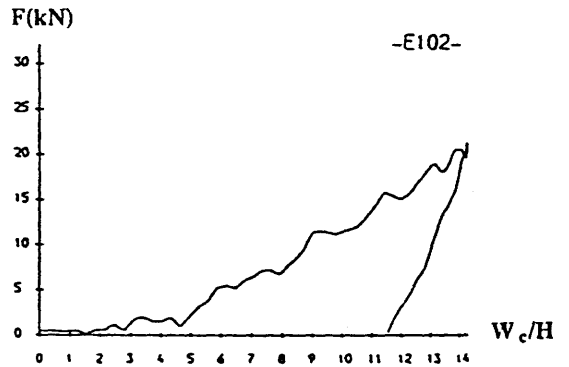
(a) CENTRAL DEFLECTION-TIME HISTORY



(c) ACCELERATION-TIME HISTORY OF STRIKER



(b) VELOCITY-TIME HISTORY OF STRIKER



(d) IMPACT FORCE-INDENTATION CURVE

Fig. 6.4 Results from numerical method using elasto-plastic work-hardening material

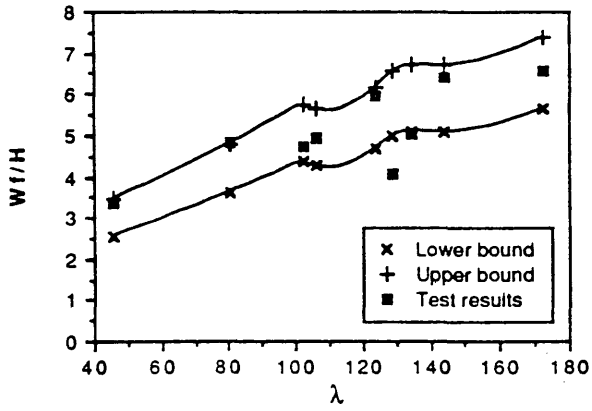
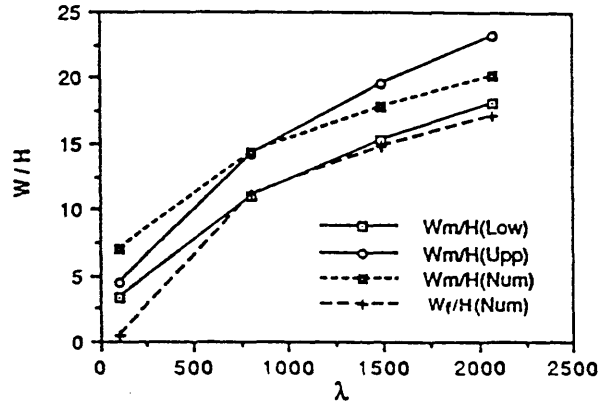
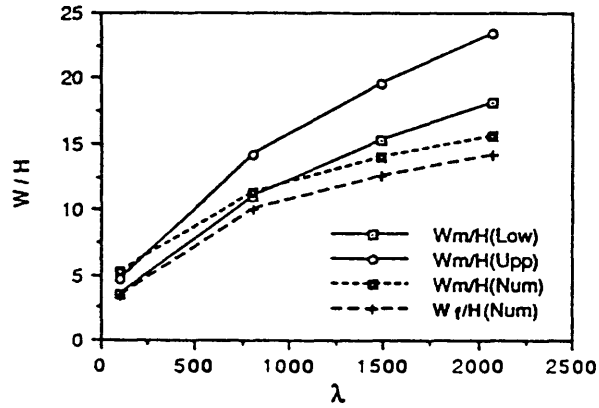


Fig. 6.5 Comparison between the rigid perfectly plastic solutions and test results on the permanent deflection of aluminium plates



(a) Plate thickness $H=0.8$ mm



(b) Plate thickness $H=1.6$ mm

Fig. 6.6 Maximum and permanent deflections of plates with different thickness

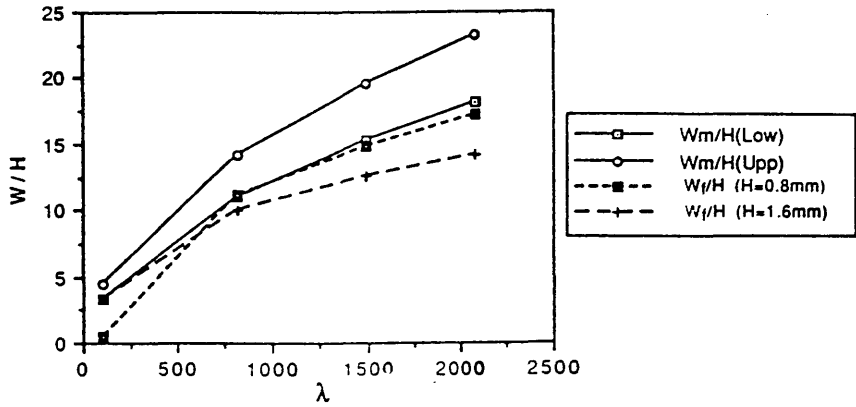


Fig. 6.7 Maximum deflection by rigid perfectly plastic analysis and permanent deflection by numerical analysis

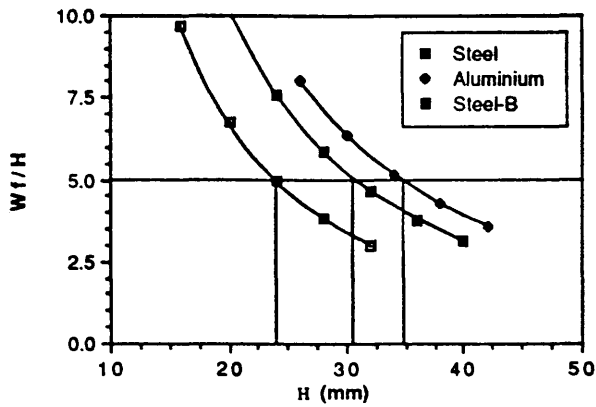


Fig. 6.8 Determination of thicknesses of struck steel and aluminium plates

CHAPTER SEVEN

DYNAMIC RESPONSE OF PLATE UNDER REPEATED IMPACTS

7.1 Introductory Remarks

Marine structure subjected to repeated loading is a practical engineering problem. When the loading is static the classical shakedown phenomenon is defined, in which elastic, perfectly plastic structural model is adopted with infinitesimal displacements. Little work has been done on the shakedown problem when the structures are under dynamic loads caused by slamming, dropped objects, collisions, ice damage and explosions.

The phenomenon of pseudo-shakedown was introduced by Jones [1973] for a rigid, perfectly plastic rectangular plate subjected to repeated dynamic pressure pulse. If a rigid perfectly plastic structure is subjected to a pressure pulse with a magnitude p_m and a short duration τ_1 , then the maximum permanent transverse displacement W_{p1} , for sufficiently short pressure pulse, may be smaller than the corresponding maximum permanent transverse displacement due to static load, W_s . If the same dynamic pressure pulse were repeated, the rigid perfectly plastic structure might reach a final state with a maximum permanent transverse displacement W_{p2} , say, which might still be smaller than W_s . This process could continue until the permanent set from the repeated dynamic pressure pulse equalled, eventually, W_s . A rigid perfectly plastic structure would have reached a pseudo-shakedown state, and would not then deform for further repetitions of the same dynamic pressure pulse. This phenomenon was

observed for the repeated wave impact of ship bows [Jones, 1977]. Recently a conjecture was derived by Shen and Jones [1989] for the pseudo-shakedown of beams and plates under repeatedly applied, rectangular shaped pressure. As the stretching effect due to axial restraint plays a dominant role in the pseudo-shakedown, the rigid perfectly plastic model can satisfactorily feature in the pseudo-shakedown problem.

A government sponsored report published recently by Lloyd's Register of Shipping has revealed that most floating and fixed structures are simply too weak to take repeated impact from supply boats [Dickey, 1986]. It was suggested that the existing rules governing their design should be changed.

In this chapter the dynamic response of a fully clamped rectangular plate under two identical impacts was studied by numerical analysis and rigid perfectly plastic analysis. A very good agreement between these two methods is achieved which is validated by the experimental results. The conditions of using the Rigid Perfectly Plastic Method are discussed. The rigid perfectly plastic model was also used to study the dynamic inelastic response of plate subjected to any number of identical impacts. From the analytical solution it is found that no pseudo-shakedown occurs in the case described above.

7.2 Numerical Simulation of Elasto-Plastic Plates

The dynamic inelastic response of clamped rectangular plates impacted by a knife edge indenter was studied in the previous chapters. The striker hits the plate and keeps contact with the dent line. After the plate reaches its maximum deflection it bounces back. When the interactive force between the plate and the striker decreases to zero, the striker separates from the plate, then the plate vibrates elastically. Due to damping effects the plate finally comes to rest, which is defined as the residual state of the plate

after first impact. The residual deformations, strains and stresses can be obtained by the program. The program was developed to study the dynamic response of the plate under second impact. The residual deformations, strains and stresses after the first impact can be stored dynamically and serve as initial conditions for the subsequent impact. It is assumed that in the second impact the striker hits the same position of the plate as in the first one. In spite of that, the mass and impact velocity of the striker can be different from the first one.

The numerical simulation is made on an aluminum plate of length 150 mm, width 200 mm and thickness 1.65 mm (see Fig. 2.1). The dent line is 100 mm and the impact velocity is 2.0 m/s. The overall dynamic response of the plate under two identical impacts is depicted in Figs 7.1(a) - (c), with the dynamic impact force-indentation curve in Fig. 7.1(d). It should be noted that a time interval was set between the two impacts and in the case A3P2 the second impact starts at time 12.22 ms, as shown in Fig. 7.1.

Figure 7.1(a) shows the central deflection time history of the impacted plate in which the rise of the maximum deflection in the second impact is $1.92 H$ - about 30% of the first impact. A 43% reduction in the response time can also be observed in Fig. 7.1(a). However, the rebound velocity increases from $0.35 V_0$ for the first impact to $0.38 V_0$ for the second (see Fig. 7.1(b)). It is observed from Fig. 7.1(c) that the acceleration in the second impact rises steeply to the value of the first maximum acceleration at the beginning of the second impact. The interactive impact force between the striker and the plate is plotted in Fig. 7.1(d) which illustrates the whole process of the two impacts. It is shown in Fig. 7.1(d) that at the beginning of the second impact the $F - W_c/H$ curve rises along the unloading curve of the first impact. When the impact force reaches the value of maximum impact force of the first impact, the curve rises steadily at the slope of the loading curve of the first impact. The unloading curve is approximately parallel to that of the first impact.

The strain time histories at four different points are shown in Fig. 7.2, from which detailed information about the dynamic strain during the impact process can be obtained. In the case A3P2, the maximum x-strain at the end of the dent line is larger than strains at other positions. At this point the maximum x-strain increases from $125 \epsilon_s$ for the first impact to $175 \epsilon_s$ for the second, which may cause the rupture of the plate due to bi-axial tension.

The x-stress and strain distribution at the maximum deformation of the second impact are presented in Fig. 7.3. It can be seen that there is significant stress and strain concentration at the end of the dent line. The x-stress and strain distribution in the residual state are plotted in Fig. 7.4.

7.3 Rigid Perfectly Plastic Analysis

The same co-ordinate system defined in Fig. 6.1 is used for the formulation of the rigid perfectly plastic analysis under repeated impacts.

7.3.1 Second Impact

An approximate theoretical procedure based on the Rigid Perfectly Plastic Method is developed to give the lower and upper bound of the dynamic plastic solution to the impacted rectangular plate with finite deflections.

The general form of dynamic equation to rectangular plates in Eqn. (6.1) can be simplified to Eqn. (7.1) if the deformed plate is assumed to be subdivided into a number of rigid regions separated by s straight line hinges:

$$\int_A (p - \mu \ddot{w}) \dot{w} dA = \sum_{m=1}^s \int_{l_m} (Nw - M) \dot{\theta}_m dl_m \quad (7.1)$$

where w is the transverse deflection, M and N denote the resultant moment and membrane force along the yield hinge, and θ_m is the rotation of adjacent rigid parts of the plate.

Using the Wood's mode the plate can be divided into two regions I and II shown in Fig. 6.1. The displacements are given:

$$w_I = \frac{W_{2c}(B_r \tan \Phi - x')}{B_r \tan \Phi} \quad \text{for region I} \quad (7.2a)$$

$$w_{II} = \frac{W_{2c}(B_r - y)}{B_r} \quad \text{for region II} \quad (7.2b)$$

where W_{2c} is the displacement at the centre of the plate in second impact.

For the uniformly distributed impact loading along the dent line, the impact force is:

$$F = -m_{20} \ddot{W}_{2c} \quad (7.3)$$

$$p = \frac{F}{2l'_d} \quad (7.4)$$

where m_{20} is mass of the striker in second impact.

If the square yield criterion is chosen, then we have:

$$D = M_0 \left(1 + \frac{4w}{H}\right) \dot{\theta}_m \quad (7.5)$$

The governing equation of the dynamics of the plate is:

$$\ddot{W}_{2c} + h_2 W_{2c} = d_2 \quad (7.6)$$

where:

$$h_2 = \frac{8M_0(2L_r - B_r \tan \Phi + B_r \cot \Phi)}{HB_r \left[m_{20} + \frac{2}{3} \mu B_r (2L_r - B_r \tan \Phi) \right]} \quad (7.7)$$

$$\omega_2 = \sqrt{h_2} \quad (7.8)$$

$$d_2 = - \frac{8M_0(L_r + B_r \cot \Phi)}{B_r \left[m_{20} + \frac{2}{3} \mu B_r (2L_r - B_r \tan \Phi) \right]} \quad (7.9)$$

$$\tan \Phi = \frac{L_r - l'_d}{B_r} \quad (7.10)$$

The initial conditions for Eqn. (7.6) is:

$$W_{2c}(0) = W_{1m} \quad (7.11)$$

$$\dot{W}_{2c}(0) = V_{20} \quad (7.12)$$

where W_{1m} is the maximum deflection caused by the first impact and V_{20} is the initial impact velocity of the striker in the second impact.

The solution to Eqn. (7.6) which satisfies the above initial condition is written as:

$$W_{2c}(t) = \frac{V_{20}}{\omega_2} \sin \omega_2 t + \left(W_{1m} - \frac{d_2}{h_2} \right) \cos \omega_2 t + \frac{d_2}{h_2} \quad (7.13)$$

The velocity and acceleration are:

$$\dot{W}_{2c}(t) = V_{20} \cos \omega_2 t - (W_{1m} - \frac{d_2}{h_2}) \omega_2 \sin \omega_2 t \quad (7.14)$$

$$\ddot{W}_{2c}(t) = -V_{20} \omega_2 \sin \omega_2 t + (W_{1m} - \frac{d_2}{h_2}) h_2 \cos \omega_2 t \quad (7.15)$$

Taking the right hand side of Eqn. (7.14) to zero we can obtain the duration of the second impact:

$$t_{2m} = \frac{1}{\omega_2} [\tan^{-1}(\frac{V_{20} \omega_2}{W_{1m} h_2 - d_2})] \quad (7.16)$$

The corresponding maximum permanent deflection is:

$$W_{2m} = \frac{\sqrt{(W_{1m} h_2 - d_2)^2 + (V_{20} \omega_2)^2} + d_2}{h_2} \quad (7.17)$$

The initial acceleration is:

$$a_{20} = -(W_{1m} h_2 - d_2) \quad (7.18)$$

It can be shown that the initial acceleration of the second impact is equal to the maximum one of the first impact.

The maximum acceleration is:

$$a_{2m} = -\sqrt{(W_{1m} h_2 - d_2)^2 + (V_{20} \omega_2)^2} \quad (7.19)$$

which occurs at the same time as the maximum deflection.

The analytic procedure outlined above is used to study the case A3P2, which has been simulated by the elasto-plastic numerical analysis program. The same input data is used to obtain the rigid perfectly plastic solutions. In Fig. 7.5, using circumscribing and inscribing square yield curves the rigid perfectly plastic solutions are given for the transverse deflection, velocity and acceleration of the striker as well as interactive impact force. Therefore, for the maximum permanent deflection and impact duration the 'lower bound' was predicted by a theoretical solution using a square yield curve which circumscribes the maximum normal stress yield curve, while the 'upper bound' corresponds to an inscribing yield curve (see Fig. 6.2).

The starting point of the second impact is set at 10.89 ms in Fig. 7.5. The central deflection time history of the plate is shown in Fig. 7.5(a), with the rise in the maximum deflection being 44 - 45% that of the first impact and with 46.3 - 47.3% drop in the response time. It can be found that the amplitude of the maximum acceleration increases from 47.08 g (36.96 g)² for the first impact to 65.22 g (51.16 g)² for the second (Fig. 7.5(c)). As the rigid perfectly plastic model was used and no elastic effect was accounted for, the impact force in Fig. 7.5(d) rises vertically at the beginning of each impact.

7.3.2 ith Impact

For a fully clamped rectangular plate under repeated identical impacts it is necessary to investigate the pseudo-shakedown phenomenon.

The procedure used to analyse the second impact is adopted for subsequent impacts. It can be shown for the repeated identical impacts with striker mass m_0 and impact velocity V_0 , that:

² Values predicted by using the inscribing square yield curve.

1st impact

$$W_{1m} = \frac{\sqrt{d^2 + hV_0^2} + d}{h} \quad (7.20)$$

$$t_{1m} = \frac{1}{\omega} \left[\tan^{-1} \left(\frac{V_0 \omega}{-d} \right) \right] \quad (7.21)$$

$$a_{1m} = -\sqrt{d^2 + hV_0^2} \quad (7.22)$$

$$a_{10} = -d \quad (7.23)$$

2nd impact

$$W_{2m} = \frac{\sqrt{d^2 + 2hV_0^2} + d}{h} \quad (7.24)$$

$$t_{2m} = \frac{1}{\omega} \left[\tan^{-1} \left(\frac{V_0 \omega}{\sqrt{d^2 + hV_0^2}} \right) \right] \quad (7.25)$$

$$a_{2m} = -\sqrt{d^2 + 2hV_0^2} \quad (7.26)$$

$$a_{20} = -\sqrt{d^2 + hV_0^2} \quad (7.27)$$

ith impact

$$W_{im} = \frac{\sqrt{d^2 + ihV_0^2} + d}{h} \quad (7.28)$$

$$t_{im} = \frac{1}{\omega} \left[\tan^{-1} \left(\frac{V_0 \omega}{\sqrt{d^2 + (i-1)hV_0^2}} \right) \right] \quad (7.29)$$

$$a_{im} = -\sqrt{d^2 + ihV_0^2} \quad (7.30)$$

$$a_{i0} = -\sqrt{d^2 + (i-1)hV_0^2} \quad (7.31)$$

where coefficients h , ω and d were given in Eqns (6.12), (6.13) and (6.14).

As can be seen from the above formulae, the maximum deflection W_{im} and amplitude of deceleration a_{im} increase with the number of the impacts i , but the impact duration t_{im} becomes smaller with the increase of the number of impacts. Unfortunately there is no bound for the maximum deflection W_{im} (see Eqn. (7.28)) when i tends to be infinite. In other words, the pseudo-shakedown phenomenon does not occur for the fully clamped rectangular plates under repeated identical impacts.

7.4 Discussions

The case A3P2 has been studied by the elasto-plastic numerical analysis program and by the Rigid Perfectly Plastic Method, with overall response results being shown in Figs. 7.1 and 7.5 respectively. It was shown for both impacts that the maximum deflection, response time for maximum deflection and the amplitude of the maximum acceleration predicted by the elasto-plastic numerical program are between the rigid perfectly plastic analytical solutions using circumscribing and inscribing square yield curves. A surprisingly good agreement between these two methods has been achieved. The measured acceleration time history in case A3P2 is given in Fig. 3.26. The acceleration time curves predicted by the elasto-plastic numerical analysis program (Fig. 7.1(c)) and Rigid Perfectly Plastic Method (Fig. 7.5(c)) are well validated by the experimental results. Moreover, a comparison among these three kinds of results can also help us to get a better understanding of the impact phenomena and numerical and rigid perfectly plastic analysis. It is worth emphasising that the rigid perfectly plastic solution can be easily obtained by hand or by calculator, which provides engineers and designers with a convenient and economical way to evaluate the dynamic response of repeatedly impacted plates.

As indicated in the last chapter, it is important to explore the conditions of using the Rigid Perfectly Plastic Method. In the following case A4P2, all the input data are the

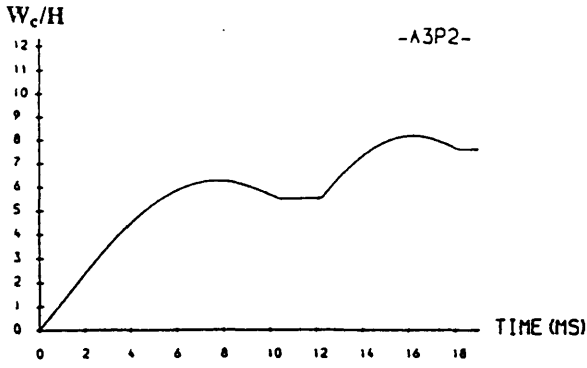
same as those in the case A3P2 except that the plate length (L) is 300 mm (see Fig.2.1). These two cases have the same value of λ . The overall response results generated from the elasto-plastic numerical program and from the Rigid Perfectly Plastic Method are plotted in Figs. 7.6 and 7.7 respectively. A comparison between Fig. 7.1(d) for case A3P2 and Fig. 7.6(d) for case A4P2 shows a difference between the characteristics of the impact force-indentation relationship. It is suggested from Fig.7.6(d) that the elastic effects are significant, which can not be neglected in the case of A4P2. The severe plastic deformation only occurs near the denting area (Fig. 7.8) and the overall response of the plate is not dominated by membrane behaviour. In this circumstance, the use of the Rigid Perfectly Plastic Method associated with Wood deformation mode may result in appreciable errors (see Figs. 7.6 and 7.7). It is usually assumed that elastic effects may be neglected when the dynamic energy is at least three times larger than the maximum elastic strain capacity, and that the pulse duration is smaller than the fundamental period of the structure. For locally impacted plates a large energy ratio is still essential. How the ratio of impact duration and the fundamental period of the plate affects the error of rigid perfectly plastic solution need further investigation. In the case A3P2 ($T_d/T_e=4.7$), the rigid perfectly plastic solution gave a good estimate on the response of the impacted plate. Therefore, whether the Rigid Perfectly Plastic Method can be used should be judged by numerical results before the dynamic response of locally impacted plates has been studied fully.

The rigid perfectly plastic analysis indicates that the plastic deformations are accumulated in repeated identical impacts and no pseudo-shakedown occurs. This was examined by repeated tests on steel plate ST03 (see Fig. 3.28) which was subjected to identical repeated impacts up to 17 times when the plate had just cracked at the end of the dent line in the test. It was observed in the experiment that, when significant rupture occurred in the plate, the rebound velocity of the striker fell dramatically. The corresponding rigid perfectly plastic analytical solutions for case ST03 are plotted in Fig. 7.9 which give the same tendency for maximum deflection and response time as

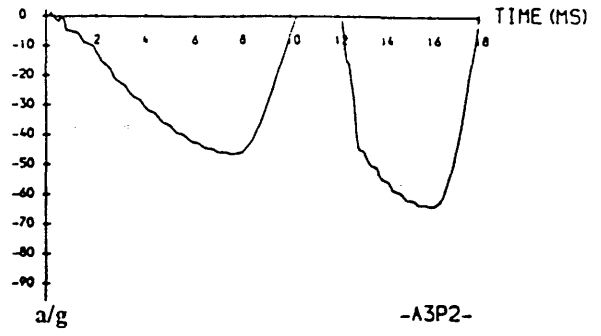
the experimental measurements. Nevertheless, due to difficulties in the dynamic test after the 5th impact, the maximum acceleration in Fig. 3.28 began to decline and then fluctuated.

Figure 7.10 presents comparisons between the test results and rigid perfectly plastic solutions for maximum permanent deflection and response time for repeatedly impacted plate ST03. As can be seen from Fig. 7.10(a), the lower bound of rigid perfectly plastic solution for maximum deflection gives a good estimate for the permanent deflection of the plate for the first four impacts. After four impacts the lower bound curve diverges from the test curve because the error for each impact has been accumulated. Figure 7.10(b) shows that the rigid perfectly plastic solution underestimates the real response time. Yet, the overall shape of the curves for rigid perfectly plastic solutions on either maximum permanent deflection or response time is coherent with the corresponding test curve. Hence, the conclusion that no pseudo-shakedown occurs for repeatedly impacted plates is supported by the experiment. Pseudo-shakedown does not occur for a repeated mass impact loading on structures because the finite energy input must be absorbed plastically [Jones and Zhu, 1989]. If a dynamic pressure acts on a structure which has shaken down, then no external work is done when the structure remains rigid [Shen and Jones, 1989].

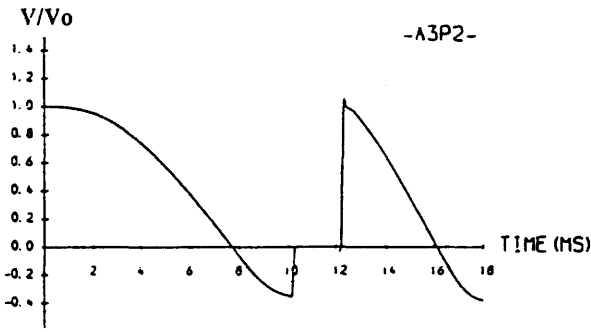
It should be stated that, even though in reality there is little possibility that one ship repeatedly collides with another at the same position, the experimental investigation in chapter 3 indicates that this scenario is more dangerous than those caused by repeated impacts at different positions.



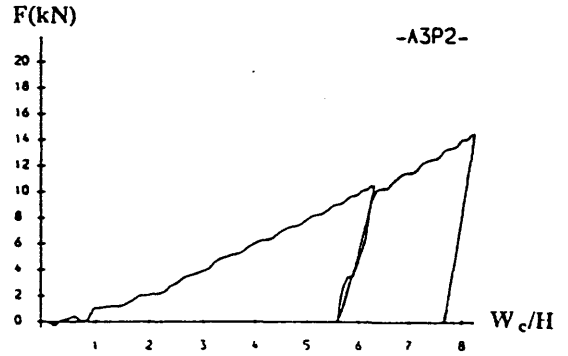
(a) CENTRAL DEFLECTION-TIME HISTORY



(c) ACCELERATION-TIME HISTORY OF STRIKER

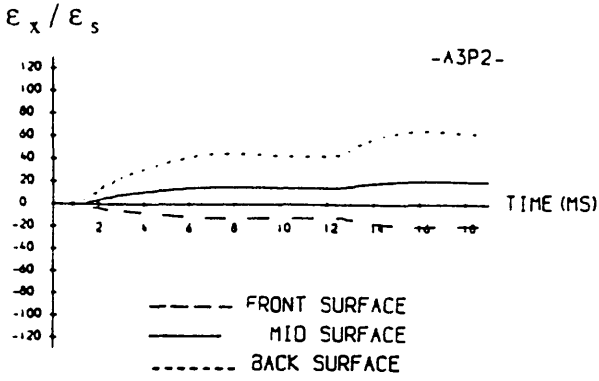


(b) VELOCITY-TIME HISTORY OF STRIKER

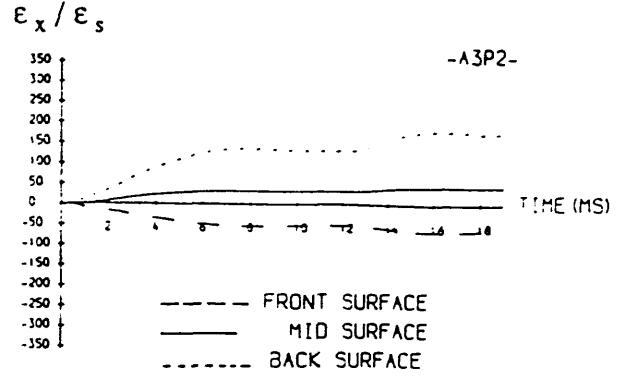


(d) IMPACT FORCE-INDENTATION CURVE

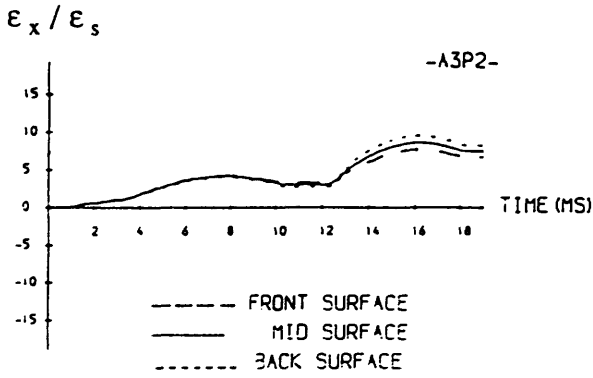
Fig. 7.1 Overall response of plate A3P2 (Numerical method using elasto-plastic work-hardening material)



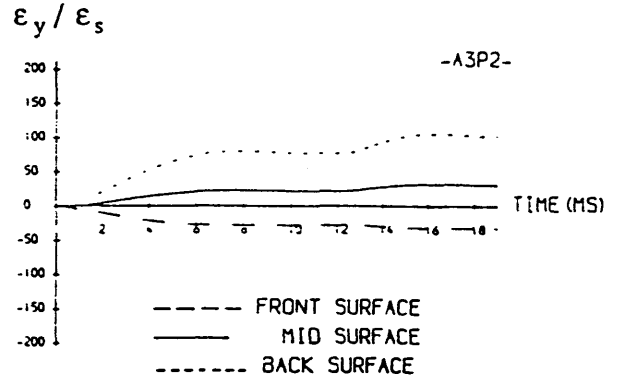
(a) STRAIN-TIME HISTORY (1)



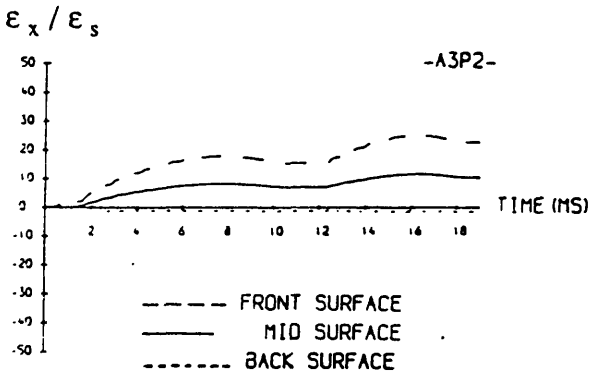
(d) STRAIN-TIME HISTORY (4)



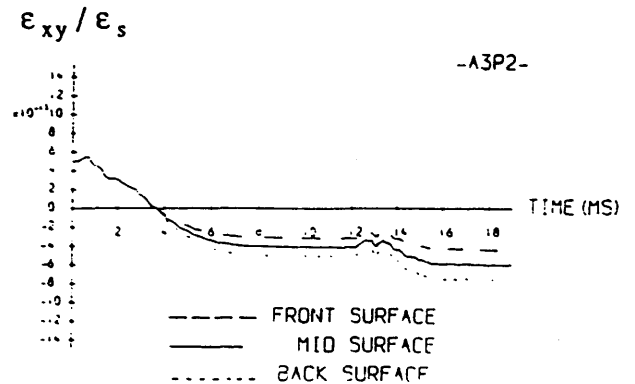
(b) STRAIN-TIME HISTORY (2)



(e) STRAIN-TIME HISTORY (4)

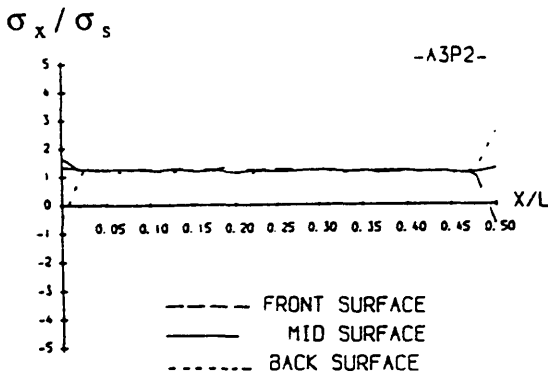


(c) STRAIN-TIME HISTORY (3)

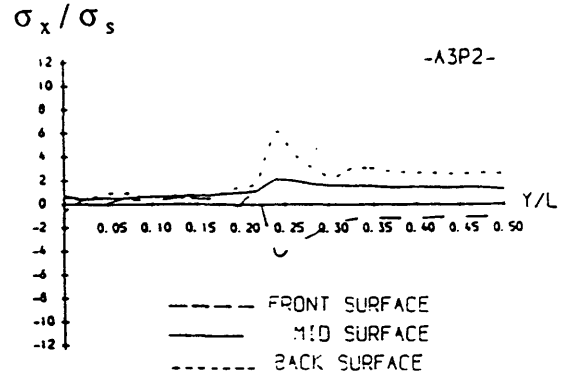


(f) STRAIN-TIME HISTORY (4)

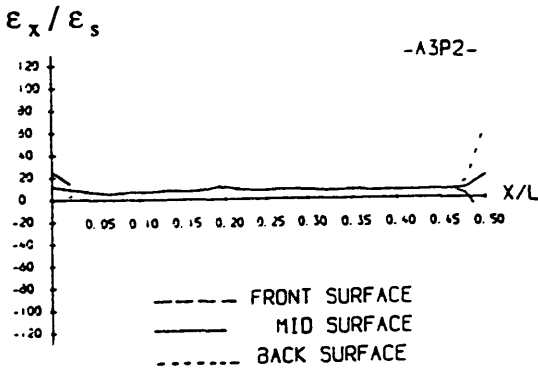
Fig. 7.2 Strain time histories on plate -A3P2-
by numerical method
(ϵ_s - Static uniaxial yield strain)



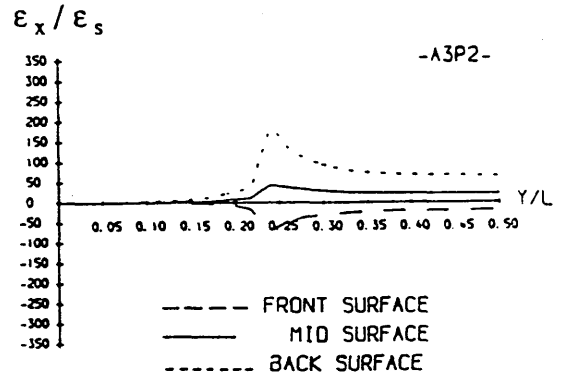
(a) STRESS AT MAXIMUM DEFLECTION



(b) STRESS AT MAXIMUM DEFLECTION



(c) STRAIN AT MAXIMUM DEFLECTION

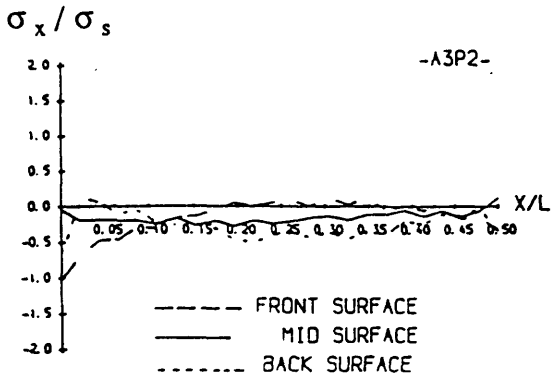


(d) STRAIN AT MAXIMUM DEFLECTION

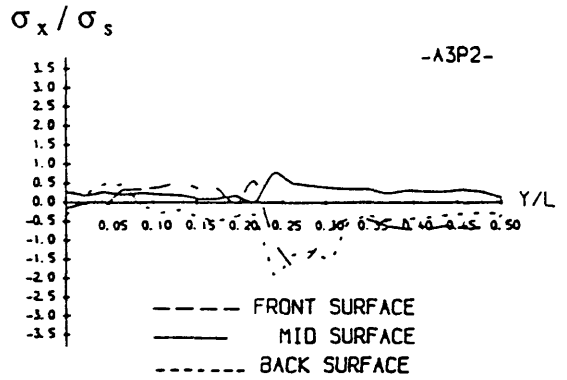
Fig. 7.3 Stress and strain distributions at maximum deflection

σ_s -- Static uniaxial yield strain, and

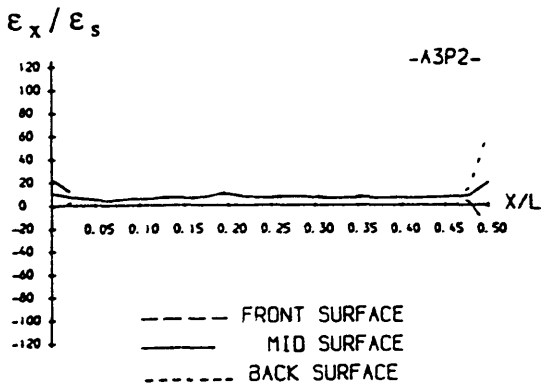
ϵ_s -- Static uniaxial yield stress.



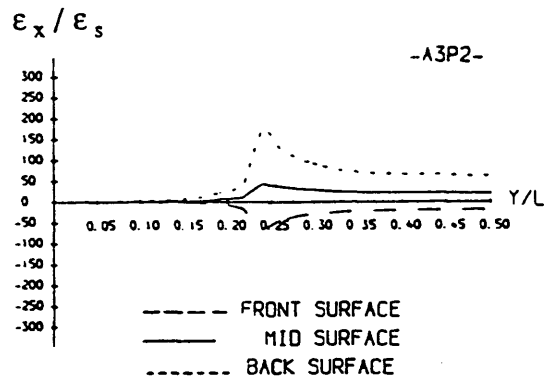
(a) STRESS IN RESIDUAL STATE



(b) STRESS IN RESIDUAL STATE



(c) STRAIN IN RESIDUAL STATE

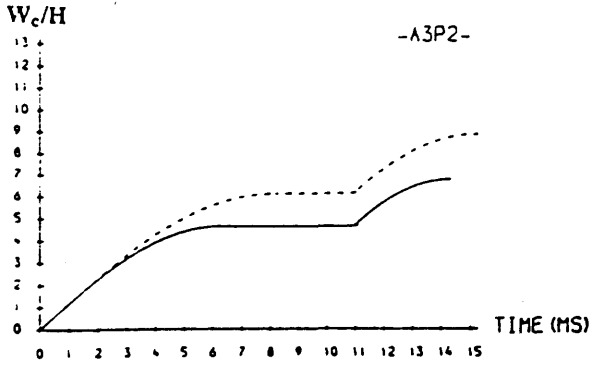


(d) STRAIN IN RESIDUAL STATE

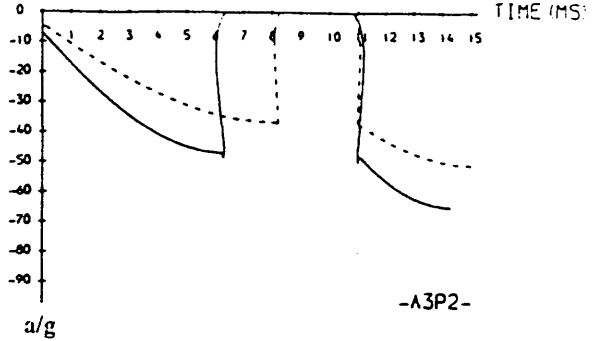
Fig. 7.4 Stress and strain distributions in residual state

σ_s -- Static uniaxial yield stress, and

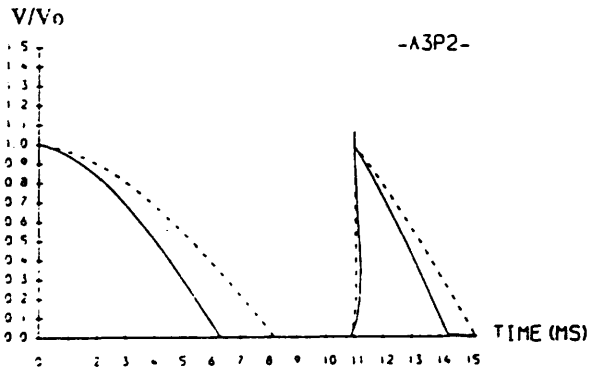
ϵ_s -- Static uniaxial yield strain.



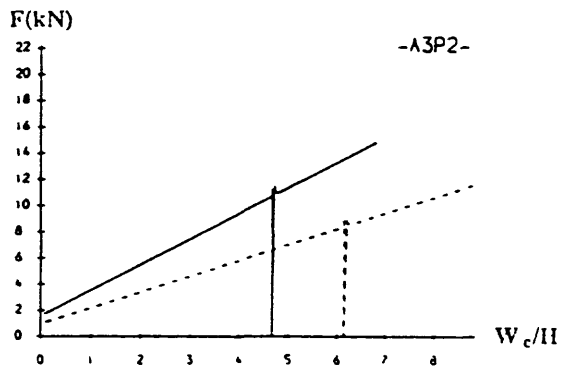
(a) CENTRAL DEFLECTION-TIME HISTORY



(c) ACCELERATION-TIME HISTORY OF STRIKER

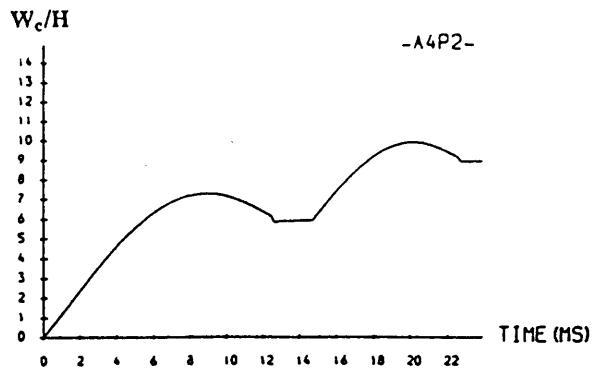


(b) VELOCITY-TIME HISTORY OF STRIKER

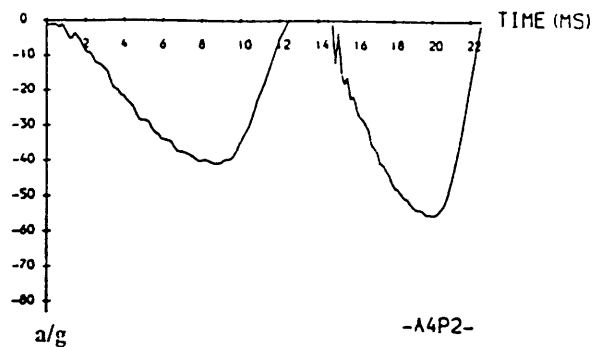


(d) IMPACT FORCE-INDENTATION CURVE

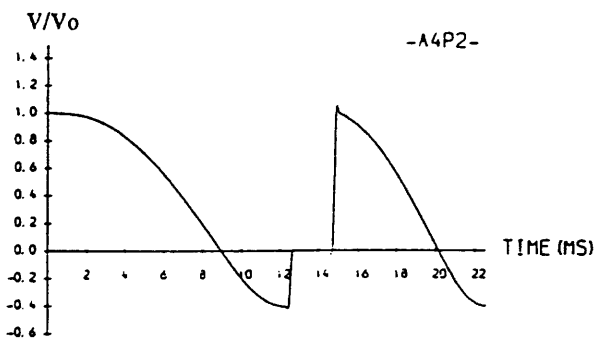
Fig. 7.5 Overall response of plate -A3P2-
 (rigid perfectly plastic method)
 -----for inscribing square yield curve
 —————for circumscribing square yield curve



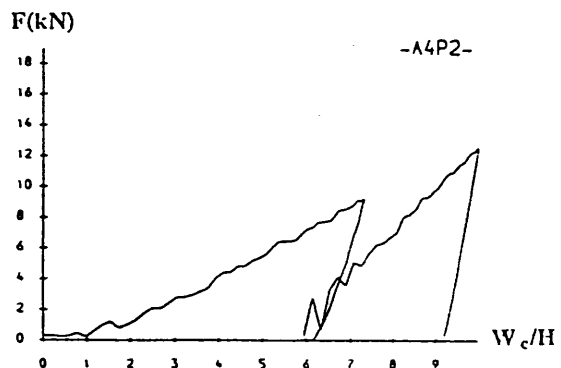
(a) CENTRAL DEFLECTION-TIME HISTORY



(c) ACCELERATION-TIME HISTORY OF STRIKER

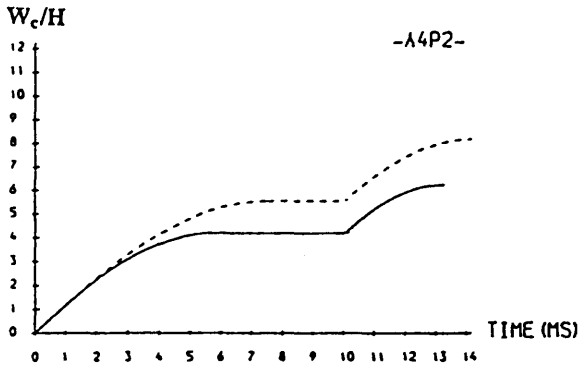


(b) VELOCITY-TIME HISTORY OF STRIKER

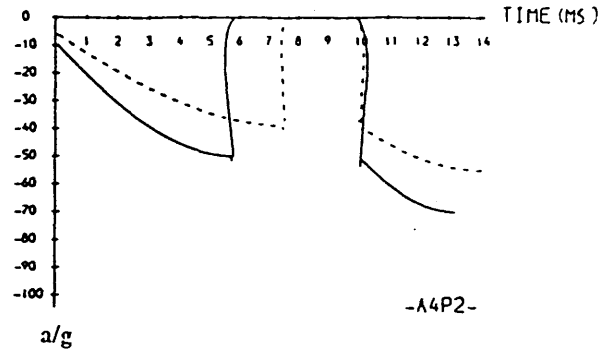


(d) IMPACT FORCE-INDENTATION CURVE

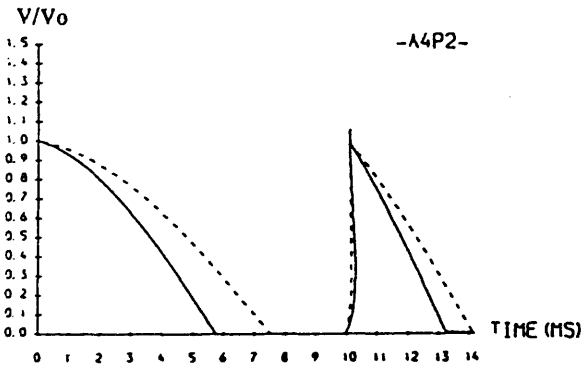
Fig. 7.6 Overall response of plate -A4P2- (Numerical method using elasto-plastic work-hardening material)



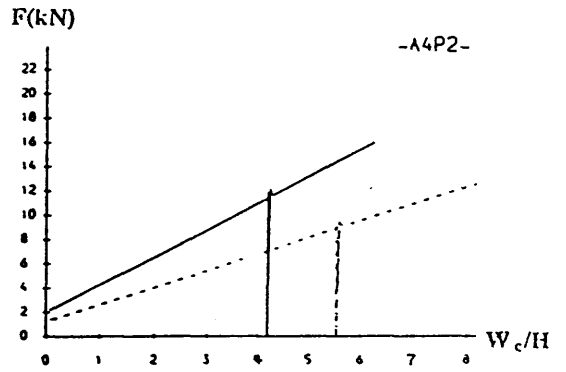
(a) CENTRAL DEFLECTION-TIME HISTORY



(c) ACCELERATION-TIME HISTORY OF STRIKER

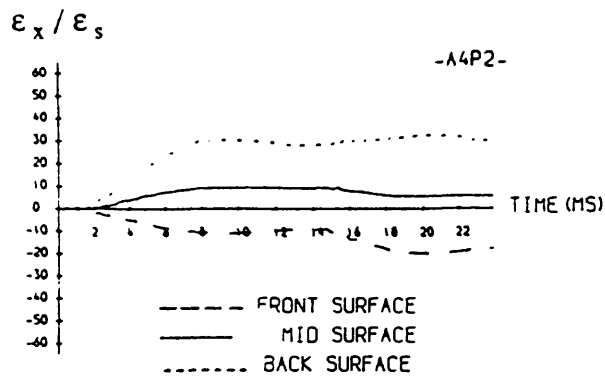


(b) VELOCITY-TIME HISTORY OF STRIKER

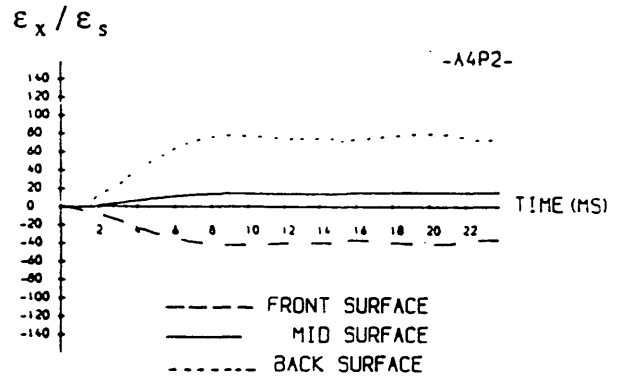


(d) IMPACT FORCE-INDENTATION CURVE

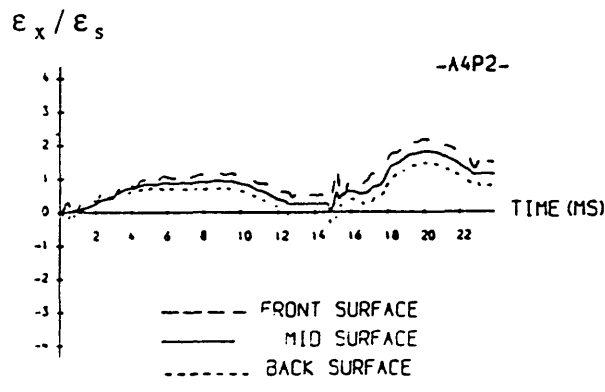
Fig. 7.7 Overall response of plate -A4P2-
 (rigid perfectly plastic method)
 ----- for inscribing square yield curve
 ————— for circumscribing square yield curve



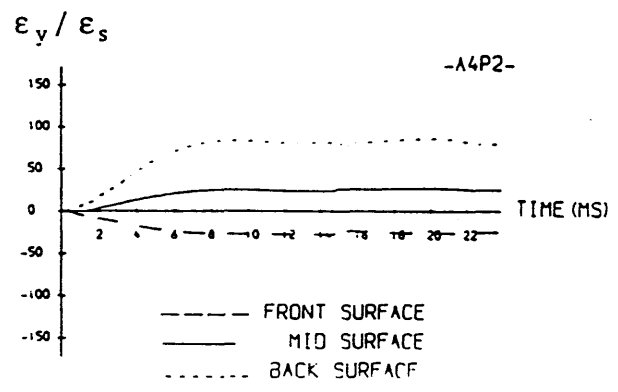
(a) STRAIN-TIME HISTORY (1)



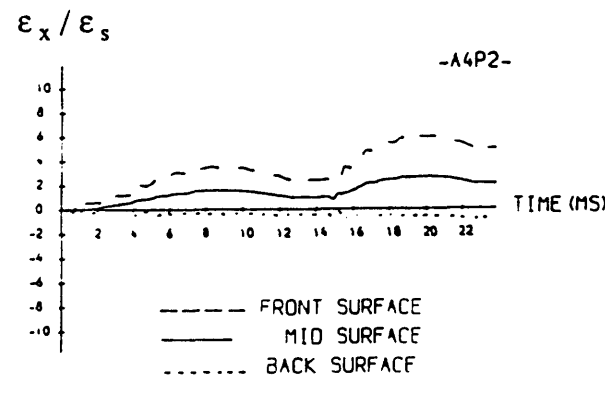
(d) STRAIN-TIME HISTORY (4)



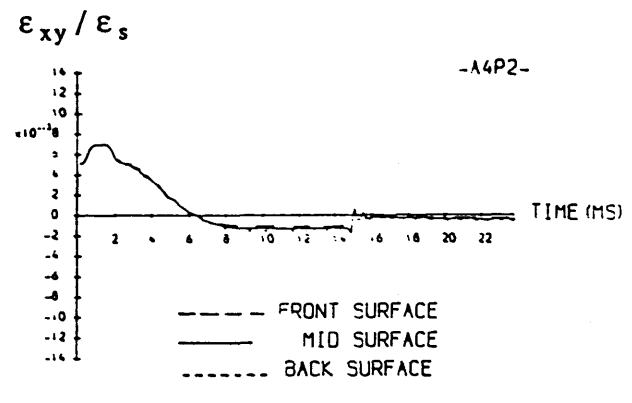
(b) STRAIN-TIME HISTORY (2)



(e) STRAIN-TIME HISTORY (4)

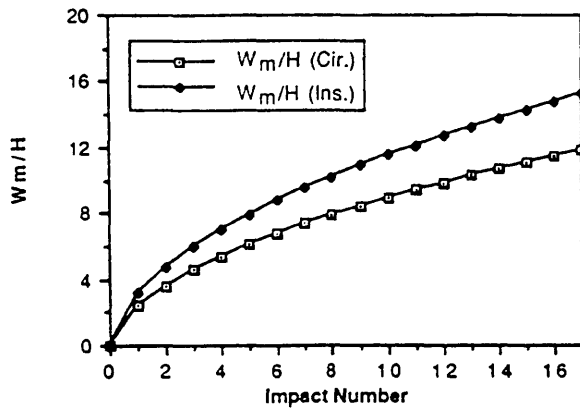


(c) STRAIN-TIME HISTORY (3)

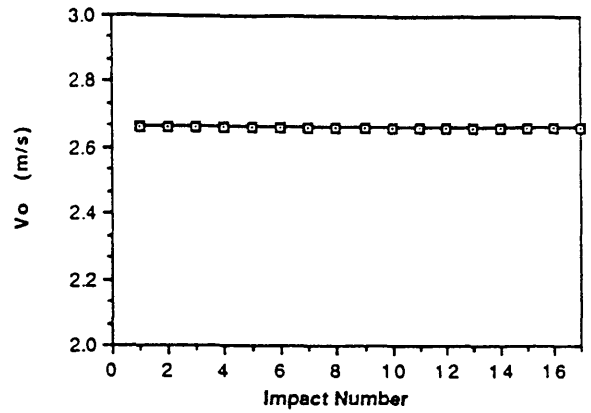


(f) STRAIN-TIME HISTORY (4)

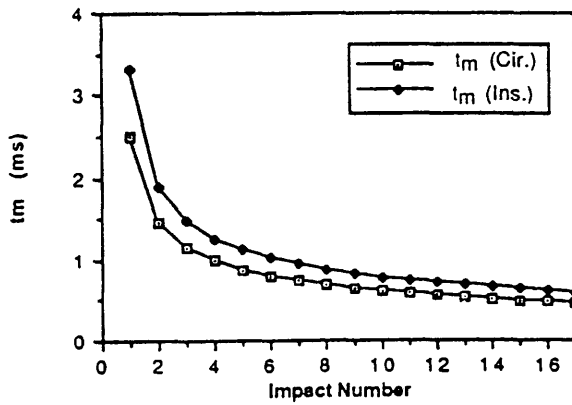
Fig. 7.8 Strain time histories on plate -A4P2-
by numerical method
(ϵ_s - Static uniaxial yield strain)



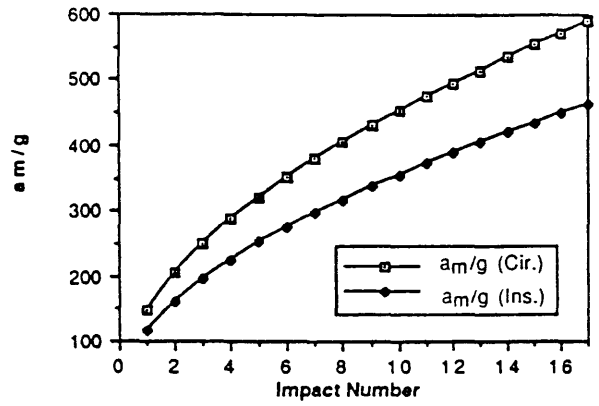
(a) Maximum deflection



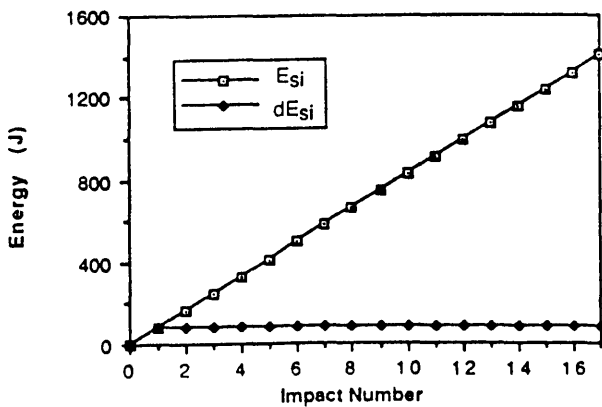
(b) Impact velocity



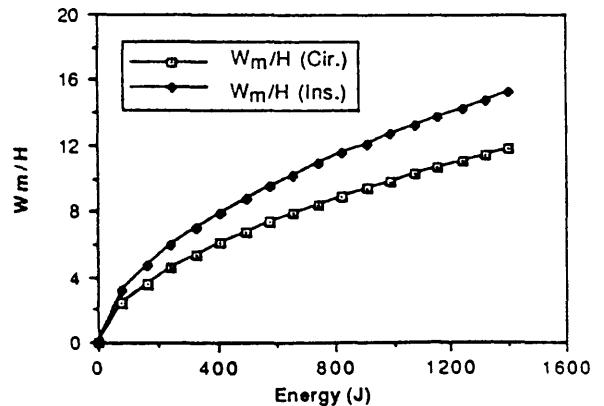
(c) Maximum response time



(d) Acceleration

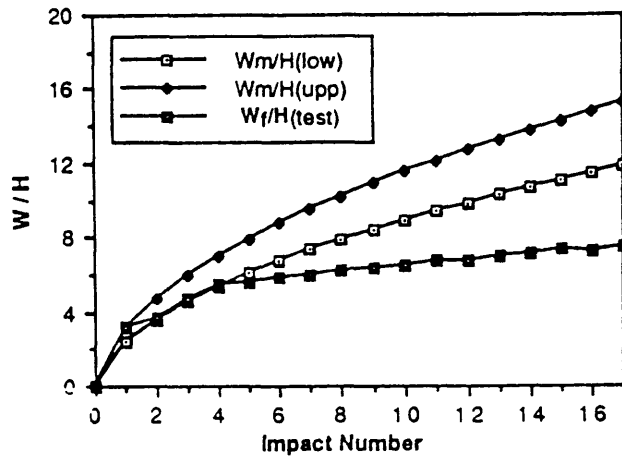


(e) Energy absorbed by the plate

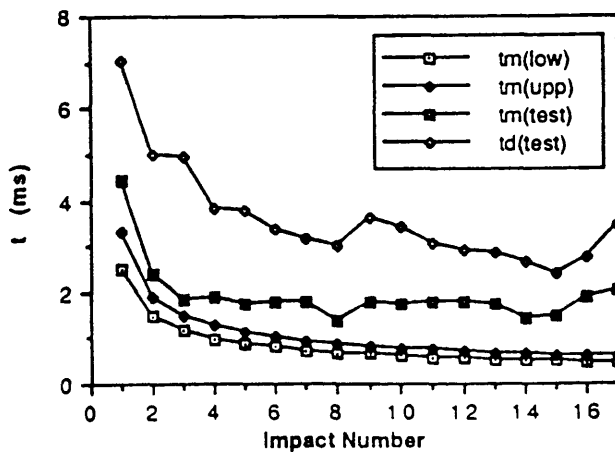


(f) Maximum deflection - energy relation

Fig. 7.9 Rigid perfectly plastic solutions for repeatedly impacted plate -ST03-
 Cir. - Circumscribing square yield curve
 Ins. - Inscribing square yield curve



(a) Maximum permanent deflection



(b) Response time

Fig. 7.10 Comparisons between test results and rigid perfectly plastic solutions for repeatedly impacted plate-ST03-

CHAPTER EIGHT

CONCLUSIONS AND PROPOSALS FOR FUTURE WORK

8.1 Conclusions

This thesis presents a numerical procedure to study the dynamic structural response for ship collisions. The numerical results are compared with experimental data and with approximate analytical methods. A wide range of structural behaviour in collision has been investigated. The important parameters governing ship collision are included in the simplified model which justifies itself satisfactorily by its good results. Both energy absorption behaviour and local stress and strain analysis are performed in the work. The understanding gained aids the development of an approximate design method.

Numerical Modelling

- The numerical model was based on the Variational Finite Difference Method, in which the influence of finite deflection, axial restraints, bending moments, material elasticity and strain hardening were included. The interface condition was established on the basis that the striking object has the same deformation as the struck plate in the contact area. The program written in Fortran was developed on the University's mainframe IBM-3090 and proved to be very efficient. The running time for one case is normally less than 30 minutes.

- The numerical approach provides information on the impact force, deformation, stress

and strain everywhere in the plate. These results give a full picture of the collision process and could not be obtained experimentally or by simple plastic formulations.

- Numerical predictions favourably match the results from experiments on clamped plates. Satisfactory correlation is also obtained with data from small scale ship model tests conducted in the University's Department of Naval Architecture and Ocean Engineering during 1981-1982. For plate tests, the dynamic yield stress coefficient was obtained by comparison of test data on aluminium and steel plates. For small scale ship models, the strain rate at different points in the plate was given by the program. The average dynamic yield stress can be adopted according to the Cowper-Symonds formula.

Experimental Investigation

- Impact tests to support the numerical analysis were performed on simplified plate structures to simulate the collision process. Both aluminium and steel plates were tested. Detailed information was obtained on impact and rebound velocities, permanent deformation, accelerations, dynamic strains and failure modes.

- The effect of strain-rate sensitivity was observed in the test. For 1.65 mm thick aluminium and steel plates, two $W_f/H - \lambda$ curves were plotted. By adjusting the dynamic yield stress coefficient for steel plates, these two curves coincided. For the test condition given, the coefficient is approximately 1.5.

- The failure process of the struck plate was investigated. At the beginning of the impact bending, membrane stretching and transverse shearing developed at the end of the dent line. Afterwards the plate failure began with either denting through plate thickness or cracking due to large tensile strain. These two types of failure initiated at

the end of the dent line. The failure caused by the transverse shear force should be avoided in practice, as the failure due to ductile deformation can absorb more impact energy. It is emphasised that although allowance of in-plane sliding along the top and bottom boundaries increases the maximum deflection a little, the above change in boundary condition has significant effect in the failure mode of the plate, and makes crack at the end of the dent line appear less easily.

- For repeated, identical impacts when the dent lines do not coincide, the maximum deflection is smaller than when coincided. This is because the impact energy is partly dissipated on developing new plastic hinges.

- To explore the mechanism of plate failure it is important to experimentally monitor the crack and rupture process. The strain gauge time history provides an ideal way to detect cracking of the plate.

Rigid Perfectly Plastic Method

- A simple approximate procedure was developed based on the Rigid Perfectly Plastic Method to predict the dynamic response of an impacted plate, including deformation and impact force. Correlations with numerical results and experimental data were examined. There are some differences in the response between the local impact and uniformly distributed pressure. For instance, the rebound velocity of a locally impacted plate is still significant even though the value of W_0/H is larger than 10. It is suggested that a suitable range of λ for using the Rigid Perfectly Plastic Method should be tested by a numerical program. The conditions for using the Rigid Perfectly Plastic Method on locally impacted plate need to be explored further.

- The simple approximate procedure was also developed to study the response of plate

subjected to a number of identical impacts. It was proved that the phenomenon of pseudo-shakedown does not occur, and this was validated by the test results.

- The influence of boundary conditions was examined by allowing free rotation along two sides of the plate. It was found that there is a little increase in the maximum permanent deflection and impact duration, but a decrease in maximum impact force.

Applications of this Work

- The combined work of numerical modelling, experimental investigation and the rigid perfectly plastic analysis enable one to gain a better understanding of the collision process, especially the dynamic characteristics of ship collision as the assumption of it being a quasi-static process is removed. This makes possible the study of relatively higher velocity impacts. Since the boundary of the impacted plate is unmovable, which implies that the mass of struck ship is assumed to be very large, it is suggested that when the mass of the striking vessel is 10 times smaller than the struck ship this theory can be accurately applied. As the research is fundamental, it can be used not only for ships but for platforms.

- Using the numerical method parametric studies on some important structural parameters governing ship collisions provide designers with useful information for design.

- Research on the failure mode of ships reveals that there are extreme stress and strain concentrations at the end of the dent line. Therefore the traditional energy method should be combined with stress and strain analysis to account for the local failure of the plate. As plate failure is linked to the critical speed of ships, which is particularly important to the design of ships with hazardous cargoes, the numerical program can be used to calculate the 'critical speed' in terms of the failure criterion chosen.

- Given the impact condition, size and material properties of the struck plate, the design thickness can be determined by using the numerical program and the rigid perfectly plastic formulae. For each thickness assumed, the $W_f/H - H$ curve is plotted and the design thickness can be chosen according to the design requirement, say, to limit the indent to five thicknesses.

- The above design method can also be extended to design of the plate of a ship or a platform subjected to repeated impacts of supply vessels. From a service and maintenance point of view, this specific problem requires the attention of researchers and designers.

8.2 Proposals for Future Work

Reliability Aspects of Ship Collisions

Given specified material properties and impact conditions, the structural response of the impacted plate can be calculated by the prescribed procedures. However, there are many uncertainties in the phenomenon of ship collision which can not be explained by the deterministic approach. In the simplified model presented in this thesis uncertainties exist, for example, in material properties, impact mass and velocity, and ultimate limit states. To rationally assess the safety of the impacted structures, a reliability approach should also be incorporated with the deterministic method. The main object of ship plate design against impact is to ensure that, at an acceptable probability level of collision, the plate will not become unfit for its intended purpose at any time during its specified design life. This can be achieved by using the Advanced Level Two Method. The important parameters governing the response to collision are selected as basic variables. The failure surface is obtained by using the program or the rigid perfectly plastic formula with the specified failure criterion. If the means and standard deviations

of the basic variables are given according to the statistical data, then the design point can be determined. The sensitivity factors and PSFs can also be obtained for any required level of safety.

Locally Impacted Stiffened Plate

As flat stiffened panels are a basic component of ships, stiffened plates should be studied as the continuation of the work on flat plates. There is no substantial difficulty in extending the numerical program to locally impacted stiffened plates. The structural response consists of bending and membrane behaviour. However, the plate and stiffeners need to be treated as a whole and no interaction is considered between them. This means that interactive tripping behaviour can not be accounted for but this may not be serious for essentially normal impacts.

From an experimental point of view the design of stiffened panels for further test is proposed. The first two models are suggested using 1 mm plate thickness and vertical bar stiffeners 10*1 at 50 mm spacing with two and four stiffeners respectively. The model should be stress relieved and a vertical striker should aim mid-way between the central stiffeners.

Locally Impacted Cylinder

The cylinder is an important structural type which is found widely throughout the field of marine and offshore engineering. The problem of ship impact damage on offshore platforms has attracted a great deal of research since the risk from collision is significant for the cylindrical elements. The study of cylinders under local impact is proposed to extend the previous work, which will enable this work to progress to the important practical area of pipes and shells. The failure modes, local stress and strain behaviour

and relationship between structural absorbed energy and structural parameter should be the emphasis of the study. In developing the numerical program the "gap element" is recommended to model the interface condition between the striker and the surface of the cylinder.

REFERENCES

Amdahl, J., 1983, 'Energy absorption in ship-platform Impacts', Norwegian Institute of Technology, Division of Marine Structures, Report No. UR-83-34, Trondheim.

Akita, Y., Ando, N., Fujita, Y. and Kitamura, K., 1972, 'Studies on collision-protective structures in nuclear powered ships', Nuclear Engineering and Design, Vol. 19, /365/.

Akita, Y. and Kitamura, K., 1972, 'A study on collision by an elastic stem to a side structure of ships', Trans. Soc. of Naval Architects of Japan, Vol. 131, /307/.

Ando, N. and Arita, K., 1976, 'A study on the strength of double-hull structures in collision', Trans. Soc. of Naval Architects of Japan, /139/.

Chang, P.Y., Seibold, F. and Thasanatorn, C., 1980, 'A rational methodology for the prediction of structural response due to collision of ships', Transactions SNAME, Vol. 88, /173/.

Cheresh, M.C. and McMichael, S., 1987, 'Instrumented impact test data interpretation', **Instrumented Impact Testing of Plastics and Composite Materials**, ASTM 936. Ed. by S.L. Kessler, G.C. Adams, S.B. Driscoll and D.R. Ireland, American Society for Testing and Materials, Philadelphia, /9/.

Cho, S.R., 1987, 'Design approximations for offshore tubulars against collisions', Ph.D. Thesis, Glasgow University.

Cox, A.D. and Morland, L.W., 1959, 'Dynamic plastic deformations of simply-supported square plates', *J. Mech. Phys. Solids*, Vol.7, /229/.

Davies, I. Li., 1980, 'A method for the determination of the reaction forces and structural damage arising in ship collisions', *European Offshore Petroleum Conference and Exhibition, London*, /245/.

de Oliveira, J.G., 1981, 'Design of steel offshore structures against impact load due to dropped objects', *Proc. 2nd Int. Symp. on Offshore Eng. Struct.*, Ed. by Carpeiro, et al., *Coppe Rio de Janeiro*, /466/.

Dickey, A., 1986, 'New rules for when the going gets tough', *The Engineer*, 22 May, /20/.

Ellinas, C.P. and Valsgard, S., 1985 'Collision and damage of offshore structures: A state-of-the-art', *J. of Energy Resources Tech.*, Vol. 107, /297/, September.

Embury, J.D. and LeRoy, G.H., 1977, 'Failure maps applied to metal deformation process', *4th Int. Conf. on Fracture, Waterloo*, Vol. 1, /15/.

Frieze, P.A. and Sachinis, A., 1983, 'Compressive strength of stress-relieved ring-stiffened cylinders including local damage', paper 18, *Proceedings of Int. Conf. on Marine Safety, Glasgow University*.

Fung, Y. C., 1965, *Foundations of Solid Mechanics*, Prentice-Hall, Inc.

Harima, T. et al. 1962, 'Research on the collision-resisting construction of the sides of a nuclear-powered ship', *Mitsubishi Nippon Industries Technical Review*.

Incecik, A. and Samuelides, E., 1981, 'Analytical and experimental studies on ship-ship and ship-platform collisions', Proceedings of the Dynamic Modelling of Structures, published jointly by the Institute of Structural Engineers and Building Research Establishment, U.K.

ISSC, 1967, 'Plastic and limit design', Committee Rep. 3e, Proc. 3rd Int. Ship Structures Congress, Hamburg, /68/.

ISSC, 1982, 'Transient dynamic loading and response', Committee Rep. II. 3, Proc. 8th Int. Ship Structures Congress, Paris, Vol. II. /3/.

Ito, H., Kondo, K., Yoshimura, N., Kawashima, M. and Yamamoto, S., 1984, 'A simplified method to analyze the strength of double hulled structures in collision (1st report)', Read at the Autumn Meeting of the Society of Naval Architecture of Japan, J. Soc. of Naval Architects of Japan, Vol. 156, /283/.

Ito, H., Kondo, K., Yoshimura, N., Kawashima, M. and Yamamoto, S., 1985, 'A simplified method to analyze the strength of double hulled structures in collision (2nd report)', Read at the Autumn Meeting of the Society of Naval Architecture of Japan, J. Soc. of Naval Architects of Japan, Vol. 158, /543/.

Jones, N., 1968, 'Finite-deflections of a rigid-viscoplastic strain-hardening annular plate loaded impulsively', J. of Appl. Mech., Vol. 35, /349/.

Jones, N., Uran, T.O. and Teken, S.A., 1970, 'The dynamic plastic behaviour of fully clamped rectangular plates', Int. J. Solids & Struct., Vol. 6, /1499/.

Jones, N., 1971, 'A theoretical study of the dynamic plastic behaviour of beams and plates with finite-deflections', Int. J. Solids & Struct., Vol. 7, /1007/.

Jones, N., 1972, 'Review of the plastic behaviour of beams and plates', *Int. Ship Building Progress*, Vol. 19, No.218, /313/.

Jones, N., 1973, 'Slamming damage', *J. of Ship Research*, Vol. 17, No.2, /80/.

Jones, N., 1974, 'Some remarks on the strain-rate sensitive behaviour of shells', **Problem of Plasticity**, Ed. by Sawczuk, A., Leyden, /403/.

Jones, N., 1976, 'Plastic failure of ductile beams loaded dynamically', *J. Engrg. Indus.*, Trans. ASME, Vol. 98(B), /131/.

Jones, N., 1977, 'Damage estimate for plating of ships and marine vehicles', *Int. Symp. on Practical Design in Shipbuilding(PRADS)*, Society of Naval Architects of Japan, Tokyo, /121/.

Jones, N., 1979, 'A literature survey on the collision and grounding protection of ships', *Ship Structure Committee Report, SSC-283*, U.S. Coastguard, Washington.

Jones, N., 1983, 'Structural aspects of ship collision', **Structural Crashworthiness**, Ed. by Jones, N. and Wierzbicki, T., Butterworths, /308/.

Jones, N., 1988, 'On the dynamic inelastic failure of beams', **Structural Failure**, Ed. by Wierzbicki, T. and Jones, N., John Wiley & Sons, /133/.

Jones, N., 1989-a, 'Some comments on structural impact', **Supercomputing In Engineering Structures**, Ed. by Melli, P. and Brebbia, C.A., Computational Mechanics Publications, Southampton, Boston, /133/.

Jones, N., 1989-b, 'Some comments on the modelling of material properties for dynamic structural plasticity', Int. Conf. Mech. Prop. of Materials at High Rates of Strain, Oxford.

Jones, N. and Zhu, L., 1989, Personal communication.

Kinkead, A.N., 1983, 'Some collision and grounding consideration for refrigerated gas carriers', *Marine and Offshore Safety*, Ed. by Frieze, P.A., McGregor, R.C. and Winkle, I.E., Applied Science Publishers, /59/.

Lee, E.H. and Symonds, P.S., 1952, 'Large plastic deformation of beams under transverse impact', *J. App. Mechs.*, Vol. 19, /308/.

Lee, L.H.N. and Ni, C.M., 1973, 'A minimum principle in dynamics of elastic-plastic continua at finite deformation', *Arch. Mech.* Vol. 25, /456/.

Liu, J. H. and Jones, N., 1987 'Experimental investigation of clamped beams struck transversely by a mass', *Int. J. Impact Engng*, Vol. 6, No. 4, /303/

Liu, J. H. and Jones, N., 1988 'Dynamic response of a rigid plastic clamped beams struck by a mass at any point on the beam', *Int. J. Solid Structures*, Vol. 24, No.3, /251/

Manjoine, M.J., 1944, 'Influence of rate of strain and temperature on yield stresses of mild steel', *J. of Appl. Mech.*, Vol. 11, /A-211/.

Marsh, K.J. and Campell, J.D., 1963, 'The effect of strain-rate on post-yield flow of mild steel', *Int. J. Mech. and Physics of Solids*, Vol. 11, /49/.

Martin, J.B., 1964, 'Impulsive loading theorems for rigid-plastic continua', Proc. ASCE, Vol.90, No. EM5, /27/.

Martin, J and Symonds, P., 1966, 'Mode approximation for impulsively-loaded rigid plastic structures', J. Eng. Mechs. Div., ASCE, EM5, /43/.

Martin, J. and Ponter, A., 1972, 'Bounds for impulsively loaded plastic structures', J. Eng. Struc. Div., ASCE, EM1, /107/

McDermott, J.F., Kline, R.G., Jones, E.L., Maniar, N.M. and Chiang, W.P., 1974, 'Tanker structural analysis for minor collisions', Trans SNAME, Vol. 82, /382/.

Menkes, S.B. and Opat, H.J., 1973, 'Broken beams', Exptl. Mech., Vol. 13, /480/.

Minorsky, V. U., 1959, 'An analysis of ship collisions with reference to protection of nuclear power plants', J. of Ship Research, Vol. 3, /1/.

Morales, W.J. and Nevill, G.E., 1970, 'Lower bounds on deformations of dynamically loaded rigid-plastic continua', AIAA Journal, Vol.8, /2043/.

Ni, C.M. and Lee, L.H.N., 1974, 'Dynamic behavior of inelastic cylindrical shells at finite deformation', Int. J. Non-Linear Mech., Vol. 9, /193 /.

Ni, C.M., 1982, ' A quadrilateral finite difference plate element for nonlinear transient analysis of panels', J. Comp. & Struc. Vol. 15, /1/.

NMAB, 1980, 'Safety aspects of liquefied natural gas in the marine environment', Report of Panel on LNG Safety Evaluation, National Materials Advisory Board, Pub. NMAB 354, National Academy of Sciences, Washington, D.C.

Onoufriou, A and A.S. Elnashai et al. 1987, 'Numerical modelling of damage to ring stiffened cylinders', Proc. of 6th Int. Conf. on Offshore Mechanics and Arctic Engineering, Houston, /281/.

Parkes, E.W., 1958, 'The permanent deformation of an encastre beam struck transversely at any point in its span', Proc. Instn. of Civil Engrs, Vol. 10, /277/.

Perrone, N., 1965, 'On a simplified method for solving impulsively loaded structures of rate-sensitive materials', J. of Appl. Mech., Vol. 32, /489/.

Perrone, N., 1967, 'Impulsively loaded strain-rate-sensitive plates', J. of Appl. Mech., Vol.34, /380/.

Perzyna, P.,1980, 'Modified theory of viscoplasticity, Application to advanced flow and instability phenomena', Archives of Mechanics, Vol.32, /403/.

Pettersen, E., 1981, 'Assessment of impact damage by means of a simplified non-linear approach', **Integrity of Offshore Structures**, Applied Science Publishers, /317/.

Ronalds, B.F. and Dowling, P.J., 1986, 'Finite deformations of stringer stiffened plate and shells under knife edge loading', Proc. of 5th Int. Conf. on Offshore Mechanics and Arctic Engineering, /323/.

Samuelides, E., 1984, 'Structural dynamic and rigid body response coupling in ship collisions', Ph.D. Thesis, Glasgow University.

Sawczuk, A., 1964, 'On initiation of the membrane action in rigid-plastic plates', *Journal de Mecanique*, Vol. 3, No.1, /15/.

Shen, W. Q. and Jones, N., 1989, 'The pseudo-shakedown of beams and plates when subjected to repeated dynamic loads', ASME Winter Annual Meeting, San Francisco.

Soreide, T. H. and Amdahl, J., 1982, 'Deformation characteristics of Tubular members with reference to impact loads from collision and dropped objects', *Norwegian Maritime Research*, Vol. 10, No.2, /3/.

Symonds, P.S., 1965, 'Viscoplastic behaviour in response of structures to dynamic loadings, **Behaviour of Materials under Dynamic Loading**, Ed. by N.J.Huffington, ASME, /106/.

Symonds, P.S. and Wierzbicki, T., 1979, 'Membrane mode solutions for impulsively loaded circular plates', *J. App. Mechs.*, Vol.49, No.1, /58/.

Ueda, Y., Murakawa, H and Xiang, D., 1989, 'Classification of dynamic response of a tubular beam under collision', *Proc. of 8th Int. Conf. on Offshore Mechanics and Arctic Engineering*, /645/.

Valsgard, S. and Pettersen, E., 1982, 'Simplified nonlinear analysis of ship/ship collisions', *Norwegian Maritime Research*, Vol. 10, No.3, /2/.

Van Mater, P. R. Jr. and Giannotti, J.G., Jones, N. and Genalis, P., 1979, 'Critical evaluation of low energy ship collision - damage and design methodologies, Appendix B.', *Ship Structure Committee Report SSC-285*.

Van Mater, P. R. Jr., Giannotti, J.G., McNatt, T.R. and Edinberg, D.C., 1980, 'Vessel collision damage resistance', Report CG-D-21-80, US Coast Guard.

Vaughan, H., 1978, 'Bending and tearing of plate with application to ship-bottom damage', The Naval Architect, May 1978, /97/.

Wierzbicki, T., 1983, 'Crashing behaviour of plate intersections', **Structural Crashworthiness**, Ed. by Jones, N. and Wierzbicki, T., Butterworths, /66/.

Woisin, G., 1979, 'Design against colision', Int. Symp. on Advances in Marine Technology, Trondheim, Norway, /1/.

Woisin, G., 1986, 'The transferability of collision model tests to real collisions, part 4: Model test techniques for investigating ship collisions', Unpublished paper.

Wood, R., 1961, **Plastic and Elastic Design of Slabs and Plates**, The Ronald Press, New York.

Yang, P.D.C. and Caldwell, J.B., 1988, 'Collision energy absorption of ship's bow structures', Int. J. Impact Engng, Vol. 7, No.2, /181/.

Yu, J. L. and Jones, N., 1989, 'Numerical simulation of a clamped beam under impact loading', J. Computers & Structures, Vol. 32, No. 2, /281/.

Zhu, L., 1989, 'Rigid plastic solution for the impacted rectangular plates with finite deflections', Department Report NAOE 89-45, University of Glasgow.

Zhu, L. and Faulkner, D., 1989, 'Dynamic behaviour of ship plates in collision', Department Report NAOE 89-26, University of Glasgow.

Zhu, L. and Jones, N., 1989, Personal communication.

Zhu, L., 1990, 'Dynamic response of plates under repeated impacts', Department Report NAOE 90-01, University of Glasgow.

Zhu, L. and Faulkner, D., 1990, 'Numerical modelling of dynamic inelastic response of clamped rectangular plates impacted by a knife edge indenter', Proc. of 9th Int. Conf. on Offshore Mechanics and Arctic Engineering, Houston, Vol.1, Part B, /595/.

Zukas, J.A. et al, 1982, **Impact Dynamics**, John Wiley & Sons, Inc.

APPENDIX

-Expressions for the coefficients in (2.40) - (2.42)

$$C_1 = \frac{H}{L} \frac{1}{2\Delta x}$$

$$C_2 = \frac{H}{L} \frac{1}{2\Delta y}$$

$$C_3 = \frac{H}{L} \frac{1}{(\Delta x)^2}$$

$$C_4 = \frac{H}{L} \frac{1}{(\Delta y)^2}$$

$$C_5 = \frac{H}{L} \frac{1}{2\Delta x \Delta y}$$

$$C_6 = \frac{H}{L} \frac{1}{2\Delta x}$$

$$C_7 = \frac{H}{L} \frac{1}{2\Delta y}$$

$$Q = \frac{\rho L}{EH}$$

$$A_{i,j}^1 = \frac{1}{2\Delta x} (u_{i+1,j} - u_{i-1,j})$$

$$A_{i,j}^2 = \frac{1}{2\Delta x} (v_{i+1,j} - v_{i-1,j})$$

$$A_{i,j}^3 = \frac{1}{2\Delta x} (w_{i+1,j} - w_{i-1,j})$$

$$A_{i,j}^4 = \frac{1}{2\Delta y} (u_{i,j+1} - u_{i,j-1})$$

$$A_{i,j}^5 = \frac{1}{2\Delta y} (v_{i,j+1} - v_{i,j-1})$$

$$A_{i,j}^6 = \frac{1}{2\Delta y} (w_{i,j+1} - w_{i,j-1})$$

$$A_{i,j}^7 = \frac{1}{(\Delta x)^2} (w_{i+1,j} - 2w_{i,j} + w_{i-1,j})$$

$$A_{i,j}^8 = \frac{1}{(\Delta y)^2} (w_{i,j+1} - 2w_{i,j} + w_{i,j-1})$$

$$A_{i,j}^9 = \frac{1}{4\Delta x \Delta y} (w_{i+1,j+1} - w_{i-1,j+1} - w_{i+1,j-1} + w_{i-1,j-1})$$

$$(N_{xx})_{i,j} = \frac{1}{E} \sum_{k=-1}^1 (s_{xx})_{i,j,k} - \frac{1}{2E} [(s_{xx})_{i,j,-1} + (s_{xx})_{i,j,1}]$$

$$(N_{yy})_{i,j} = \frac{1}{E} \sum_{k=-1}^1 (s_{yy})_{i,j,k} - \frac{1}{2E} [(s_{yy})_{i,j,-1} + (s_{yy})_{i,j,1}]$$

$$(N_{xy})_{i,j} = \frac{1}{E} \sum_{k=-1}^1 (s_{xy})_{i,j,k} - \frac{1}{2E} [(s_{xy})_{i,j,-1} + (s_{xy})_{i,j,1}]$$

$$(M_{xx})_{i,j} = \frac{1}{E} \sum_{k=-1}^1 k(s_{xx})_{i,j,k} - \frac{1}{2E} [-1(s_{xx})_{i,j,-1} + 1(s_{xx})_{i,j,1}]$$

$$(M_{yy})_{i,j} = \frac{1}{E} \sum_{k=-1}^1 k(s_{yy})_{i,j,k} - \frac{1}{2E} [-1(s_{yy})_{i,j,-1} + 1(s_{yy})_{i,j,1}]$$

$$(M_{xy})_{i,j} = \frac{1}{E} \sum_{k=-1}^1 k(s_{xy})_{i,j,k} - \frac{1}{2E} [-1(s_{xy})_{i,j,-1} + 1(s_{xy})_{i,j,1}]$$

